

1. THE SPANWISE PERTURBATION OF TWO-DIMENSIONAL  
BOUNDARY LAYERS
2. THE TURBULENT RAYLEIGH PROBLEM
3. THE PROPAGATION OF FREE TURBULENCE IN  
A MEAN SHEAR FLOW

Thesis by  
Steven Collins Crow

In Partial Fulfillment of the Requirements  
For the Degree of  
Doctor of Philosophy

California Institute of Technology  
Pasadena, California

1966

(Submitted May 27, 1966)

## ACKNOWLEDGMENTS

Peter Bradshaw and Trevor Stuart at the National Physical Laboratory in England suggested the boundary-layer problem solved in the first chapter of this thesis. I began the work under their inspiration and continued with the guidance of Philip Saffman at Caltech. Peter Bradshaw's desire to incorporate the Townsend stress-shear relation in turbulent boundary-layer similarity solutions led me to develop the turbulent Rayleigh problem. Bradshaw's enthusiasm and his experiments motivated my work during my stay in England. Philip Saffman suggested the problem of propagation of turbulence through a mean shear flow. He helped me through initial difficulties and made many suggestions which have been incorporated in the thesis. He was always ready to talk about the essential ideas behind the work, and he was also willing to help on troublesome mathematical details. I thank Peter Bradshaw, Trevor Stuart, and especially Philip Saffman for their encouragement and their contributions to my research.

Elizabeth Fox worked as hard typing the thesis as I did writing it. I thank her for a beautiful job on a long and complicated project.

Finally, I thank the National Science Foundation for the Fellowship which made my graduate study possible.

## ABSTRACT

### 1. The Spanwise Perturbation of Two-Dimensional Boundary Layers

Large spanwise variations of boundary-layer thickness have recently been found in wind tunnels designed to maintain two-dimensional flow. Bradshaw argues that these variations are caused by minute deflections of the free-stream flow rather than an intrinsic boundary-layer instability. The effect of a small, periodic transverse flow on a flat-plate boundary layer is studied in this chapter. The transverse flow is found to produce spanwise thickness variations whose amplitude increases linearly with distance downstream.

### 2. The Turbulent Rayleigh Problem

Rayleigh flow is the non-steady motion of fluid above a flat plate accelerated suddenly into motion. Laminar Rayleigh flow is closely analogous to laminar boundary-layer flow but does not involve the analytical difficulty of non-linear convection. In this chapter, turbulent Rayleigh flow is studied to illuminate physical ideas used recently in boundary-layer theory. Boundary layers have nearly similar profiles for certain rates of pressure change. The Rayleigh problem is shown to have a class of exactly similar solutions. Townsend's energy balance argument for the wall layer and Clauser's constant eddy viscosity assumption for the outer layer are adapted to the Rayleigh problem to fix the relation between shear and stress. The resulting non-linear, ordinary differential equation of motion is solved exactly for constant wall stress, analogous to zero pressure gradient in the boundary-layer problem, and for zero wall stress, analogous to continuously separating flow. Finally, the boundary-

layer equations are expanded in powers of the skin friction parameter  $\gamma = \sqrt{C_f/2}$ , and the zeroth order problem is shown to be identical to the Rayleigh problem. The turbulent Rayleigh problem is not merely an analogy, but is a rational approximation to the turbulent boundary-layer problem.

### 3. The Propagation of Free Turbulence in a Mean Shear Flow

This chapter begins with the assumption that the propagation of turbulence through a rapidly shearing flow depends primarily on random stretching of mean vorticity. The Reynolds stress  $\sigma(y,t)$  acting on a mean flow  $U(y) = \Omega y$  in the  $x$  direction is computed from the linearized equations of motion. Turbulence homogeneous in  $x, z$  and concentrated near  $y = 0$  was expected to catalyze the growth of turbulence further out by stretching mean vorticity, but  $\sigma(y,t)$  is found to become steady as  $\Omega t \rightarrow \infty$ . As far as Reynolds stress is a measure of turbulent intensity, random stretching of mean vorticity alone cannot yield steadily propagating turbulence.

The problem is simplified by assuming that all flow properties are independent of  $x$ . Eddy motion in the  $y, z$  plane is then independent of the  $x$  momentum it transports, and the mean speed  $U(y,t)$  is diffused passively. The equations of motion are partially linearized by neglecting convection of eddies in the  $y, z$  plane, and wave equations for  $\sigma(y,t)$  and  $U(y,t)$  are derived. The solutions are worthless, however, for large times. Turbulence artificially steady in the  $y, z$  plane forces the mean speed gradient steadily to zero. In a real flow the eddies disperse as fast as  $U$  diffuses.

Numerical experiments are designed to find how quickly concentrated vortex columns parallel to  $x$  disperse over the  $y, z$  plane and how effectively they diffuse  $U$ . It is shown that unless a lower limit on the distance between any two vortices is imposed, computational errors can dominate the solution no matter how small a time increment is used. Vortices which approach closely must be united. Uniting vortices during the computations is justified by finding a capture cross section for two vortices interacting in a strain field. The experiments confirm the result that columnar eddies disperse as fast as they transport momentum.

TABLE OF CONTENTS

PART	TITLE	PAGE
I.	THE SPANWISE PERTURBATION OF TWO-DIMENSIONAL BOUNDARY LAYERS	1
	1. Introduction	1
	2. Statement of the Problem	2
	3. Solution Far Upstream	4
	4. Outer Expansion	6
	5. Inner Expansion	7
	6. Matching	8
	7. Initial Steps in Solving the Problem	9
	8. Final Steps to Determine $F_2$	14
	9. Conclusion	20
	REFERENCES	21
II.	THE TURBULENT RAYLEIGH PROBLEM	22
	1. Introduction	22
	2. Similarity Form of the Rayleigh Problem for Self-Preserving Solutions	28
	3. Some Properties of the Self-Preserving Solutions	30
	A. Momentum Conservation	30
	B. Laminar Sublayer	32
	4. Assumptions for the $\Omega\{\sigma\}$ Relation	34
	A. Wall Layer	35
	B. Outer Layer	37
	5. Equations of Motion under the $\Omega\{\sigma\}$ Assump- tions – Some General Consequences	39

TABLE OF CONTENTS (Cont'd)

PART	TITLE	PAGE
	6. Solution for the Constant Stress Case, $c = 0$	42
	7. Solution for the Continuously Separating Case, $c = -1$	44
	8. Analogy with the Equilibrium Boundary Layer	50
	REFERENCES	66
	APPENDIX	67
III.	THE PROPAGATION OF FREE TURBULENCE IN A MEAN SHEAR FLOW	71
	1. Introduction	71
	2. Basic Equations of the Problem	77
	3. The Linearized Problem with Constant $\Omega$	83
	A. Fourier Transformation and Solution of the Linearized Equations of Motion	83
	B. Correlation and Spectrum Functions of the Solutions to the Linear Problem	89
	C. Reynolds Stress above a Sheet of Random Vorticity	92
	D. Reynolds Stress in the Limit $\Omega t \rightarrow \infty$ of the General Problem	102
	4. Flow Uniform in the x Direction	106
	A. The $\partial F / \partial x = 0$ Assumption	106
	B. The Random Vortex Sheet Problem with $\partial F / \partial x = 0$	117
	C. Steady Induction by Line Vortices of	

TABLE OF CONTENTS (Cont'd)

PART	TITLE	PAGE
	Alternating Sign	129
5.	The Numerical Experiments	136
	A. Basis of the Numerical Approach	136
	B. Generation of Random Vortex Strengths a Specified Correlation	145
	C. Error Drift	149
	D. Flow Velocity and Error Velocity	159
	E. Vortex Capture	164
	F. Flow Visualization Experiments	172
	G. Background for the Momentum Transfer Experiments	182
	H. Momentum Transfer Experiments	193
6.	Summary	206
	REFERENCES	209
	APPENDICES	211
	A. Evaluation of $L_{ij}(k, k_{02})$	211
	B. Evaluation of the Stress Integrals in the Vortex Sheet Problem	213
	C. Proof that Equation 31 is Valid in the Limit $\Omega t \rightarrow \infty$	216
	D. Singular Perturbation Solution for $s(\eta, \tau), r(\eta, \tau)$	218
	E. Derivation of $T(\psi)$ and $\psi(y, 0)$ for the Steady Vortex Street	224

TABLE OF CONTENTS (Cont'd)

PART	TITLE	PAGE
F.	Derivation of the Mean Square Error Velocity $\overline{v_{\epsilon c}^2}$	227
G.	Motion of the Center of a Continuous Vorticity Distribution in a Uniform Translation and Strain Field	230

# I. THE SPANWISE PERTURBATION OF TWO-DIMENSIONAL BOUNDARY LAYERS

## 1. Introduction

In a series of wind-tunnel tests under nominally two-dimensional conditions, Klebanoff and Tidstrom [1] found quasi-periodic spanwise variations of boundary-layer thickness of order  $\pm 8\%$ . Recently the phenomenon recurred in a National Physical Laboratory tunnel specifically designed for the study of two-dimensional boundary layers. Bradshaw [2] sought a remedy as well as an explanation and found that these variations could result from lateral convergence or divergence of the flow downstream of slightly non-uniform settling-chamber damping screens. A rough analysis suggested that a boundary layer is surprisingly sensitive to spanwise velocity variations. The thickness variations found by Klebanoff could have been produced by variations in the free-stream flow direction of around 0.04 degree, much too small to be measured directly. This chapter is a rigorous analysis of the effect of a small, periodic spanwise component of velocity on the boundary layer of a flat plate. The flow is assumed to be incompressible, steady and laminar.

Three-dimensional effects in the boundary layer will depend on the transverse flow field chosen for the incident flow. Suppose  $U_0$  characterizes the chordwise component of free-stream flow,  $\gamma U_0$  the amplitude of the transverse perturbation. Suppose the frequency of the spanwise flow is specified by a wave-number  $k$ . The Reynolds number of the perturbation is then

$$R = \gamma U_0 / k\nu .$$

If Bradshaw's explanation is correct, the value of  $R$  corresponding to Klebanoff's data can be computed, and it is found to be around 3. It is not surprising that  $R$  is of order 1, since the transverse velocity variations are supposed to arise from the non-uniform drag of damping screens—a viscous phenomenon to begin with.  $R$  will be regarded as a parameter of order 1 throughout the analysis.

## 2. Statement of the Problem

The momentum and continuity equations are

$$\underline{U} \cdot \nabla \underline{U} = -\frac{\nabla P}{\rho} + \nu \nabla^2 \underline{U},$$

$$\nabla \cdot \underline{U} = 0,$$

for a steady, incompressible flow field  $\underline{U} = (U, V, W)$ . The coordinates and physical situation are shown in figure 1. For a characteristic speed  $U_0$  and perturbation wave-number  $k$ , the following non-dimensional variables are appropriate:

$$(\xi, \eta, \zeta) = (kx, ky, kz),$$

$$(u, v, w) = \left( \frac{U}{U_0}, \frac{V}{U_0}, \frac{W}{U_0} \right),$$

$$p = \frac{P}{\rho U_0^2}.$$

The equations of motion in non-dimensional form are:

$$(\xi\text{-momentum}) \quad uu_\xi + vu_\eta + wu_\zeta = -p_\xi + \epsilon^2(u_{\xi\xi} + u_{\eta\eta} + u_{\zeta\zeta}),$$

$$(\eta\text{-momentum}) \quad uv_\xi + vv_\eta + wv_\zeta = -p_\eta + \epsilon^2(v_{\xi\xi} + v_{\eta\eta} + v_{\zeta\zeta}),$$

$$(\zeta\text{-momentum}) \quad uw_\xi + vw_\eta + ww_\zeta = -p_\zeta + \epsilon^2(w_{\xi\xi} + w_{\eta\eta} + w_{\zeta\zeta}),$$

$$(\text{continuity}) \quad u_\xi + v_\eta + w_\zeta = 0,$$

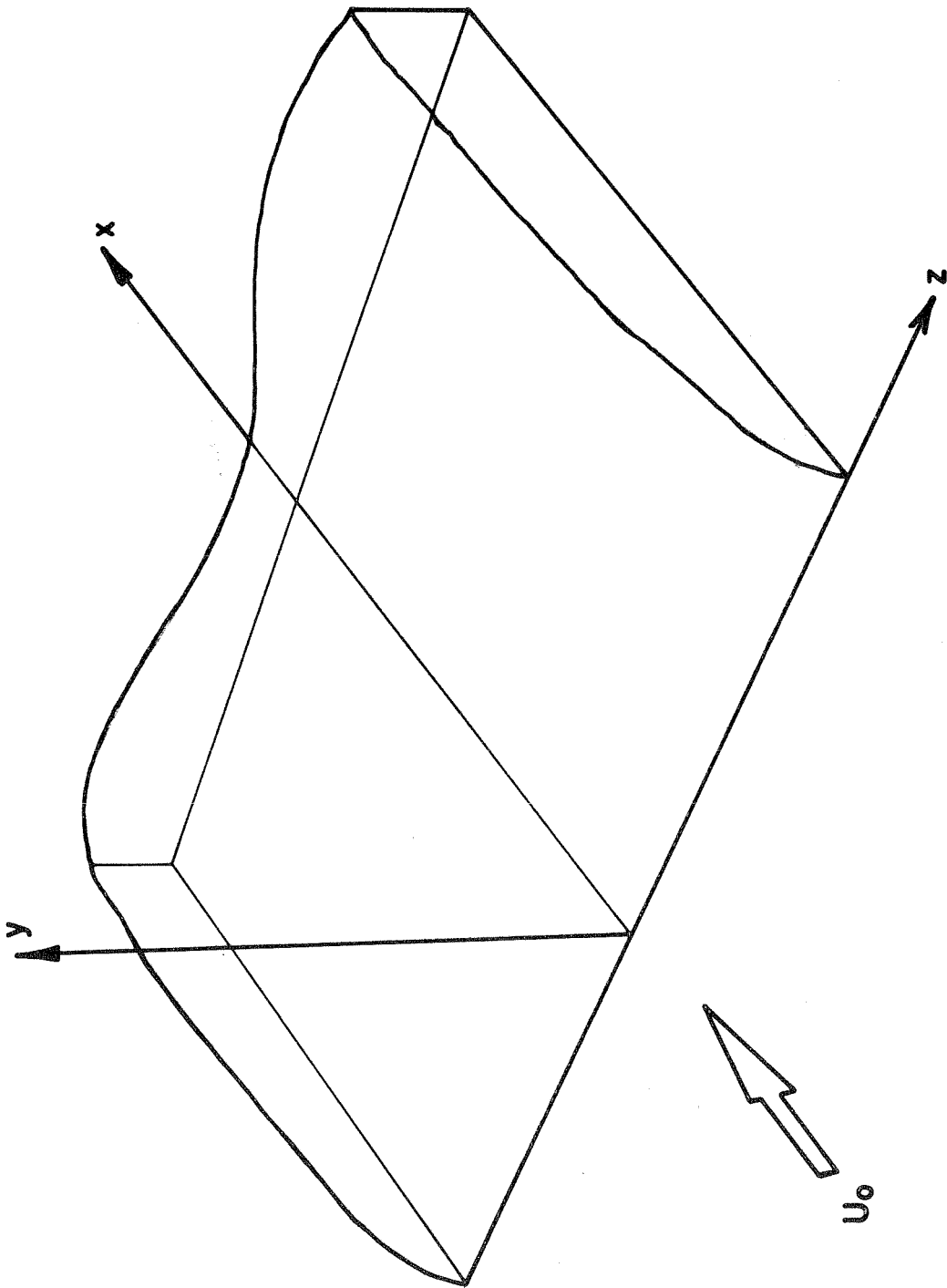


FIG. 1 THE PERTURBED BOUNDARY LAYER

where  $\epsilon^2 \equiv \nu k/U_0$ . If  $\gamma$  is the amplitude of the angular variation of free-stream flow direction, the perturbation Reynolds number is

$$R = \gamma U_0 / k\nu = \gamma / \epsilon^2 \sim O(1).$$

In Klebanoff's experiments  $\gamma$  was typically  $0.40^\circ \sim 0.001$  rad., so  $\epsilon$  was about 0.02. In this chapter  $\epsilon$  is used as an expansion parameter in a perturbation scheme.

The boundary condition at the plate is

$$(u, v, w) = (0, 0, 0).$$

The upstream flow can be specified in any convenient way as long as the field chosen carries the desired transverse perturbation and is an adequate approximation to a solution of the equations of motion. Let the expansions for  $u$  and  $w$  in the outer flow begin

$$\begin{aligned} u &= 1 + \dots, \\ w &= \gamma \cos \zeta + \dots = R\epsilon^2 \cos \zeta + \dots \end{aligned}$$

### 3. Solution Far Upstream

The velocity components above cannot be worked into a uniformly convergent solution to the equations of motion. Since the Reynolds number of the perturbation is of order 1, the transverse field of the incident stream must decay under the action of viscosity. Suppose we try a solution of the form

$$\begin{aligned} u &= 1, \\ v &= R(\xi)\epsilon^2 \eta \sin \zeta, \\ w &= R(\xi)\epsilon^2 \cos \zeta, \end{aligned}$$

where  $v$  has been chosen to satisfy the continuity equation. The approximate momentum equation

$$\tilde{u}_\xi = \epsilon^2 (\tilde{u}_{\eta\eta} + \tilde{u}_{\zeta\zeta})$$

is satisfied for

$$R(\xi) = R_0 e^{-\epsilon^2 \xi}.$$

In fact, a uniformly convergent approximate solution to the equations of motion is

$$\begin{aligned} u &= 1 + O(\epsilon^4), \\ v &= R\epsilon^2 \eta \sin \zeta + O(\epsilon^4), \\ w &= R\epsilon^2 \cos \zeta + O(\epsilon^4), \\ p &= p_0 + \frac{1}{2}R^2\epsilon^4 (\sin^2 \zeta - \eta^2) + O(\epsilon^6), \end{aligned}$$

for that  $R(\xi)$ .

An expansion of the outer solution in powers of  $\epsilon$  cannot be uniformly convergent. But such an expansion converges over an arbitrarily large interval  $\Delta\xi$ , where

$$\Delta\xi \ll 1/\epsilon^2.$$

As long as attention is confined to such an interval  $\Delta\xi$ , a straightforward expansion in powers of  $\epsilon$  can be carried out, and the upstream boundary conditions may be taken as

$$\begin{aligned} u &= 1 + O(\epsilon^4), \\ v &= R\epsilon^2 \eta \sin \zeta + O(\epsilon^4), \\ w &= R\epsilon^2 \cos \zeta + O(\epsilon^4), \end{aligned}$$

where change in R is now contained in the  $O(\epsilon^4)$  corrections.

#### 4. Outer Expansion

Let  $\xi$ ,  $\eta$ ,  $\zeta$  remain fixed, and allow  $\epsilon$  to tend to zero. The dependent variables are expanded in powers of  $\epsilon$  as follows:

$$u = 1 + \epsilon f_1(\xi, \eta, \zeta) + \epsilon^2 f_2(\xi, \eta, \zeta) + \dots,$$

$$v = \epsilon g_1(\xi, \eta, \zeta) + \epsilon^2 g_2(\xi, \eta, \zeta) + \dots,$$

$$w = R\epsilon^2 \cos \zeta + \dots,$$

$$p = p_0 + \epsilon p_1(\xi, \eta, \zeta) + \epsilon^2 p_2(\xi, \eta, \zeta) + \dots$$

When the coefficients of consecutive powers of  $\epsilon$  in the equations of motion are set equal to zero, the following system of equations results:

$\xi$  momentum

$$O(\epsilon) \quad f_{1\xi} = -p_{1\xi}, \quad (1)$$

$$O(\epsilon^2) \quad f_{11\xi} + f_{2\xi} + g_1 f_{11\eta} = -p_{2\xi}. \quad (2)$$

$\eta$  momentum

$$O(\epsilon) \quad g_{1\xi} = -p_{1\eta}, \quad (3)$$

$$O(\epsilon^2) \quad f_{1g_{1\xi}} + g_{2\xi} + g_1 g_{1\eta} = -p_{2\eta}. \quad (4)$$

$\zeta$  momentum

$$O(\epsilon) \quad p_{1\zeta} = 0, \quad (5)$$

$$O(\epsilon^2) \quad p_{2\zeta} = 0. \quad (6)$$

Continuity

$$O(\epsilon) \quad f_{1\xi} + g_{1\eta} = 0, \quad (7)$$

$$O(\epsilon^2) \quad f_{2\xi} + g_{2\eta} - R \sin \zeta = 0. \quad (8)$$

No boundary conditions are available at the plate. The outer expansion must be matched to an inner (boundary-layer) expansion there. In accordance with the discussion of the previous section, the conditions far upstream are  $f_1, f_2, f_3, g_1 \rightarrow 0$ . 'Far upstream' means  $-\xi \gg 1$ ; we cannot really permit  $-\xi \rightarrow \infty$ , since the expansion form assumed is valid only in an interval  $\Delta\xi \ll \epsilon^{-2}$ .

### 5. Inner Expansion

An expanded boundary-layer variable  $\tilde{\eta} = \eta/\epsilon$  must be used to bring out the behaviour of the fluid near the plate. Then let  $\xi, \tilde{\eta}, \zeta$  remain fixed, and allow  $\epsilon$  to approach zero. The dependent variables are again expanded in powers of  $\epsilon$ :

$$u = F_0(\xi, \tilde{\eta}, \zeta) + \epsilon F_1(\xi, \tilde{\eta}, \zeta) + \epsilon^2 F_2(\xi, \tilde{\eta}, \zeta) + \dots,$$

$$v = \epsilon G_1(\xi, \tilde{\eta}, \zeta) + \epsilon^2 G_2(\xi, \tilde{\eta}, \zeta) + \dots,$$

$$w = \epsilon^2 H_2(\xi, \tilde{\eta}, \zeta) \dots,$$

$$p = p_0 + \epsilon P_1(\xi, \tilde{\eta}, \zeta) + \epsilon^2 P_2(\xi, \tilde{\eta}, \zeta) + \dots$$

The equations of motion split up into the following system:

$\xi$  momentum

$$O(1) \quad F_0 F_{0\xi} + G_1 F_{0\tilde{\eta}} = F_0 \tilde{\eta}\tilde{\eta}, \quad (9)$$

$$O(\epsilon) \quad F_1 F_{0\xi} + F_0 F_{1\xi} + G_2 F_{0\tilde{\eta}} + G_1 F_{1\tilde{\eta}} = -P_{1\xi} + F_{1\tilde{\eta}\tilde{\eta}}, \quad (10)$$

$$O(\epsilon^2) \quad F_0 F_{2\xi} + F_1 F_{1\xi} + F_2 F_{0\xi} + G_1 F_{2\tilde{\eta}} + G_2 F_{1\tilde{\eta}} + G_3 F_{0\tilde{\eta}} \\ + H_2 F_{0\zeta} = -P_{2\xi} + F_{0\xi\xi} + F_{2\tilde{\eta}\tilde{\eta}} + F_{0\zeta\zeta}. \quad (11)$$

$\eta$  momentum

$$O(1) \quad P_{1\tilde{\eta}} = 0, \quad (12)$$

$$O(\epsilon) \quad F_0 G_{1\xi} + G_1 G_{1\tilde{\eta}} = -P_{2\tilde{\eta}} + G_{1\tilde{\eta}\tilde{\eta}} \quad (13)$$

$\zeta$  momentum

$$O(\epsilon) \quad P_{1\zeta} = 0, \quad (14)$$

$$O(\epsilon^2) \quad F_0 H_{2\xi} + G_1 H_{2\tilde{\eta}} = -P_{2\zeta} + H_{2\tilde{\eta}\tilde{\eta}}. \quad (15)$$

Continuity

$$O(1) \quad F_{0\xi} + G_1 \tilde{\eta} = 0, \quad (16)$$

$$O(\epsilon) \quad F_{1\xi} + G_2 \tilde{\eta} = 0, \quad (17)$$

$$O(\epsilon^2) \quad F_{2\xi} + G_3 \tilde{\eta} + H_{2\zeta} = 0. \quad (18)$$

At the plate all terms in the expansions of  $u$ ,  $v$ ,  $w$  are zero. Further conditions are provided by matching the inner and outer solutions in an intermediate region where they are simultaneously valid.

## 6. Matching

The forms assumed for the inner and outer expansions are valid only if the solutions based on them can be matched. Since matching must be done step-by-step in the analysis which follows, general equations for the procedure are derived here.

Consider the inner and outer expansions of any dependent variable  $a$ :

$$(\text{inner}) \quad a = A_0(\xi, \tilde{\eta}, \zeta) + \epsilon A_1(\xi, \tilde{\eta}, \zeta) + \epsilon^2 A_2(\xi, \tilde{\eta}, \zeta) + \dots,$$

$$(\text{outer}) \quad a = a_0(\xi, \eta, \zeta) + \epsilon a_1(\xi, \eta, \zeta) + \epsilon^2 a_2(\xi, \eta, \zeta) + \dots$$

The matching is done on an intermediate variable  $\eta^* = \eta/\lambda(\epsilon)$  such that, for  $\eta^*$  fixed and  $\epsilon \rightarrow 0$ ,

$$\eta = \lambda(\epsilon)\eta^* \rightarrow 0, \quad \tilde{\eta} = \frac{\lambda(\epsilon)}{\epsilon} \eta^* \rightarrow \infty.$$

The outer solution may be expanded around  $\eta = 0$  in the form

$$a = a_0 + \lambda \eta^* a_{0\eta} + \epsilon a_1 + \epsilon \lambda \eta^* a_{1\eta} + \frac{1}{2} (\lambda \eta^*)^2 a_{0\eta\eta} + \epsilon^2 a_2 + \dots,$$

where the arguments of each function on the right are  $(\xi, 0, \zeta)$ . The inner solution has the form

$$a = A_0 \left( \xi, \frac{\lambda}{\epsilon} \eta^*, \zeta \right) + \epsilon A_1 \left( \xi, \frac{\lambda}{\epsilon} \eta^*, \zeta \right) + \epsilon^2 A_2 \left( \xi, \frac{\lambda}{\epsilon} \eta^*, \zeta \right) + \dots$$

In order for the two expansions to match for  $\eta^*$  fixed and  $\epsilon \rightarrow 0$ , the following conditions must hold:

$$A_0(\xi, \infty, \zeta) = a_0(\xi, 0, \zeta),$$

$$\lim_{\tilde{\eta} \rightarrow \infty} A_1(\xi, \tilde{\eta}, \zeta) = \tilde{\eta} a_{0\eta}(\xi, 0, \zeta) + a_1(\xi, 0, \zeta),$$

$$\lim_{\tilde{\eta} \rightarrow \infty} A_2(\xi, \tilde{\eta}, \zeta) = \frac{1}{2} \tilde{\eta}^2 a_{0\eta\eta}(\xi, 0, \zeta) + \tilde{\eta} a_{1\eta}(\xi, 0, \zeta) + a_2(\xi, 0, \zeta).$$

## 7. Initial Steps in Solving the Problem

The solution must be carried to second order in  $\epsilon$  to show the most interesting effects produced by the transverse field of the incident flow. The program can be carried out by finding solutions to a sequence of groups of the equations (1)-(18). The functions  $F_0, F_1, G_1, G_2, H_2, f_1, f_2, g_1, g_2$  are found that way in the five steps of this section. That is preliminary. The effect of the transverse field on the chordwise flow is uncovered only when  $F_2$  is found, and that is deferred to §8.

At the beginning of each of the steps below the ingredients needed are listed—the equations from the system (1)-(18), the boundary conditions, and the matching conditions.

First step—determining  $F_0$  and  $G_1$

equations: (9), (16)

boundary conditions:  $F_0(\xi, 0, \zeta) = 0$ , (a)

$G_1(\xi, 0, \zeta) = 0$ , (b)

matching condition:  $F_0(\xi, \infty, \zeta) = 1$ . (c)

Let  $F_0 = \Psi_{\tilde{\eta}}$ . Then equation (16) becomes

$$\Psi_{\tilde{\eta}\xi} + G_{1\tilde{\eta}} = 0.$$

Hence  $G_1 = -\Psi_{\xi} + f_n(\xi, \zeta)$ ,

where  $f_n(\xi, \zeta)$  is zero if (b) is satisfied by putting  $\Psi_{\xi}(\xi, 0, \zeta) = 0$ .

Equation (9) becomes

$$\Psi_{\tilde{\eta}} \Psi_{\tilde{\eta}\xi} - \Psi_{\xi} \Psi_{\tilde{\eta}\tilde{\eta}} = \Psi_{\tilde{\eta}\tilde{\eta}\tilde{\eta}}.$$

Set  $\Psi = \sqrt{(2\xi)} \mathcal{F}(s)$ ,  $s = \tilde{\eta}/\sqrt{(2\xi)}$ .

Then  $\mathcal{F}(s)$  satisfies

$$\mathcal{F}''' + \mathcal{F}\mathcal{F}'' = 0.$$

$F_0$  and  $G_1$  become

$$F_0 = \mathcal{F}'(s),$$

$$G_1 = (1/\sqrt{(2\xi)}) [s\mathcal{F}'(s) - \mathcal{F}(s)],$$

so conditions (a), (b), (c) are

$$\mathcal{F}'(0) = \mathcal{F}(0) = 0, \quad \mathcal{F}'(\infty) = 1.$$

$\mathcal{F}(s)$  is thus the Blasius function. Suppose  $\beta$  is defined as follows:

$$\lim_{s \rightarrow \infty} \mathcal{F}(s) = s - \beta .$$

Then

$$\lim_{\tilde{\eta} \rightarrow \infty} G_1(\xi, \tilde{\eta}) = (1/\sqrt{2\xi}) \lim_{s \rightarrow \infty} (s\mathcal{F}' - \mathcal{F}) = \beta/\sqrt{2\xi} .$$

Notice  $F_0$  and  $G_1$  do not depend on  $\zeta$ .

Second step—determining  $H_2$

$$\text{equations:} \quad (5), (6), (13), (15)$$

$$\text{boundary condition:} \quad H_2(\xi, 0, \zeta) = 0, \quad (a)$$

$$\text{matching conditions:} \quad H_2(\xi, \infty, \zeta) = R \cos \zeta, \quad (b)$$

$$\lim_{\tilde{\eta} \rightarrow \infty} P_2(\xi, \tilde{\eta}, \zeta) = \tilde{\eta} p_{1\tilde{\eta}}(\xi, 0, \zeta) + p_2(\xi, 0, \zeta). \quad (c)$$

The matching conditions here, as elsewhere, are applications of the general matching equations derived earlier. (c), for example, is the second-order matching condition for  $p$  with  $p_{0\tilde{\eta}\tilde{\eta}} = 0$ . Equation (13) may be written

$$P_{2\tilde{\eta}} = G_{1\tilde{\eta}\tilde{\eta}} - F_0 G_{1\xi} - G_1 G_{1\tilde{\eta}} .$$

Since  $F_0$  and  $G_1$  do not depend on  $\zeta$ ,  $P_{2\tilde{\eta}\zeta} = 0$ , so  $P_{2\zeta} = \text{fn}(\xi, \zeta)$ . Differentiating (c) on  $\zeta$  and using equations (5) and (6) yield  $\lim_{\tilde{\eta} \rightarrow \infty} P_{2\zeta} = 0$ .

Thus

$$P_{2\zeta} = 0$$

everywhere. Equation (15) then becomes

$$F_0 H_{2\xi} + G_1 H_{2\tilde{\eta}} = H_{2\tilde{\eta}\tilde{\eta}} ,$$

which is the same as equation (9) if  $H_2 = \text{fn}(\zeta)F_0(\xi, \tilde{\eta})$ . The solution

satisfying conditions (a) and (b) is

$$H_2 = RF_0 \cos \zeta = R\mathcal{F}'(s) \cos \zeta .$$

Thus the spanwise flow follows the Blasius profile to the order considered.

Third step—determining  $f_1$ ,  $g_1$  and  $p_1$

equations: (1), (3), (5), (7)

boundary conditions:  $f_1, g_1 \rightarrow 0$  far upstream, (a)

matching condition:  $G_1(\xi, \infty) = g_1(\xi, 0, \zeta)$ . (b)

Equations (1) and (3),  $f_{1\xi} = -p_{1\xi}$  and  $g_{1\xi} = -p_{1\eta}$ , combine to give the equation for conservation of spanwise vorticity,

$$(g_{1\xi} - f_{1\eta})_{\xi} = 0.$$

By the upstream conditions (a),

$$g_{1\xi} - f_{1\eta} = 0.$$

Equations (1), (3) and (5) then imply

$$p_1 = -f_1 .$$

Since the spanwise vorticity is zero, there is a potential function  $\phi$  such that

$$f_1 = \phi_{\xi}, \quad g_1 = \phi_{\eta},$$

and equation (7) becomes

$$\phi_{\xi\xi} + \phi_{\eta\eta} = 0.$$

Condition (b) and the expression for  $G_1(\xi, \infty)$  found in the first step give

$$\phi_\eta(\xi, 0) = \beta/\sqrt{2\xi}$$

over the plate.  $\phi$  is thus the linearized potential for flow around a thin parabolic cylinder (van Dyke [3]). The solution satisfies

$$f_1(\xi, 0) = -p_1(\xi, 0) = 0$$

next to the plate, and  $f_1$  and  $g_1$  do not depend on  $\zeta$ .

Fourth step—determining  $F_1$  and  $G_2$

equations:	(10), (12), (14), (17)	
boundary conditions:	$F_1(\xi, 0, \zeta) = 0,$	(a)
	$G_2(\xi, 0, \zeta) = 0,$	(b)
matching conditions:	$F_1(\xi, \infty, \zeta) = f_1(\xi, 0) = 0,$	(c)
	$P_1(\xi, \infty, \zeta) = p_1(\xi, 0) = 0.$	(d)

Since equations (12) and (14) imply  $P_1 = P_1(\xi)$ , condition (d) requires  $P_1 = 0$ . Equations (10) and (17) are thus homogeneous and linear in  $F_1$  and  $G_2$ , and the only solution compatible with conditions (a), (b) and (c) is

$$F_1 = G_2 = 0.$$

Fifth step—determining  $f_2$ ,  $g_2$  and  $p_2$

equations:	(2), (4), (6), (7), (8)	
boundary condition:	$f_2 \rightarrow 0$ far upstream,	(a)
matching condition:	$\tilde{\eta}g_{1\eta}(\xi, 0) + g_2(\xi, 0, \zeta) = \lim_{\tilde{\eta} \rightarrow \infty} G_2 = 0.$	(b)

By equation (7)  $g_{1\eta} = -f_{1\xi}$ , and from the third step  $f_1(\xi, 0) = 0$ .

Hence

$$g_{1\eta}(\xi, 0) = 0,$$

and (b) becomes

$$g_2(\xi, 0, \zeta) = 0.$$

In the third step it was shown that  $f_{1\eta} = g_{1\xi}$ , so equations (2), (4), (6) and (8) can be written

$$f_{2\xi} = -\left\{\frac{1}{2}(f_1^2 + g_1^2) + p_2\right\}_{\xi},$$

$$g_{2\xi} = -\left\{\frac{1}{2}(f_1^2 + g_1^2) + p_2\right\}_{\eta},$$

$$p_{2\xi} = 0,$$

$$f_{2\xi} + g_{2\eta} = R \sin \zeta,$$

and the solution satisfying conditions (a) and (b) is

$$f_2 = 0,$$

$$g_2 = R_{\eta} \sin \zeta,$$

$$p_2 = -\frac{1}{2}(f_1^2 + g_1^2).$$

## 8. Final Steps to Determine $F_2$

In the last section it was shown that the first-order correction to the chordwise boundary-layer profile is zero. If the theory is going to account for the large boundary-layer thickness and shear variations observed by Klebanoff and Bradshaw, those effects will have to show up in the function  $F_2$  yet to be calculated. The trouble is that even in

the strictly two-dimensional case there is a second-order correction to the Blasius profile. Since the perturbation equations are linear in the functions still uncomputed, solutions can be superposed, and the contribution of the transverse field can be separated from the two-dimensional part of the solution. The two-dimensional part decreases toward zero downstream, but the part driven by the transverse field increases rapidly.

{The pressure function  $P_2$ }

By means of the expressions for  $F_0$  and  $G_1$  derived in the last section, equation (13) can be written

$$P_{2\tilde{\eta}} = \frac{1}{2\sqrt{(2)}\xi^{\frac{3}{2}}} [\mathcal{F}'' + s\mathcal{F}'^2 - \mathcal{F}\mathcal{F}'] .$$

$P_{2\xi}$  was found to be zero. If  $P_2$  takes the form

$$P_2 = R(s)/\xi,$$

then  $R$  must satisfy

$$R' = \frac{1}{2}[\mathcal{F}'' + s\mathcal{F}'^2 - \mathcal{F}\mathcal{F}'] .$$

As  $s \rightarrow \infty$ ,  $R' \rightarrow \frac{1}{2}\beta$ , and the form assumed for  $P_2$  is valid only if that limit is compatible with the matching condition

$$\lim_{\tilde{\eta} \rightarrow \infty} P_2 = \tilde{\eta} p_{1\eta}(\xi, 0) + p_2(\xi, 0).$$

But from equation (3) and the work of §7

$$\begin{aligned} p_{1\eta}(\xi, 0) &= -g_{1\xi}(\xi, 0) = -G_{1\xi}(\xi, \infty) = \beta/2\xi\sqrt{(2\xi)}, \\ p_2(\xi, 0) &= -\frac{1}{2}g_1^2(\xi, 0) = -\beta^2/4\xi. \end{aligned}$$

Hence

$$\lim_{\tilde{\eta} \rightarrow \infty} P_2 = \beta s / 2\xi - \beta^2 / 4\xi,$$

which is compatible with the form assumed earlier if the constant of integration for  $R$  is chosen such that

$$R(s) \rightarrow \frac{1}{2}\beta s - \frac{1}{4}\beta^2 \text{ as } s \rightarrow \infty.$$

{ Transformation of the equation for  $F_2$  }

Since  $F_1 = G_2 = F_{0\zeta} = 0$  and  $H_2 = RF_0 \cos \zeta$ , equations (11) and (18) are

$$F_0 F_{2\xi} + F_2 F_{0\xi} + G_1 F_{2\tilde{\eta}} + G_3 F_{0\tilde{\eta}} = -P_{2\xi} + F_{0\xi\xi} + F_{2\tilde{\eta}\tilde{\eta}},$$

$$F_{2\xi} + G_{3\tilde{\eta}} = R \sin \zeta F_0.$$

Let  $F_0 = \Psi_{\tilde{\eta}}$  as before, and let  $F_2 = \chi_{\tilde{\eta}}$ . Then the continuity equation becomes

$$\chi_{\xi\tilde{\eta}} + G_{3\tilde{\eta}} = R \sin \zeta \Psi_{\tilde{\eta}}.$$

Hence

$$G_3 = R \sin \zeta \Psi - \chi_{\xi} + \text{fn}(\xi, \zeta)$$

and  $\text{fn}(\xi, \zeta) = 0$  if the boundary condition  $G_3(\xi, 0, \zeta) = 0$  is satisfied by requiring  $\chi_{\xi}(\xi, 0, \zeta) = 0$ . Now transform

$$(\xi, \tilde{\eta}, \zeta) \Rightarrow (\xi, s, \zeta), \quad s = \tilde{\eta} / \sqrt{2\xi},$$

in the momentum equation. Thus

$$\chi(\xi, \tilde{\eta}, \zeta) = X(\xi, s, \zeta),$$

and  $F_0$ ,  $G_1$  and  $P_2$  are already known in terms of the new variables.

The equation becomes

$$\begin{aligned} X_{sss} + \mathcal{F}X_{ss} - 2\xi\mathcal{F}'X_{s\xi} + 2\xi\mathcal{F}''X_{\xi} + \mathcal{F}'X_s \\ = 2\sqrt{(2)\xi}^{\frac{3}{2}}R\sin\zeta\mathcal{F}\mathcal{F}'' - \frac{2\sqrt{2}}{\sqrt{\xi}}\left[\mathcal{R} + \frac{1}{2}s\mathcal{R}' + \frac{1}{4}(s^2\mathcal{F}'''' + 3s\mathcal{F}''')\right]. \end{aligned}$$

The boundary conditions at the plate are

$$X_s(\xi, 0, \zeta) = 0, \quad X_{\xi}(\xi, 0, \zeta) = 0,$$

and, say,

$$\chi(\xi, 0, \zeta) = 0.$$

The matching condition for  $F_2$  is

$$\lim_{\tilde{\eta} \rightarrow \infty} F_2 = \tilde{\eta}f_{1\eta}(\xi, 0) + f_2(\xi, 0).$$

From the last section  $f_2 = 0$  and  $f_{1\eta}(\xi, 0) = g_{1\xi}(\xi, 0) = -\beta/2\xi\sqrt{(2\xi)}$ .

Hence

$$\lim_{\tilde{\eta} \rightarrow \infty} F_2 = -\beta s/2\xi,$$

and

$$\lim_{s \rightarrow \infty} X_s(\xi, s, \zeta) = -\beta s/\sqrt{(2\xi)}.$$

It is easy to show by direct substitution that that limit is compatible with the transformed momentum equation.

{Separation of  $X$  into two- and three-dimensional parts}

In the transformed momentum equation there is one term which is

modulated by  $R \sin \zeta$ ; there are no such terms in the boundary conditions. That term reflects the  $R \sin \zeta \Psi$  part of  $G_3$  and is a forcing function imposed by the transverse field through the continuity condition.  $X$  can be written as a sum of two parts, one proportional to  $R \sin \zeta$  and the other not involving  $\zeta$  at all. The first term responds to the forcing function proportional to  $R \sin \zeta$  and obeys zero boundary conditions all around. The second term responds to the two-dimensional forcing function and satisfies the  $X_s$  limit for  $s \rightarrow \infty$ . Thus write

$$X = \frac{1}{\sqrt{2\xi}} [R \xi^2 \sin \zeta N(s) + M(s)] .$$

$N(s)$  and  $M(s)$  are defined by separate differential equations and boundary conditions:

$$\left. \begin{aligned} N'''' + \mathcal{F}N'' - 2\mathcal{F}'N' + 3\mathcal{F}''N &= 4\mathcal{F}\mathcal{F}'' , \\ N(0) = N'(0) = 0, \quad N'(\infty) &= 0, \end{aligned} \right\}$$

$$\left. \begin{aligned} M'''' + \mathcal{F}M'' + 2\mathcal{F}'M' - \mathcal{F}''M &= -4R - 2sR' - s^2\mathcal{F}''' - 3s\mathcal{F}'' , \\ M(0) = M'(0) = 0, \quad \lim_{s \rightarrow \infty} M(s) &= -\beta s. \end{aligned} \right\}$$

If the spanwise vorticity is to decay exponentially far from the plate,  $N(s)$  must contain an  $O(\log \epsilon)$  term (Van Dyke [3]). There is no need to find out more about  $N(s)$ . The important point is that the two-dimensional contribution  $X$  approaches zero as  $\xi$  becomes large, and the three-dimensional term grows as  $\xi^{3/2}$ .

{ $F_2$  and the boundary-layer profile }

The  $N$  equation with its boundary conditions has a simple solution –

$$N = \mathcal{F} - s\mathcal{F}' .$$

That can be verified by direct substitution using the Blasius equation

$$\mathcal{F}''' + \mathcal{F}\mathcal{F}'' = 0$$

and its derivative. Then

$$F_2 = \chi_{\eta}^{\sim} = X_s / \sqrt{2\xi} = -\frac{1}{2}R\xi \sin \zeta_s \mathcal{F}'' + M' / 2\xi .$$

The boundary-layer profile is

$$u = \mathcal{F}'(s) - \frac{1}{2}R\epsilon^2 \xi \sin \zeta_s \mathcal{F}''(s) + \epsilon^2 (M'(s) / 2\xi) + O(\epsilon^3) .$$

Notice the expansion is not uniformly convergent. The second term is much smaller than the first only if  $\xi \ll 1/\epsilon^2$ , but that is assured by the restriction  $\Delta\xi \ll 1/\epsilon^2$  already imposed to make the outer flow tractable. The third term is small if  $\xi \gg \epsilon^2$ , the usual requirement for convergence of the boundary-layer expansion.

The first two terms of the profile expansion can be combined into a single function

$$\mathcal{F}' \left( \frac{s}{1 + \frac{1}{2}R\epsilon^2 \xi \sin \zeta} \right)$$

with third-order accuracy. Then

$$u = \mathcal{F}'(s^*) + (\epsilon^2 / 2\xi) M'(s^*) + O(\epsilon^2)$$

where

$$s^* = s / (1 + \frac{1}{2} \gamma \xi \sin \zeta),$$

and  $\gamma = R \epsilon^2$ . Thus the shape of the profile is unaffected by the transverse field. Even in the second-order approximation, the only three-dimensional effect is a spanwise variation in boundary-layer thickness.

### 9. Conclusion

For the profile expansion to be valid,  $\xi$  must satisfy  $\epsilon^2 \ll \xi \ll 1/\epsilon^2$ . In physical variables the inequality can be written

$$\nu k / U_0 \ll kx \ll R / \gamma,$$

and in that interval, expressions good to  $O(\gamma)$  for  $U$  and  $W$  are

$$U = U_0 [\mathcal{F}'(y/\delta) + \nu / U_0 x \mathcal{M}'(y/\delta)],$$

$$W = \gamma U_0 \cos kz \mathcal{F}'(y/\delta),$$

where

$$\delta = \sqrt{\frac{2\nu x}{U_0}} (1 + \frac{1}{2} \gamma kx \sin kz).$$

Thus the boundary layer takes on the wavy character illustrated in figure 1. The practical significance of these results is discussed by Bradshaw [2].

REFERENCES

1. Klebanoff, P. S. and Tidstrom, K. D., "Evolution of Amplified Waves Leading to Transition in a Boundary Layer with Zero Pressure Gradient," NASA TN D 195 (1959).
2. Bradshaw, P., "The Effect of Wind Tunnel Screens on Nominally Two-Dimensional Boundary Layers," Journal of Fluid Mechanics, Vol. 22 (1965), pp. 679-688.
3. Van Dyke, M., Perturbation Methods in Fluid Mechanics, New York, Academic Press (1964), pp. 121-147.

## II. THE TURBULENT RAYLEIGH PROBLEM

### 1. Introduction

The essential physical problem of turbulent shear flow – to find the relationship between mean flow distribution and turbulent structure – is still unsolved. For the time being, ad hoc physical hypotheses must be injected into any theory of turbulent shear flow, and the best a theoretician can do is inject at the least sensitive point in the structure of a problem. For example, suppose we describe properties of a boundary layer above a wall in a coordinate system  $(x, y, z)$  where  $x$  points downstream and  $y$  is perpendicular to the wall. Let  $(U, V, 0)$  be the corresponding mean velocity components and  $(u, v, w)$  be turbulent fluctuations from the mean. The boundary-layer momentum equation is

$$U \frac{\partial U}{\partial x} + V \frac{\partial U}{\partial y} = - \frac{1}{\rho} \frac{dP}{dx} + \frac{\partial \sigma}{\partial y}, \quad (1)$$

where  $dP/dx$  is the mean pressure gradient and  $\sigma$  is the kinematic shear stress (Townsend [1]). The full expression for the stress is

$$\sigma = -\overline{uv} + \nu \frac{\partial U}{\partial y},$$

but in the fully turbulent region the viscous term is negligible. In terms of  $\sigma$  and the mean velocity gradient

$$\Omega \equiv \frac{\partial U}{\partial y},$$

a quantity with the dimensions of viscosity can be defined as

$$\nu_e \equiv \frac{\sigma}{\Omega}. \quad (2)$$

Then the calculated mean velocity profile  $U(y)$  is fairly insensitive to assumptions made about the "eddy viscosity."

The Prandtl mixing length theory, which gave

$$v_e = \kappa^2 y^2 |\Omega|$$

in the region of a boundary layer near the wall, amounted to little more than a plausible assumption on the eddy viscosity. But the relation above can be derived without the mixing length hypothesis by making certain assumptions about the turbulent energy equation. At the same time it becomes evident where the original Prandtl relation will break down. By balancing turbulent energy generation, turbulent diffusion and dissipation, and by making certain similarity assumptions for the wall layer, Townsend [2] shows that

$$\Omega = \frac{\sqrt{\sigma}}{\kappa y} \left( 1 - B \frac{y}{\sigma} \left| \frac{\partial \sigma}{\partial y} \right| \right), \quad (3)$$

where the term with the coefficient B represents the effect of turbulent diffusion. The derivation of that equation and the assumptions involved will be discussed later in connection with the turbulent Rayleigh problem. The important thing for now is the form of the relation:  $\Omega$  is a functional of the stress distribution. That will be true of any velocity gradient-stress relation derived from energy considerations. If equation 3 is combined as it stands with the equation of motion, an integro-differential equation is the result. Equation 3 may be regarded as an ordinary first-order differential equation for  $\sqrt{\sigma}$  and solved:

$$\sqrt{\sigma} = f(x) + y \pm \frac{1}{2B} \left[ \int y \mp \frac{1}{2B} \Omega(y) dy + g(x) \right]$$

When that is inserted in equation 1, an integral term remains. Alternately the momentum equation can be differentiated with respect to  $y$ , and with the aid of the continuity relation

$$\frac{\partial U}{\partial x} + \frac{\partial V}{\partial y} = 0,$$

it may be rewritten in terms of  $\Omega$  and  $\sigma$ :

$$U \frac{\partial \Omega}{\partial x} + V \frac{\partial \Omega}{\partial y} = \frac{\partial^2 \sigma}{\partial y^2} . \quad (4)$$

But  $U$  and  $V$  must still be expressed as integrals of  $\Omega$ .

The Rayleigh problem of shear flow involves none of the purely kinematic difficulties of the boundary-layer problem, yet the same physical ideas apply. In this problem the non-steady flow above an infinite plate moving in the  $x$ -direction in the  $x$ - $z$  plane is examined; the independent variables are  $y$  and  $t$ . The situation is sketched in figure 1. The mean flow continuity equation is automatically satisfied, since  $V = 0$  and the problem is statistically homogeneous in  $x$ . The momentum equation is

$$\frac{\partial U}{\partial t} = \frac{\partial \sigma}{\partial y} \quad (5)$$

or

$$\frac{\partial \Omega}{\partial t} = \frac{\partial^2 \sigma}{\partial y^2} , \quad (6)$$

a form closely analogous to equation 4. The turbulent Rayleigh problem is discussed in detail in this chapter.

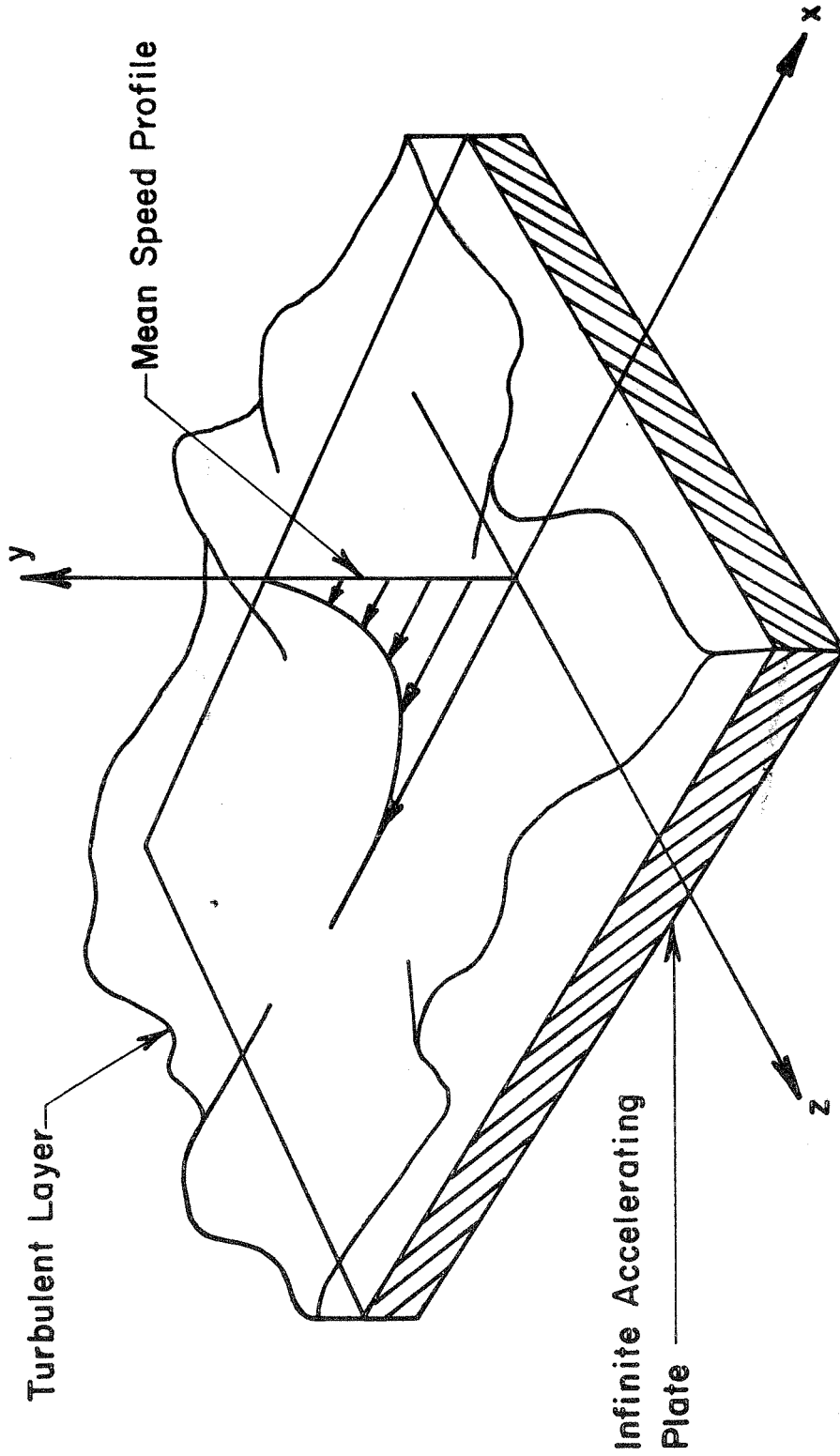


FIG. I TURBULENT RAYLEIGH FLOW

In 1956, Clauser [3] suggested that approximately similar solutions could be obtained for "equilibrium" turbulent boundary layers, those for which the parameter

$$\beta = \frac{\delta^*}{\rho \sigma_w} \frac{dP}{dx}$$

remains constant.  $\delta^*$  is a measure of the boundary-layer thickness,  $\sigma_w$  is the wall stress, so  $\beta$  is the ratio of pressure force across the boundary layer to shear force. But a skin friction parameter

$$\gamma = \frac{\sqrt{\sigma_w}}{U_\infty} = \sqrt{\frac{C_f}{2}}$$

also enters the boundary-layer momentum equation and prevents exact similarity (or "self-preservation," cf. Townsend [1,2]). Since  $\gamma$  has only a small effect on the results, useful quasi-similar solutions can be obtained, and that program was recently carried out by Mellor and Gibson [4A, B]. One of the simplifications of the Rayleigh problem is that exactly self-preserving solutions are possible. It is that family of exactly similar solutions which is treated here.

Rayleigh proposed his non-steady shear flow situation as an analog to the laminar boundary layer. The convective terms on the left hand side of equation 1 can be written

$$U_T \frac{\partial U_T}{\partial s}$$

where  $U_T$  is the mean flow speed and  $s$  is a streamline coordinate.

If this term is approximated by

$$U_{\infty} \frac{\partial U}{\partial x}$$

then  $t$  and  $x/U_{\infty}$  play analogous parts in the non-steady and steady problems. Since a turbulent boundary layer is much fuller than a laminar boundary layer, the velocities at corresponding points being more nearly equal to the free-stream velocity in the turbulent case, it might be conjectured that a Rayleigh type analogy would be more significant for the turbulent layers. In fact it is found that if the equation of motion for the equilibrium boundary layer is written in similarity form and expanded in powers of  $\gamma$ , the zeroth-order term is the similarity equation for the Rayleigh problem. Thus the Rayleigh problem contains all the essential features of the boundary-layer problem except for non-similarity.

The plan of this chapter is then as follows: in order to find the self-preserving solutions, the Rayleigh problem is put in similarity form, and some general consequences of that form are discussed; the physical ideas used by Clauser, Townsend and lately by Mellor and Gibson are cast into a form suitable for the Rayleigh problem; exact solutions for the constant wall stress and zero wall stress cases are derived under the physical assumptions, and properties of other solutions are discussed; the analogy between the turbulent boundary layer and the Rayleigh situation is developed. The  $\sigma$ - $\Omega$  forms of the equations of motion, equations 4 and 6, will be used so Townsend's velocity gradient-stress relation can be used when the time comes. That means that shear stress will be specified at the moving wall rather than the wall speed. Then the stress

distribution for the Rayleigh flow can be found without explicitly including any assumptions about the laminar sublayer – that is not strictly possible for the boundary layer.

## 2. Similarity Form of the Rayleigh Problem for Self-Preserving Solutions

The problem first will be restated. The equation of motion is

$$\frac{\partial \Omega}{\partial t} = \frac{\partial^2 \sigma}{\partial y^2}, \quad (6)$$

and in order to solve a practical problem a relation  $\Omega\{\sigma\}$  will have to be found. The boundary and initial conditions are

$$\begin{aligned} \sigma(y, 0) &= 0, \\ \sigma(0, t) &= \sigma_w(t), \\ \sigma(\infty, t) &= 0. \end{aligned} \quad (7)$$

If exactly similar solutions exist,  $\sigma$  and  $\Omega$  must have the forms

$$\left. \begin{aligned} \sigma &= \sigma_0 s(\eta), \\ \Omega &= \frac{\sqrt{\sigma_0}}{\ell_0} g(\eta), \\ \eta &= \frac{y}{\ell_0}, \end{aligned} \right\} \quad (8)$$

where

and  $\ell_0$  and  $\sigma_0$  are functions of time only. The boundary condition at the wall must be compatible with the similarity solutions,

$$\sigma_w(t) = \text{const. } \sigma_0(t)$$

and the equation of motion 6 becomes

$$-\left[ \frac{\sqrt{\sigma_0} \ell_0}{\ell_0^2} \right] \eta g' + \left[ \frac{\sigma_{0t}}{2\sqrt{\sigma_0} \ell_0} - \frac{\sqrt{\sigma_0} \ell_{0t}}{\ell_0^2} \right] g = \left[ \frac{\sigma_0}{\ell_0^2} \right] s'' . \quad (9)$$

Similarity is obtained when the coefficients in brackets are mutually proportional. For a Rayleigh type flow, where the fluid is stationary until  $t = 0$  and then is driven by the motion of a plate, it must be assumed that  $\ell_0(0) = 0$ . Then it is easy to show that similarity solutions are obtained only when

$$\begin{aligned} \sigma_0 &= \text{const. } t^c , \\ \ell_0 &= \text{const. } t^{1+c/2} , \end{aligned}$$

with  $c > -2$  for a growing turbulent layer. It has been found convenient to write  $\sigma_w$ ,  $\sigma_0$  and  $\ell_0$  as follows:

$$\begin{aligned} \sigma_w &= (1+c)Pt^c , \\ \sigma_0 &= Pt^c , \\ \ell_0 &= \sqrt{kP} t^{1+c/2} . \end{aligned} \quad (10)$$

$k$  is a dimensionless constant defined in section 4B. The reason for including it here will become clear later. The self-preserving solutions 8 take the form

$$\left. \begin{aligned} \sigma &= Pt^c s(\eta) , \\ \Omega &= \frac{1}{\sqrt{k} t} g(\eta) , \\ \eta &= \frac{y}{\sqrt{kP} t^{1+c/2}} . \end{aligned} \right\} \quad (11)$$

where

Equation 9 becomes

$$s'' + \sqrt{k} \left(1 + \frac{c}{2}\right) \eta g' + \sqrt{k} g = 0, \quad (12)$$

and conditions 7 reduce to

$$s(0) = 1 + c, \quad s(\infty) = 0. \quad (13)$$

The condition  $c > -2$  insures that the turbulent layer grows, as it must for Rayleigh flow. The condition is more restrictive than is necessary in the analogous boundary-layer case, since boundary layers may actually contract under highly favorable pressure gradients. The case  $c = -1$  corresponds to continuously separating flow with zero wall stress. The cases  $-1 > c > -2$  involve various degrees of separation and negative stresses, and they are not discussed further. It is assumed throughout that all stresses are positive to avoid cumbersome absolute value signs.

### 3. Some Properties of the Self-Preserving Solutions

#### A. Momentum Conservation

The equation for conservation of total momentum is

$$L \equiv \int_0^{\infty} U(y, t) dy = - \int_0^t \sigma_w(t') dt' = -Pt^{1+c}. \quad (14)$$

The last equality follows from equation 10 except in the case  $c = -1$ , for then  $\sigma_w = 0$ . But in that case we assume that an amount of momentum  $L = -P$  has been injected into the field prior to  $t = 0$ . The velocity at any point in the field can be found from the momentum equation. From equations 5 and 11,

$$\frac{\partial U}{\partial t} = \sqrt{\frac{P}{k}} \frac{s'}{t^{1-c/2}} ,$$

$$U(y, t) = \sqrt{\frac{P}{k}} \int_0^t \frac{s'[\eta(y, t')]}{t'^{1-c/2}} dt' ,$$

or

$$U(\eta, t) = \sqrt{\frac{Pt^c}{k}} \frac{\eta^{r-1}}{1+\frac{c}{2}} \int_{\eta}^{\infty} \frac{s'(\eta')}{\eta'^r} d\eta' , \quad (15)$$

where

$$r = \frac{1+c}{1+\frac{c}{2}} ,$$

and the last of equations 11 has been used to find  $t'(y, \eta')$ .

Since  $U$  has been expressed in terms of  $s$  through the equation of motion, it is obvious that  $\int_0^{\infty} U dy$  must equal  $-Pt^{1+c}$  automatically except perhaps in the case  $c = -1$ . It is interesting to demonstrate that explicitly though. By equations 11 and 15,

$$\begin{aligned} L &= \sqrt{kP} t^{1+c/2} \int_0^{\infty} U(\eta, t) d\eta \\ &= \frac{Pt^{1+c}}{1+\frac{c}{2}} \int_0^{\infty} \int_{\eta}^{\infty} \frac{s'(\eta')}{\eta'^r} \eta^{r-1} d\eta' d\eta . \end{aligned}$$

The order of integration can be reversed and the integral evaluated explicitly:

$$\begin{aligned} L &= \frac{Pt^{1+c}}{1+\frac{c}{2}} \int_0^{\infty} \int_0^{\eta'} \frac{s'(\eta')}{\eta'^r} \eta^{r-1} d\eta d\eta' \\ &= \frac{Pt^{1+c}}{(1+\frac{c}{2})r} \int_0^{\infty} \frac{s'(\eta')}{\eta'^r} \eta'^r d\eta' = -Pt^{1+c} . \end{aligned}$$

The first of equations 13 was used. The proof holds as  $c$  approaches

-1 but fails for  $c = -1$ . Going back to equation 15 for that case,

$$U = -\sqrt{\frac{P}{kt}} \frac{2s}{\eta}, \quad (16)$$

$$L = -2P \int_0^{\infty} \frac{s}{\eta} d\eta,$$

and in order that  $L = -P$ ,  $s$  must satisfy

$$\int_0^{\infty} \frac{s}{\eta} d\eta = \frac{1}{2}, \quad (c = -1). \quad (17)$$

It may seem strange that in this special case an extra condition like equation 17 is imposed on the stress distribution  $s$ . But equation 12 for the  $c = -1$  case with the boundary conditions  $s(0) = s(\infty) = 0$  gives a non-unique result, and equation 17 removes the non-uniqueness. The physical reason why an integral momentum condition is needed for the continuously separating case is clear: in every other case the momentum in the field is determined by the history of the stress at the wall, but in that case the wall stress is zero and the momentum is injected into the field by unspecified means.

### B. Laminar Sublayer

An important tacit assumption has been made up to this point which will now be justified. Immediately adjacent to the wall the flow must be laminar, and the self-preserving solutions cannot be expected to hold in the laminar sublayer. The sublayer will extend to some height  $\delta_v$  and the stress will undergo some change  $\Delta\sigma$  through it. Corresponding to  $\delta_v$ , there will be some non-dimensional thickness  $\eta_v$  on the similarity scale, and the similarity solutions of equation 12 will be valid only when

(i)  $\eta_\nu \ll 1$ ,

(ii)  $\frac{\Delta\sigma}{\sigma_w} \ll 1$ .

These two requirements are discussed below.

(i) The laminar sublayer becomes unstable at a critical Reynolds number given by

$$\frac{\delta_\nu \sqrt{\sigma_w}}{\nu} \approx 12,$$

(Clauser [3]). The corresponding similarity thickness  $\eta_\nu$  is

$$\eta_\nu = \frac{\delta_\nu}{\sqrt{kP} t^{1+c/2}} = \frac{12}{\sqrt{k(c+1)} R}, \quad (18)$$

where R is the Reynolds number based on momentum in the field,

$$R = \frac{|L|}{\nu}.$$

(ii) Suppose  $\sigma = \sigma_w + \alpha y$  to an adequate approximation in the laminar sublayer. Then

$$\frac{\partial\sigma}{\partial y} = \alpha = \frac{\partial U}{\partial t},$$

and since  $\alpha$  is constant and  $\partial U / \partial t = \dot{U}_w$  at the wall, where  $\dot{U}_w$  is the acceleration of the wall,

$$\frac{\Delta\sigma}{\sigma_w} = \frac{\delta_\nu \dot{U}_w}{\sigma_w}.$$

$U_w$  can be related to  $\sigma_w$  through a friction coefficient:

$$\sigma_w = \frac{1}{2} C_f U_w^2.$$

By using that expression to find  $\dot{U}_w$ , equations 10 for  $\sigma_w$ , and the

expression for  $L$ , it is easily shown that

$$\frac{\Delta\sigma}{\sigma_w} = \frac{12c}{\sqrt{2C_f} (c+1)R} . \quad (19)$$

Except in the separating flow case, where the laminar sub-layer does not have to transmit a mean stress boundary condition anyway and is generally supposed to be irrelevant, both  $\eta_\nu$  and  $\Delta\sigma/\sigma_w$  go to zero as  $R \rightarrow \infty$ . The constant  $k$ , discussed in the next section, is known to be about .015, and  $C_f$  could be about .003 for a smooth plate under a wide range of Reynolds numbers. Then conditions (i) and (ii) become

$$\eta_\nu \sim \frac{100}{\sqrt{c+1} R} \ll 1, \quad (20)$$

$$\frac{|\Delta\sigma|}{\sigma_w} \sim \frac{150|c|}{(c+1)R} \ll 1 .$$

#### 4. Assumptions for the $\Omega\{\sigma\}$ Relation

The reason for doing the Rayleigh problem is that it illuminates the ideas used in boundary-layer theory more clearly than the boundary-layer problem does. The purpose here is not to introduce new physical assumptions, but to adapt the ones ordinarily used to the Rayleigh problem. The two-layer model of Clauser and Townsend will be used, with a wall layer in energy equilibrium and an outer layer of constant eddy viscosity. The object is to find an expression for  $\Omega$  as a functional of  $\sigma$  reasonably well founded on physical arguments. It must be emphasized that the work up to now holds independently of any assumptions about the relation  $\Omega\{\sigma\}$  except that it be compatible with the similarity form of the equations of motion.

The wall layer and outer layer will be treated separately.

A. Wall Layer

Townsend's energy equilibrium argument [2] can be taken over with little alteration. The turbulent energy equation for the Rayleigh problem is

$$\frac{\partial}{\partial t} \left( \frac{1}{2} \overline{q^2} \right) + \overline{uv} \frac{\partial U}{\partial y} + \frac{\partial}{\partial y} \overline{v(p + \frac{1}{2} q^2)} + \mathcal{E} = 0,$$

where  $q^2 = u^2 + v^2 + w^2$  and  $p$  is the pressure fluctuation. The first term represents the rate of change of turbulent energy at a point, the second – the rate of generation of turbulent energy by interaction with the mean field, the third – the rate of lateral diffusion of energy, the fourth – the rate of energy dissipation. Energy equilibrium means that generation and dissipation are closely balanced, and the first term is small compared with the second or fourth. Townsend's arguments from dimensionality and structural similarity then imply the following relations:

$$\begin{aligned} |-\overline{uv}| &= a_1 \overline{q^2}, \\ \overline{v(p + \frac{1}{2} q^2)} &= -a_2 (\overline{q^2})^{3/2} \operatorname{sgn} \left( \frac{\partial \overline{q^2}}{\partial y} \right), \\ \mathcal{E} &= \frac{(\overline{q^2})^{3/2}}{L_\epsilon} \end{aligned}$$

and since deep in the turbulent layer near the wall the only possible length scale is  $y$ ,

$$L_\epsilon = a_3 y.$$

Now suppose the rate of change of turbulent energy in the wall layer

is indeed small compared with the rate of energy generation,

$$\left| \frac{\partial}{\partial t} \left( \frac{1}{2} \overline{q^2} \right) \right| \ll \left| \overline{uv} \frac{\partial U}{\partial y} \right| ,$$

or

$$\frac{1}{2a_1} \left| \frac{\partial \sigma}{\partial t} \right| \ll \sigma |\Omega| . \quad (21)$$

Then it follows from the energy balance equation that

$$\Omega = \frac{\sqrt{\sigma}}{\kappa y} \left( 1 - B \frac{y}{\sigma} \left| \frac{\partial \sigma}{\partial y} \right| \right) . \quad (3)$$

From equations 3 and 11,  $g(\eta)$  for the wall layer may be found:

$$g = \frac{\sqrt{s}}{\kappa \eta} b ,$$

where

(22)

$$b = 1 - B \frac{\eta}{s} |s'| .$$

It is known from experiments on boundary layers that  $\kappa \approx 0.41$  (the Kármán constant) and  $B \sim 0.2$  [1, 2], and there is no reason to doubt that the same values hold for the Rayleigh problem.  $B = 0$  gives the old Prandtl expression again.

The meaning of inequality 21 becomes clearer when it is put in similarity form. Suppose the lateral diffusion term in equation 3 is neglected for simplicity. Equations 3 and 6 are then

$$\Omega = \frac{\sqrt{\sigma}}{\kappa y} ,$$

$$\frac{\partial \sigma}{\partial t} = 2\kappa y \sqrt{\sigma} \frac{\partial^2 \sigma}{\partial y^2} .$$

Inequality 21 then becomes

$$\frac{k^2 y^2}{a_1} \left| \frac{\partial^2 \sigma}{\partial y^2} \right| \ll \sigma,$$

or

$$0.4 \eta^2 |s''| \ll s, \quad (23)$$

since  $a_1$  is known to be about 0.4 [Bradshaw, P., unpublished]. Inequality 23 is simply a condition that the stress distribution curve be roughly linear over most of the equilibrium region. It is very strongly satisfied for calculated shear stress profiles in the wall region, so it is surely the breakdown of the length scale hypothesis  $L_\epsilon = a_3 y$  which ends the validity of equation 3.

### B. Outer Layer

The argument for the outer layer is less involved and less convincing. Consider the boundary-layer problem first, and define a displacement thickness

$$\delta^*(x) \equiv \int_0^\infty \left[ 1 - \frac{U(x,y)}{U_\infty(x)} \right] dy,$$

where  $U_\infty(x) = U(x, \infty)$ . The eddy viscosity  $\nu_e \equiv \sigma/\Omega$  can be used to define a turbulent Reynolds number  $k^{-1}$ ,

$$k^{-1} \equiv \frac{U_\infty \delta^*}{\nu_e},$$

as a function of  $x$  and  $y$ . Clauser [3] found that the existing boundary-layer profile data were surprisingly compatible with a  $k^{-1}$  constant with respect to  $x$  and  $y$  some distance from the wall. In boundary-layer theory, the eddy viscosity in the outer layer is thus taken to be

$$\nu_e = k \int_0^{\infty} (U_{\infty} - U) dy$$

with  $k$  a universal constant about equal to 0.015 [3, 4A]. The eddy viscosity for the Rayleigh problem should thus be

$$\nu_e = k \left| \int_0^{\infty} U dy \right| = k |L| .$$

Thus

$$\Omega = \frac{\sigma}{k |L|} , \quad (24)$$

and by equations 11 and 14,

$$g = \frac{s}{\sqrt{k}} \quad (25)$$

in the outer layer.

The complete gradient function  $g(\eta)$  is now found simply by joining expressions 22 and 25 at their point of equality. For convenience, let us define the square root of the stress

$$r \equiv \sqrt{s} .$$

Then expressions 22 and 25 give equal results for  $g$  where

$$\eta_e r_e = \epsilon b_e , \quad (26)$$

with

$$\epsilon \equiv \frac{\sqrt{k}}{K} \approx 0.30 . \quad (27)$$

That defines the junction between wall and outer layers. In practice the wall layer spans about 20% of the total turbulent layer thickness.

5. Equations of Motion under the  $\Omega\{\sigma\}$  Assumptions – Some General Consequences

When equations 22 and 25 are combined with equation 12, the equation of motion assumes the following forms in the wall and outer layers:

$$\text{(Wall) } s'' = \frac{\epsilon}{2} \left[ \frac{c(br)}{\eta} - (2+c) (br)' \right] , \quad (28)$$

$$\text{(Outer) } s'' + \left(1 + \frac{c}{2}\right) \eta s' + s = 0 . \quad (29)$$

The equation of motion 12, involving the stress  $s$  and velocity gradient  $g$  with an unspecified relationship between them, has been supplemented by the physical assumptions of the last section and superseded by equations 26 to 29. None of these equations involves  $\kappa$  or  $k$  separately – only combined into  $\epsilon$ . Under the present  $\Omega\{\sigma\}$  assumptions, the stress distribution for any  $c$  is governed by the single empirical constant  $\epsilon$ . This is the reason  $k$  was introduced in equations 10;  $k$  fixes the relationship between turbulent layer momentum and length scale, but does not separately influence the non-dimensional shear stress distribution  $s(\eta)$ .

In practice equations 28 and 29 must be solved separately and the solutions matched at a point  $\eta_e$  determined by condition 26. The single boundary condition  $s(0) = 1 + c$  is applied to the wall solution, and  $s(\infty) = 0$  is required of the outer solution. Since both equations 28 and 29 are second order, two matching conditions are required. One of these is continuity of  $s$ ; it is easy to show the other is then continuity of slope  $s'$ . Equations 28 and 29, taken together, have

the form

$$s'' = \mathcal{F}(\eta, s, s'; \epsilon),$$

where  $\mathcal{F}$  changes its functional form at  $\eta_e$ . Since  $s$  is continuous, the most  $s'$  can do is jump. Consequently  $\mathcal{F}$  and hence  $s''$  can have at most a jump discontinuity at  $\eta_e$ . Hence  $s'$  is continuous.

The outer equation 29 is well known [1, 5] and can be written in the standard form

$$\left. \begin{aligned} & s''_{\tilde{\eta}\tilde{\eta}} + \tilde{\eta} s''_{\tilde{\eta}} - ns = 0, \\ \text{with} \quad & \tilde{\eta} = \sqrt{1 + \frac{c}{2}} \eta, \\ \text{and} \quad & n = - \left(1 + \frac{c}{2}\right)^{-1}. \end{aligned} \right\} \quad (30)$$

The general solution is written

$$s = A H h_n(\tilde{\eta}).$$

Some special  $H h_n$  functions [5] are

$$\left. \begin{aligned} H h_0 &= \int_{\tilde{\eta}}^{\infty} e^{-x^2/2} dx, \\ H h_{-1} &= e^{-\tilde{\eta}^2/2}, \\ H h_{-2} &= \tilde{\eta} e^{-\tilde{\eta}^2/2}. \end{aligned} \right\} \quad (31)$$

For very small  $\eta$ , equation 28 can be treated generally too.

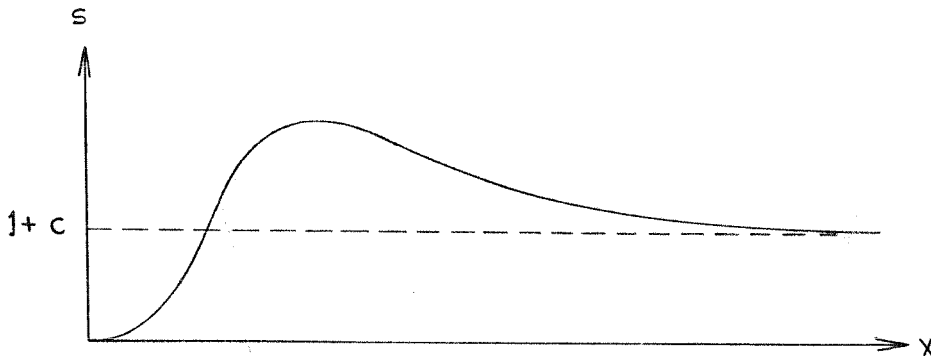
Substitute

$$x = \frac{1}{\eta}$$

The resulting equation for  $s(x)$  is

$$s_{xx} + \frac{2s}{x} = \frac{\epsilon}{2} \left[ \frac{c(br)}{x^3} + (2+c) \frac{(br)x}{x^2} \right] . \quad (32)$$

The function  $s(x)$  must have the general form shown below, and it will be found that  $b \rightarrow 1$  as  $x \rightarrow \infty$  except in the case  $c = -1$ :



For large  $x$  equation 32 thus approaches

$$s_{xx} + \frac{2s}{x} \Rightarrow \frac{\epsilon c \sqrt{1+c}}{2x^3} + O\left(\frac{\epsilon s}{x^2 \sqrt{1+c}}\right) ,$$

where the last term becomes negligible compared with the second term on the left. The asymptotically valid solution of equation 32 is then

$$s(x) = 1+c + \frac{a}{x} - \frac{\epsilon c \sqrt{1+c}}{2x} \log x ,$$

or

$$\lim_{\eta \rightarrow 0} s = 1 + c + a\eta + \frac{\epsilon c \sqrt{1+c}}{2} \eta \log \eta, \quad (33)$$

for some constant  $a$  which can be determined only by a complete solution of the problem.  $s'$  has a log singularity at  $\eta = 0$  unless  $c = 0$  or  $c = -1$ , but it is easy to see that  $b \rightarrow 1$  at the origin anyway from its definition in equation 22. Though the analysis leading to equation 33 breaks down in the case  $c = -1$ , the equation is in fact valid in that case too. The same singularity in the stress gradient was noted by Mellor [4B] for boundary layers, but it apparently was passed up in the computer solutions of [4A].

#### 6. Solution for the Constant Stress Case, $c = 0$

In the last section it was pointed out that the stress gradient is well behaved at the origin only in the special cases  $c = 0$  and  $c = -1$ . In those cases it is possible to find complete, exact solutions for arbitrary  $B$  — that is the real justification for posing the problem in stress form in the first place. For the case  $c = 0$  the first integration of equation 28 is trivial, and the outer solution is the second of equations 31. The integrated wall equation, the matching point location, and the outer stress distribution are written below:

$$\begin{aligned} \text{(i)} \quad s' + \epsilon br &= A, \\ \text{(ii)} \quad \eta_e r_e &= \epsilon b_e, \\ \text{(iii)} \quad s &= Ae^{-\eta^2/2}. \end{aligned} \quad (34)$$

$A$  can be found immediately by matching slopes at  $\eta_e$ :

$$\begin{aligned}
 s'_e &= -\eta_e s_e && \text{by (iii) ,} \\
 &= -\eta_e r_e^2 \\
 &= -\epsilon b_e r_e && \text{by (ii) ,} \\
 &= a - \epsilon b_e r_e && \text{by (i) .}
 \end{aligned}$$

Hence

$$A = 0 .$$

Equation 34(i) may now be written

$$2r' + \epsilon b = 0 ,$$

and from equation 22 (anticipating the fact that  $s'$  will be negative),

$$2r' + \epsilon + \epsilon B \eta \frac{2r'}{r} = 0 . \quad (35)$$

The equation may be inverted so  $\eta$  becomes the dependent variable:

$$\frac{d\eta}{dr} + \frac{2B}{r} \eta + \frac{2}{\epsilon} = 0 .$$

The solution satisfying the boundary condition  $\eta(1) = 0$  is

$$\eta = \frac{2}{\epsilon(2B+1)} (r^{-2B} - r) . \quad (36)$$

In the case  $B = 0$  equation 36 can be written

$$r = 1 - \frac{\epsilon}{2} \eta \quad (37)$$

The quantities  $A$  (the coefficient in the outer solution),  $\eta_e$ , and  $s_e$  can now be computed by solving equations 34(ii), (iii) and 36 at the matching point. The results for two values of  $B$  are as follows:

B	A	$\eta_e$	$s_e$
0	.954	.315	.908
.2	.954	.309	.908

In this case then, Townsend's B correction makes essentially no difference. The stress distribution curve good for either  $B = 0$  or  $B = 0.2$  is shown in figure 2.

7. Solution for the Continuously Separating Case -  $c = -1$

Again the outer solution is known - the second of equations 31 - and the equation of motion for the wall layer can be integrated once as follows. Equation 28 for  $c = -1$  can be written

$$\eta s'' = -\frac{\epsilon}{2} [(br) + \eta(br)'] ,$$

or

$$(\eta s' - s)' = -\frac{\epsilon}{2} (\eta br)' .$$

Integrating and using the boundary condition  $s(0) = 0$ ,

$$\eta s' - s + \frac{\epsilon}{2} \eta br = 0 .$$

The integrated wall layer equation, the matching point location, and the outer solution are then

$$\left. \begin{aligned} \text{(i)} \quad 2\eta r' - r + \frac{\epsilon}{2} b\eta &= 0 , \\ \text{(ii)} \quad \eta_e r_e &= \epsilon b_e , \\ \text{(iii)} \quad r &= \sqrt{A\eta} e^{-\eta^{2/8}} . \end{aligned} \right\} \quad (38)$$

But now the matching on slopes is identically satisfied. That can be seen as follows:

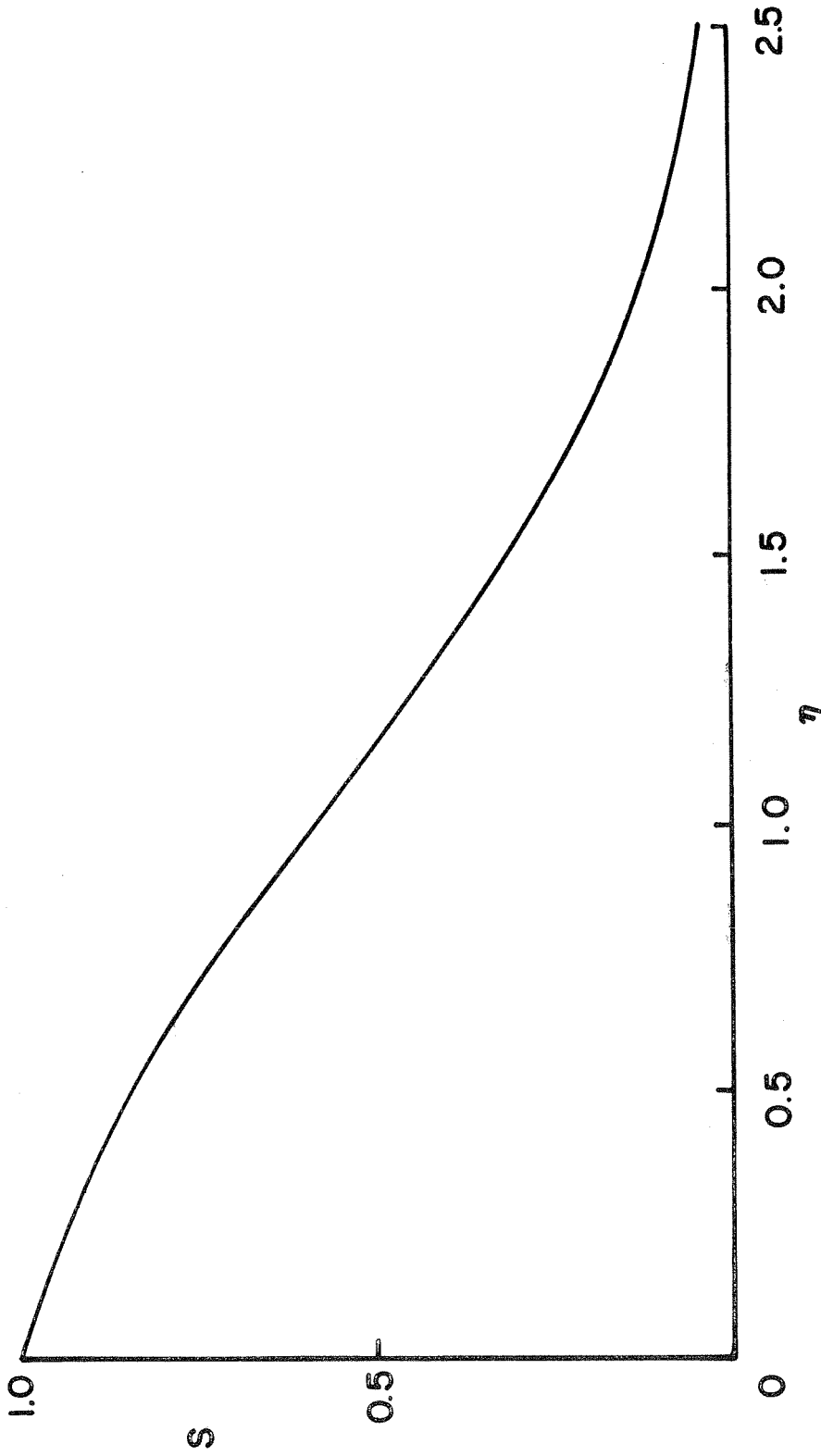


FIG. 2 STRESS PROFILE C = 0

$$\begin{aligned} r'_e &= \frac{r_e}{2\eta_e} - \frac{\eta_e r_e}{4} \quad \text{by (iii),} \\ &= \frac{r_e}{2\eta_e} - \frac{\epsilon b_e}{4} \quad \text{by (ii),} \end{aligned}$$

and the last equality holds identically for any  $r$  satisfying 38(i) in the wall layer. Thus one of the matching conditions is superfluous, and the apparent non-uniqueness mentioned earlier arises. The non-uniqueness is removed by the momentum condition 17:

$$\int_0^{\infty} \frac{s}{\eta} d\eta = \frac{1}{2}. \quad (17)$$

Equation 38(i) written out in full (under the correct assumption  $s' > 0$ ) is

$$2\eta r' - r + \frac{\epsilon\eta}{2} - \epsilon B \eta^2 \frac{r'}{r} = 0.$$

With the substitutions

$$X = \sqrt{\eta}, \quad Y = \frac{r}{\sqrt{\eta}},$$

the equation becomes

$$\frac{dY}{dX} \left(1 - \frac{\epsilon BX}{2Y}\right) + \frac{\epsilon}{2} (1-B) = 0,$$

or

$$\frac{dX}{dY} - \frac{B}{(1-B)Y} X + \frac{2}{\epsilon(1-B)} = 0.$$

The solution satisfying  $Y(0) = a$  or  $X(a) = 0$  is

$$X = \frac{2a}{\epsilon(1-2B)} \left[ \left( \frac{Y}{a} \right)^{B/1-B} - \left( \frac{Y}{a} \right) \right]. \quad (39)$$

If  $B = 0$  this becomes

$$r = a\sqrt{\eta} - \frac{\epsilon\eta}{2}. \quad (40)$$

Equations 17, 38(ii), (iii) and 39 determine  $a$ ,  $A$ ,  $\eta_e$  and  $s_e$  -

for non-zero B a good deal of numerical work is required. The steps of a strongly convergent iteration procedure are described in the Appendix. The stress curve is nearly linear in the wall layer, that is

$$s \sim a^2 \eta .$$

If the stress curve were exactly linear, then b would be 1-B. In the actual case that must be nearly correct. The group  $\epsilon b$  appearing in equations 38 must be nearly constant and equal to  $\epsilon(1-B)$ , and an equation analogous to 40,

$$r \approx a\sqrt{\eta} - \frac{\epsilon(1-B)\eta}{2} \quad (41)$$

must be very accurate for all reasonable B. For B = 0.2, the value proposed by Townsend [2], the difference between 39 and 41 is entirely inconsequential. Values for a, A,  $\eta_e$ ,  $s_e$  for the three cases B = 0, b = 0.8 (the approximation to B = 0.2), and B = 0.2 are given below:

	a	A	$\eta_e$	$s_e$
B = 0	.618	.273	.721	.173
b = 0.8	.596	.276	.611	----
B = 0.2	.5981	.2766	.6331	.1585

The shear stress distributions for B = 0 and B = 0.2 are shown in figure 3.

The speed distribution for  $c = -1$  has already been given in equation 16. The only function of the wall in the zero stress case is to sustain fluctuating pressure forces. There is no mean flow in the laminar sublayer, and its thickness is of order  $\sqrt{\nu\tau}$  where  $\tau$  is the time scale of the turbulence. Thus the mean speed equation

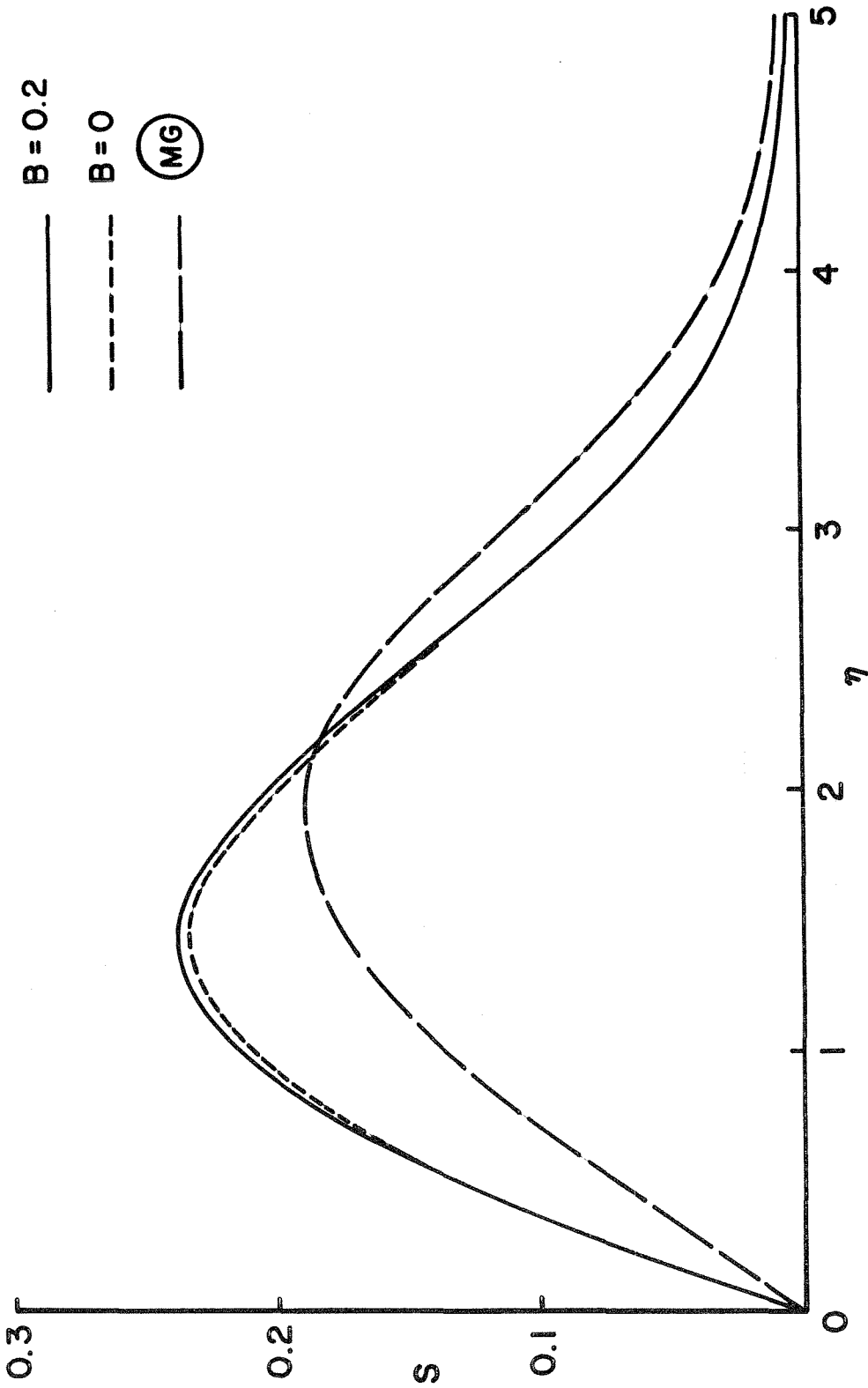


FIG. 3 STRESS PROFILE  $C = -1$

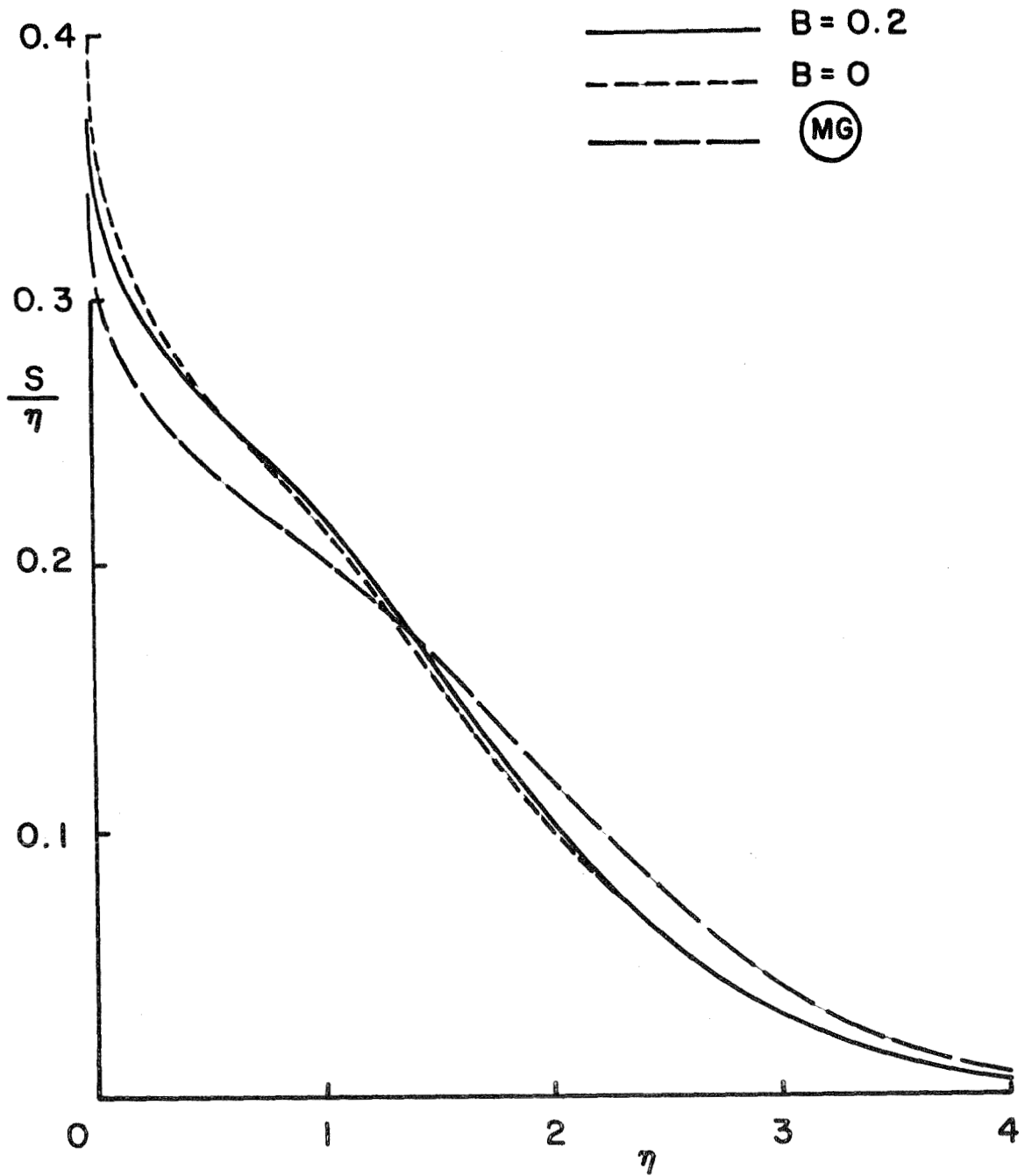


FIG. 4 SPEED PROFILE  $C = -1$

$$U = -2 \sqrt{\frac{P}{kt}} \frac{s}{\eta} \quad (16)$$

should hold right up to the wall, where

$$U_w = -2a^2 \sqrt{\frac{P}{kt}} \quad (42)$$

The function  $s/\eta$  is graphed in figure 4.

### 8. Analogy with the Equilibrium Boundary Layer

The ideas and notation of Mellor and Gibson [4A, B] will be followed as closely as possible here. The main differences are that equation 4, instead of equation 1, will be used as the equation of motion from the outset, and the eddy viscosity notation, cumbersome and deceptive in this context, will not be used at all. The boundary-layer momentum and continuity equations are

$$U \frac{\partial \Omega}{\partial x} + V \frac{\partial \Omega}{\partial y} = \frac{\partial^2 \sigma}{\partial y^2} \quad (4)$$

$$\frac{\partial U}{\partial x} + \frac{\partial V}{\partial y} = 0 \quad (43)$$

Define a "skin friction velocity"  $u_\tau$  and length scale  $\Delta$  as follows:

$$u_\tau^2(x) = \sigma_w(x), \quad (44)$$

$$\int_0^\infty \frac{U_\infty(x) - U(x, y)}{u_\tau(x)} dy = \Delta(x),$$

where  $\sigma_w(x)$  is the wall stress, and  $U_\infty(x) = U(x, \infty)$ . Mellor and Gibson use the following boundary conditions:

- (i)  $\sigma(\mathbf{x}, 0) = u_{\tau}^2(\mathbf{x})$
- (ii)  $\Delta(\mathbf{x})$  exists (45)
- (iii)  $V(\mathbf{x}, 0) = 0$

Condition (i) seems true by definition of  $u_{\tau}$ . But the full expression for the shear stress  $\sigma$ ,

$$\sigma = -\overline{uv} + \nu \Omega ,$$

is truncated to  $\sigma = -\overline{uv}$  in the turbulent region. The laminar sublayer intervening between the turbulence and the wall, where the viscous contribution to  $\sigma$  becomes important, is patched on later. Condition (i) thus asserts that the wall stress is transmitted intact through the laminar sublayer (cf. section 3B for the equivalent situation in the Rayleigh problem). Condition (ii) guarantees that  $U(\mathbf{x}, y) \rightarrow U_{\infty}(\mathbf{x})$  as  $y \rightarrow \infty$  and that the difference between  $U$  and  $U_{\infty}$  is integrable. Condition (iii) sets the mean velocity normal to the wall equal zero at the wall.

Clauser found that approximately similar solutions for  $U$  could be obtained in the "velocity defect" form

$$\frac{U_{\infty}(\mathbf{x}) - U(\mathbf{x}, y)}{u_{\tau}(\mathbf{x})} = f(H) ,$$

where

$$H = \frac{y}{\Delta} .$$

Thus let us write  $\sigma$  and  $\Omega$  in the forms

$$\begin{aligned} \sigma &= u_{\tau}^2 S(H) \\ \Omega &= u_{\tau}/\Delta G(H) \end{aligned}$$

(46)

so that

$$f'' = - \mathcal{G} . \quad (47)$$

$f(0)$  can be set equal to zero. Then boundary conditions 45(i) and (ii) become

$$\begin{aligned} S(0) &= 1 \\ f(\infty) &= \int_0^{\infty} f'(H) dH = \int_0^{\infty} \int_H^{\infty} \mathcal{G}(H') dH' dH = 1 \end{aligned} \quad (48)$$

and condition 45(iii) is used in the integration of the continuity equation 43 to get  $V$  in terms of  $U$ .

When forms 46 and the expression for  $V$  are used in the equation of motion 4,  $u_{\tau}$  and  $U_{\infty}$  must appear together in the ratio

$$\gamma(x) = \frac{u_{\tau}(x)}{U_{\infty}(x)} .$$

Now there is no reason why  $u_{\tau}$  and  $U_{\infty}$  should be proportional.  $u_{\tau}$  is governed by the stress-bearing capacity of turbulent flow, but  $U_{\infty}(x)$  is measured with respect to the wall, and the laminar sublayer intervenes. Thus we cannot expect to reduce the boundary layer momentum equation to a fully similar form. The equation of motion for the Rayleigh problem, on the other hand, does not contain the convective terms which make non-similarity inevitable. If similarity solutions to the Rayleigh problem are sought with velocities non-dimensionalized on  $u_{\tau}$ , they can be found. The reader should recall that at no point in the discussion of the Rayleigh problem was the

actual wall speed  $U_w(t)$  required to generate the similarity solutions discussed – except in the continuously separating case  $c = -1$  where the laminar sublayer is irrelevant to the mean dynamics. In order to specify the wall speed programs  $U_w(t)$  for an experiment in which the similarity flows would be generated, assumptions about the connection between the laminar sublayer and the turbulent region would have to be made. The reader can find such assumptions in [4A] and make his own judgement on their reliability.

The transformed equation of motion 4 is

$$\begin{aligned} S'' + \beta \mu H G' + \beta(2+\mu) G \\ = \gamma \beta f (\mu - \gamma \omega) G' + \gamma \beta (2 + \mu - \gamma \omega + \gamma^2 \omega f') G, \end{aligned} \quad (49)$$

where

$$f = \int_0^H \int_{H'}^{\infty} G(H'') dH'' dH'$$

from 47, and

$$-\beta = \frac{\Delta U_{\infty x}}{\gamma U_{\infty}}, \quad \omega = \frac{\gamma_x U_{\infty}}{\gamma^2 U_{\infty x}}, \quad \mu = - \left( 1 + \frac{\Delta_x U_{\infty}}{\Delta U_{\infty x}} \right).$$

Quasi-similar solutions are sought for  $\beta$  fixed – the equilibrium turbulent boundary layers of Clauser [3]. Notice equation 49 is an integro-differential equation on  $S$  and  $G$  as promised in the Introduction.

Suppose there is a region very close to the wall in which the following conditions are satisfied:

- (i) the flow is fully turbulent, so the speed profile can be written in defect form (first of equations 46);
- (ii) the length characterizing the rate of stress variation is large compared with the distance from the wall (region of constant stress), so that the only physical length available is  $\nu/u_\tau$ .

Then  $U$  must simultaneously have the forms

$$U = U_\infty - u_\tau f' \left( \frac{y}{\Delta} \right)$$

and 
$$U = u_\tau \mathcal{F} \left( \frac{u_\tau y}{\nu} \right)$$

That is possible only if

$$U = u_\tau \left( \frac{1}{\kappa} \log \frac{u_\tau y}{\nu} + D \right) \tag{50}$$

where  $D$  and Kármán's constant  $\kappa$  are universal constants. This argument fails if no such "overlap" region satisfying (i) and (ii) exists, and no such region exists if the pressure gradient  $U_\infty U_{\infty x}$  is severe enough, since a large stress gradient in the  $y$ -direction is required to balance a large pressure gradient in the  $x$ -direction for steady flow. Where such a region does exist, equation 50 permits the evaluation of  $\omega$  and  $\mu$  in terms of  $\gamma$ ,  $\beta$  and a shape factor

$$\mathcal{G} = \int_0^\infty f'^2 dH.$$

Mellor and Gibson [4B] find that

$$\omega = \frac{\mu}{\kappa + \gamma} = \frac{\mu}{\kappa} - \frac{\gamma \mu}{\kappa^2} + \dots, \tag{51}$$

and that the integrated boundary-layer momentum equation takes the form

$$\begin{aligned} \mu &= \left(1 + \frac{\gamma}{K}\right) \frac{1/\beta + 2 - \gamma G}{1 - \gamma G + \gamma^2 G/K} \\ &= 2 + \frac{1}{\beta} + \gamma \left[ \frac{2 + 1/\beta}{K} + G(1 + 1/\beta) \right] + \dots \quad (52) \end{aligned}$$

$\gamma$  is a small quantity ( $\gamma = \sqrt{C_f/2} \sim .04$  for a flat plate in a typical experimental situation) and can be used as an expansion parameter in an asymptotic series solution to equation 49. Thus write  $\mathcal{S}$ ,  $\mathcal{G}$  and  $f$  as follows:

$$\begin{aligned} \mathcal{S} &= \sum_{i=0}^{\infty} \gamma^i \mathcal{S}_i(H), \\ \mathcal{G} &= \sum_{i=0}^{\infty} \gamma^i \mathcal{G}_i(H), \\ f &= \sum_{i=0}^{\infty} \gamma^i f_i(H), \end{aligned}$$

so that

$$f_i(H) = \int_0^H \int_{H'}^{\infty} \mathcal{G}_i(H'') dH'' dH'.$$

The expansions for  $\omega$  and  $\mu$  have already been indicated in equations 51 and 52, and the expansion for  $G$  begins

$$G = \sum_{i=0}^{\infty} \gamma^i G_i = \int_0^{\infty} f_0'^2 dH + \gamma 2 \int_0^{\infty} f_0' f_1' dH + \dots$$

The boundary conditions 48 are met as follows:

$$\begin{aligned}
 S_0(0) = 1, \quad & \int_0^\infty \int_H^\infty G_0(H') dH' dH = 1; \quad (53) \\
 S_i(0) = 0, \quad & \int_0^\infty \int_H^\infty G_i(H') dH' dH = 0, \quad i \neq 0.
 \end{aligned}$$

Thus the zeroth order solution contains the entire momentum defect. When the quantities in equation 49 are expanded in powers of  $\gamma$  as described, the coefficients of the various powers must satisfy the following sequence of equations:

$$S_0'' + (1+2\beta)H G_0' + (1+4\beta) G_0 = 0, \quad (54(0))$$

$$S_1'' + (1+2\beta)H G_1' + (1+4\beta) G_1 = (1+4\beta)G_0$$

$$\begin{aligned}
 + \left[ \frac{1+2\beta}{K} + G_0(1+\beta) \right] (G_0 - H G_0') + (1+2\beta) f_0 G_0' \\
 = \mathcal{F}_1 \{ G_0 \},
 \end{aligned}$$

·  
·  
·

$$S_i'' + (1+2\beta)H G_i' + (1+4\beta)G_i = \mathcal{F}_i \{ G_{i-1}, G_{i-2}, \dots \} \quad (54(i))$$

·  
·  
·

The  $\mathcal{F}_i$ 's are complicated functionals involving derivatives and multiple integrals of lower order  $G$ 's. But if  $\beta$  is held fixed for the equilibrium solutions and some relationship between  $G$  and  $S$  is assumed, equations 54 with their boundary conditions 53 can be solved one by

one and the asymptotic series for  $S$  constructed. Each function  $S_i$ ,  $G_i$  and  $f_i$  will depend on  $H$  only, and the non-similarity will be taken care of by the  $\gamma(x)^i$ .

The nature of the analogy between the boundary layer and Rayleigh problems can now be seen by comparing equations 54(0) and 12 — they have exactly the same form. The first of boundary conditions 53 and 13 also have the same form; the second of conditions 53 insures that  $G_0(H) \rightarrow 0$  as  $H \rightarrow \infty$ , and for a reasonable assumption on the  $G$ - $S$  relation for large  $H$  (e.g., Clauser's), it should insure  $S(H) \rightarrow 0$  as well. Thus the similarity solution for self-preserving Rayleigh flow is formally identical to the zeroth-order approximation for the equilibrium boundary layer.

Suppose we have the solution  $s(\eta)$ ,  $g(\eta)$  to the Rayleigh problem for some  $c$ , and we want the zeroth order solution  $S_0(H)$ ,  $G_0(H)$  to the equivalent boundary-layer problem ("equivalent" will become precise when  $\beta(c)$  is found). We expect to have

$$\begin{aligned} S_0(H) &= A s(BH), \\ G_0(H) &= C g(BH) \end{aligned} \tag{55}$$

for some  $A$ ,  $B$ ,  $C$ . Since the physical stress, velocity gradient and  $y$ -coordinate must be the same in the two problems, equations 8 and 46 imply

$$(i) \quad \sigma = \sigma_o s(\eta) = u_{\tau}^2 A_s(BH) \quad ,$$

$$(ii) \quad \Omega = \frac{\sqrt{\sigma_o}}{\ell_o} g(\eta) = \frac{u_{\tau}}{\Delta} C_g(BH) \quad ,$$

$$(iii) \quad y = \ell_o \eta = \frac{\Delta BH}{B} \quad .$$

We shall require  $\eta = BH$ . Squaring (ii), dividing by (i) and multiplying by the square of (iii) gives

$$\frac{C^2}{AB^2} = 1 \quad , \quad (56)$$

a constraint on  $A$ ,  $B$ ,  $C$  arising because the physical solutions contain one velocity and one length scale only. When forms 55 are used in the first boundary condition 53 and the zeroth-order equation of motion 54, the following equations result:

$$A_s(0) = 1 \quad ,$$

$$s''(BH) + \frac{C}{AB^2} (1+2\beta) BH g'(BH) + \frac{C}{AB^2} (1+4\beta) g(BH) = 0 \quad .$$

These are exactly the same as the Rayleigh problem equations 12 and 13 if  $\eta = BH$ , and

$$A = \frac{1}{1+c} \quad ,$$

$$\frac{C}{AB^2} (1+2\beta) = \sqrt{k} \left(1 + \frac{c}{2}\right) \quad , \quad (57)$$

$$\frac{C}{AB^2} (1+4\beta) = \sqrt{k} \quad .$$

Equations 56 and 57 can be solved simultaneously to give

$$\left. \begin{aligned} A &= \frac{1}{1+c} , \\ B &= \frac{1}{\sqrt{k(1+c)}} , \\ C &= \frac{1}{\sqrt{k(1+c)}} , \\ \beta &= \frac{-c/4}{1+c} . \end{aligned} \right\} \quad (58)$$

Thus, given the solution  $s(\eta)$ ,  $g(\eta)$  to a Rayleigh problem for some  $c$ , the zeroth-order solution to the equilibrium boundary-layer problem with  $\beta = -c/4(1+c)$  is known through the prescription 55 and the quantities  $A, B, C$  given in equations 58.  $\beta(c)$  is graphed in figure 5; interesting limiting cases for the boundary-layer and Rayleigh problems are marked on the graph.

In the limit  $\beta \rightarrow \infty$  when the flow becomes continuously separating, the boundary-layer equations become intractable as they stand, and the following transformation [4A] is useful:

$$\left. \begin{aligned} \gamma &= \frac{\lambda}{\sqrt{\beta}} , \\ H &= \frac{\tilde{H}}{\sqrt{\beta}} , \\ S(H) &= \beta \tilde{S}(\tilde{H}) , \\ G(H) &= \beta \tilde{G}(\tilde{H}) , \\ f(H) &= \tilde{f}(\tilde{H}) , \end{aligned} \right\} \quad (59)$$

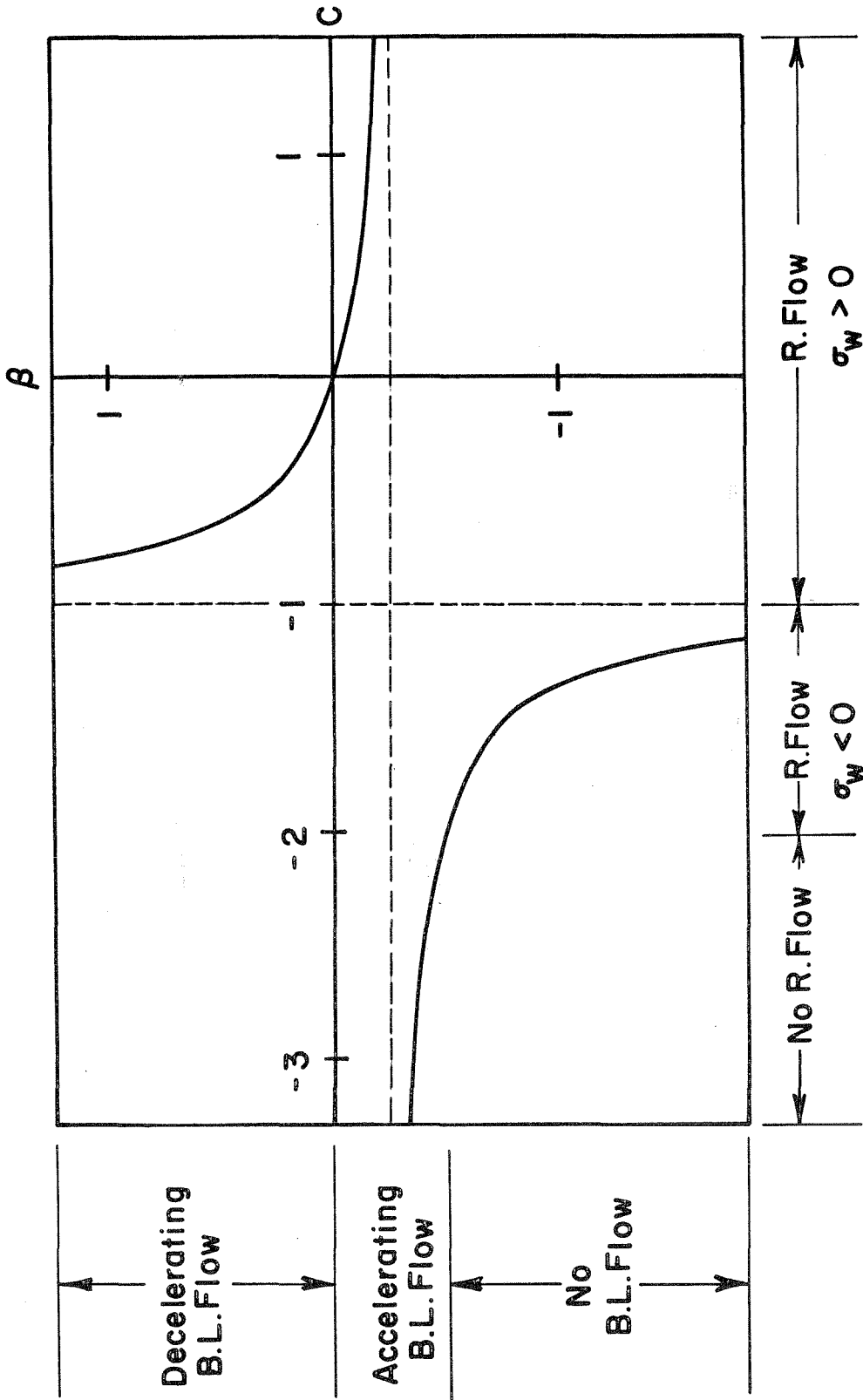


FIG. 5  $\beta(C)$  FOR ANALOGOUS B.L. AND RAYLEIGH FLOWS

so that

$$\tilde{f}'' = -\tilde{G}. \quad (60)$$

The essential reason transformation 59 becomes necessary as  $\beta \rightarrow \infty$  is that the wall shear  $\sigma_w$  becomes dynamically irrelevant in that case, — the "skin friction velocity"  $u_\tau = \sqrt{\sigma_w}$  is no longer an appropriate scale. From the definition of  $\beta$  below equation 49,

$$\beta = -\frac{\Delta U_\infty}{\gamma U_\infty} \frac{x}{U_\infty} = -\frac{\left(\frac{u_\tau}{U_\infty} \Delta\right) U_\infty U_\infty x}{u_\tau^2} = \frac{\delta^* \frac{1}{\rho} \frac{dp}{dx}}{u_\tau^2} = \frac{u_p^2}{u_\tau^2},$$

where  $\delta^*$  is the boundary-layer displacement thickness

$$\delta^*(x) = \int_0^\infty \left[ 1 - \frac{U(x,y)}{U_\infty(x)} \right] dy,$$

and  $u_p$  is a "pressure velocity" defined as  $\sqrt{\delta^*/\rho \, dP/dx}$ . Transformation 59 rescales the physical variables on  $u_p$  so that

$$\left. \begin{aligned} \tilde{H} &= \frac{y}{\tilde{\Delta}}, \\ \sigma &= u_p^2 \tilde{S}(\tilde{H}), \\ \Omega &= \frac{u_p}{\tilde{\Delta}} \tilde{G}(\tilde{H}), \\ \frac{U_\infty(x) - U(x,y)}{u_p(x)} &= \tilde{f}'(\tilde{H}), \end{aligned} \right\} \quad (61)$$

with

$$\tilde{\Delta}(x) = \int_0^\infty \frac{U_\infty(x) - U(x,y)}{u_p(x)} dy$$

from equations 44 and 46.

The last case one would expect a close analogy between the boundary-layer and Rayleigh problems is the case of separating flow, yet the analogy is very close indeed. The equation of motion 49 can be rewritten in terms of the new variables 59 and the various quantities expanded in powers of  $\lambda$ . The zeroth-order equation of motion and the conditions on its solution become

$$\begin{aligned} \tilde{S}_0'' + \left(2 + \frac{1}{\beta}\right) \tilde{H} \tilde{G}_0' + \left(4 + \frac{1}{\beta}\right) \tilde{G}_0 &= 0, \\ \tilde{S}_0(0) &= \frac{1}{\beta}, \\ \int_0^\infty \int_{\tilde{H}}^\infty \tilde{G}_0(\tilde{H}') d\tilde{H}' d\tilde{H} &= 1. \end{aligned} \tag{62}$$

For  $\beta^{-1} = 0$  the equation of motion may be written

$$\tilde{H} \tilde{S}_0'' + 2(\tilde{H}^2 \tilde{G}_0)' = 0,$$

and since

$$\tilde{H} \tilde{S}_0'' = (\tilde{H} \tilde{S}_0' - \tilde{S}_0)',$$

a first integration can be performed. The constant of integration is fixed by the condition  $\tilde{S}_0(0) = 0$ , and the result is

$$\tilde{G}_0 = -\frac{1}{2} \left( \frac{\tilde{S}_0}{\tilde{H}} \right)'$$

$\tilde{G}_0$  can be written in terms of  $\tilde{f}_0$  through equation 60 and the equation integrated once more —

$$\tilde{f}'_0 = \frac{1}{2} \frac{\tilde{J}_0}{\tilde{H}},$$

where  $\tilde{f}'(\infty) = 0$  has been used. This result is analogous to equation 16 for the  $c = -1$  Rayleigh problem, where the non-dimensional mean speed appears as  $s/\eta$ . Suppose now we have the zeroth-order boundary-layer solution  $\tilde{J}_0, \tilde{f}'_0$  for the case  $\beta^{-1} = 0$ , and we want to find the solution  $s, s/\eta$  to the  $c = -1$  Rayleigh problem. That is, we expect

$$\begin{aligned} s(\eta) &= \tilde{a} \tilde{J}_0(\tilde{b}\eta), \\ \frac{s(\eta)}{\eta} &= \tilde{c} \tilde{f}'_0(\tilde{b}\eta) \end{aligned} \tag{63}$$

and want  $\tilde{a}, \tilde{b}, \tilde{c}$ . Then by the same kind of argument that produced equations 58 it is easy to show

$$\left. \begin{aligned} \tilde{a} &= \frac{1}{4}, \\ \tilde{b} &= \frac{\sqrt{k}}{2}, \\ \tilde{c} &= \frac{\sqrt{k}}{4}. \end{aligned} \right\} \tag{64}$$

If Mellor and Gibson had given their numerical results for the zeroth-order boundary-layer solution, equations 64 would have permitted a direct check on their calculations against the exact results of section 7 (with  $B = 0$  — Mellor and Gibson use the Prandtl eddy viscosity equation for their wall layer). In fact they show plots of the combined zeroth and first-order solutions only, but their results are rescaled and plotted in figures 3 and 4 anyway.

For  $\beta^{-1} = 0$ , the only parameter left in the boundary-layer similarity solution  $\tilde{S}(\tilde{H}), \tilde{G}(\tilde{H})$  is  $\lambda$ . The quantities  $\kappa$  and  $k$  associated with the stress-velocity gradient assumptions remain, of course, but their values are supposed to be universal and known. The quantity  $\tilde{f}'(0)$ , in particular, depends on  $\lambda$  only. The wall stress is zero, and under any of the stress-gradient assumptions  $U(x, 0) = 0$  (thus the flow is "continuously separating"). By the definition of  $\gamma$  and the first of equations 59,

$$\lambda = \frac{u_p}{U_\infty} .$$

By the fourth of equations 61,

$$\frac{1}{\lambda} = \tilde{f}'(0) , \tag{65}$$

and since the right-hand side is a function of  $\lambda$  known once the similarity problem is solved, equation 65 determines  $\lambda$  uniquely. The profile for continuously separating flow is thus unique, and it is the first-order approximation to that solution which is rescaled and plotted in figures 3 and 4. Mellor and Gibson find  $\lambda^{-1} = 10.27$  to first order. The zeroth-order approximation can be found through equations 63, 64 and the work of section 7:

$$\lambda_o^{-1} = \tilde{f}'_o(0) = \frac{4}{\sqrt{k}} \left( \frac{s(\eta)}{\eta} \right)_{\eta=0} = \frac{4a^2}{\sqrt{k}} = 12.4$$

for Townsend's  $B = 0$ , the computed  $a = .618$ , and  $k = .015$ .

Since Mellor and Gibson carry their analysis to first order in  $\lambda$  and use the  $B = 0$  stress-gradient relation, the differences between the curves labeled (MG) and the Rayleigh problem curves for  $B = 0$

must be the first-order corrections. The corrections are fairly large, especially in the stress profile, but the qualitative features of the analogous curves are the same. It can be seen from Mellor and Gibson's papers ([4A] figure 5 or [4B] figure 10) that the experimental data deviate from the computed velocity profile in just the same way as the  $B = 0.2$  curve deviates from the  $B = 0$  curve for the Rayleigh problem solution of figure 4. The Townsend relation, equation 3, should thus fit the data much better than the Prandtl eddy viscosity relation in the extreme case of continuously separating flow.

REFERENCES

1. Townsend, A. A., The Structure of Turbulent Shear Flow, Cambridge (Eng.) University Press (1956).
2. Townsend, A. A., "Equilibrium Layers and Wall Turbulence," Journal of Fluid Mechanics, Vol. 11 (1961), pp. 97-120.
3. Clauser, F., "The Turbulent Boundary Layer," Advances in Applied Mechanics, Vol. 4 (1956), pp. 1-51.
- 4A. Mellor, G. L., and Gibson, D. M., "Equilibrium Turbulent Boundary Layers," Mechanical Engineering Report FLD 13, Princeton University (1963).
- 4B. Mellor, G. L., "The Effects of Pressure Gradients on Turbulent Flow near a Smooth Wall," Mechanical Engineering Report FLD 14, Princeton University (1964).
5. Jeffreys, H., and Jeffreys, B., Methods of Mathematical Physics, 3rd ed., Cambridge (Eng.) University Press (1956), p. 622.

APPENDIX

A Numerical Technique for Finding  $a$ ,  $A$ ,  $\eta_e$ ,  $s_e$  for the Case  $c = -1$

The analytical expressions for the stress distribution derived in section 7 contain the constants  $a$  and  $A$ . Two conditions must be satisfied by the wall and outer layer stress distributions: they must match at a point  $\eta_e$  fixed by equation 26, and the integral  $\int_0^{\infty} s/\eta \, d\eta$  must be  $1/2$ . The stress slopes match automatically as explained in section 7.

The steps of a strongly convergent iteration procedure for finding  $a$ ,  $A$  and the matching point  $(\eta_e, s_e)$  between wall and outer layers are outlined below. The essential point is that the area under the  $s/\eta$  curve is very nearly proportional to  $A$ ; the proportionality would be exact if the outer solution spanned the whole field. The integral  $\int_0^{\infty} s/\eta \, d\eta = I$  is computed on the basis of a guess for  $A$ , say  $A^{(0)}$ , then a new estimate  $A^{(1)}$  is found:

$$\frac{A^{(1)}}{A^{(0)}} = \frac{1/2}{I} \tag{A1}$$

The cycle can then be started again with  $A^{(1)}$ . The reason this operation is interesting enough to be discussed in an appendix is that it may be carried out by hand despite the fact  $s$  is not given as an explicit function of  $\eta$  by the wall solution for non-zero  $B$ .

① guess  $A = A^{(0)}$

The superscript (0) will be dropped until step 6 .

② compute  $\eta_e$

The outer solution and the matching condition are required:

$$s = A\eta_e e^{-\eta_e^2/4} \quad (A2)$$

$$\eta_e r_e = \epsilon b_e = \epsilon (1 - B\eta_e \frac{s'_e}{s_e}) \quad (A3)$$

By A2,

$$\frac{s'_e}{s_e} = \frac{1}{\eta_e} - \frac{\eta_e}{2}$$

Then A2 and A3 both yield expressions for  $r_e$ :

$$r_e = \sqrt{A\eta_e} e^{-\eta_e^2/8} = \frac{\epsilon}{\eta_e} (1 - B + \frac{B\eta_e^2}{2})$$

An equation for  $\eta_e$  is the result:

$$\eta_e^{3/2} = \frac{\epsilon}{\sqrt{A}} (1 - B + \frac{B\eta_e^2}{2}) e^{\eta_e^2/8} \quad (A4)$$

Since  $B\eta_e^2/2$  and  $\eta_e^2/8$  are small compared to 1, that equation may be solved by iteration very quickly.

③ compute  $s_e, X_e, Y_e$

The outer solution and the definitions of X and Y are used:

$$s_e = A\eta_e e^{-\eta_e^2/4} \quad (A5)$$

$$X_e = \sqrt{\eta_e} \quad (A6)$$

$$Y_e = \sqrt{\frac{s_e}{\eta_e}} \quad (A7)$$

④ compute a

Equation 39 is now used:

$$X = \frac{2a}{\epsilon(1-2B)} \left\{ \left( \frac{Y}{a} \right)^{\frac{B}{1-B}} - \left( \frac{Y}{a} \right) \right\} \quad (A8)$$

That can be rewritten as an expression for a and evaluated at the matching point using the computed values of  $X_e, Y_e$ :

$$a = \left\{ \frac{\frac{\epsilon}{2}(1-2B)X_e + Y_e}{Y_e \frac{B}{1-B}} \right\}^{\frac{1-B}{1-2B}} \quad (A9)$$

⑤ evaluate  $I = \int_0^{\infty} \frac{s}{\eta} d\eta$

$$I = \int_0^{\eta_e} \frac{s}{\eta} d\eta + \int_{\eta_e}^{\infty} A e^{-\eta^2/4} d\eta$$

$$= \int_0^{\eta_e} Y^2 d\eta + A \sqrt{\pi} \operatorname{erfc} \left( \frac{\eta_e}{2} \right)$$

Performing an integration by parts,

$$I = s_e + \int_{Y_e^2}^{a^2} \eta d(Y^2) + A \sqrt{\pi} \operatorname{erfc} \left( \frac{\eta_e}{2} \right)$$

Substituting  $y = Y^2$  and using equation A8, I may be written as an explicit function of  $s_e, \eta_e, a, A$ :

$$I = s_e + A \sqrt{\pi} \operatorname{erfc} \left( \frac{\eta_e}{2} \right) + \frac{4}{\epsilon^2(1-2B)^2} \int_{\frac{s_e}{\eta_e}}^{a^2} \left\{ a \frac{1-2B}{1-B} y^{\frac{B}{2-2B}} - y^{\frac{1}{2}} \right\}^2 dy \quad (A10)$$

⑥ compute  $A^{(1)}$  and renew cycle

By A1,

$$\frac{A^{(1)}}{A^{(0)}} = \frac{1}{2I} \quad (A1)$$

$A^{(1)}$  can be used as a second guess for  $A$  in step ① . The iteration cycle is thus closed.

### III. THE PROPAGATION OF FREE TURBULENCE IN A MEAN SHEAR FLOW

#### 1. Introduction

Since the work of Corrsin and Kistler [1], it has become clear that one of the most distinctive features of turbulence is its spotty or intermittent character. A hot wire record of a real flow shows periods of great agitation erupting sporadically between quiescent intervals. It now appears that any theory of turbulence, even turbulence homogeneous in the sense that ensemble averages of flow properties are invariant under translation, must take into account the severe inhomogeneity present in each realization of the flow.

Corrsin and Kistler discussed the sharp fronts that bound the turbulent portions of wakes and boundary layers embedded in regions of potential flow. The turbulent side of a front is supposed to be characterized by random vorticity, while the flow on the other side is vorticity free. The rate of propagation of such a front, at high Reynolds numbers, is governed by the intensity of the turbulence itself and is independent of viscosity. Yet there is no way to transmit vorticity to the irrotational flow beyond the front except by viscous diffusion. Corrsin and Kistler resolved the apparent contradiction by pointing out that the interface between rotational and irrotational flow wrinkles up until its area is adequate to transmit the right amount of vorticity.

The phenomenon of intermittency also occurs in situations where the flow beyond intensely turbulent regions is not irrotational. Turbulent slugs in pipe flow, spiral turbulent bands in circular

Couette flow, wedge-shaped spots of turbulence in boundary layers on the verge of transition, turbulent wakes behind the bow shocks of hypersonic projectiles are examples of intermittent turbulence in a mean shear flow. Saffman [ 2 ] noticed the similarity between turbulent slugs and slugs of diffusing dye in pipe flow, and conjectured that turbulence might behave like a diffusible scalar quantity in such situations. He proposed a model equation for the 'turbulence density'  $T$ ,

$$\frac{\partial T}{\partial t} + \underline{U} \cdot \nabla T = \alpha T + \nabla \cdot (\nu \cdot T) ,$$

where  $\underline{U}$  is the mean velocity, and the convected time derivative of  $T$  is set equal to a production term proportional to  $T$  plus a diffusion term depending on a tensor diffusivity  $\nu$ . Turbulence propagating into an irrotational flow cannot diffuse at all, if 'turbulence' means random vorticity fluctuations. Vorticity must stay behind the surging interface. But if the flow beyond the turbulent region is already rotational, velocity fluctuations induced by the turbulence will stretch the vorticity in the laminar region and produce random vorticity fluctuations, that is, turbulence. Thus an initially sharp turbulent front will propagate into a mean shear flow, and Saffman proposed that this propagation might be described by a diffusion equation.

One of the problems with this proposal is that the quantity  $T$  which is supposed to diffuse is hard to define in terms of mechanical properties of the flow. An outright identification of  $T$  with some moment of the fluctuation vorticity  $\omega$  cannot be defended by the vorticity equation. Since the diffusion should depend on random stretching of mean vorticity, an interaction between the turbulence already

present and the mean field, the physics of the propagation should remain after linearization of the vorticity fluctuation equation. Suppose the mean vorticity  $\bar{\Omega}$  is constant in space. The linearized equation for  $\omega$  is

$$\frac{\partial \omega}{\partial t} + \bar{u} \cdot \nabla \omega = \omega \cdot \nabla \bar{u} + \bar{\Omega} \cdot \nabla \bar{u}$$

The last term represents propagation of turbulence by random stretching of mean field vorticity. It must be written in terms of the turbulent velocity  $\bar{u}$ , and  $\bar{u}$  is a non-local functional of  $\omega$  found by uncurling the equation  $\omega = \nabla \times \bar{u}$ . The equations for statistical moments of  $\omega$  similarly involve the velocity field  $\bar{u}$ . It is hard to see how  $T$  could be defined as a local functional of the vorticity and still satisfy Saffman's diffusion equation (unless, of course,  $\nu$  is itself a non-local functional of the turbulent field, but then the point would be lost). In the situations where turbulent regions embedded in shear flows have been observed, spiral bands in Couette flow for example, the turbulence is more of a visual than a mechanical phenomenon anyway. Regions are called turbulent which display so much commotion that the eye cannot pick up the details. These turbulent regions appear to be bounded by sharp fronts just like turbulent regions embedded in irrotational flow (see Coles' review article [3] for examples).

Whether turbulence diffuses or not, it is certain that a turbulent region embedded in a mean shear flow excites random vorticity around it, and it would be interesting to know how the effect propagates. A straightforward way to assess the intensity

of the turbulence is to find the average rate at which it transports momentum through the mean flow — the Reynolds stress. Suppose, for example, that the mean flow is in the  $x$  direction and the mean speed  $U$  is a function of  $y$  and  $t$  only. The  $(x, y, z)$  components of turbulent velocity and vorticity are  $(u, v, w)$  and  $(\xi, \eta, \zeta)$  respectively. The turbulence satisfies the continuity equation  $\nabla \cdot \underline{u} = 0$  and is statistically homogeneous in  $x$  and  $z$ . Then the mean field momentum equation is

$$\frac{\partial U}{\partial t} = \frac{\partial}{\partial y} (-\overline{uv}) ,$$

where  $-\overline{uv}$  is the Reynolds stress. By continuity and homogeneity,

$$\begin{aligned} \frac{\partial}{\partial y} (-\overline{uv}) &= -\overline{u \frac{\partial v}{\partial y}} - \overline{v \frac{\partial u}{\partial y}} = \overline{u \left( \frac{\partial u}{\partial x} + \frac{\partial w}{\partial z} \right)} + \overline{v \left( \frac{\partial v}{\partial x} - \frac{\partial u}{\partial y} \right)} \\ &= \overline{u \frac{\partial w}{\partial z}} + \overline{v \omega} = \overline{w \left( \frac{\partial w}{\partial x} - \frac{\partial u}{\partial z} \right)} + \overline{v \omega} \\ &= \overline{v \omega} - \overline{w \eta} \end{aligned}$$

so the gradient of the Reynolds stress is zero if no random vorticity is present. If the Reynolds stress is zero at  $\infty$  and has a finite value at some height  $y$ , then random vorticity fluctuations must have propagated beyond  $y$ . The object of this chapter is to find how the Reynolds stress evolves and the mean flow reacts as the turbulence propagates.

The first approach to this problem was patterned after Phillips' model for the random potential flow above a turbulent boundary layer [4]. The original turbulence was supposed to lie below the  $x, z$  plane in the region  $y < 0$  and excite random vorticity fluctuations in

the region  $y > 0$ . The  $x, z$  plane was idealized as a wall of pistons continually forcing the flow above. The trouble with this model is that it assumes a qualitative distinction between the flow above the plane and the flow below. Such a distinction may be appropriate when the flow above is irrotational, but it is surely unjustified when both parts of the flow contain random vorticity. The work of Moffatt [5] on homogeneous turbulence under mean shear suggested a more sensible formulation of the problem. In this chapter the propagation of turbulence is treated as an initial value problem. At time zero, random impulses, homogeneous in  $x$  and  $z$  and closely confined to the region  $y = 0$ , generate an infinite slab of random vorticity. This vorticity then propagates into an unbounded, parallel mean shear flow, and the reaction of that mean flow to the propagating turbulence is the object of study. The physical setup is sketched in figure 1. Throughout the rest of this chapter the coordinate labels  $(x, y, z)$  and  $(x_1, x_2, x_3)$  will be used interchangeably, and the turbulent velocity components will be written either  $(u, v, w)$  or  $(u_1, u_2, u_3)$ . Unit vectors in the  $x, y, z$  directions are written  $\underline{i}, \underline{j}, \underline{k}$ .

The chapter can be divided into three main parts, sections 3, 4 and 5, corresponding to three tacks taken in an effort to understand the problem just outlined. In section 3, the evolution of the Reynolds stress under the linearization mentioned earlier is studied. The result is surprising and disappointing: the stress stops propagating once the turbulence is highly sheared. In the next section, the problem is greatly simplified by permitting initial turbulent fields uniform in the direction of mean flow only, and some aspects

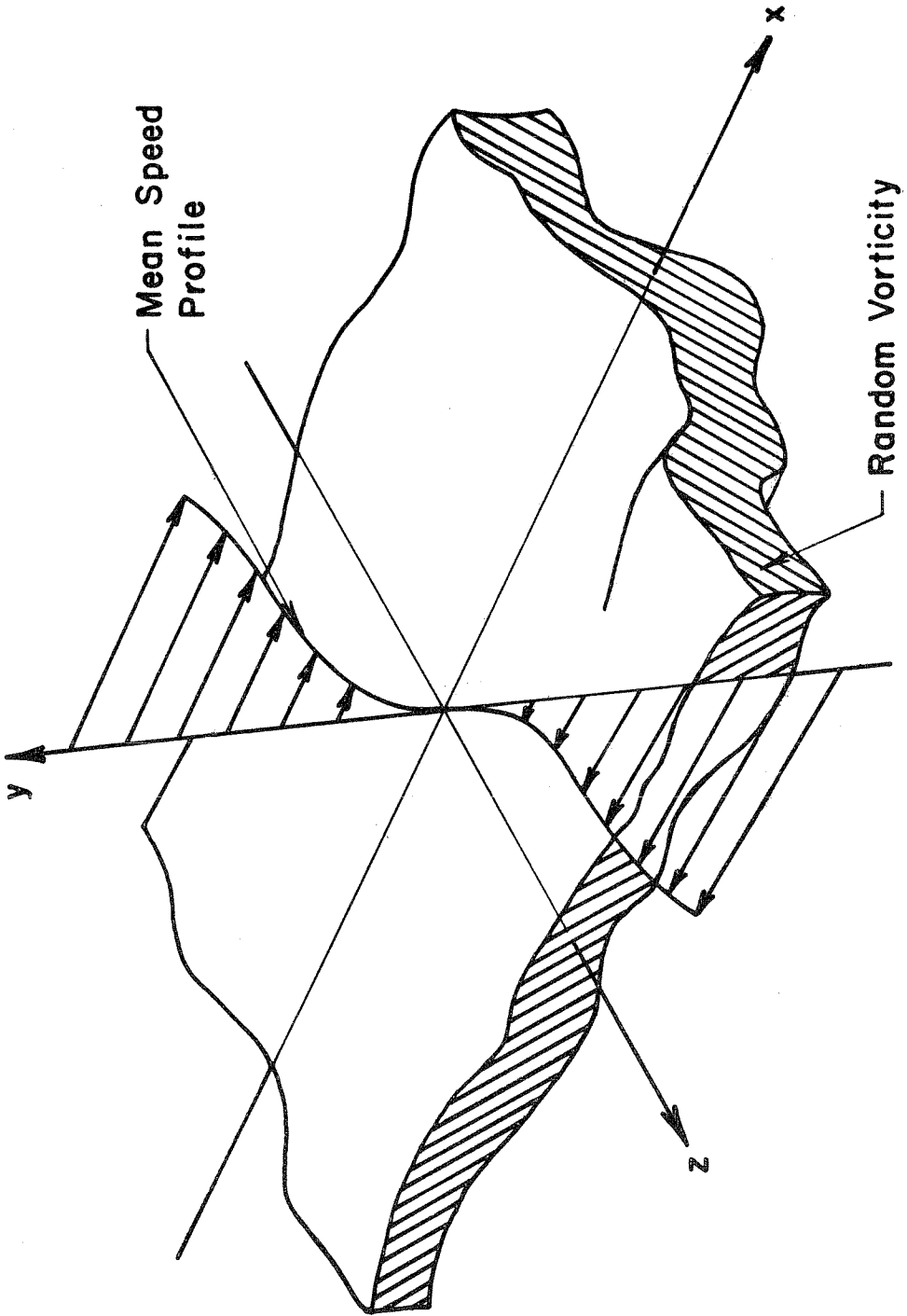


FIG. I TURBULENCE IN A MEAN SHEAR FLOW

of non-linearity are reintroduced. No general estimate of the power of such turbulence to distort the mean flow can be found analytically, however. The convection of momentum depends critically on the convection of random vorticity by the fluctuating velocity field, and that problem cannot be solved. When it became clear that analytical models would be unreliable, numerical flow visualization and momentum transfer experiments were programmed and carried out. The background for these and the results obtained are described in section 5.

## 2. Basic Equations of the Problem

The problem to be studied can be posed as follows. At time zero an ensemble of initial velocity fields  $\underline{v}_0(\underline{x})$  is given, and the flow for each initial condition evolves under the Navier-Stokes equations of motion:

$$\frac{\partial \underline{v}}{\partial t} + \underline{v} \cdot \nabla \underline{v} + \nabla \pi = \nu \nabla^2 \underline{v}, \quad (1)$$

$$\nabla \cdot \underline{v} = 0,$$

where  $\nu$  is the kinematic viscosity and  $\pi$  is the kinematic pressure. Each initial condition can be written as the sum of two parts:

$$\underline{v}_0(\underline{x}) = \underline{U}_0(y) + \underline{u}_0(\underline{x}). \quad (2)$$

$\underline{U}_0(y)$  is the same from experiment to experiment, and  $\underline{u}_0(\underline{x})$  satisfies the following properties: the ensemble average of  $\underline{u}_0(\underline{x})$  is zero; statistical quantities based on the ensemble of  $\underline{u}_0(\underline{x})$  are homogeneous

in  $x$  and  $z$ , and symmetrical under reflection through a plane perpendicular to  $z$ ;  $u_0(x, y, z) \rightarrow 0$  as  $y \rightarrow \pm \infty$ . Solutions  $\underline{u}, \pi$  based on these initial conditions can be written

$$\begin{aligned} \underline{u}(\underline{x}) &= \underline{u}U(y, t) + \underline{u}(\underline{x}, t) , \\ \pi(\underline{x}) &= P(\underline{x}, t) + p(\underline{x}, t) , \end{aligned} \tag{3}$$

where  $\overline{\underline{u}}$  and  $\overline{p}$  are zero. The overbars denote averages taken over the ensemble of initial value experiments.  $P(\underline{x}, t)$  is required to approach a constant pressure  $P_0$  as  $y \rightarrow \infty$ , so no mean pressure gradient is imposed in the far field. When the equations of motion are written in terms of the quantities defined in 3 and averaged, the result is

$$\begin{aligned} \frac{\partial \underline{U}}{\partial t} + \underline{U} \cdot \nabla \underline{U} + \overline{\underline{u} \cdot \nabla \underline{u}} + \nabla P &= \nu \nabla^2 \underline{U} , \\ \nabla \cdot \underline{U} &= 0 . \end{aligned} \tag{4}$$

The averages may be subtracted from the original equations to give

$$\begin{aligned} \frac{\partial \underline{u}}{\partial t} + \underline{U} \cdot \nabla \underline{u} + \underline{u} \cdot \nabla \underline{U} + \underline{u} \cdot \nabla \underline{u} + \nabla p &= \overline{\underline{u} \cdot \nabla \underline{u}} + \nu \nabla^2 \underline{u} , \\ \nabla \cdot \underline{u} &= 0 . \end{aligned} \tag{5}$$

But

$$\begin{aligned} \overline{\underline{u} \cdot \nabla \underline{u}} &= \overline{u_j \frac{\partial u_i}{\partial x_j}} = \frac{\partial}{\partial x_j} (\overline{u_i u_j}) = \frac{\partial}{\partial y} (\overline{u_i v}) \\ &= \underline{i} \frac{\partial}{\partial y} (\overline{uv}) + \underline{j} \frac{\partial}{\partial y} (\overline{v^2}) , \end{aligned}$$

where the continuity equation and the assumption of homogeneity in  $x$  and  $z$  have been used. Since the mean velocity has the form  $\underline{U} = \underline{j}U(y,t)$ , the second of equations 4 is automatically satisfied, and the  $y$  component of the first is

$$\frac{\partial}{\partial y} (\overline{v^2}) + \frac{\partial P}{\partial y} = 0 .$$

Integrating from  $y \rightarrow \infty$ , and using the condition  $P(x, \infty, z, t) = P_0$ ,

$$P(\underline{x}, t) = P_0 - \overline{v^2}(y, t) = P(y, t) .$$

Thus a mean pressure depending on  $y$  and  $t$  only is consistent with the assumption  $\underline{U} = \underline{j}U$ . Equations 5 and the  $x$  component of the mean momentum equation are now

$$\frac{\partial \underline{u}}{\partial t} + \underline{U} \frac{\partial \underline{u}}{\partial x} + \underline{i} v \frac{\partial U}{\partial y} + \nabla P = \left[ \underline{i} \frac{\partial}{\partial y} (\overline{uv}) + \underline{j} \frac{\partial}{\partial y} (\overline{v^2}) \right] - \underline{u} \cdot \nabla \underline{u} + \nu \nabla^2 \underline{u} , \quad (6)$$

$$\nabla \cdot \underline{u} = 0 ,$$

$$\frac{\partial U}{\partial t} + \frac{\partial}{\partial y} (\overline{uv}) = \nu \frac{\partial^2 U}{\partial y^2} . \quad (7)$$

Suppose the viscous term in equation 7 is negligible, and define the mean field momentum change

$$M = \int_{-\infty}^{\infty} [U(y, t) - U_0(y)] dy$$

and angular momentum change

$$L = \int_{-\infty}^{\infty} y [U(y, t) - U_0(y)] dy .$$

From equation 7 and the assumption that turbulent fluctuations approach zero as  $y \rightarrow \infty$ ,

$$\dot{M} = \int_{-\infty}^{\infty} \frac{\partial U}{\partial t} dy = - \int_{-\infty}^{\infty} \frac{\partial(\overline{uv})}{\partial y} dy = - \overline{uv} \Big|_{-\infty}^{\infty} = 0 ,$$

but

$$\dot{L} = \int_{-\infty}^{\infty} y \frac{\partial U}{\partial t} dy = - \int_{-\infty}^{\infty} y \frac{\partial(\overline{uv})}{\partial y} dy = \int_{-\infty}^{\infty} \overline{uv} dy \neq 0 .$$

It may seem surprising that angular momentum (or rather, angular momentum per unit length in the x direction, and that is the catch) is not necessarily conserved. The same thing happens in the laminar flow case, where equation 7 becomes

$$\frac{\partial U}{\partial t} = \nu \frac{\partial^2 U}{\partial y^2} ,$$

and the kind of situation shown in figure 2 might be considered. Then

$$\dot{L} = \int_{-\infty}^{\infty} y \frac{\partial U}{\partial t} dy = \nu \int_{-\infty}^{\infty} y \frac{\partial^2 U}{\partial y^2} dy = -\nu \int_{-\infty}^{\infty} \frac{\partial U}{\partial y} dy = -\nu \Delta U .$$

Here again, 'angular momentum' is being lost, and at a rate  $-\nu \Delta U$ .

Why is no pressure gradient needed to create a torque consistent with this loss? The answer can be seen by considering the thought experiment shown in figure 3. Two long, thin boards pass by each other and suddenly connect. Their angular momentum is proportional to their length  $\ell$ . If their tendency to rotate after connection is resisted by a graded impulse per unit length  $I = -px$ , then the total angular impulse delivered is proportional to  $p\ell^3$ , and this must

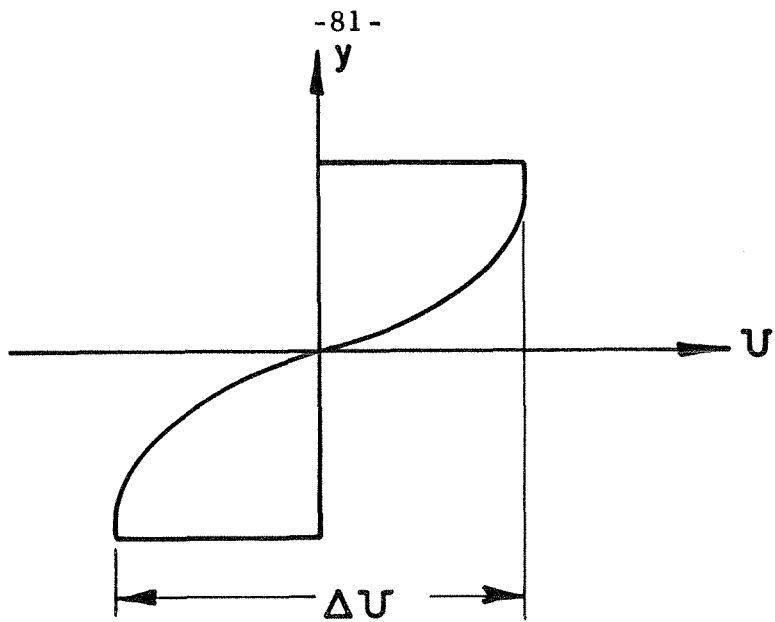


FIG. 2 LAMINAR FLOW LOSING "ANGULAR MOMENTUM"

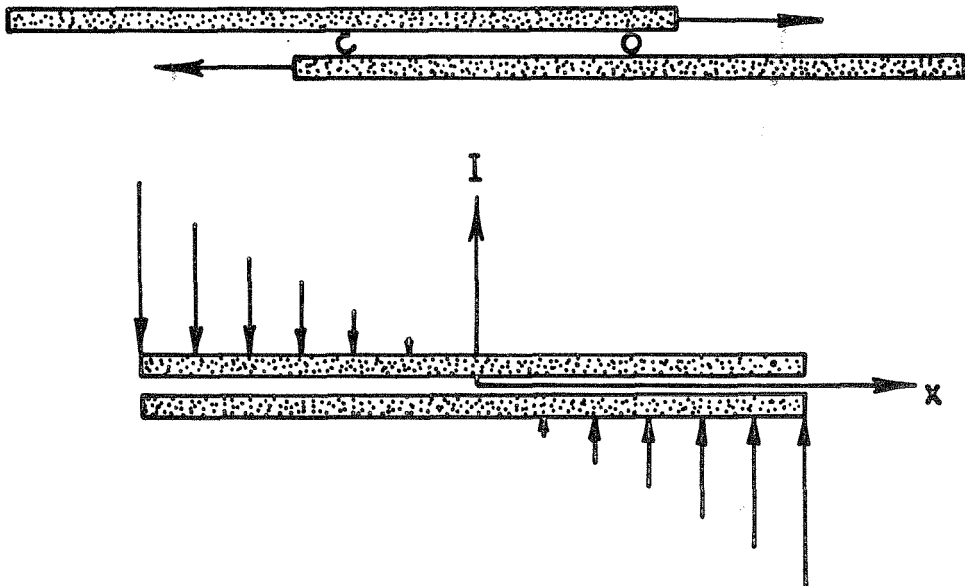


FIG. 3 SUDDEN CONNECTION OF TWO BOARDS

be proportional to  $l$ . Thus  $p \sim l^{-2}$ , and the impulse gradient required drops as the length of the boards increases. As  $l \rightarrow \infty$ ,  $p \rightarrow 0$ , just as the pressure gradient in the fluid flow problem goes to zero as the flow is made homogeneous over larger and larger intervals in the  $x$  direction.

In this chapter various restrictions on the allowable initial conditions and various truncations of equations of motion 6 and 7 will be considered. The viscous terms in the equations, for example, will always be dropped. In section 4 a truncation called the mean field equations will be used, in which the non-linear action of the turbulence on itself is dropped, but the turbulent interaction with the mean field is retained. The inviscid mean field equations are

$$\frac{\partial \underline{y}}{\partial t} + U \frac{\partial \underline{y}}{\partial x} + \underline{j} \cdot \nabla \frac{\partial U}{\partial y} + \nabla p = 0 ,$$
$$\nabla \cdot \underline{y} = 0 , \tag{8}$$

$$\frac{\partial U}{\partial t} + \frac{\partial}{\partial y} (\overline{uv}) = 0 ,$$

where  $U = U(y, t)$ . The mean field equations are not a rational approximation to the full equations in the sense of being a valid perturbation limit for small times, but they do preserve some of the qualitative features of the flow which are lost in a full linearization. In the language of the theory of homogeneous turbulence, the mean field equations retain the interaction between the large eddies (the mean flow) and the small eddies, but neglect the interaction of the small eddies with each other.

If the non-linear terms are dropped altogether, the linearized equations of motion result:

$$\frac{\partial \underline{u}}{\partial t} + U \frac{\partial \underline{u}}{\partial x} + \underline{i}v\Omega + \nabla p = 0 ,$$

$$\nabla \cdot \underline{u} = 0 , \tag{9}$$

$$U(y, t) = U_0(y) ,$$

where

$$\Omega \equiv \frac{\partial U}{\partial y} .$$

The case  $\Omega(y) = \text{const}$  is discussed in detail in the next section. Suppose the initial turbulent disturbance  $\underline{u}_0(\underline{x})$  is characterized by a magnitude  $U$  and a length scale  $L$ . The convective terms dropped to get equation 9 become important after a time  $L/U$ , and the time scale associated with the mean field interaction terms is  $\Omega^{-1}$ . Hence equations 9 are valid and interesting for times satisfying

$$\Omega^{-1} \sim t \ll L/U ,$$

and  $\Omega L/U \gg 1$  is required for the linearized equations to be valid at all.

### 3. The Linearized Problem with Constant $\Omega$

#### A. Fourier Transformation and Solution of the Linearized Equations of Motion

The turbulent velocity field can be expressed as a Fourier integral

$$u(\underline{x}, t) = \int \underline{a}(\underline{k}, t) e^{i\underline{k} \cdot \underline{x}} d\underline{k} ,$$

where

(10)

$$\underline{a}(\underline{k}, t) = \frac{1}{(2\pi)^3} \int u(\underline{x}, t) e^{-i\underline{k} \cdot \underline{x}} d\underline{x} .$$

$\underline{a}$  is a generalized function and can be considered the limit of the integral over physical space as the domain of integration becomes arbitrarily large. Lighthill [6] gives formal definitions of quantities like  $\underline{a}$  and techniques for manipulating them. Fourier transformations will be abbreviated to expressions like  $FT(u) = \underline{a}$ . Then

$$FT\left(\frac{\partial u}{\partial t}\right) = \frac{\partial \underline{a}}{\partial t} ,$$

$$FT(\nabla \cdot u) = i\underline{k} \cdot \underline{a}$$

follow at once, and if  $FT(p) = b(\underline{k}, t)$ ,

$$FT(\nabla p) = i\underline{k} b .$$

For  $\Omega$  constant and  $(1, 0, 0)$  a unit vector in the  $k_1$  direction,

$$FT(\underline{i} \cdot \nabla \Omega) = \Omega a_2(1, 0, 0) .$$

Finally, for constant  $\Omega$  and  $U = \Omega x_2$ ,  $FT(U \partial u / \partial x)$  is found as follows:

$$\begin{aligned} FT\left(U \frac{\partial u}{\partial x}\right) &= \frac{1}{(2\pi)^3} \int \Omega x_2 \frac{\partial u}{\partial x_1} e^{-i\underline{k} \cdot \underline{x}} d\underline{x} \\ &= i\Omega k_1 \frac{1}{(2\pi)^3} \int x_2 u e^{-i\underline{k} \cdot \underline{x}} d\underline{x} \\ &= i\Omega k_1 \left[ i \frac{\partial}{\partial k_2} FT(u) \right] = -\Omega k_1 \frac{\partial \underline{a}}{\partial k_2} . \end{aligned}$$

The Fourier transforms of the linearized momentum and continuity equations are thus

$$\frac{\partial \tilde{a}}{\partial t} - \Omega k_1 \frac{\partial \tilde{a}}{\partial k_2} + \Omega a_2(1, 0, 0) + i \tilde{k} b = 0 ,$$

$$\tilde{k} \cdot \tilde{a} = 0 .$$

Differentiating the continuity equation with respect to time and  $k_2$  gives

$$\tilde{k} \cdot \frac{\partial \tilde{a}}{\partial t} = 0 ,$$

and

$$\tilde{k} \cdot \frac{\partial \tilde{a}}{\partial k_2} + a_2 = 0 .$$

An expression for  $b$  is obtained by using these relations and dotting the momentum equation with  $\tilde{k}$ ,

$$b = \frac{2i\Omega k_1 a_2}{k^2}$$

where  $k^2 = k \cdot k$ . The momentum equation in terms of  $\tilde{a}$  alone is

$$\frac{\partial \tilde{a}}{\partial t} - \Omega k_1 \frac{\partial \tilde{a}}{\partial k_2} + \Omega a_2(1, 0, 0) - \frac{2\Omega k_1 \tilde{k} a_2}{k^2} = 0 . \quad (11)$$

The initial condition is

$$\tilde{a}(\tilde{k}, 0) = FT(y_0) = \tilde{a}_0(\tilde{k}) . \quad (12)$$

For given  $k_1, k_3$ , equation 11 is a linear wave equation on  $k_2$  and  $t$ . Thus substitute

$$\tilde{a}(k_1, k_2, k_3, t) = \tilde{A}(k_1, k_2, k_3, k_2 + \Omega t k_1) ,$$

and write

$$k_{o2} = k_2 + \Omega t k_1 .$$

Then

$$\frac{\partial \tilde{a}}{\partial t} - \Omega k_1 \frac{\partial \tilde{a}}{\partial k_2} = -\Omega k_1 \frac{\partial \tilde{A}}{\partial k_2} ,$$

and equation 11 becomes

$$k_1 \frac{\partial \tilde{A}}{\partial k_2} = A_2(1, 0, 0) - \frac{2k_1 k A_2}{k^2} ,$$

with the initial condition

$$\tilde{A}(k_1, k_{o2}, k_3, k_{o2}) = \tilde{a}_o(k_1, k_{o2}, k_3) .$$

In subscript form,

$$\frac{\partial A_i(k_2, k_{o2})}{\partial k_2} = T_i(k_2) A_2, \quad A_i(k_{o2}, k_{o2}) = a_{oi}(k_{o2}) ,$$

where the functional dependence on  $k_1, k_3$  is understood, and

$$T_i = \frac{1}{k_1} \left( \delta_{i1} - \frac{2k_i k_1}{k^2} \right) .$$

The solutions  $A_i$  can be written in the form

$$A_i(k_2, k_{o2}) = L_{ij}(k_2, k_{o2}) a_{oj}(k_{o2})$$

where

$$L_{ij}(k_{o2}, k_{o2}) = \delta_{ij} . \tag{13}$$

Then the equation of motion is

$$\frac{\partial L_{ij}}{\partial k_2} = T_i(k_2) L_{2j} \quad (14)$$

with the initial condition 13. Equation 14 is integrated in Appendix A.

The result is

$$L_{ij} = \left\{ \begin{array}{ccc} 1 & - \left( \frac{k_3^2 k_o^2}{k_1 \ell^3} [\theta] + \frac{k_1 k_o^2}{\ell^2} \left[ \frac{k_2}{k^2} \right] \right) & 0 \\ 0 & \frac{k_o^2}{k^2} & 0 \\ 0 & \frac{k_o^2 k_3}{\ell^3} \left( [\theta] - \ell \left[ \frac{k_2}{k^2} \right] \right) & 1 \end{array} \right\} \quad (15)$$

where the index j designates columns, and

$$k^2 = k_1^2 + k_2^2 + k_3^2,$$

$$\ell^2 = k_1^2 + k_3^2$$

$$k_o^2 = k_1^2 + k_{o2}^2 + k_3^2,$$

$$\left[ \frac{k_2}{k^2} \right] = \frac{k_2}{k^2} - \frac{k_{o2}}{k_o^2},$$

$$[\theta] = \tan^{-1} \left( \frac{\ell}{k_2} \right) - \tan^{-1} \left( \frac{\ell}{k_{o2}} \right).$$

$[f_n(k_2)]$  means  $f_n(k_2) - f_n(k_{o2})$ .  $\theta$  is the polar angle of  $\underline{k}$  measured from the  $k_2$  axis and has values between 0 and  $\pi$ . The solution for  $\underline{a}$  is thus

$$a_i(\underline{k}, t) = L_{ij}(\underline{k}, k_{o2}) a_{oj}(k_1, k_{o2}, k_3), \quad (16)$$

where

$$k_{o2} = k_2 + \Omega t k_1 ,$$

and  $L_{ij}$  is given in equation 15.\*

If the initial turbulent field consists of eddies whose dimensions are roughly  $L$  in all directions, then  $a_o(k_1, k_{o2}, k_3)$  should tend to zero as any one of its arguments becomes large compared with  $L^{-1}$ . But for  $\Omega t \gg 1$ ,  $k_{o2}$  is indeed very large unless  $k_1$  is very small compared with  $L^{-1}$ . Thus equation 16 implies that, as time passes, only Fourier modes with  $k_1 \ll L^{-1}$  can become excited. If it is legitimate to translate that statement into eddy language, the implication is that after a long time the turbulent motion will consist of eddies greatly elongated in the x direction. Furthermore, equation 15 shows that the  $L_{12}$  component of  $L_{ij}$  is large for  $k_1$  small, so the  $a_1$  components of the Fourier modes which remain excited for  $\Omega t \gg 1$  should be excited very strongly. The qualitative picture that emerges, based, to be sure, on the analogy between Fourier modes and physical eddies, is that of elongated columns of fluid surging in the direction of mean flow.

---

\* I have followed the notation but not the approach of Moffatt [5], who derives equations 15 and 16 by watching the evolution of a single Fourier mode whose wave vector  $\underline{k}$  is a function of time. His approach is physically illuminating for the specific problem of the evolution of a shear wave, but the connection between his Fourier modes with time varying wave vectors and the modes  $a(\underline{k}, t)$  ordinarily discussed in turbulence theory is not quite clear and leads me to some confusion when he sums his modes for the turbulence problem.

B. Correlation and Spectrum Functions of the Solutions to the Linear Problem

The correlation function for the turbulent velocity field  $u_i(\underline{x})$  is defined as

$$R_{ij}(\underline{x}, \underline{r}) = \overline{u_i(\underline{x})u_j(\underline{x}+\underline{r})} ,$$

and since the field is statistically homogeneous in the  $x_1$  and  $x_3$  directions,

$$R_{ij}(\underline{x}, \underline{r}) = R_{ij}(y, \underline{r}) .$$

The time argument in all quantities is understood. Homogeneity further requires

$$R_{ij}(y, \underline{r}) = R_{ji}(y+r_2, -\underline{r}) . \quad (17)$$

The flow should be statistically invariant under reflection through a plane perpendicular to the  $x_3$  axis. Since the only velocity component which changes its sign under such a reflection is  $u_3$ ,

$$R_{ij}(y, r_1, r_2, r_3) = R_{ij}(y, r_1, r_2, -r_3), \quad i, j \neq 3 .$$

For  $i$  or  $j = 3$ , the relation holds with a minus sign on the right, and for both  $i$  and  $j = 3$ , the relation is true as it stands. A final condition is imposed on  $R_{ij}$  by the continuity equation:

$$\frac{\partial}{\partial r_j} R_{ij}(y, \underline{r}) = 0 .$$

If  $u_i(\underline{x})$  and  $u_j(\underline{x}+\underline{r})$  are Fourier analyzed according to equation 10, then  $R_{ij}$  can be written

$$R_{ij}(y, \underline{r}) = \iint \frac{1}{a_i(\underline{k}')a_j(\underline{k})} e^{i(\underline{k}+\underline{k}') \cdot \underline{r}} e^{i\underline{k} \cdot \underline{r}} d\underline{k}' d\underline{k} .$$

Since the left side does not depend on  $x_1$  or  $x_3$ ,

$$\overline{a_i(\underline{k}')a_j(\underline{k})} = A_{ij}(k'_2, \underline{k}) \delta(k'_1+k_1) \delta(k'_3+k_3) .$$

The spectrum function  $A_{ij}$  defined by this relation depends on  $k_1, k_3$  and both  $k_2$  and  $k'_2$ , since the velocity field is inhomogeneous in the  $y$  direction. The integrations over  $k'_1$  and  $k'_3$  in the expression for  $R_{ij}$  can be performed immediately to give

$$R_{ij}(y, \underline{r}) = \int A_{ij}(k'_2, \underline{k}) e^{i(k_2+k'_2)y} e^{i\underline{k} \cdot \underline{r}} dk'_2 d\underline{k} . \quad (18)$$

Since  $R_{ij}$  is real,

$$A_{ij}^*(k'_2, \underline{k}) = A_{ij}(-k'_2, -\underline{k}) .$$

The symmetry condition 17 imposes a further restriction on  $A_{ij}$ , since

$$\begin{aligned} R_{ji}(y+r_2, -\underline{r}) &= \int A_{ji}(k'_2, \underline{k}) e^{i(k_2+k'_2)y} e^{-i(k_1 r_1 + k_3 r_3) + ik'_2 r_2} dk'_2 d\underline{k}, \\ &= \int A_{ji}(k_2, -k_1, k'_2, -k_3) e^{i(k_2+k'_2)y} e^{i\underline{k} \cdot \underline{r}} dk'_2 d\underline{k} . \end{aligned}$$

Comparing that with equation 18,

$$A_{ij}(k'_2, k_1, k'_2, k_3) = A_{ji}(k_2, -k_1, k_2, -k_3) .$$

The condition on the reflectional symmetry of  $R_{ij}$  implies

$$A_{ij}(k'_2, k_1, k_2, k_3) = A_{ij}(k'_2, k_1, k_2, -k_3), \quad i, j \neq 3 . \quad (19)$$

The incompressibility condition imposes a final restriction —

$$k_j A_{ij}(k'_2, \underline{k}) = 0 .$$

The linearized solution of the last subsection can be used to find  $A_{ij}$  as an explicit function of time. From equation 16,

$$\begin{aligned} A_{ij}(k'_2, \underline{k}, t) \delta(k'_1+k_1) \delta(k'_3+k_3) &= \overline{a_i(\underline{k}', t) a_j(\underline{k}, t)} , \\ &= L_{i\ell}(\underline{k}', k'_{o2}) L_{jm}(\underline{k}, k_{o2}) \overline{a_{o\ell}(k'_1, k'_{o2}, k'_3) a_{om}(k_1, k_{o2}, k_3)} , \\ &= L_{i\ell}(\underline{k}', k'_{o2}) L_{jm}(\underline{k}, k_{o2}) A_{\ell m}(k'_{o2}, \underline{k}_o, 0) \delta(k'_1+k_1) \delta(k'_3+k_3) , \end{aligned}$$

where

$$\begin{aligned} k_{o2} &= k_2 + \Omega t k_1 , \\ k'_{o2} &= k'_2 + \Omega t k'_1 , \end{aligned}$$

and  $\underline{k}_o$  denotes the vector  $(k_1, k_{o2}, k_3)$ . The expression for  $A_{ij}$  as a function of time is now obtained by integrating the equation above over  $k'_1$  and  $k'_3$ :

$$\begin{aligned} A_{ij}(k'_2, \underline{k}, t) &= L_{i\ell}(-k'_1, k'_2, -k'_3, k'_{o2}) L_{jm}(k_1, k_2, k_3, k_{o2}) \quad (20) \\ &A_{\ell m}^o(k'_{o2}, k_1, k_{o2}, k_3) , \end{aligned}$$

where now

$$k'_{o2} = k'_2 - \Omega t k_1 ,$$

and

$$A_{\ell m}^o(k'_{o2}, \underline{k}_o) = A_{\ell m}(k'_{o2}, \underline{k}_o, 0) .$$

Equations 18 and 20 give  $R_{ij}(y, \underline{r}, t)$  when the initial spectrum function  $A_{lm}^0$  is known and the linearized equation of motion is valid. Only  $R_{ij}(y, 0, t)$  will be considered from now on, and in that case the integration in equation 18 is more easily carried out over  $k'_{o2}, k_1, k_{o2}, k_3$  than over  $k'_2, k_1, k_2, k_3$ . The Jacobian of the transformation is 1, since

$$k_2 = k_{o2} - \Omega t k_1 ,$$

$$k'_2 = k'_{o2} + \Omega t k_1 .$$

Thus

$$R_{ij}(y, 0, t) = \int_{-\infty}^{\infty} \int_{-\infty}^{\infty} \int_{-\infty}^{\infty} L_{i\ell}(-k_1, k'_2, -k_3, k'_{o2}) L_{jm}(k_1, k_2, k_3, k_{o2}) A_{lm}^0(k'_{o2}, k_1, k_{o2}, k_3) e^{i(k_{o2} + k'_{o2})y} dk'_{o2} dk_{o2} dk_1 dk_3 . \quad (21)$$

In the next subsection, the Reynolds stress  $\sigma(y, t) = -R_{21}(y, 0, t)$  is found for a special case where equation 21 simplifies for arbitrary  $t$ . After that, some general consequences of equation 21 in the limit  $\Omega t \gg 1$  are derived.

### C. Reynolds Stress above a Sheet of Random Vorticity

Suppose prior to time  $t = 0$  there are no turbulent fluctuations in the velocity field, and at  $t = 0$  a random impulse per unit area  $f(x, y)$  is applied at  $y = 0$  over the  $x, z$  plane. A collection of lifting surfaces might be shot over the  $x, z$  plane at  $t = 0$ , for example. The inviscid equation of motion for the total velocity  $\underline{y}$  is

$$\frac{\partial \underline{y}}{\partial t} + \underline{y} \cdot \nabla \underline{y} + \nabla \pi = \int \underline{f}(x, z) \delta(y) \delta(t) \cdot$$

By integrating the equation across  $t = 0$ , a new initial field  $\underline{y}_0$  is found,

$$\underline{y}_0(\underline{x}) - \underline{U}_0(\underline{x}) + \nabla \phi = \int \underline{f}(x, z) \delta(y)$$

where  $\phi$  is the impulse of the pressure. The initial turbulent field  $\underline{y}_0(\underline{x})$  then satisfies

$$\underline{y}_0(\underline{x}) + \nabla \phi = \int \underline{f}(x, z) \delta(y) \quad (22)$$

and the continuity condition

$$\nabla \cdot \underline{y}_0(\underline{x}) = 0.$$

Thus  $\underline{y}_0$  is a potential flow,  $\underline{y}_0 = -\nabla \phi$ , for  $y \neq 0$ . Phillips [4] treated a similar situation in his paper on the potential flow above a wall of random pistons, an idealization of the flow above a turbulent boundary layer or wake. The difference here is that there is no wall of random pistons, but a sheet of random vorticity; there must be a legitimate velocity field over all physical space. Suppose the potential just above the  $x, z$  plane is  $\phi_1$  and just below is  $\phi_2$ . Since the  $y$  component of  $\underline{y}_0$  must be continuous at  $y = 0$ , equation 22 can be integrated across  $y = 0$  to give

$$\phi_1 - \phi_2 = f(x, z).$$

There is thus a velocity slip  $\Delta \underline{y}_0$  through the  $x, z$  plane given by

$$\Delta \underline{y}_0 = -\nabla_1(\phi_1 - \phi_2) = -\nabla_1 f, \quad (23)$$

where  $\nabla_1$  means a gradient in the  $x, z$  directions only. After the impact at  $t = 0$ , the  $x, z$  plane is covered by a sheet of random concentrated vorticity, and the initial turbulent flow is potential out of

the plane. Since there is no random vorticity beyond  $y = 0$ , there is no initial Reynolds stress. That is a consequence of integrating the equation

$$\frac{\partial(-\overline{uv})}{\partial y} = \overline{v\omega} - \overline{w\eta}$$

down from  $y \rightarrow \infty$ . The problem of the initial random vortex sheet is thus ideal for the examination of random vorticity generation by turbulent interaction with the mean field.

The object now is to find  $A_{lm}^0$  corresponding to the  $u_0(\underline{x})$  given by equation 22 and to use equation 21 to find the Reynolds stress as a function of  $y$  and  $t$ . The Fourier transformations of  $u_0$ ,  $\phi$  and  $f$  are needed, say

$$\text{FT}(u_0) = a_0(\underline{k}) ,$$

$$\text{FT}(\phi) = \tilde{\phi}(\underline{k}) ,$$

$$\text{FT}_1(f) = \tilde{f}(\underline{l}) ,$$

where  $\text{FT}_1$  means Fourier transformation over the  $x, z$  plane only, and  $\underline{l} = (k_1, k_3)$ . Then

$$\text{FT}(\nabla\phi) = i\underline{k}\tilde{\phi} ,$$

$$\text{FT}(f(x, z)\delta(y)) = \frac{1}{2\pi}\tilde{f} ,$$

$$\text{FT}(\nabla \cdot u_0) = i\underline{k} \cdot a_0 ,$$

and the Fourier transformed momentum and continuity equations are

$$\underline{a}_0(\underline{k}) + i\underline{k}\tilde{\phi}(\underline{k}) = j \frac{1}{2\pi} \tilde{f}(\underline{\ell}) ,$$

$$\underline{k} \cdot \underline{a}_0(\underline{k}) = 0 .$$

Dotting the momentum equation with  $\underline{k}$  and using continuity gives

$$\tilde{\phi} = \frac{\tilde{f}}{2\pi i} \frac{k_2}{k} ,$$

so

$$\underline{a}_0(\underline{k}) = \frac{\tilde{f}}{2\pi} \left( j - \frac{\underline{k}k_2}{k^2} \right) .$$

In particular,

$$\begin{aligned} a_{01} &= - \frac{\tilde{f}}{2\pi} \frac{k_1 k_2}{k^2} , \\ a_{02} &= \frac{\tilde{f}}{2\pi} \frac{\ell^2}{k} . \end{aligned} \tag{24}$$

Suppose the spectrum function of  $f$  is  $\psi(\underline{\ell}) -$

$$\overline{\tilde{f}(\underline{\ell}) \tilde{f}(\underline{\ell}')} = \psi(\underline{\ell}) \delta(\underline{\ell} + \underline{\ell}') .$$

A relationship between  $\psi(\underline{\ell})$  and the spectrum function  $\Theta(\underline{\ell})$  of the upwash distribution used by Phillips can be found. The upwash at  $y = 0$  is  $u_{02}(x, 0, z)$ ; suppose

$$FT_1(u_{02}(x, 0, z)) = a(\underline{\ell}) .$$

But

$$\begin{aligned} u_{02}(x, 0, z) &= \int a_{02} e^{i(k_1 x_1 + k_3 x_3)} d\underline{k} , \\ &= \int \frac{\tilde{f}(\underline{\ell})}{2\pi} \frac{\ell^2}{\ell^2 + k_2^2} e^{i\underline{\ell} \cdot \underline{x}} dk_2 d\underline{\ell} , \end{aligned}$$

$$= \int \frac{\ell f(\underline{\ell})}{2} e^{i\underline{\ell} \cdot \underline{x}} d\underline{\ell} .$$

Thus

$$a(\underline{\ell}) = \frac{\ell \tilde{f}(\underline{\ell})}{2} ,$$

where  $\ell$  is the magnitude of  $\underline{\ell}$ , and

$$\Theta(\underline{\ell}) = \frac{\ell^2}{4} \psi(\underline{\ell}) .$$

As  $\underline{\ell} \rightarrow 0$ ,

$$\Theta(\underline{\ell}) \Rightarrow \frac{\ell^2}{2} \psi(0) . \tag{25}$$

The large scale contribution to the upwash is thus isotropic with respect to rotations in the  $x, z$  plane regardless of the character of  $\psi$ , an interesting example of pressure forces leading to isotropy. Furthermore,  $\Theta$  is  $O(\ell^2)$  when  $\psi$  has a finite value at  $\underline{\ell} = 0$ . This leads to a surprising physical conclusion as follows.  $\psi$  is the Fourier transform of the impulse correlation function  $\overline{f(x, z)f(x', z')}$ ,

$$\overline{f(x, z)f(x', z')} = \int \psi(\underline{\ell}) e^{i\underline{\ell} \cdot (\underline{x} - \underline{x}')} d\underline{\ell} .$$

By inverse Fourier transformation,

$$\psi(0) = \int \overline{f(x, z)f(x', z')} d(\underline{x} - \underline{x}') .$$

If  $f$  satisfies an ergodic property, so ensemble averages can be replaced with averages over large portions of the  $x, z$  plane,

$$\begin{aligned} \psi(0) &= \lim_{A \rightarrow \infty} \left[ \frac{1}{A} \int \int_{AA} f(x, z) f(x', z') \, dx \, dx' \right] \\ &= \lim_{A \rightarrow \infty} \left[ \frac{1}{\sqrt{A}} \int_A f(x, z) \, dx \right]^2 . \end{aligned}$$

If the  $f(x, z)$  over separate patches of the plane behave like uncorrelated random impulses, the integral diverges like  $\sqrt{A}$ , and  $\psi(0) \neq 0$ . Similarly,

$$\Theta(0) = \lim_{A \rightarrow \infty} \left[ \frac{1}{\sqrt{A}} \int_A u_{o2}(x, 0, z) \, dx \right]^2 .$$

But equation 25 requires  $\Theta(0) = 0$  even if  $\psi(0) \neq 0$ . Thus a spatially random impulse generates an upwash with negative correlation between neighboring patches; in other words, if fluid is slammed down in one place, it is likely to squirt up nearby. Since

$$FT_1(\Delta u_o) = -FT_1(\nabla_1 f) = -i\ell \tilde{f}$$

from equation 23, the spectral distribution of the slip velocity is also  $O(\ell^2)$  as  $\ell \rightarrow 0$  for  $\psi(0) \neq 0$ . Phillips used  $\Theta(0) = 0$  and got results in good agreement with experiment, but his demonstration for  $\Theta(0) = 0$  was in error. It is now apparent that if the turbulence is generated by impulses in the fluid itself rather than by pistons in a wall,  $\Theta(0) = 0$  is a natural result.

The Reynolds stress  $\sigma(y, t)$  equals  $-R_{12}(y, 0, t)$  or  $-R_{21}(y, 0, t)$ . The way equation 21 is set up, fewer primes have to be written if  $R_{21}$  is computed. Since  $L_{13}$ ,  $L_{21}$  and  $L_{23}$  are zero, the integrand for

$R_{21}$  in equation 21 has the form

$$L_{2\ell} L_{1m} A_{\ell m}^{\circ} = L_{22} L_{11} A_{21}^{\circ} + L_{22} L_{12} A_{22}^{\circ} . \quad (26)$$

From equations 24,

$$A_{21}^{\circ}(k_2', k) = \frac{\Theta(\tilde{\ell})}{\pi^2} \frac{k_1 k_2}{k^2 k'^2} ,$$

$$A_{22}^{\circ}(k_2', k) = \frac{\Theta(\tilde{\ell})}{\pi^2} \frac{\ell^2}{k^2 k'^2} ,$$

where  $k' = (k_1, k_2', k_3)$ . Equations 15 and 21 give the Reynolds stress as a sum of complicated integrals:

$$\begin{aligned} \sigma(y, t) = -R_{21}(y, 0, t) &= I_1 + I_2 + I_3 , \\ I_1 &= \int \frac{k_o'^2}{k'^2} \frac{\Theta(\tilde{\ell})}{\pi^2} \frac{k_1 k_{o2}}{k_o^2 k_o'^2} e^{i(k_{o2} + k_{o2}')y} dk_{o2}' dk_{o2} d\tilde{\ell} , \\ I_2 &= \int \frac{k_o'^2}{k'^2} \frac{k_3^2 k_o^2}{k_1 \ell^3} [\theta] \frac{\Theta(\tilde{\ell})}{\pi^2} \frac{\ell^2}{k_o^2 k_o'^2} e^{i(k_{o2} + k_{o2}')y} dk_{o2}' dk_{o2} d\tilde{\ell} , \\ I_3 &= \int \frac{k_o'^2}{k'^2} \frac{k_1 k_o^2}{\ell^2} \left[ \frac{k_2}{k} \right] \frac{\Theta(\tilde{\ell})}{\pi^2} \frac{\ell^2}{k_o^2 k_o'^2} e^{i(k_{o2} + k_{o2}')y} dk_{o2}' dk_{o2} d\tilde{\ell} . \end{aligned} \quad (27)$$

The geometrical quantities appearing in the integrals have been defined under equation 15 and in equations 21. The great advantage of the vortex sheet problem is that the integrals  $I_1$  and  $I_3$  cancel identically. That is shown in Appendix B, and the integrations over  $k_{o2}$  and  $k_{o2}'$  in  $I_2$  are also carried out to give the final result

$$\sigma(y, t) = \int \Theta(\tilde{\ell}) \frac{k_3^2}{\ell^2} \frac{\sin(\Omega t k_1 y)}{k_1 y} e^{-2\ell |y|} d\tilde{\ell} . \quad (28)$$

The implications of equation 28 become clear when several limiting cases are studied.

(i)  $\Omega t \rightarrow 0$ . Then

$$\sigma(y, t) \Rightarrow \Omega t \int_{\Theta} (\underline{\ell}) \frac{k_3^2}{\ell^2} e^{-2\ell |y|} d\ell = \Omega t f_n(y) ,$$

so the Reynolds stress is zero at  $t = 0$ , a result anticipated earlier, and begins to grow linearly with time.

(ii)  $\Omega t \rightarrow \infty$ . Substitute  $k = \ell |y|$  in equation 28 -

$$\sigma(y, t) = \frac{1}{y^2} \int_{\Theta} \left( \frac{k}{|y|} \right) \frac{k_3^2}{k^2} \frac{\sin(\Omega t k_1)}{k_1} e^{-2|k|} dk . \quad (29)$$

As  $\Omega t \rightarrow \infty$ ,  $\sin(\Omega t k_1)/k_1$  behaves like a  $\delta$ -function of weight  $\pi$  in the integration over  $k_1$ , and except at  $y = 0$ ,

$$\sigma(y, t) \Rightarrow \frac{\pi}{y^2} \int_{-\infty}^{\infty} \Theta \left( 0, \frac{k_3}{|y|} \right) e^{-2|k_3|} dk_3 = f_n(y) , \quad (30)$$

provided  $\Theta(0, k_3)$  exists. The case where  $\Theta(0, k_3)$  does not exist, where all the initial turbulent vorticity is aligned in the  $x_1$  direction, is discussed in section 4. For a roughly isotropic initial turbulent flow, the stress relaxes into a steady distribution except at  $y = 0$ .

(iii)  $y \rightarrow 0$ . Hold  $t$  fixed and take the limit  $y \rightarrow 0$  in equation 28:

$$\sigma(0, t) = \Omega t \int_{\Theta} (\underline{\ell}) \frac{k_3^2}{\ell^2} d\ell .$$

The Reynolds stress at  $y = 0$  grows linearly with time for all time.

(iv)  $y \rightarrow \infty$ . Take the limit  $y \rightarrow \infty$  in equation 29. For  $\ell$  small,

$$\Theta(\ell) \Rightarrow \frac{\ell^2}{4} \psi(0)$$

from equation 25. That relation can be substituted in the integrand of equation 29 except where  $\kappa$  is large, and the exponential factor eliminates contributions to the integral from regions of large  $\kappa$  anyway. Thus

$$\sigma(y, t) \Rightarrow \frac{\psi(0)}{4y^4} \int \kappa_3^2 \frac{\sin(\Omega t \kappa_1)}{\kappa_1} e^{-2|\kappa|} d\kappa = \frac{\psi(0)}{4y^4} f_n(t).$$

Hence the stress decreases as  $y^{-4}$ , for  $y$  large compared with the length scale of the original fluctuations, for all time. Phillips [4] found a  $y^{-4}$  decrease for the fluctuation mean energy density in his potential flow problem.

(v)  $\Omega t \rightarrow \infty$ ,  $y \rightarrow \infty$ . As  $\Omega t \rightarrow \infty$  in the last equation,  $\sin(\Omega t \kappa_1)/\kappa_1$  again behaves like a  $\delta$ -function, and

$$\sigma(y, t) \Rightarrow \frac{\pi \psi(0)}{4y^4} \int_{-\infty}^{\infty} \kappa_3^2 e^{-2|\kappa_3|} d\kappa_3 = \frac{1}{8} \left(\frac{\pi}{2}\right)^{3/2} \frac{\psi(0)}{y^4}.$$

The evolving stress profile is sketched in figure 4. The details, of course, depend on a detailed specification of  $\psi(\ell)$ , the spectral distribution of the impulse. The important point is that the stress relaxes into a steady profile as  $\Omega t$  becomes large, except at the sheet of concentrated vorticity itself. This behavior is not peculiar to the vortex sheet problem, but occurs for any (roughly isotropic) initial conditions. That is shown in the next subsection.

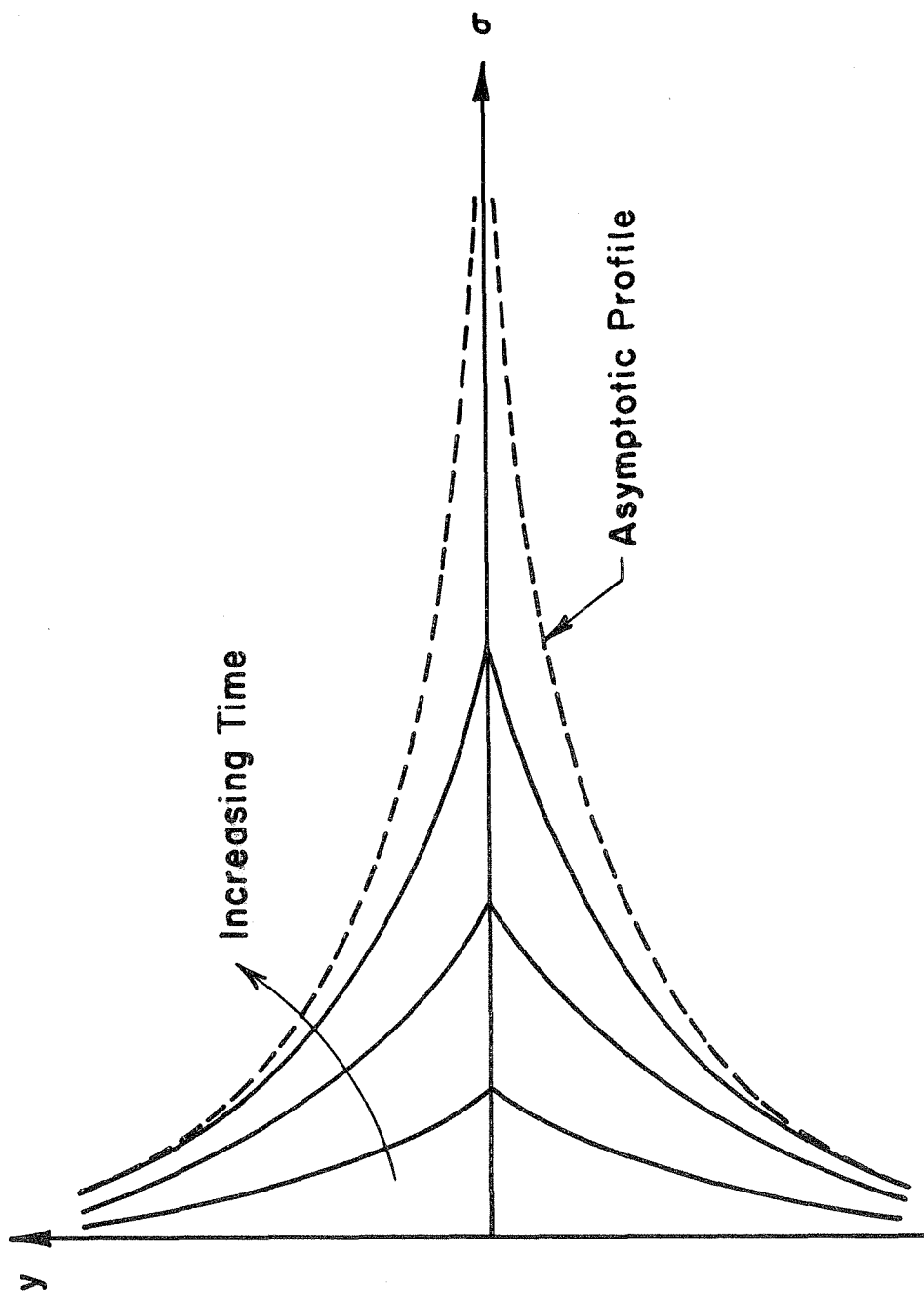


FIG. 4 STRESS HISTORY NEAR A VORTEX SHEET

D. Reynolds Stress in the Limit  $\Omega t \rightarrow \infty$  of the General Problem

In the general case, the integrand for  $R_{21}$  in equation 21 still has the form given in equation 26. Since  $k'_2 = k'_{o2} + \Omega t k_1$  from equations 21, the factor  $L_{22} = (\ell^2 + k'_{o2}{}^2)/(\ell^2 + k'_2{}^2)$  in front of both terms in equation 26 forces the integrand to zero as  $\Omega t \rightarrow \infty$ , except in regions of small  $k_1$ . But equation 15 shows that the first term of  $L_{12}$  has a  $k_1$  in the denominator, and the portion of the integrand containing that factor should give the dominant contribution to the Reynolds stress for large times. Thus the Reynolds stress should be approximately

$$\sigma(y, t) = \int \frac{(\ell^2 + k'_{o2}{}^2)(\ell^2 + k'_2{}^2) k_3^2}{k_1 \ell^3 [\ell^2 + (k'_{o2} + \Omega t k_1)^2]} \left[ \cot^{-1} \left( \frac{k_{o2} - \Omega t k_1}{\ell} \right) - \cot^{-1} \left( \frac{k_{o2}}{\ell} \right) \right] \quad (31)$$

$$A_{22}^o(k'_{o2}, k_1, k_{o2}, k_3) e^{i(k_{o2} + k'_{o2})y} dk'_{o2} dk_{o2} dk_1 dk_3 .$$

This corresponds to the quantity  $I_2$  defined in equations 27 for the vortex sheet problem. In that problem the other terms,  $I_2$  and  $I_3$ , cancelled identically. Generally they do not cancel, but the fact that they are negligible in the limit  $\Omega t \rightarrow \infty$  is established in Appendix C.

Transform the variables of integration in equation 31 as follows:

$$\begin{aligned} k_{o2} &= \ell \beta , \\ k'_{o2} &= \ell \beta' , \\ k_1 &= \ell \cos \phi , \\ k_3 &= \ell \sin \phi . \end{aligned} \quad (32)$$

The Jacobian of the transformation is  $l^3$ . Thus

$$\sigma(y, t) = \int_{-\infty}^{\infty} \int_{-\infty}^{\infty} \int_0^{\infty} \int_0^{2\pi} \frac{(1+\beta^2)(1+\beta'^2)l^3 \sin^2 \phi}{\cos \phi [1+(\beta'+\Omega t \cos \phi)^2]} [\cot^{-1}(\beta-\Omega t \cos \phi) - \cot^{-1} \beta] A_{22}^0(\beta'l, l \cos \phi, \beta l, l \sin \phi) e^{i(\beta+\beta')ly} d\phi dl d\beta d\beta'.$$

It can be shown easily that

$$\int_0^{2\pi} f(\sin \phi, \cos \phi) d\phi = 2 \int_0^{\pi} f(\sin \phi, \cos \phi) d\phi$$

for a function  $f$  symmetric on its first argument.  $A_{22}^0$  is symmetric on its last argument by equation 19, so  $\phi$  may be integrated from 0 to  $\pi$  only, and the result multiplied by 2. Now substitute

$$\xi = -\Omega t \cos \phi. \tag{33}$$

Then

$$\frac{\sin^2 \phi}{\cos \phi} d\phi = -\sqrt{1 - \left(\frac{\xi}{\Omega t}\right)^2} \frac{d\xi}{\xi}$$

for  $0 \leq \phi \leq \pi$ , and the stress integral is

$$\sigma(y, t) = -2 \int_{-\infty}^{\infty} \int_{-\infty}^{\infty} \int_0^{\infty} \int_{-\Omega t}^{\Omega t} \frac{(1+\beta^2)(1+\beta'^2)l^3}{\xi [1+(\beta'-\xi)^2]} [\cot^{-1}(\beta+\xi) - \cot^{-1} \beta] \sqrt{1 - \left(\frac{\xi}{\Omega t}\right)^2} A_{22}^0(\beta'l, -\frac{l\xi}{\Omega t}, \beta l, l\sqrt{1 - \left(\frac{\xi}{\Omega t}\right)^2}) e^{i(\beta+\beta')ly} d\xi dl d\beta d\beta'.$$

So far no approximations have been made in transforming the particular term of  $\sigma(y, t)$  retained in equation 31. The next step is to

find the limit of  $\sigma(y,t)$  as  $\Omega t \rightarrow \infty$ . The limit can be taken in the expression above before an explicit integration is carried out if the resulting integral converges for large  $\xi$ . But the integrand is of order  $\xi^{-3}$  for large  $\xi$ , the integral thus converges, and in the limit  $\Omega t \rightarrow \infty$ ,

$$\sigma(y,t) \Rightarrow -2 \int_{-\infty}^{\infty} \int_{-\infty}^{\infty} \int_0^{\infty} \int_{-\infty}^{\infty} \frac{(1+\beta^2)(1+\beta'^2)\ell^3}{\xi[1+(\beta'-\xi)^2]} [\cot^{-1}(\beta+\xi) - \cot^{-1}\beta] A_{22}^0(\beta'\ell, 0, \beta\ell, \ell) e^{i(\beta+\beta')\ell y} d\xi d\ell d\beta d\beta' . \quad (34)$$

Equation 34 is the general analog of equation 30 for the vortex sheet problem and shows that in the general case the stress relaxes into a steady profile as  $\Omega t \rightarrow \infty$ . Again, the assumption that the initial flow is 'roughly isotropic,' i.e., that  $A_{\ell m}^0(k'_2, 0, k_2, k_3)$  exists, has been made. The same chain of transformations that led to equation 34 is used in Appendix C to show that the largest term left out of equation 31 is  $O(\Omega t)^{-1}$  in the limit  $\Omega t \rightarrow \infty$ .

The physical situation behind the asymptotically steady stress  $\sigma(y,t) = -\overline{uv}$  can be seen more clearly by considering the mean square values of  $u$  and  $v$  separately.  $\overline{v^2}$  is easy to find, since the integrand of equation 21 for  $R_{22}$  contains only one non-zero term,  $L_{22}L_{22}A_{22}^0$ . The integrand for  $\overline{u^2}$  contains several terms, the dominant one being  $L_{12}L_{12}A_{22}^0$  as  $\Omega t \rightarrow \infty$ . There is no point in repeating the kind of argument which led from equation 31 to 34. Provided the transformed integral of a term in equation 21 converges as  $\xi \rightarrow \infty$  (and it does for  $\overline{v^2}$  or the dominant term of  $\overline{u^2}$ ), the term is  $O(\Omega t)^{n-1}$

as  $\Omega t \rightarrow \infty$ , where  $n$  is the power of  $k_1$  in the denominator of the integrand. A glance at equation 15 shows that

$$\overline{u^2} \Rightarrow O(\Omega t)$$

$$\overline{v^2} \Rightarrow O(\Omega t)^{-1},$$

as  $\Omega t \rightarrow \infty$ . Thus mean field interaction with the turbulence imposes a heavy veto on vertical fluctuations but promotes high-speed surges in the direction of mean flow. This observation was made by Moffatt for the case of homogeneous turbulence, and was already apparent from equations 15 and 16. A rough physical description of the process goes as follows. A blob of fluid may be moving upward at  $t = 0$ . As it moves it tends to retain its original speed in the  $x$  direction, but it is sheared out flat perpendicular to the  $y$  axis and loses upward momentum to the fluid around it. It is left as an elongated and flattened slab of fluid lagging behind the mean flow of its surroundings. The Reynolds stress  $-\overline{uv}$  becomes steady as the  $u$  fluctuations become large because of vertical convection, and the  $v$  fluctuations themselves drop to zero.

Equations 30 or 34 are embarrassing results in a study aimed at the propagation of turbulence through mean shear flows. As  $\Omega \rightarrow \infty$ , the turbulence stops propagating. Apparently, any properties of the equations of motion that would have led to a diffusion of Reynolds stress have been lost in the linearization. In the next section a more restricted class of initial conditions is considered, and non-linear effects, in some measure, are restored.

4. Flow Uniform in the x Direction

A. The  $\partial F / \partial x = 0$  Assumption

If a roughly symmetrical blob of fluid begins to rise, it is elongated and flattened against its line of ascent by the mean shear flow, its apparent mass (associated with displacement of the fluid around it) increases, its rate of ascent decreases, and the blob becomes a shaft of fluid lagging behind the mean flow of its surroundings. This picture is appropriate if the initial turbulent flow can be blocked off into roughly symmetrical and independent blobs. The picture is meaningless when the original turbulence consists of eddies uniform and infinitely elongated in the x direction, when distinguishable fluid blobs are columns to begin with. If the original eddies are independent of x, all flow properties are independent of x for all time. The inviscid equations of motion for the total velocity  $\mathbf{x}$  and pressure  $\pi$  are then

$$\frac{Dv_1}{Dt} = 0, \tag{35}$$

$$\left. \begin{aligned} \frac{Dv_2}{Dt} + \frac{\partial \pi}{\partial y} &= 0, \\ \frac{Dv_3}{Dt} + \frac{\partial \pi}{\partial z} &= 0, \\ \frac{\partial v_2}{\partial y} + \frac{\partial v_3}{\partial z} &= 0, \end{aligned} \right\} \tag{36}$$

where

$$\frac{D}{Dt} = \frac{\partial}{\partial t} + v_2 \frac{\partial}{\partial y} + v_3 \frac{\partial}{\partial z} .$$

The first equation states that the x component of momentum of a fluid column is conserved as the column is transported in the y, z plane. The next three equations, the y and z momentum equations and the continuity equation, are completely independent of  $v_1$  and describe the dynamics of two-dimensional, incompressible flow. Given an initial flow  $\underline{v}_0(y, z)$ ,  $v_2(y, z, t)$  and  $v_3(y, z, t)$  are found by solving the two-dimensional problem governed by equations 36, then  $v_1(y, z, t)$  is found by integrating equation 35 using the known histories of  $v_2$  and  $v_3$ . Averages are taken over an ensemble of  $\underline{v}_0(y, z)$ . If the initial fields have the form

$$\underline{v}_0(y, z) = \underline{i}U_0(y) + \underline{j}v_0(y, z) + \underline{k}w_0(y, z) ,$$

for example, where  $\overline{\underline{v}_0} = \underline{i}U_0$  and the initial perturbation velocity component  $u_0(y, z)$  is zero, then the initial Reynolds stress  $-\overline{uv}$  is zero, and the mean flow profile is  $U(y, t) = \overline{v_1(y, z, t)}$  for all t. The fluctuating part of the vorticity field which evolves from such an initial condition is not two-dimensional in the sense that the turbulent vorticity is aligned in the x direction. The initial turbulent vorticity is aligned in the x direction (for  $u_0(y, z) = 0$ ), but the field it induces stretches the mean field vorticity and produces a three-dimensional random vorticity field  $\underline{\omega} = (\xi, \eta, \zeta)$ . The assumption that  $\partial F / \partial x = 0$  for any flow property F implies only that  $\underline{\omega} = \underline{\omega}(y, z)$ .

The simplest example of the type of situation studied in this section is a line vortex on the x axis in a shear flow with an initial linear profile  $v_{01} = \Omega y$ . The geometry of the problem is shown in figure 5. Equations 36 are satisfied by a steady, tangential velocity

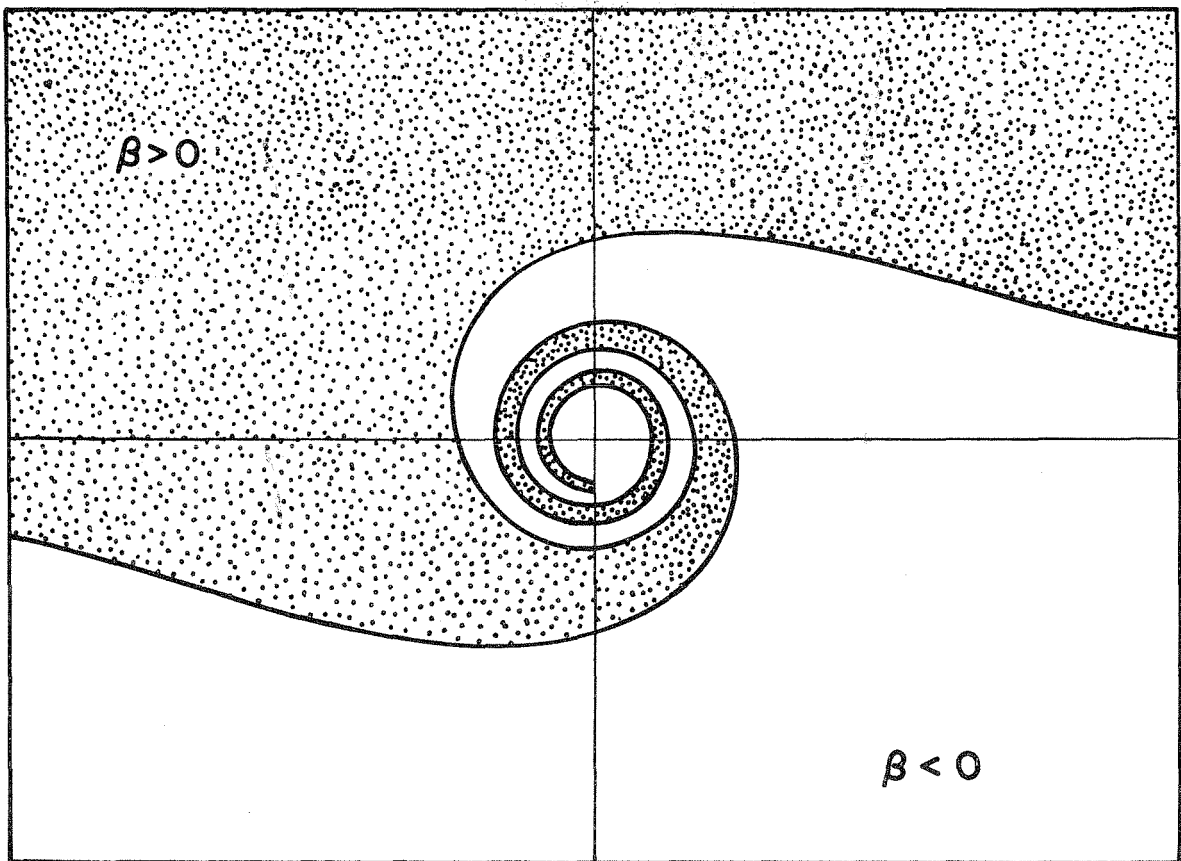
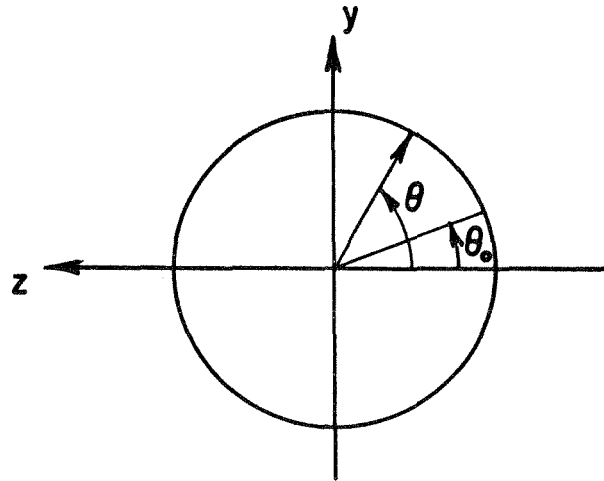


FIG. 5 A SHEAR FLOW WRAPPING AROUND A VORTEX

$v_\theta = k/2\pi r$ , where  $k$  is the circulation around the vortex and  $r$  is the distance from the origin in the  $y, z$  plane. A fluid column at  $r, \theta$  at time  $t$  originated at  $r, \theta_0$  at time 0, where

$$\theta_0 = \theta - \frac{kt}{2\pi r^2} .$$

The height  $y_0$  corresponding to its original location is  $r \sin \theta_0$ , and the original and, by equation 35, the final speed of the column in the  $x$  direction is  $\Omega y_0$ . Hence

$$v_1(r, \theta, t) = \Omega r \sin \left( \theta - \frac{kt}{2\pi r^2} \right) .$$

Set

$$v_1 = \Omega \sqrt{\frac{kt}{2\pi}} \beta ,$$

$$r = \sqrt{\frac{kt}{2\pi}} \rho .$$

Then

$$\beta = \rho \sin \left( \theta - \frac{1}{\rho^2} \right) .$$

A contour map of  $\beta(\rho, \theta)$  is shown in figure 5. The portion of the plane where  $\beta > 0$  is shaded. In physical space, the picture would expand with  $\sqrt{t}$ , and the speed at geometrically similar points would grow with  $\sqrt{t}$  as well.

A single vortex thus wraps the initial shear field into an expanding and tightening spiral of speeds of alternating sign, a surprisingly complicated flow for such a simple initial condition. Suppose  $v_1$  is measured over a circular patch in the  $y, z$  plane centered at

$r, \theta$  with a radius  $\delta \ll r$ . Initially the speed is about  $\Omega r \sin \theta$  everywhere on the patch. As the field induced by the vortex redistributes fluid columns, the speed trace over the patch distorts, forms loops, and eventually goes through high-pitched sinusoidal oscillations in the radial direction. The amplitude of the oscillations is  $\Omega r$  over the patch, and the wave length  $\lambda$  is  $2\pi^2 r^3 / kt$ . For  $t$  so large that  $\lambda \ll \delta$ , the average of the trace over the patch tends to zero. As  $t \rightarrow \infty$ , the speed  $v_1$  averaged in the vicinity of any point  $y, z$  approaches zero; a single vortex eventually stops the area-averaged flow anywhere. The radius  $R$  inside of which the flow is 'stopped' in this sense must satisfy  $2\pi R^2 / kt \lll 1$  so a  $\delta$  such that  $\lambda \ll \delta \ll R$  can be found. Thus  $R \ll \sqrt{kt/2\pi^2}$ , and  $r < \sqrt{kt}/40$ , say, in the region of 'stopped' (but highly striated) flow. The 'stopping power' of a single vortex thus depends on steady induction over a long interval of time. If the vortex itself moves in a turbulent field, no such interval is available, and the picture must change entirely.

What bearing does the  $\partial F / \partial x = 0$  problem have on the more general problem, where flow properties depend on  $x$  as well as  $y$  and  $z$ ? An obvious answer is that the  $\partial F / \partial x = 0$  problem can be used as a testing ground for approximate theories. The fact that  $v_2$  and  $v_3$  are independent of  $v_1$  is an enormous simplification. For example, consider the linearized problem, the problem solved by Fourier transformation in section 3. The linearized, inviscid equations of motion 9 for the fluctuation quantities become

$$\left. \begin{aligned} \frac{\partial u}{\partial t} + \Omega(y)v &= 0 , \\ \frac{\partial v}{\partial t} + \frac{\partial p}{\partial y} &= 0 , \\ \frac{\partial w}{\partial t} + \frac{\partial p}{\partial z} &= 0 , \\ \frac{\partial v}{\partial y} + \frac{\partial w}{\partial z} &= 0 , \end{aligned} \right\} \quad (37)$$

when  $\partial F/\partial x = 0$ . The last three equations imply  $(\partial^2/\partial y^2 + \partial^2/\partial z^2)p=0$ . Thus  $p = \text{const.} = 0$ , since  $\bar{p} = 0$ , and the second and third equations show  $v$  and  $w$  remain equal to their initial values,

$$v(y, z, t) = v_0(y, z) ,$$

$$w(y, z, t) = w_0(y, z) .$$

If the initial value of  $u$  is zero, then

$$u(y, z, t) = -\Omega(y)t v_0(y, z)$$

from the first equation. The Reynolds stress is

$$-\overline{uv} = \Omega(y)t \overline{v_0^2}(y) . \quad (38)$$

Three steps were required to produce the analog of the result that took all the algebra of section 3 to derive in general! Notice the Reynolds stress grows linearly with  $t$  for all time instead of tending asymptotically to a steady state as it did in the roughly isotropic case. Equations 15 and 16 show that the Fourier modes which are strongly excited when  $\Omega t \gg 1$  depend on initial modes occupying the  $k_1 \leq (\Omega t)^{-1}/L$  sector of wave-number space ( $L$  is the length scale of

the turbulence). If all the turbulent energy is loaded into the  $k_2, k_3$  plane, as it is in the  $\partial F / \partial x = 0$  problem, then all the initial modes remain effective for all time. In the roughly isotropic case, where modes are distributed over  $k_1, k_2, k_3$  with no singular concentration in the  $k_2, k_3$  plane, fewer and fewer of the initial modes remain effective for large times, and  $\overline{u^2}$ ,  $\overline{v^2}$  and  $\overline{uv}$  grow less rapidly (Moffatt [5] presents this argument more quantitatively).

The general problem is complicated enough even when linearized. It would be extremely hard to use a better approximation, the mean field equations 8, in a practical problem. But the mean field equations reduce to a simple form when  $\partial F / \partial x = 0$ . The last three of equations 37 are the same in the mean field approximation, so  $v(y, z, t) = v_0(y, z)$  and is independent of time. The momentum equation for  $u$  is

$$\frac{\partial u}{\partial t} + v \frac{\partial}{\partial y} U(y, t) = 0 .$$

The result of multiplying the equation through by  $v$  and averaging is

$$(i) \quad \frac{\partial \sigma}{\partial t} - \overline{v^2}(y) \frac{\partial U}{\partial y} = 0$$

for the Reynolds stress  $\sigma(y, t) = -uv$ .

The equation of mean motion is

$$(ii) \quad \frac{\partial U}{\partial t} - \frac{\partial \sigma}{\partial y} = 0 ,$$

(39)

so the mean field equations lead to a one-dimensional wave propagation problem with a variable phase velocity  $\sqrt{\overline{v^2}(y)}$ . Consider the rather artificial problem sketched in figure 6.

The initial speed profile is linear,

$$U(y, 0) = \Omega y ,$$

and the turbulence is confined to a band between  $y = \pm h$ .  $\overline{v_o^2}$  equals a constant  $c^2$  where  $|y| > h$ . If the initial stress is zero everywhere (that is, the turbulence is initially two dimensional,  $u_o(y, z) = 0$ ),

$$\frac{\partial U}{\partial t}(y, 0) = 0 ,$$

from 39(ii). Equation 39(i) implies  $\sigma(y, t) = 0$  for  $|y| > h$ . Integrating 39(ii) across  $y = \pm h$  gives the jump condition on  $\sigma$ ,  $[\sigma] = 0$ , so  $\sigma(\pm h, t) = 0$  just inside  $|y| = h$ . Then from 39(i),

$$\frac{\partial U}{\partial y}(\pm h, t) = 0 .$$

Equations 39(i) and (ii) combine to give

$$\frac{\partial^2 U}{\partial t^2} - c^2 \frac{\partial^2 U}{\partial y^2} = 0$$

in the region  $|y| < h$ , and a general solution is  $U = F(y-ct) + G(y+ct)$ . The initial and boundary conditions determine the final result,

$$U(y, t) = \frac{\Omega h}{2} \left[ f\left(\frac{y-ct}{h}\right) + f\left(\frac{y+ct}{h}\right) \right] ,$$

where  $f$  is the periodic function shown in figure 7.  $U(y, t)$  is itself periodic with period  $4h/c$ . The history of  $U$  over one period is shown in figure 8.

The rocking, periodic speed profile of figure 8 cannot be a good approximation to a real flow, but it is far more plausible than the equivalent result from the fully linearized equations. From

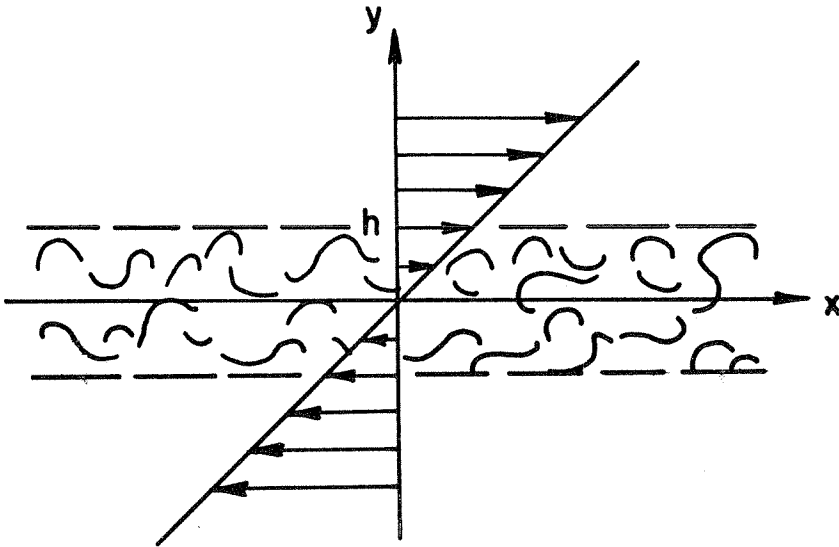


FIG. 6 TURBULENT BAND IN INITIALLY UNIFORM SHEAR

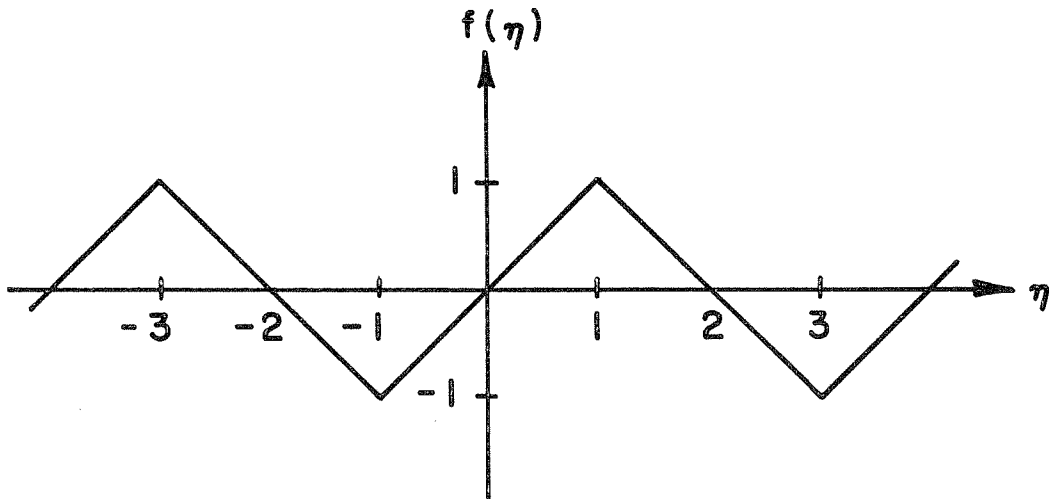


FIG. 7 THE PERIODIC FUNCTION  $f$

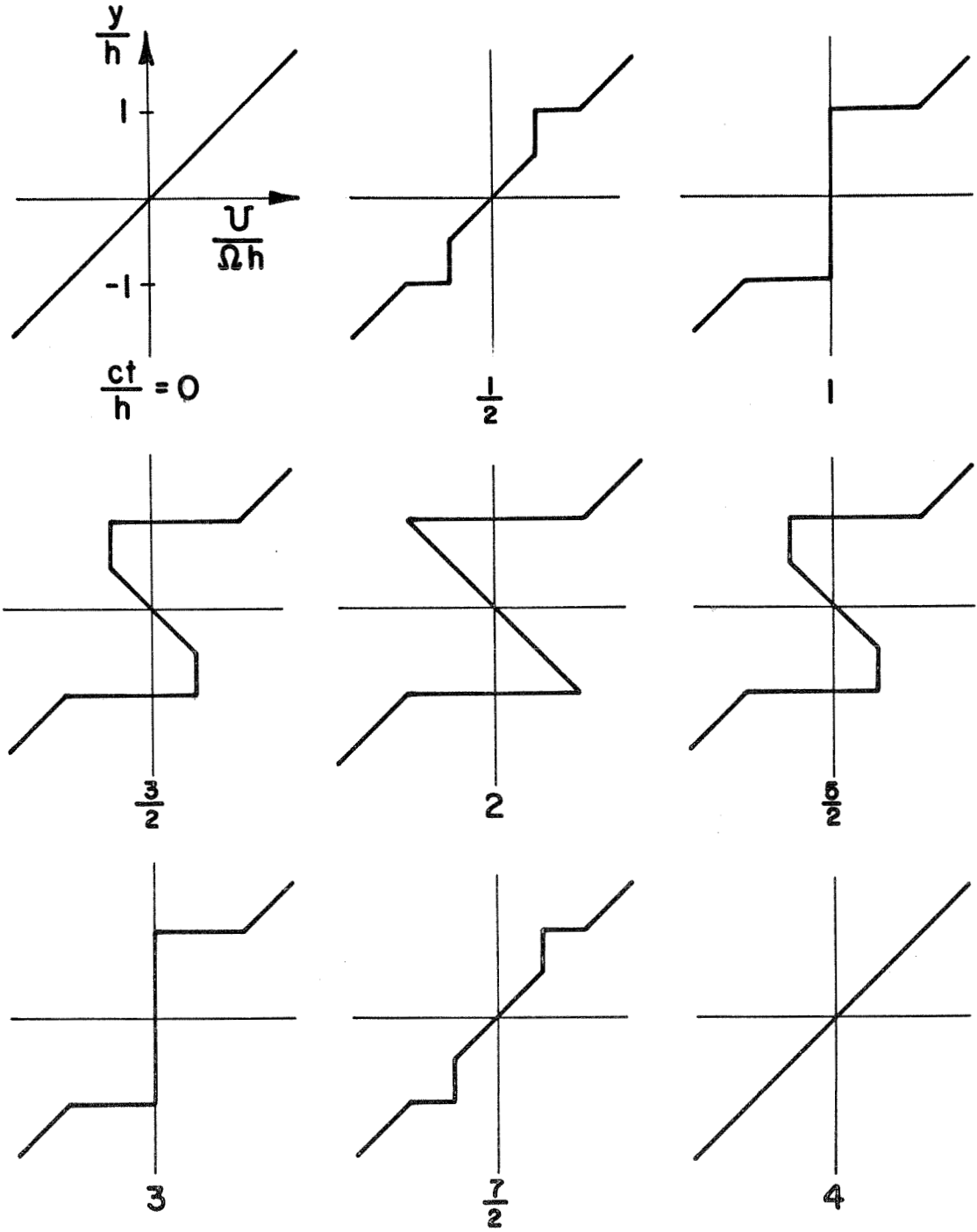


FIG. 8 SPEED PROFILE ONE PERIOD

equation 38,  $\sigma = c^2 \Omega t$  for  $|y| < h$ , and  $\sigma = 0$  for  $|y| > h$ , based on the full linearization. If this stress is used in the mean momentum equation 39(ii) to find a first approximation for  $U$  (the zeroth approximation being  $U = \Omega y$ ), the result is

$$U(y,t) = \Omega y - \frac{\Omega(ct)^2}{2h} \left[ \delta\left(\frac{y}{h} - 1\right) - \delta\left(\frac{y}{h} + 1\right) \right].$$

Sheets of concentrated momentum and infinite speed form at  $y = \pm h$ . This particular problem is physically unrealistic, of course, but it does show that the mean field equations can give qualitatively reasonable results when the linearized equations give nonsense. It is only in the case  $\partial F / \partial x = 0$  that the mean field equations can be used without overwhelming algebraic complexity.

The consequences of any theory of Reynolds stress generation can be drawn out much more quickly when the flow is independent of  $x$  than otherwise. The  $\partial F / \partial x = 0$  problem is at least a useful heuristic analogy to the general problem. Possibly it may be more than an analogy. According to the linear analysis of section 3, Fourier modes whose wave vectors lie close to the  $k_2, k_3$  plane (that is, Fourier modes which represent eddies nearly aligned in the  $x$  direction) are preferred in the sense that they contain most of the turbulent energy when  $\Omega t \gg 1$ . The non-linear terms dropped to produce that result may retard this tendency to anisotropy. On the other hand, they may accelerate the transfer of excitation into the preferred modes. If  $\partial F / \partial x = 0$  for any flow property  $F$ , then the velocity correlation function  $R_{ij}(y, \underline{r})$  is independent of  $r_1$ ; correlation contours are infinite cylinders aligned in the  $x$  direction. Experiments on turbulent wall

layers, where the turbulence also interacts strongly with a mean shear flow, show that the correlation functions are very much elongated in the  $x$  direction [8,9]. Even if  $R_{ij}$  were completely independent of  $r_1$ , it would be impossible to conclude that the flow is independent of  $x$ , since higher moments could still depend on spatial separation in the  $x$  direction. But insofar as the propagation of turbulence in a mean shear flow depends on low-order statistical moments like  $R_{ij}$ , it is possible that highly sheared turbulence spreads as if the eddies were independent of  $x$ .

B. The Random Vortex Sheet Problem with  $\partial F/\partial x = 0$

If the turbulence is initiated by an impulse concentrated in the  $x, z$  plane and independent of  $x$ , the flow is independent of  $x$  for all time. In that case the linear and mean field equations for the evolution of Reynolds stress, equations 38 and 39, can be compared easily. The only property of the initial flow required in equations 38 and 39 is the mean square upwash  $\overline{v_0^2}(y)$ , and that can be obtained directly from the work of section 3C on the generation of an initial field by an area impulse  $f(x, z)$ . However, the argument leading to  $\overline{v_0^2}$  is simpler and more illuminating when  $f$  is assumed independent of  $x$  from the beginning, so the argument is reviewed quickly here.

The equations of motion for the total velocity  $\underline{v}$  and pressure  $\pi$  are

$$\frac{\partial \underline{v}}{\partial t} + \underline{v} \cdot \nabla \underline{v} + \nabla \pi = \underline{j} f(z) \delta(y) \delta(t),$$

$$\nabla \cdot \underline{v} = 0 .$$

Equations for the pressure impulse  $\phi$  and the turbulent part of the initial velocity field  $\underline{u}_0$  are obtained by integrating the momentum equation across  $t = 0$ :

$$\begin{aligned} \underline{u}_0 + \nabla\phi &= j f(z)\delta(y) , \\ \nabla \cdot \underline{u}_0 &= 0 . \end{aligned} \tag{40}$$

Since the forcing function  $f(z)\delta(y)$  is independent of  $x$ ,  $\phi$  is independent of  $x$ , and the  $x$  component of  $\underline{u}_0$  is zero. For  $y \neq 0$ ,  $\underline{u}_0 = -\nabla\phi$ , a two-dimensional potential flow. Suppose the potential is  $\phi_1$  just above the  $x, z$  plane and  $\phi_2$  just below. Since the  $y$  component of velocity must be continuous across  $y = 0$ , the first of equations 40 can be integrated to give

$$\phi_1 - \phi_2 = f(z) .$$

Thus there is a speed slip  $\gamma$  across  $y = 0$ , where

$$\gamma = \frac{d}{dz} (\phi_2 - \phi_1) = - \frac{df}{dz} . \tag{41}$$

In section 3C it was suggested that a random area-impulse could be simulated by shooting lifting surfaces over the  $x, z$  plane. When the impulse is independent of  $x$ , a much less fanciful setup is required. Suppose a steady shear flow

$$S(x, y) = S_0 + U(x, y)$$

passes over a high aspect ratio wing with random lift per unit length  $L(z)$  fixed in a wind tunnel at  $x, y = 0$ . The situation is shown in

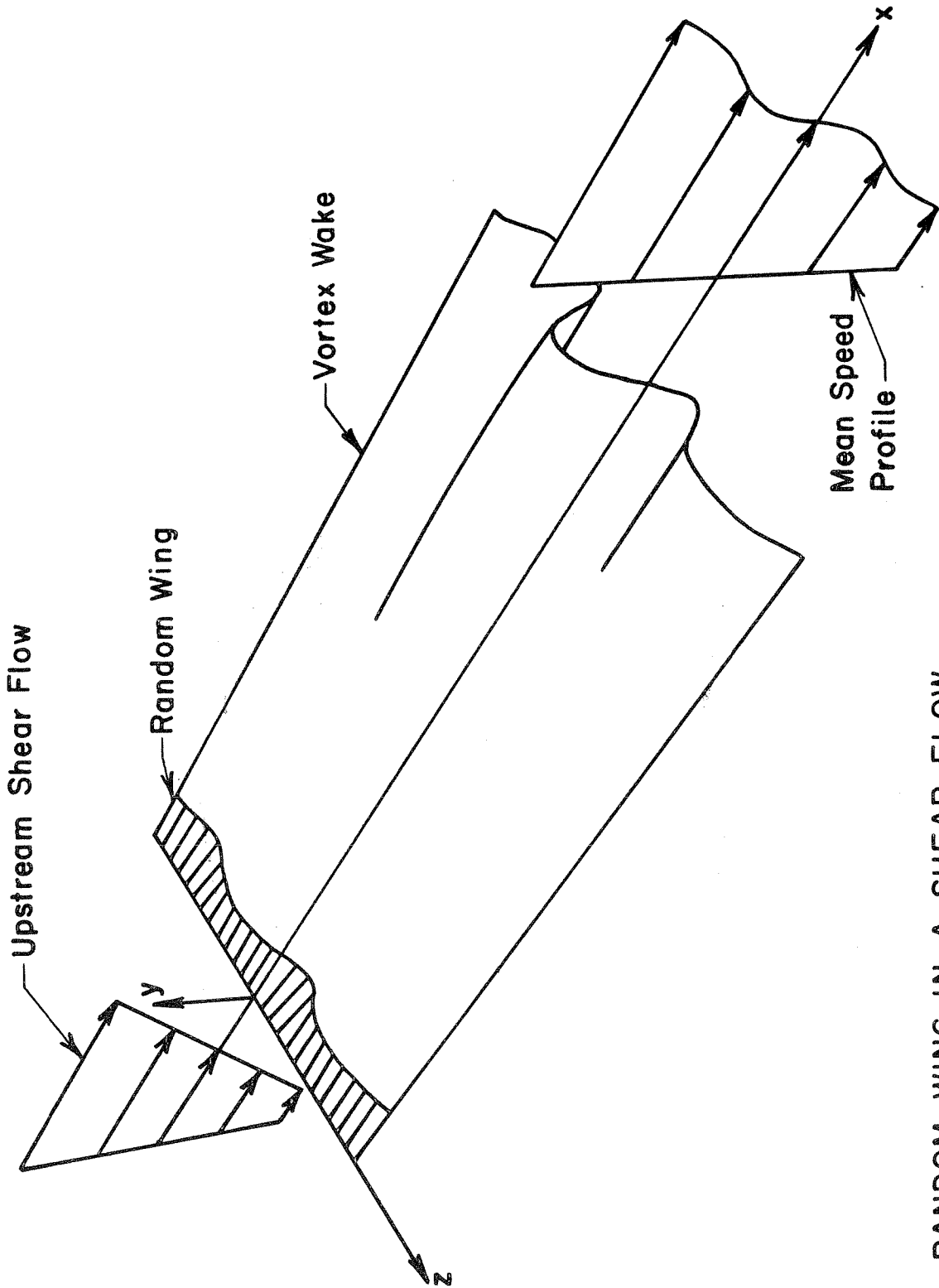


FIG. 9 RANDOM WING IN A SHEAR FLOW

figure 9. The speed profile might be linear far upstream,  $S \rightarrow S_0 + \Omega y$  as  $x \rightarrow -\infty$ , but downstream the flow is distorted by the random vorticity shed from the wing. The wing delivers a concentrated impulse  $-L(z)/S_0$  to the fluid passing over it, and the velocity jump through the wake is

$$\gamma = \frac{1}{S_0} \frac{dL}{dz} ,$$

analogous to equation 41. For  $S_0$  much larger than a typical downwash speed, the flow varies only slowly with  $x$ , and the time  $t$  in the non-steady problem is analogous to the ratio  $x/S_0$ . Any results found in the non-steady problem can be turned into predictions about the wind-tunnel experiment through the prescription

$$t \rightarrow x/S_0 ,$$

$$f(z) \rightarrow -L(z)/S_0 .$$

Equation 41 gives the slip speed  $\gamma$  as a function of the impulse  $f$ , but it can also be integrated to give the  $f$  required to generate a given  $\gamma$ :

$$f(z) - f(0) = - \int_0^z \gamma(z') dz' .$$

$f$  is forced through a random walk to generate a random slip speed  $\gamma$ , and by the transformation of variables usual in random walk problems,

$$\overline{[f(z) - f(0)]^2} = \int_0^z \int_0^z \overline{\gamma(z')\gamma(z'')} dz' dz'' = 2 \int_0^z (z-\zeta) \Gamma(\zeta) d\zeta$$

for  $\gamma$  homogeneous in  $z$  with a correlation function  $\overline{\gamma(z)\gamma(z+\zeta)} = \Gamma(\zeta)$ .  $f$  should also be homogeneous, and for  $z$  large enough,  $f(z)$  and  $f(0)$  should be independent. Then as  $z \rightarrow \infty$

$$\overline{f^2} \Rightarrow z \int_0^\infty \Gamma(\zeta) d\zeta - \int_0^\infty \zeta \Gamma(\zeta) d\zeta .$$

The equation cannot be satisfied for an impulse with finite variance unless

$$\int_0^\infty \Gamma(\zeta) d\zeta = 0 . \tag{42}$$

Equation 42 imposes a severe constraint on the kind of vortex sheet that can be generated by finite and homogeneous random impulses, or the kind of wake that can be generated by a random wing. Regardless of the correlation between neighboring random impulses, even if neighboring impulses are completely independent, the vorticity over neighboring parts of the wake must be negatively correlated so the integral of the correlation function is zero. The equivalent result was obtained for the general problem in section 3C, but not so directly.

Equations 40 can be solved by Fourier transformation just as before. Thus if  $\tilde{f}(k_3)$  is the Fourier transform of  $f$  over  $z$  and  $\tilde{a}_0(k_2, k_3)$  is the Fourier transform of  $u_0$  over  $y$  and  $z$ ,

$$\tilde{a}_0(\underline{k}) = \frac{\tilde{f}}{2\pi} \left( \tilde{j} - \frac{\tilde{k}k_2}{k^2} \right)$$

where  $\underline{k} = (k_2, k_3)$ . In particular

$$a_{o2} = \frac{\tilde{f}}{2\pi} \frac{k_3^2}{k^2}$$

and the upwash at  $y, z$  is

$$v_o(y, z) = \int \frac{\tilde{f}(k_3)}{2\pi} \frac{k_3^2}{k^2} e^{i\mathbf{k} \cdot \mathbf{x}} d\mathbf{k} .$$

Suppose  $f$  has a spectral distribution  $\psi(k_3)$ , so that

$$\overline{\tilde{f}(k_3)\tilde{f}(k'_3)} = \psi(k_3) \delta(k_3+k'_3) .$$

Then the initial upwash correlation at a height  $y$  is

$$\begin{aligned} Q(y, \zeta) &= \overline{v_o(y, z)v_o(y, z+\zeta)} \\ &= \int \frac{\psi(k_3)}{(2\pi)^2} \frac{k_3^4}{(k_2^2+k_3^2)(k_2'^2+k_3^2)} e^{i(k_2+k_2')y} e^{ik_3\zeta} dk_2' dk_2 dk_3 \\ &= \int_{-\infty}^{\infty} \frac{\psi(k_3)}{4} k_3^2 e^{-2|k_3 y|} e^{ik_3\zeta} dk_3 . \end{aligned}$$

The spectral distribution of the upwash at the vortex sheet  $\Theta(k_3)$  is the Fourier transform of  $Q(0, \zeta)$ . Thus

$$\Theta(k_3) = \frac{k_3^2}{4} \psi(k_3) ,$$

analogous to the general result discussed in detail in section 3C. In order to get a specific result, suppose

$$\psi(k_3) = A e^{-\mu|k_3|} .$$

Then

$$Q(y, \zeta) = A (\mu+2|y|) \frac{[(\mu+2|y|)^2 - 3\zeta^2]}{[(\mu+2|y|)^2 + \zeta^2]^3} . \quad (43)$$

Finally,

$$\overline{v}_0^2(y) = Q(y, 0) = \frac{A}{(\mu + 2|y|)^3} . \quad (44)$$

Now that  $\overline{v}_0^2$  is known, the stress can be computed according to the linear approximation, equation 38, or the mean field approximation, equations 39,

In subsection A it was shown that a discontinuity in  $\overline{v}_0^2$  leads to the formation of a sheet of concentrated momentum under the linear approximation. According to equation 38,

$$\sigma = \frac{\Omega At}{(\mu + 2|y|)^3}$$

for the vortex sheet problem.  $\sigma$  is continuous but has a discontinuous first derivative with respect to  $y$  at  $y = 0$ . This time, the first approximation to the mean speed,

$$U = \Omega y - \frac{3\Omega At^2}{(\mu + 2|y|)^4} \text{sgn}(y) ,$$

jumps across  $y = 0$ . This more modest singularity is still unacceptable. Any such jump must be preceded by a steepening of the speed profile near  $y = 0$ , but the integration of the momentum equation for  $u$  to give  $u = -\Omega t v_0$ , in the derivation of equation 38, requires  $\Omega$  to be constant in time.

The mean field equations 39 give a more realistic result, since they do take into account the change of mean speed that invalidates the linear approach. Suppose non-dimensional variables are defined as follows:

$$\overline{v_0^2} = c^2 g(\eta) ,$$

$$U = S r(\eta, \tau) ,$$

$$\sigma = c S s(\eta, \tau) ,$$

$$y = l \eta ,$$

$$t = \frac{l}{c} \tau .$$

Then equations 39 transform to

$$(i) \frac{\partial s}{\partial \tau} - g \frac{\partial r}{\partial \eta} = 0 ,$$

(45)

$$(ii) \frac{\partial r}{\partial \tau} - \frac{\partial s}{\partial \eta} = 0 .$$

The Reynolds stress is non-dimensionalized on the typical mean speed  $S$  times the fluctuation speed  $c$ . If the flow is 'highly sheared,'  $S \gg c$ , then  $\sigma \gg c^2$ . Random stretching of the mean field vorticity produces a stress much larger than the original turbulent energy density. The time characterizing changes is properly non-dimensionalized on  $l/c$ ; in a time of order  $l/c$  the mean flow reacts to the stress. But  $l/c$  is also the time scale for non-linear convection of turbulent vorticity, the phenomenon neglected in the mean field approximation. Thus the mean field equations are not a consistent approximation and can give only a qualitative description of the real flow.

If  $l$ ,  $c$  and  $S$  are related to  $\mu$ ,  $A$  and  $\Omega$  by the equations

$$l = \frac{\mu}{2},$$

$$c = \sqrt{\frac{A}{3\mu}},$$

$$S = \frac{\Omega\mu}{2},$$

then the non-dimensional form of equation 44 is

$$g = \frac{1}{(1+|\eta|)^3}, \quad (46)$$

and the initial and boundary conditions are

$$s(\eta, 0) = 0, \quad r(\eta, 0) = \eta, \quad (47)$$

$$\lim_{|\eta| \rightarrow \infty} s(\eta, \tau) = 0, \quad \lim_{|\eta| \rightarrow \infty} r(\eta, \tau) = \eta,$$

for a mean speed profile linear at  $t = 0$ . Equations 45, 46 and 47 determine the history of the flow according to the mean field approximation for all time.

The mean field equations are only a qualitative approximation for any time  $t$ , and for  $t$  large compared with the turbulent convection time  $l/c$ , they must be a bad qualitative approximation. The cylindrical eddies inducing the mean square upwash  $\overline{v_0^2}$  themselves disperse after a time of order  $l/c$ . Assuming  $\overline{v_0^2}$  is unchanging for all time led to the peculiar periodic solution of figure 9. Thus the solution to equations 45, 46, 47 is relevant only in the limit  $\tau \ll 1$ . In that case it is reasonable to rewrite the problem in terms of an expanded coordinate

$$\tilde{\tau} = \tau/\epsilon$$

and try to find asymptotic series expansions of  $r(\eta, \tilde{\tau}; \epsilon)$  and  $s(\eta, \tilde{\tau}; \epsilon)$  in powers of  $\epsilon$ . In Appendix D, it is shown that the expansions begin

$$\begin{aligned} s &= \epsilon \tilde{\tau} g(\eta) + O(\epsilon^3) , \\ r &= \eta + \epsilon^2 \frac{\tilde{\tau}^2}{2} g'(\eta) + O(\epsilon^4) , \end{aligned} \tag{48}$$

the same as the linear solution. However, the ordering of the terms breaks down where  $\eta \sim \epsilon$ , and in that region it is necessary to use a second expanded variable

$$\tilde{\eta} = \eta/\epsilon .$$

A function  $g$  which is symmetric and peaked like the function in equation 46 can be expanded around  $\eta = 0$  in the form

$$g = 1 - \alpha |\eta| + \dots = 1 - \epsilon \alpha |\tilde{\eta}| + \dots .$$

If  $g = (1 + |\eta|)^{-3}$ ,  $\alpha = 3$ . It is shown in Appendix D that equations 48 are correct even for small  $\eta$  as long as  $|\tilde{\eta}| > \tilde{\tau}$ , and that the expansions for  $s(\tilde{\eta}, \tilde{\tau}; \epsilon)$  and  $r(\tilde{\eta}, \tilde{\tau}; \epsilon)$  begin

$$\begin{aligned} s &= \epsilon \tilde{\tau} - \epsilon^2 \frac{\alpha}{2} (\tilde{\eta}^2 + \tilde{\tau}^2) + O(\epsilon^3) , \\ r &= \epsilon \tilde{\eta} - \epsilon^2 \alpha \left( |\tilde{\eta}| \tilde{\tau} - \frac{\tilde{\eta}^2}{2} \right) \text{sgn}(\tilde{\eta}) + O(\epsilon^3) , \end{aligned} \tag{49}$$

where  $|\tilde{\eta}| < \tilde{\tau}$ . To second order in  $\epsilon$ , the singularity at the vortex sheet affects only the portion of the  $\eta, \tau$  plane between the particular zeroth-order characteristics,  $\eta = \pm \tau$ , which originate at  $\eta = 0$  when  $\tau = 0$ . Expansions 48 and 49 become

$$\left. \begin{aligned} s &= \tau g(\eta) + \dots, \\ r &= \eta + \frac{\tau^2}{2} g'(\eta) + \dots, \end{aligned} \right\} |\eta| > \tau,$$

$$\left. \begin{aligned} s &= \tau - \frac{\alpha}{2} (\eta^2 + \tau^2) + \dots, \\ r &= \eta - \alpha \left( |\eta| \tau - \frac{\eta^2}{2} \right) \operatorname{sgn}(\eta) + \dots, \end{aligned} \right\} |\eta| < \tau,$$

when rewritten in terms of the original non-dimensional variables  $\eta, \tau$ . The non-dimensional stress  $s(\eta, \tau)$  and speed change  $r(\eta, \tau) - r(\eta, 0) = r(\eta, \tau) - \eta$  are sketched in figure 10. In the region  $|\eta| < \tau$  where the linear and mean field results differ, the linear results are shown as dotted lines.

The speed slip of the linear approximation is patched up in the region  $|\eta| < \tau$ , and the mean field profiles are plausible. However, the sheet of concentrated vorticity that generated the peaked  $\overline{v}_0^2(y)$  at the start must wrinkle and occupy the band  $|\eta| < \tau$  itself.  $\overline{v}_0^2(y)$  should be blunted about as fast as  $\sigma$ , so the mean field approximation is suspect in the only region it makes any difference. That is inevitable. The mean field approximation is not consistent, and the only advantage it has over the full linearization is that it gives more reasonable results near singularities in  $\overline{v}_0^2(y)$ .

The limits of  $s$  and  $r$  for  $\tau \gg 1$  can be found by Laplace transformation of equations 45, 46 and 47. One result is that  $r(\eta, \tau) \rightarrow 0$  for  $\eta$  fixed and  $\tau \rightarrow \infty$ ; the flow is eventually stopped anywhere. If the result were true it would mean random eddies exert a sustained grip on the mean flow. In fact the result is worthless. The grip

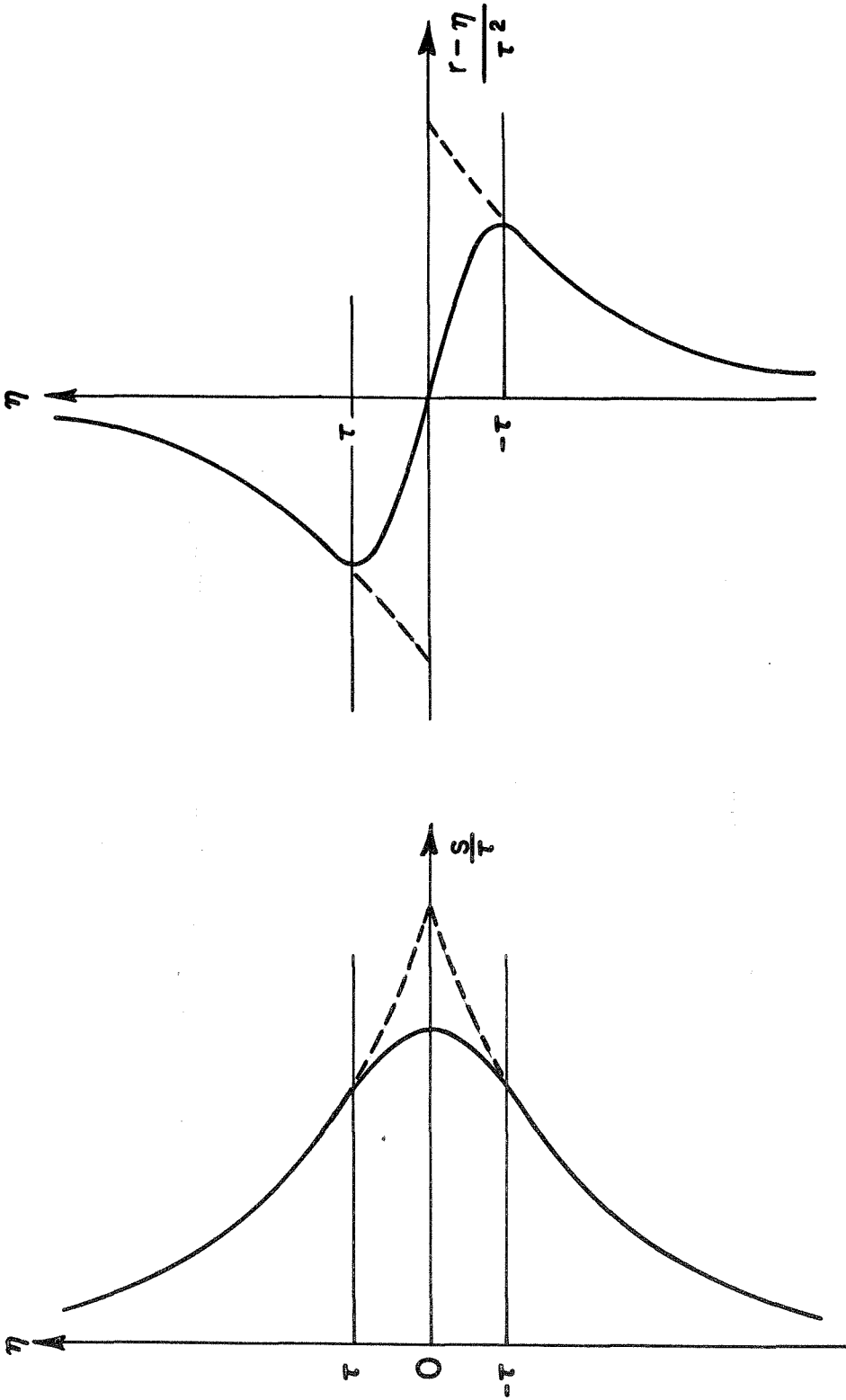


FIG. 10 STRESS AND MEAN SPEED NEAR A VORTEX SHEET

loosens rapidly as the eddies disperse in their own turbulent field. An entirely different kind of problem involving sustained induction is treated in the next subsection.

### C. Steady Induction by Line Vortices of Alternating Sign

Any physical approximation which neglects non-linear interaction between turbulent eddies leads to the conclusion that the mean flow stops anywhere after enough time. In the  $\partial F / \partial x = 0$  problem, the x component of momentum is conserved in fluid columns (equation 35) and is diffused by turbulent motions passively, like heat or chemical concentration. Without dispersion of the eddies, the intensity of turbulent mixing is constant in time, and regardless of how slow the mixing is at any particular height, given enough time it is sufficient to diffuse away any mean momentum gradient. The important question is, how much time is required to stop the flow? If the time needed were small compared with the turbulent convection time, the flow would indeed be stopped, but that is impossible since the momentum redistribution is itself a convection phenomenon. The turbulent eddies should disperse at about the same rate the x momentum diffuses, and the mean flow should be more or less distorted, but not stopped.

One situation where there is no convection of initial vorticity was described in subsection A — the case of a single vortex aligned on a streamline of an initial linear shear flow. There the flow is 'stopped,' not in a statistical sense, but stopped in the sense that the x speed averaged over a patch of finite area tends to zero as

$t \rightarrow \infty$ . Suppose that instead of one vortex there is an infinite street of vortices of alternating sign aligned parallel to  $x$  and distributed along  $z$  a distance  $\lambda$  apart. The setup is shown in figure 11. The vortices are in equilibrium, since the velocity at any particular vortex induced by all the others is zero. The equilibrium is unstable, but in principle the vortices can remain in their original locations and steadily redistribute the  $x$  momentum of an initial linear shear profile. Fluid columns move in roughly elliptical orbits as shown. Since the orbit time differs from streamline to streamline, fluid columns crossing line A-A at a large time  $t$  may have originated at greatly different heights even if their current separation is small. A speed traverse along A-A in figure 11 eventually shows high-pitched oscillations, and the  $x$  velocity component averaged over an interval  $\lambda$  at a constant height  $y$  becomes small as  $t \rightarrow \infty$ . This flow is nothing like non-steady turbulence, but it is homogeneous in the  $z$  direction, and the time it takes to stop the line-averaged flow here may give some indication of the time required by turbulence to stop a flow in the statistical sense.

Loops in the speed traverse along A-A arise after a time comparable to the orbit time in the trajectory tangent to A-A.  $T(y)$ , the orbit time in the trajectory whose apogee is  $y$ , is thus a lower bound on the time needed to stop the line-averaged flow at  $y$ . The object here is to find  $T(y)$ .

Since the flow in the  $y, z$  plane is dynamically independent of the  $x$  momentum it transports (equations 36), it can be treated as an incompressible, two-dimensional flow. It is irrotational as well,

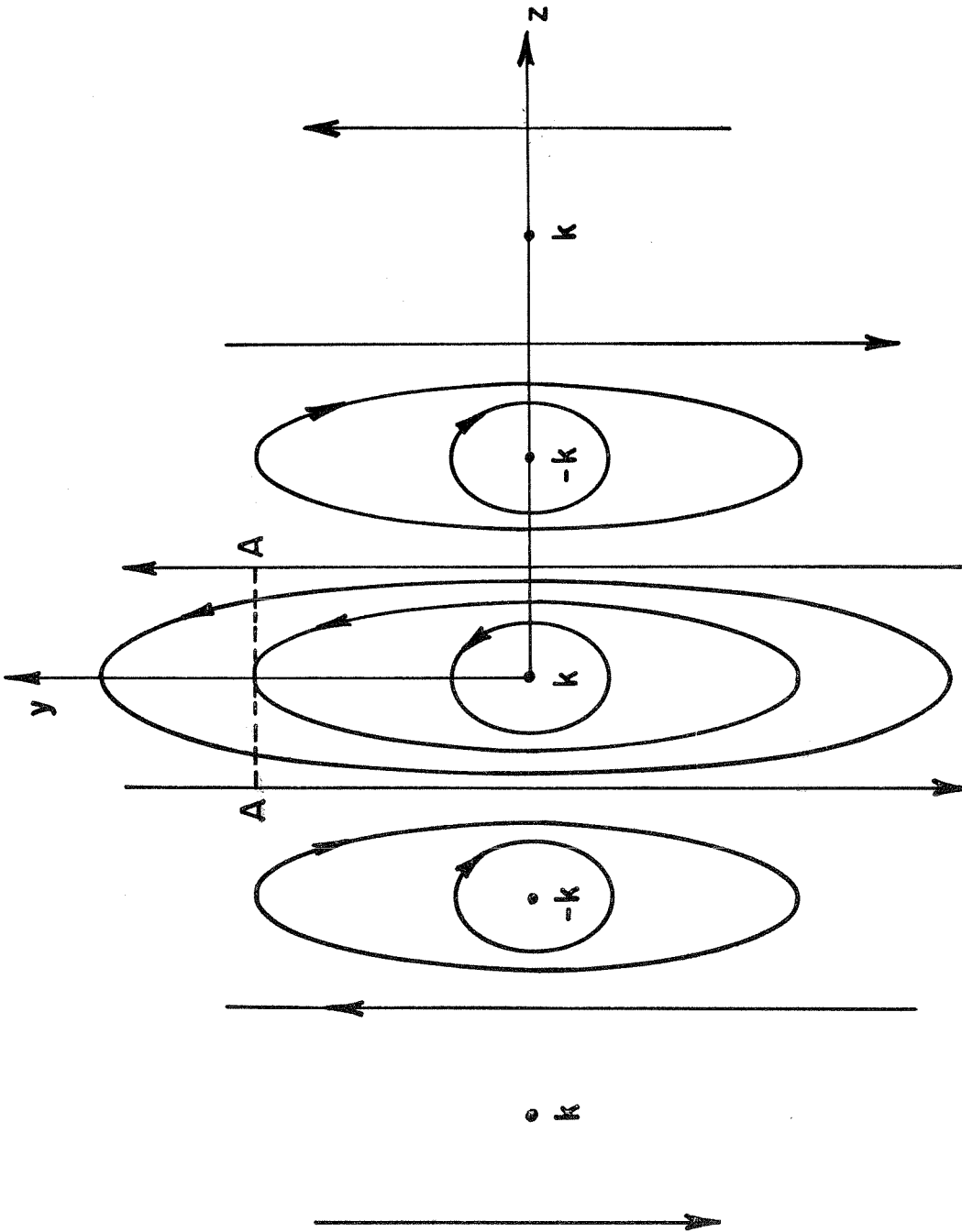


FIG. II PATHS THROUGH A VORTEX STREET

except at the vortex singularities. Thus a potential  $\phi(y, z)$  and stream function  $\psi(y, z)$  can be found such that

$$v = -\frac{\partial\phi}{\partial y} = \frac{\partial\psi}{\partial z} ,$$

$$w = -\frac{\partial\phi}{\partial z} = -\frac{\partial\psi}{\partial y} ,$$

and each location in the  $y, z$  plane can be assigned potential and streamline coordinates  $\phi, \psi$ . Suppose the speed

$$V = \sqrt{v^2 + w^2}$$

is known in terms of  $\phi, \psi$ . If  $s$  measures the arc length along a trajectory (streamline) specified by  $\psi$ , then

$$V = \frac{ds}{dt} (\psi) .$$

$V$  also satisfies

$$V = -\frac{d\phi}{ds} (\psi) .$$

Thus

$$V = \frac{ds}{d\phi} (\psi) \frac{d\phi}{dt} (\psi) = -\frac{1}{V} \frac{d\phi}{dt} (\psi)$$

or

$$\frac{d\phi}{dt} (\psi) = -V^2(\phi, \psi) .$$

The time it takes a fluid column to move from potential  $\phi_0$  to potential  $\phi_1$  along the trajectory specified by  $\psi$  is

$$t = - \int_{\phi_0}^{\phi_1} \frac{d\phi}{v^2(\phi, \psi)} .$$

Notice  $t$  is positive, since  $\phi$  must always decrease in the direction the fluid column moves. Each orbit encloses a single vortex of strength  $\pm k$ . As a column orbits once, the potential decreases an amount  $k$ , so the orbit time around the trajectory specified by  $\psi$  is

$$T(\psi) = \int_0^k \frac{d\phi}{v^2(\phi, \psi)} . \quad (50)$$

The value of  $\psi$  on the trajectory with apogee  $y$  is  $\psi(y, 0)$ . Thus

$$T(y) = T[\psi(y, 0)] = \int_0^k \frac{d\phi}{v^2[\phi, \psi(y, 0)]} ,$$

and the problem of finding  $T(y)$  is solved in principle.

Complex variable notation makes an explicit solution surprisingly easy. The details are given in Appendix E. The result is

$$T(\psi) = \frac{4\lambda^2}{k \left| \sinh \frac{2\pi\psi}{k} \right| \cosh \frac{2\pi\psi}{k}} ,$$

with

(51)

$$\psi(y, 0) = \frac{k}{2\pi} \log \left( \frac{\sinh \frac{\pi y}{\lambda}}{1 + \cosh \frac{\pi y}{\lambda}} \right) .$$

Two limits are especially interesting:

- Ⓐ as  $y/\lambda \rightarrow 0$  ,  $T(y) \Rightarrow \frac{4\pi^2 y^2}{k}$  ;
- Ⓑ as  $y/\lambda \rightarrow \infty$  ,  $T(y) \Rightarrow \frac{2\lambda^2}{k} e^{\pi y/\lambda}$  .

The orbit time at a radius  $y$  around an isolated vortex of strength  $k$  is  $4\pi^2 y^2/k$ , the same as limit a. A fluid column very close to a particular vortex is hardly affected by the other vortices in the street. Limit b is the surprising result. The orbit time around a trajectory with apogee  $y$  is exponentially large for large enough  $y$ . The two limiting cases of equations 51, derived for  $y \ll \lambda$  and  $y \gg \lambda$ , give practically the same results for intermediate values of  $y$ . For  $y = \lambda/2$ , limit a is

$$T_a = \pi^2 \frac{\lambda^2}{k} = 9.87 \frac{\lambda^2}{k},$$

and limit b is

$$T_b = 2e^{\pi/2} \frac{\lambda^2}{k} = 9.62 \frac{\lambda^2}{k}.$$

The limiting expressions agree very well around  $y = \lambda/2$ , the apogee of the orbit with major axis  $\lambda$ . Beyond that orbit, limit b must be an excellent approximation. Thus  $T(y)$ , a lower bound on the time required by the vortex street to decelerate the line-averaged flow at a height  $y$ , grows exponentially beyond  $y \sim \lambda$ . The rate of mixing  $x$  momentum is zero, for all practical purposes, outside the immediate neighborhood of the vortex street.

The apogee of the orbit that has been completed just once by time  $T$  is

$$Y = \frac{\lambda}{\pi} \log \frac{kT}{2\lambda^2}$$

for  $Y \gtrsim \lambda$ .  $Y(T)$  is the height of the 'front' where the line-averaged

flow is being significantly decelerated at time  $T$ . The front propagates at a speed  $\dot{Y} = \lambda/\pi T$ . But the slightest disturbance destroys the equilibrium of the vortex street and allows the vortices to disperse at an initial rate  $\sim k/\lambda$ . By a time of order  $\lambda^2/k$ , the vortices have dispersed past the front they are supposed to be forcing steadily through the flow. Thus no such front can develop in the first place, and the result for steady induction by a vortex street can give no indication of what happens in a real flow. The propagation of turbulence in a mean shear flow cannot be understood without considering the non-linear action of turbulence on itself. Any analogy, like the steady vortex street, or any approximate theory, like the mean field equations, which omits turbulent convection of random vorticity must lead to fundamentally unrealistic results. The mechanics of turbulence propagation through a mean shear flow is inseparable from the mechanics of the mean flow itself, and any approach which neglects non-linear interaction between random fluctuations will give a qualitatively wrong description of the mean flow.

## 5. The Numerical Experiments

### A. Basis of the Numerical Approach

According to the linear approximation of section 3, Reynolds stress stops propagating through a mean shear flow once the original turbulence is highly sheared. In section 4, the problem was simplified by assuming all flow properties are independent of  $x$ , and the non-linear interaction between turbulence and the mean field was restored. It was found that no such partial account of non-linear convection can give even qualitatively correct results for large times. Eliminating turbulent convection of random vorticity in the  $\partial F / \partial x = 0$  problem leads to a turbulent field steady in the  $y, z$  plane with a steady grip on the mean flow. Under such an approximation, the mean flow eventually stops anywhere, but in fact the turbulent eddies disperse about as fast as the mean flow decelerates, and the mean speed profile is distorted, but not driven to zero. If the propagation of turbulence through a mean shear flow is to be understood at all, non-linear action of turbulence on itself must be considered. But the fully non-linear problem is intractable. Without analytical support or the support of experiments on the propagation of free turbulence in shear flows, a guess about the effect of non-linearity would be arbitrary. Some kind of experiment is needed.

The outstanding simplification of the  $\partial F / \partial x = 0$  problem is that eddy motion in the  $y, z$  plane is dynamically independent of the momentum it convects. The motion in the  $y, z$  plane can be treated like two-dimensional turbulence, and the speed in the  $x$  direction like a scalar quantity convected in a two-dimensional turbulent field.

That does not mean that the only random vorticity in the flow is the initial vorticity. All three components of the random vorticity  $\omega = (\xi, \eta, \omega)$  are generated by mean field stretching. It means only that the velocity field in the  $y, z$  plane is unaffected by random stretching of the mean field vorticity. If the vorticity  $\xi(y, z, t)$  is given, then the two-dimensional velocity field  $\underline{v} = (v, w)$  can be found from

$$(i) \quad \underline{v}(y, z, t) = \frac{1}{4\pi} \int \int \frac{\underline{i} \times \underline{r}}{r^2} \xi(y', z', t) dy' dz'$$

where  $\underline{r} = \underline{j}(y-y') + \underline{k}(z-z')$ . From equations 36, (52)

$$(ii) \quad \frac{\partial \xi}{\partial t} + \underline{v} \cdot \nabla \xi = 0 ,$$

and the integral and differential equations can be solved step-by-step.

If the vorticity is not distributed smoothly in the  $y, z$  plane but is packed into discrete vortex columns, the problem looks even simpler. Suppose the clockwise circulation around the  $j^{\text{th}}$  vortex viewed toward negative  $x$  is  $k_j$ . Equation 52(i) becomes

$$\underline{v}(y, z, t) = - \sum_j \frac{k_j}{2\pi} \frac{\underline{i} \times \underline{r}_j}{r_j^2} , \quad (53)$$

where the  $j^{\text{th}}$  vortex is located at  $[y_j(t), z_j(t)]$ , and  $\underline{r}_j = \underline{j}(y-y_j) + \underline{k}(z-z_j)$ . Each vortex is convected in the field induced at its location by all the others. Thus

$$\begin{aligned} \dot{y}_i &= \sum_{j \neq i} \frac{k_j}{2\pi} \frac{(z_i - z_j)}{(y_i - y_j)^2 + (z_i - z_j)^2} , \\ \dot{z}_i &= - \sum_{j \neq i} \frac{k_j}{2\pi} \frac{(y_i - y_j)}{(y_i - y_j)^2 + (z_i - z_j)^2} . \end{aligned} \quad (54)$$

The path of each vortex can be found by integrating equations 54, and the statistics of the x momentum convection can be found from equation 53. Equations 54 are just as hard to deal with analytically as equations 52, but now the problem is set up for a simple step-by-step integration by computer. If a great many numerical experiments are performed over an ensemble of initial conditions  $\{k_i, y_i(0), z_i(0)\}$ , information about the turbulent grip on the mean flow can be obtained.

The value of such computer experiments rests on the physical relevance of the initial conditions chosen. Suppose the vortex sheet problem of section 4B is modeled. The discrete vortices must start in the x, z plane, so  $y_n(0) = 0$ . The continuous area-impulse  $f(z)$  must be replaced by a step-function model. Suppose the model impulse is constant over intervals  $\lambda$ , and the total impulse delivered between  $z = (n-1)\lambda$  and  $n\lambda$  is

$$F_n = \int_{(n-1)\lambda}^{n\lambda} f(z) dz .$$

The situation is shown in figure 12. The strength of the vortex whose initial position is  $y_i(0) = 0, z_i(0) = n\lambda$  is then

$$k_n = \frac{F_{n+1} - F_n}{\lambda} = \frac{\Delta F_n}{\lambda} , \quad (55)$$

from equation 41. This row of vortices could be generated in the wind tunnel experiment of figure 9 if the random wing were made of panels of span  $\lambda$  bearing uniformly distributed total lifts  $L_n = -S_o F_n$ . The initial conditions  $\{\Delta F_n / \lambda, 0, n\lambda\}$  are perfectly realizable and need not be regarded as models of random vortex sheets.

If the vortices  $k_n$  are to be generated by random, homogeneous impulses  $F_n$  of finite variance, then neighboring vortices cannot be uncorrelated. The proof is about the same as it was in the continuous case. From equation 55,

$$F_{n+1} - F_1 = \sum_{n=1}^N \Delta F_n = \lambda \sum_{n=1}^N k_n .$$

Thus

$$\overline{[F_{N+1} - F_1]^2} = \lambda^2 \sum_{m=1}^N \sum_{n=1}^N \overline{k_m k_n} .$$

For  $N$  large,  $F_{N+1}$  and  $F_1$  are independent, and the left hand side is  $\overline{2F^2}$ . If the variance of  $k_n$  is  $k^2$  and the correlation function  $R$  is defined by

$$\overline{k_m k_n} = k^2 R(n-m) ,$$

then

$$\overline{2F^2} \Rightarrow \lambda^2 k^2 \sum_{\ell=-(N-1)}^{(N-1)} (N-|\ell|) R(\ell)$$

as  $N \rightarrow \infty$ . The original sum over  $m$  and  $n$  has been transformed as shown in figure 13. Thus

$$\overline{2F^2} \Rightarrow \lambda^2 k^2 \left[ N \sum_{\ell=-\infty}^{\infty} R(\ell) - 2 \sum_{\ell=1}^{\infty} \ell R(\ell) \right] ,$$

and the relation cannot be satisfied for large  $N$  unless

$$\sum_{\ell=-\infty}^{\infty} R(\ell) = 0 . \tag{56}$$

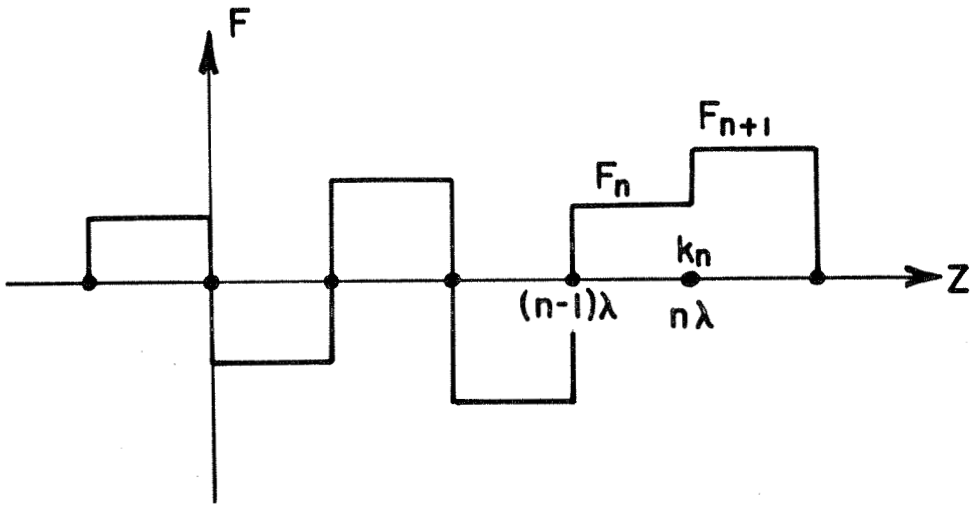


FIG. 12 STEP-FUNCTION IMPULSE

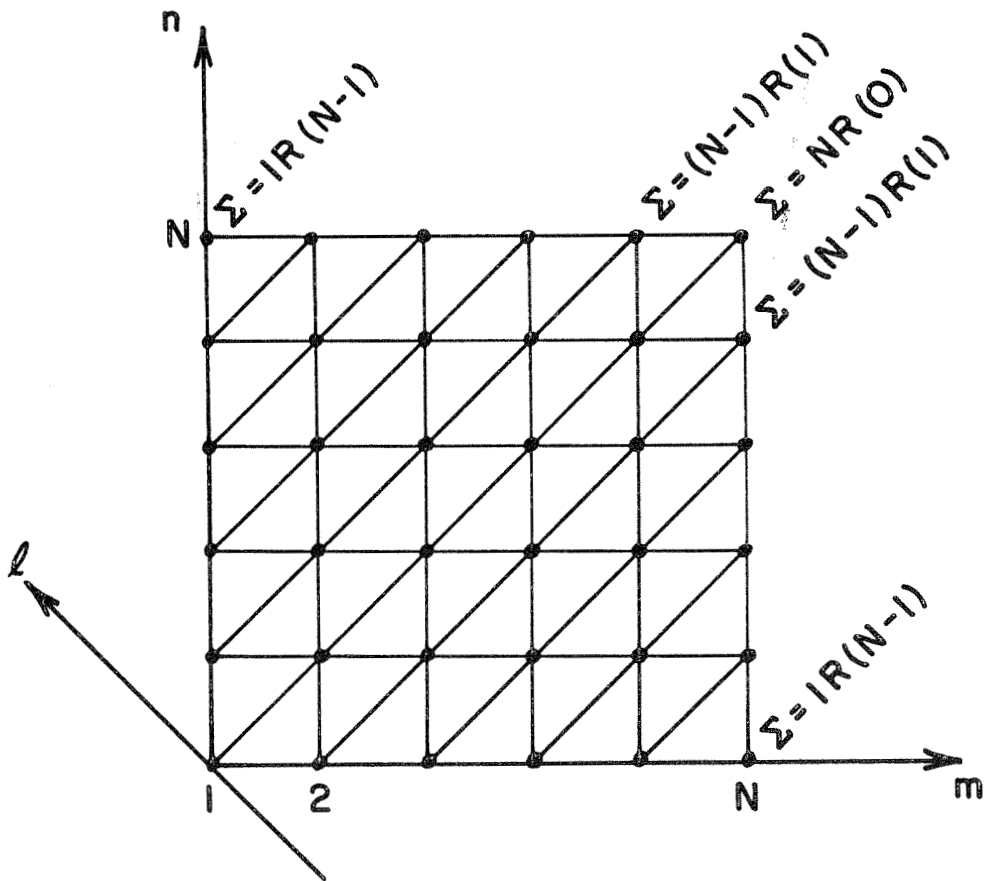


FIG. 13 METHOD FOR SUMMING  $R(n-m)$  OVER  $n, m$

The ensemble of vortex strengths must satisfy equation 56 if the computer experiments are to represent physically realizable situations.

If the impulses  $F_n$  are independent, then nearest neighbor vortices only are correlated. Thus

$$k^2 = \overline{k_n^2} = \frac{\overline{(F_{n+1} - F_n)^2}}{\lambda^2} = \frac{2\overline{F^2}}{\lambda^2},$$

$$\overline{k_n k_{n+1}} = \frac{\overline{(F_{n+1} - F_n)(F_{n+2} - F_{n+1})}}{\lambda^2} = \frac{-\overline{F^2}}{\lambda^2},$$

$$\overline{k_n k_{n+2}} = \frac{\overline{(F_{n+1} - F_n)(F_{n+3} - F_{n+2})}}{\lambda^2} = 0,$$

... .

The correlation function  $R$  satisfies

$$R(0) = 1,$$

$$R(\pm 1) = -1/2,$$

$$R(l) = 0, \quad l \neq 0, \pm 1,$$

consistent with equation 56. Nearest neighbor correlation was generally used in the computer experiments. A finite row of vortices must be used in any experiment, and correlation of nearest neighbors alone gives the maximum number of correlation lengths possible for a given number of vortices. If the correlation does not extend over a large number of vortices, the vortices can be taken to represent large scale eddies in the continuous problem, rather than elements of a vortex sheet.

From equation 53, the initial upwash above a row of such vortices is

$$v_o(y, z) = \sum_n \frac{k_n}{2\pi} \frac{z - n\lambda}{y^2 + (z - n\lambda)^2} .$$

Thus

$$\overline{v_o(y, z)v_o(y, z + \zeta)} = \frac{k^2}{4\pi^2} \sum_{n=-\infty}^{\infty} \sum_{l=-\infty}^{\infty} R(l) \frac{[z - n\lambda][z - (n-l)\lambda + \zeta]}{\{(z - n\lambda)^2 + y^2\} \{ [z - (n-l)\lambda + \zeta]^2 + y^2 \}} .$$

The upwash correlation above the discrete vortices is not independent of  $z$ . The flow is not homogeneous in  $z$  because the vortices have special determinate locations  $z = n\lambda$ . However, the upwash correlation is periodic on  $z$  with period  $\lambda$ , so an average correlation

$$Q^*(y, \zeta) = \frac{1}{\lambda} \int_0^\lambda \overline{v_o(y, z)v_o(y, z + \zeta)} dz ,$$

can be used. Then

$$\begin{aligned} Q^*(y, \zeta) &= \frac{k^2}{4\pi^2 \lambda} \sum_{n=-\infty}^{\infty} \sum_{l=-\infty}^{\infty} R(l) \int_{-n\lambda}^{-n\lambda + \lambda} \frac{x(x + l\lambda + \zeta)}{(x^2 + y^2)[(x + l\lambda + \zeta)^2 + y^2]} dx , \\ &= \frac{k^2}{4\pi^2 \lambda} \sum_{l=-\infty}^{\infty} R(l) \int_{-\infty}^{\infty} \frac{x(x + l\lambda + \zeta)}{(x^2 + y^2)[(x + l\lambda + \zeta)^2 + y^2]} dx , \\ &= \frac{k^2}{4\pi^2 \lambda y} \sum_{l=-\infty}^{\infty} R(l) G\left(\frac{\zeta + \lambda l}{y}\right) . \end{aligned}$$

By contour integration in the complex plane,

$$G(\eta) = \frac{2\pi}{4 + \eta^2} .$$

If nearest neighbor vortices only are correlated,

$$Q^*(y, \zeta) = \frac{k^2}{4\pi^2 \lambda y} \left[ G\left(\frac{\zeta}{y}\right) - \frac{1}{2} G\left(\frac{\zeta+\lambda}{y}\right) - \frac{1}{2} G\left(\frac{\zeta-\lambda}{y}\right) \right] .$$

As  $\lambda/y \rightarrow 0$ ,

$$Q^*(y, \zeta) \Rightarrow \frac{k^2}{4\pi^2 \lambda y} \left[ -\frac{1}{2} \left(\frac{\lambda}{y}\right)^2 G''\left(\frac{\zeta}{y}\right) \right] = \frac{k^2 \lambda y}{4\pi} \frac{4y^2 - 3\zeta^2}{(4y^2 + \zeta^2)^3} . \quad (57)$$

In section 4B, an expression for the upwash correlation  $Q(y, \zeta)$  for the continuous sheet was derived assuming the impulse spectrum  $\psi = A \exp(-\mu |k_3|)$ . In the limit  $\mu/y \rightarrow 0$ , equation 43 for  $Q(y, \zeta)$  becomes identical to equation 57 if

$$A = \frac{k^2 \lambda}{8\pi} .$$

Furthermore, as  $\lambda/y \rightarrow 0$ ,  $\overline{v_o(y, z)v_o(y, z+\zeta)}$  should become insensitive to  $z$  and approach  $Q^*(y, \zeta)$ . All the correlations  $R_{ij}$  between points in the potential flow region above  $y$  can be found from  $Q(y, \zeta)$ . Thus discrete vortices with nearest neighbor correlations only give a far field which is identical to the far field of a continuous sheet.

In subsection B a way of generating random vortex strengths satisfying  $\overline{k_m k_n} = k^2 R(n-m)$  for any  $R$  is described. Once a particular initial condition is chosen from the ensemble  $\{k_n, y_n(0), z_n(0)\}$ , the finite difference forms of equations 54 have to be solved step-by-step for as many time increments as a solution is desired. The computation is inherently unstable, and the computed vortex locations drift away from the locations that would be assigned by an exact solution. In computer work on deterministic problems, for

example the work of Abernathy and Kronauer [11] on the formation of vortex streets, this mechanical error drift is a serious matter and has to be kept small by using extremely small time increments. Here the object is not to follow detailed vortex paths, but to find averages over a large number of runs. Each numerical experiment can be much sloppier than the experiments of [11]; each one must be sloppier if a large number of experiments is carried out on a limited budget. Subsections C, D and E are devoted to an analysis of mechanical error drift, a discussion of how rapid a drift is permissible, and a description of a mechanism for counteracting the dispersive effect of error drift of general physical interest — vortex capture. In subsection F results for some numerical flow visualization experiments on the motion of random vortices are presented.

The flow visualization experiments show how vortices disperse: vortices pair up into dipoles and 'boil' out of the turbulent region. But no information is obtained about the rate  $x$  momentum is redistributed by the field induced by the vortices. Suppose the initial shear flow is linear,  $U_0 = \Omega y$ , and turbulent velocity fluctuations in the  $x$  direction are initially zero. If the experiment were conducted in a wind tunnel, a hot-wire measurement could be made at  $y, z$  at time  $t$ . If the hot wire intercepts a fluid column which originated at  $y_0$ , then the speed it measures is  $\Omega y_0(y, z, t)$ , since the momentum and speed of fluid columns is conserved. The mean speed is then  $U(y, t) = \overline{\Omega y_0}(y, t)$  where the average is taken over a traverse along  $z$  or over an ensemble of independent experiments. But the computer cannot tell the original height of the fluid column

at  $y, z$  at time  $t$  unless a test particle carried along with the flow from time zero happens to have landed there. In order to simulate a hot-wire traverse by computer, test particles labeled by their initial heights  $y_0$  must be scattered over the  $y, z$  plane, and their paths computed along with the paths of the vortices. At time  $t$  the particles lying near  $y$  are surveyed to find their original heights  $y_0$ . If the flow is incompressible and the test particles were originally scattered uniformly over  $y, z$ , then the mean speed is  $U(y, t) = \overline{\Omega y_0}(y, t)$  where the double-bar average is taken over the particles surveyed at  $y, t$  in each realization of the flow and over an ensemble of initial conditions. This idea is described in detail in subsection G, and the results of a series of numerical momentum transfer experiments are presented in subsection H.

#### B. Generation of Random Vortex Strengths with a Specified Correlation

The object is to generate a large number  $N$  of vortex strengths  $k_n$  which satisfy  $\overline{k_m k_n} = k^2 R(n-m)$  for any  $R$  desired. The average is taken over an ensemble of sets  $\{k_n, n = 1, \dots, N\}$  generated by the technique described here. The numbers  $k_n$  are taken to be periodic with period  $N$ , so  $k_{N+1} = k_1$  for example. Vortices near the ends of the sequence  $n = 1, \dots, N$  are then correlated, but that should make no difference in the turbulence experiments if  $N$  is much greater than the maximum  $\ell$  for which  $R(\ell)$  is non-zero. For nearest neighbor correlation, only the end vortices 1 and  $N$  are unnaturally correlated.  $N$  is assumed odd throughout the derivation to keep the work tidy.

Suppose  $n$  is regarded as a continuous variable. Then any well-behaved real function  $k(n)$  of period  $N$  can be written as a Fourier series

$$k(n) = \sum_{m=-\infty}^{\infty} c_m e^{2\pi i \frac{nm}{N}},$$

where  $c_m^* = c_{-m}$ . Where  $n$  is an integer,

$$e^{2\pi i \frac{n}{N}(m+qN)} = e^{2\pi i \frac{nm}{N}}.$$

Set  $M = (N-1)/2$ . Then

$$k_n = \sum_{m=-M}^M \left( \sum_{q=-\infty}^{\infty} c_{m+qN} \right) e^{2\pi i \frac{nm}{N}},$$

since, for example,  $c_{M+1} = c_{N-M}$ , etc.. Define

$$a_m = \sum_{q=-\infty}^{\infty} c_{m+qN}.$$

Then

$$k_n = \sum_{m=-M}^M a_m e^{2\pi i \frac{nm}{N}}, \tag{58}$$

and a periodic function defined on an integer argument can be written as a finite Fourier series (cf. Brillouin [12]). The correlation function can now be expressed as a Fourier transform —

$$k^2_R(n-m) = \overline{k_m k_n} = \sum_p \sum_q \overline{a_p a_q} e^{\frac{2\pi i}{N} (pm+qn)}$$

Since the left hand side depends on  $(n-m)$  only,

$$\overline{a_p a_q} = \overline{a_p a_p^*} \delta(p+q) = \alpha_p^2 \delta(p+q) ,$$

$$k^2 R(\ell) = \sum_{p=-M}^M \alpha_p^2 e^{2\pi i \frac{p\ell}{N}} ,$$

where  $\alpha_p^2 = \overline{a_p a_p^*}$ . The relation between  $R(\ell)$  and  $\alpha_p$  can be inverted by using the identity

$$\sum_{\ell=-M}^M e^{\frac{2\pi i}{N} \ell(p-q)} = \begin{cases} 2M+1 = N, & p = q , \\ 0, & p \neq q . \end{cases}$$

Thus

$$k^2 \sum_{\ell=-M}^M R(\ell) e^{-\frac{2\pi i}{N} q\ell} = \sum_{p=-M}^M \alpha_p^2 \sum_{\ell=-M}^M e^{\frac{2\pi i}{N} \ell(p-q)} ,$$

and

$$\alpha_m^2 = \frac{k^2}{N} \sum_{\ell=-M}^M R(\ell) e^{-2\pi i \frac{m\ell}{N}} . \tag{59}$$

If  $R(\ell)$  is given,  $\alpha_m^2 = \overline{a_m a_m^*}$  can be computed from equation 59. If random Fourier coefficients  $a_m$  can be generated satisfying  $\overline{a_m a_n} = \alpha_m^2 \delta(m+n)$  and  $a_m^* = a_{-m}$ , then sets of properly correlated random vortex strengths can be found from equation 58.

From equation 59,

$$\alpha_0^2 = \frac{k^2}{N} \sum_{\ell=-M}^M R(\ell) .$$

If the row of  $2M+1$  vortices is to represent turbulence homogeneous in  $z$ ,  $R(\ell)$  must drop to zero long before  $|\ell| \sim M$ . Then equation 56 requires  $\alpha_0^2 = 0$ . Write

$$a_m = \phi_m e^{2\pi i \theta_m}$$

where  $\phi_m$  is a real amplitude satisfying  $\overline{\phi_m^2} = \alpha_m^2$  and  $\theta_m$  is a random phase between 0 and 1. Since  $\theta_m = -\theta_{-m}$  and  $a_0 = 0$ , equation 58 becomes

$$k_n = \sum_{m=1}^M \phi_m \cos 2\pi \left( \frac{nm}{N} + \theta_m \right) .$$

If

$$\phi_m = \alpha_m = \frac{k}{\sqrt{N}} \left[ 1 + 2 \sum_{\ell=1}^M R(\ell) \cos 2\pi \frac{m\ell}{N} \right]^{1/2} ,$$

(60)

and each  $\theta_m$  is independently assigned one of the values

$$\theta_m = \begin{cases} 0 \\ .25 \\ .5 \\ .75 \end{cases}$$

at random, then the Fourier coefficients do satisfy  $\overline{a_m a_n} = \alpha_m^2 \delta(m+n)$ :

$$\overline{a_m a_{-m}} = \alpha_m^2 e^{\overline{2\pi i(\theta_m - \theta_m)}} = \alpha_m^2 ,$$

$$\overline{a_m a_m} = \alpha_m^2 e^{\overline{2\pi i(\theta_m + \theta_m)}} = \alpha_m^2 \begin{Bmatrix} +1 \\ -1 \end{Bmatrix} = 0 ,$$

$$\overline{a_m a_n} = \alpha_m \alpha_n e^{\overline{2\pi i\theta_m}} e^{\overline{2\pi i\theta_n}} = 0, \quad m \neq n .$$

It is interesting to note that the famous random phase, which plays so large a part in qualitative discussions about turbulence and no part at all in quantitative theories, is introduced here to set the initial conditions for the computer runs.

The way of selecting  $\phi_m$  and  $\theta_m$  in equations 60 may seem inflexible, and it might be thought that the probability distribution

for  $k_n$  would be a rickety step function. However, there are four  $\theta$ 's to choose from, and  $M$  choices must be made to sum the first of equations 60. If the number of vortices  $N = 51$ , say, then  $M = 25$  and the ensemble of possible initial conditions has

$$4^{25} \sim 10^{15}$$

members! The variety seems adequate. Since each  $k_n$  is the sum of 20 or 30 independent random variables of similar variance, the probability distribution for  $k_n$  should be very nearly Gaussian. In practice, the values of  $\theta_m$  for  $m = 1, \dots, M$  in each computer run were chosen by flipping a coin (twice per  $\theta_m$ ) or rolling dice. The random phases were then fed into a subroutine which computed  $k_n$  according to equations 60. The subroutine was named VEGAS, of course.

### C. Error Drift

Suppose a passive particle has a position  $\underline{x} = (y, z)$  at time  $t$ . Given the current vortex locations, the computer can calculate the velocity  $\underline{v}(\underline{x}, t)$  of the convected particle exactly (within round-off errors) from equation 53. If the time increment is  $\tau$ , then the computer assigns a new location  $\underline{x} + \delta\underline{x}$  to the particle at time  $t + \tau$ , where

$$\delta\underline{x} = \tau \underline{v}(\underline{x}, t) .$$

But an exact solution would give

$$\delta\underline{x} = \int_t^{t+\tau} \underline{v}[\underline{x}(\sigma), \sigma] d\sigma ,$$

where the integrand is evaluated at the changing location of the particle. Thus the computed trajectory and the 'real' trajectory diverge.

If the particle is convected in the field of a single vortex, the computer trajectory can be predicted analytically. Geometrical quantities are shown in figure 14. If the current radius from the vortex of strength  $k$  to the particle is  $r$ , the particle will be advanced a distance

$$\delta s = \tau \frac{k}{2\pi r}$$

after a time increment  $\tau$  along a straight line tangent to the circle of radius  $r$ . Thus the radius increases a distance  $\delta r$ , where

$$r + \delta r = \sqrt{r^2 + \delta s^2} \approx r + \frac{1}{2} \frac{\delta s^2}{r} .$$

Then

$$\frac{\delta r}{\tau} \approx \tau \frac{k^2}{8\pi^2 r^3} ,$$

$$\frac{\delta \theta}{\tau} \approx \frac{k}{2\pi r^2} ,$$

since  $\delta \theta \approx \delta s / r$ . For  $\tau$  small enough, the difference equations can be written as differential equations for the computed trajectory  $r(t)$ ,  $\theta(t)$ :

$$\frac{dr}{dt} = \frac{k^2 \tau}{8\pi^2 r^3} ,$$

$$\frac{d\theta}{dt} = \frac{k}{2\pi r^2} .$$

(61)

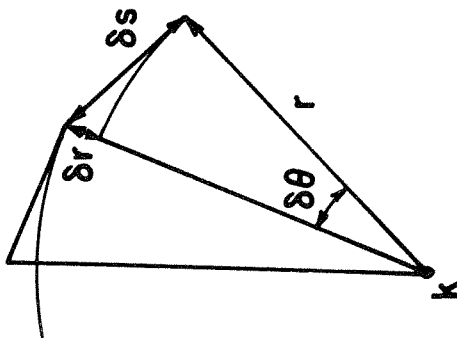
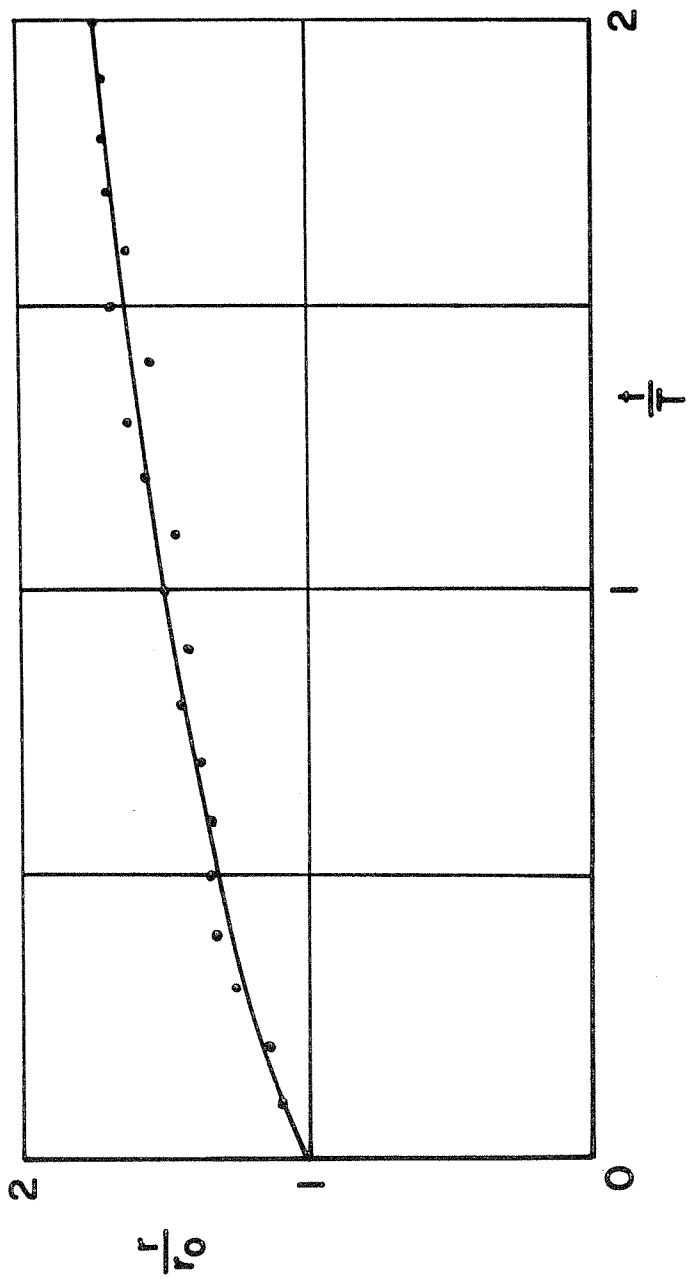


FIG. 14 COMPUTED TRAJECTORY AROUND A VORTEX

If the particle starts at  $r(0) = r_0$ ,  $\theta(0) = 0$ , then the equations give a trajectory

$$\begin{aligned} \text{(i)} \quad r(t) &= r_0 \left( 1 + \frac{k^2 \tau t}{2\pi^2 r_0^4} \right)^{1/4}, \\ \text{(ii)} \quad \theta(t) &= \frac{2\pi r_0^2}{k\tau} \left( \sqrt{1 + \frac{k^2 \tau t}{2\pi^2 r_0^4}} - 1 \right). \end{aligned} \tag{62}$$

For  $\tau \rightarrow 0$  and  $t$  fixed,  $r(t) \rightarrow r_0$  and  $\theta(t) \rightarrow kt/2\pi r_0^2$ , the expressions for the actual trajectory. But as  $t \rightarrow \infty$ ,  $r$  grows as  $t^{1/4}$  and  $\theta$  slows down to a  $t^{1/2}$  growth as the particle slides out into a weaker velocity field. A numerical flow visualization experiment was performed to check the trajectory predicted by equations 62. A time increment  $\tau$  one-twentieth of the actual orbit time  $T = (2\pi)^2 r_0^2/k$  was used,  $\tau = .05T$ , and the program was run up to  $t = 2T$ . The curve  $r(t)/r_0$  from equation 62(i) is plotted against  $t/T$  in figure 14 along with the experimental points. The agreement is excellent (the oscillation in the experimental data arises because the points are taken from an on-line computer plot, and a finer spacing is available across the print-out sheet than down it). There can be no doubt that the approximation  $\delta x = \tau \gamma(x, t)$  causes the dominant error in the numerical experiments.

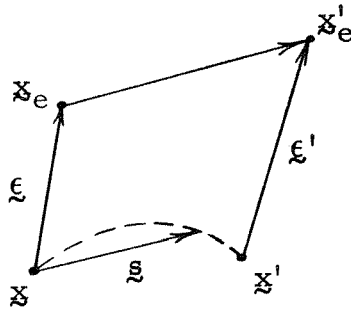
In the general case, suppose the 'real' position of a particle at time  $t$  is  $\underline{x}$  and the computed erroneous position is  $\underline{x}_e$ . The computed position at time  $t + \tau$  is then

$$\underline{x}_e' = \underline{x}_e + \tau \gamma(\underline{x}_e, t),$$

and the actual position is

$$\mathbf{x}' = \mathbf{x} + \int_t^{t+\tau} \mathbf{v}[\mathbf{x}(\sigma), \sigma] d\sigma$$

as shown in the sketch.



But

$$\mathbf{v}[\mathbf{x}(\sigma), \sigma] = \mathbf{v}(\mathbf{x}, t) + \mathbf{s} \cdot \nabla \mathbf{v}(\mathbf{x}, t) + (\sigma - t) \frac{\partial \mathbf{v}}{\partial t}(\mathbf{x}, t) + \dots,$$

where  $\mathbf{s}$  is the displacement of the particle from  $\mathbf{x}$  at time  $\sigma$ . Then

$$\mathbf{s} = (\sigma - t)\mathbf{v}(\mathbf{x}, t) + \dots,$$

and

$$\mathbf{v}[\mathbf{x}(\sigma), \sigma] = \mathbf{v}(\mathbf{x}, t) + (\sigma - t) \frac{D\mathbf{v}}{Dt}(\mathbf{x}, t) + \dots$$

The expansion can be used in the equation for  $\mathbf{x}'$  to give

$$\mathbf{x}' = \mathbf{x} + \tau \mathbf{v}(\mathbf{x}, t) + \frac{\tau^2}{2} \mathbf{a}(\mathbf{x}, t) + \dots,$$

where  $\mathbf{a} = D\mathbf{v}/Dt$  is the acceleration of the particle at time  $t$ . The computer result can also be expanded in the form

$$\mathbf{x}'_e = \mathbf{x}_e + \tau \mathbf{v}(\mathbf{x}, t) + \tau(\mathbf{x}_e - \mathbf{x}) \cdot \nabla \mathbf{v}(\mathbf{x}, t) + \dots$$

Define the error vector  $\boldsymbol{\xi} = \mathbf{x}'_e - \mathbf{x}'$ . The expansions for  $\mathbf{x}'_e$  and  $\mathbf{x}'$  can be subtracted to give

$$\xi' = \xi + \tau \xi \cdot \nabla_{\mathbf{y}}(\mathbf{x}, t) - \frac{\tau^2}{2} \mathbf{a}(\mathbf{x}, t) + \dots$$

for the new error vector  $\xi'$ . Thus

$$\frac{\delta \xi}{\tau} = \xi \cdot \nabla_{\mathbf{y}} - \frac{\tau}{2} \mathbf{a} + \dots$$

Provided  $\tau$  is small compared with the time scale of the flow and  $|\xi|$  is small compared with the typical length, that can be written as a linear differential equation for  $\xi$ ,

$$\frac{d\xi}{dt} = \xi \cdot \nabla_{\mathbf{y}} - \frac{\tau}{2} \mathbf{a}, \quad (63)$$

with

$$\xi(0) = 0.$$

Equation 63 is the fundamental equation for the machine error drift  $\xi$ , good before  $\xi$  extends clear across eddies and whenever the time increment  $\tau$  is reasonably small. The acceleration term catalyzes the build-up of error; computations based on  $\delta \mathbf{x} = \tau \mathbf{v}$  cannot keep up with an accelerating particle, and the computed position slips back along the line of acceleration. As  $\xi$  increases, the velocity at the computed location becomes significantly different from the velocity at the actual location, and the two locations shear apart. Equations 61 for the computer trajectory around a single vortex show the same behavior. The computed location slips outward at a rate  $\tau/2$  times the current centrifugal acceleration. The angular speed at any radius is the same as it would be for an actual particle, but as the computed radius grows, the computed angular displacement lags far behind the actual displacement.

Equation 63 holds for any velocity and acceleration fields  $\mathbf{y}$  and  $\mathbf{a}$  specified continuously at the actual particle location. The

steady velocity and acceleration around a single vortex drive the error up continuously and rapidly. But in a turbulence problem  $\nabla \mathbf{u}$  and  $\mathbf{a}$  are random functions of time, and it might be conjectured that the error drift is less drastic in that case, more like a random walk than an exponential divergence. Equation 63 cannot be solved analytically in closed form, but the conjecture can be tested on a simple one-dimensional model,

$$\frac{d\epsilon}{dt} = \alpha(t)\epsilon + \beta(t) , \quad (64)$$

$$\epsilon(0) = 0 ,$$

where  $\alpha(t)$  is a stochastic function analogous to a strain rate and  $\beta(t)$  is  $\tau/2$  times an acceleration. Equation 64 describes the error in computing particle location in a non-steady one-dimensional channel flow, for example. The object now is to find the variance of  $\epsilon$ ,  $\overline{\epsilon^2(t)}$ , where the average is taken over an ensemble of histories  $\alpha(\sigma)$ ,  $\beta(\sigma)$ ,  $0 \leq \sigma \leq t$ .

The exact solution of equation 64 is

$$\epsilon(t) = \int_0^t e^{\int_{\sigma}^t \alpha(t') dt'} \beta(\sigma) d\sigma .$$

Thus

$$\epsilon^2 = \int_0^t \int_0^t e^{\int_{\sigma}^t \alpha dt' + \int_{\tau}^t \alpha dt'} \beta(\sigma)\beta(\tau) d\sigma d\tau .$$

Assume  $\alpha$  and  $\beta$  are independent. Then

$$\overline{\epsilon^2} = \int_0^t \int_0^t \left\{ \overline{e^{\int_\sigma^t \alpha dt'} + \int_\tau^t \alpha dt'}} \right\} \overline{\beta(\sigma)\beta(\tau)} d\sigma d\tau .$$

Assume  $\beta$  is statistically homogeneous, so that  $\overline{\beta(\sigma)\beta(\tau)} = \beta^2 B(\sigma-\tau)$ .

The variance can then be written

$$\begin{aligned} \overline{\epsilon^2} &= \beta^2 \int_0^t d\tau \int_0^\tau d\sigma \overline{e^{2\int_\tau^t \alpha dt'} e^{\int_\sigma^\tau \alpha dt'}} B(\sigma-\tau) \\ &+ \beta^2 \int_0^t d\tau \int_\tau^t d\sigma \overline{e^{2\int_\sigma^t \alpha dt'} e^{\int_\tau^\sigma \alpha dt'}} B(\sigma-\tau) . \end{aligned}$$

Assume  $\alpha(t)$  is strictly stationary, and  $\alpha(t)$  and  $\alpha(t+T)$  are independent for  $T > \theta$ . Then for  $t \gg \theta$ ,

$$\overline{\epsilon^2} \Rightarrow \beta^2 \int_0^t d\tau \int_0^\tau d\sigma \overline{e^{2\int_0^{t-\tau} \alpha dt'} e^{\int_0^{\tau-\sigma} \alpha dt'}} B(\sigma-\tau) \quad \textcircled{a}$$

$$+ \beta^2 \int_0^t d\tau \int_\tau^t d\sigma \overline{e^{2\int_0^{\tau-\sigma} \alpha dt'} e^{\int_0^{\sigma-\tau} \alpha dt'}} B(\sigma-\tau) . \quad \textcircled{b}$$

By substituting  $x = t-\tau$ ,  $y = \tau-\sigma$  in integral  $\textcircled{a}$  and  $x = t-\sigma$ ,  $y = \sigma-\tau$  in integral  $\textcircled{b}$  it is easy to show that

$$\overline{\epsilon^2} \Rightarrow 2\beta^2 \int_0^t dx \int_0^{t-x} dy \overline{e^{2\int_0^x \alpha dt'} e^{\int_0^y \alpha dt'}} B(y) . \quad (65)$$

For  $t \gg \theta$ , the integrals  $\int_0^x \alpha dt'$  and  $\int_0^y \alpha dt'$  are carried out over many correlation times of  $\alpha$  almost everywhere in the domain spanned by  $x$  and  $y$ . Thus

$$X = \int_0^x \alpha(t) dt ,$$

for example, is a random variable of mean zero (assuming  $\alpha$  has zero mean) and has a Gaussian distribution (by the Central Limit Theorem) for almost all  $x$  in the integrand of equation 65. But

$$\overline{e^X} = e^{\frac{1}{2}X^2}$$

for Gaussian  $X$ . If  $\overline{\alpha(t)\alpha(t')} = \alpha^2 A(t-t')$ , then

$$\begin{aligned} \overline{X^2} &= \int_0^x \int_0^x \overline{\alpha(t)\alpha(t')} dt dt' = 2\alpha^2 \int_0^x (x-t)A(t)dt \\ &\Rightarrow 2\alpha^2 \Theta_x, \end{aligned}$$

for almost all  $x$ , where  $\int_0^\infty A(t)dt = \Theta$ . Equation 65 becomes

$$\begin{aligned} \overline{\epsilon^2} &\Rightarrow 2\beta^2 \int_0^t dx \int_0^{t-x} dy e^{4\alpha^2 \Theta x} e^{\alpha^2 \Theta y} B(y) \\ &= 2\beta^2 \int_0^t dy e^{\alpha^2 \Theta y} B(y) \int_0^{t-y} dx e^{4\alpha^2 \Theta x} \\ &= \frac{\beta^2}{2\alpha^2 \Theta} e^{4\alpha^2 \Theta t} \int_0^t e^{-3\alpha^2 \Theta y} B(y) \left[ 1 - e^{-4\alpha^2 \Theta(t-y)} \right] dy . \end{aligned}$$

Define the weighted correlation time for  $\beta$ ,

$$\mathfrak{S} = \int_0^\infty e^{-3\alpha^2 \Theta y} B(y) dy .$$

Then for  $t \gg \theta$  (the dependence time of  $\alpha$ ),  $\Theta$  (the correlation time for  $\alpha$ , presumably  $\sim \theta$ ), and  $\mathfrak{S}$  (the weighted correlation time for  $\beta$ ),

$$\overline{\epsilon^2} \Rightarrow \frac{\beta^2 \mathfrak{S}}{2\alpha^2 \Theta} (e^{4\alpha^2 \Theta t} - 1) . \quad (66)$$

For stochastic  $\alpha(t)$  and  $\beta(t)$ , equation 64 represents a generalized random walk for  $\epsilon(t)$ . Under the very stringent conditions assumed to solve the problem, the variance  $\overline{\epsilon^2}$  is given by equation 66. The variance diverges exponentially. It diverges even faster than the solution of equation 64 for constant  $\alpha(t) = \alpha$  if  $2\alpha\Theta > 1$ . Notice if the strain term in equation 64 is either very weak,  $\alpha \rightarrow 0$ , or varies extremely fast,  $\Theta \rightarrow 0$ , equation 66 reduces to the standard random walk result

$$\overline{\epsilon^2} \Rightarrow 2\beta^2 \delta t$$

until very large times.

The conjecture that the computer error given by equation 63 diverges slowly for stochastic  $\underline{y}$  and  $\underline{a}$  must be wrong. A numerical experiment cannot reproduce the detailed trajectories of vortices and test particles for very long times. But in a turbulence experiment the detailed record is not important. As long as the computed motion of a particle is governed primarily by the flow velocity  $\underline{y}$  at its current location, the accumulated error should be unimportant in a turbulence experiment. The computed location should be just as good as the actual location. Just beyond their point of intersection, a computed path diverges from a physical path with an error velocity  $\underline{y}_\epsilon$  given by

$$\underline{y}_\epsilon = -\frac{\tau}{2} \underline{a}$$

from equation 63. A numerical turbulence experiment is valid if

$$\delta = \sqrt{\frac{y \epsilon^2}{z^2}} < < 1, \quad (67)$$

regardless of detail differences between the computed flow and the physical flow with the same initial conditions.  $\delta$  is estimated for a random distribution of independent vortices in subsection D.

#### D. Flow Velocity and Error Velocity

The model studied in this subsection is artificial, just as equation 64 with statistically stationary  $\alpha$  and  $\beta$  is an artificial model of equation 63 with inhomogeneous vector fields  $\underline{y}$  and  $\underline{z}$ . The object is to show qualitatively that without special precautions condition 67 may not be satisfied no matter how small a time increment  $\tau$  is used.

Suppose the  $i^{\text{th}}$  vortex has strength  $k_i$  and location  $y_i, z_i$ , and a passive particle subject to a physical velocity  $\underline{y}$  and error velocity  $\underline{y}_\epsilon$  is located at  $y, z$ . Define

$$\begin{aligned} \zeta_i &= z - z_i, \\ \eta_i &= y - y_i, \\ r_i^2 &= \zeta_i^2 + \eta_i^2. \end{aligned}$$

From equation 53,

$$v = \sum_i \frac{k_i}{2\pi} \frac{\zeta_i}{r_i}, \quad w = - \sum_i \frac{k_i}{2\pi} \frac{\eta_i}{r_i}.$$

Thus

$$y_\epsilon^2 = v^2 + w^2 = \frac{1}{4\pi^2} \sum_i \sum_j k_i k_j \frac{\zeta_i \zeta_j + \eta_i \eta_j}{r_i^2 r_j^2}. \quad (68)$$

Now assume  $k_i$  and  $k_j$  are independent for  $i \neq j$ . That cannot be true for the problem solved by computer in this chapter, since the vortex strengths must be correlated to satisfy equation 56. Assume that the location of each vortex is independent of its strength, and that the vortices are distributed isotropically around  $y, z$ . Neither of those assumptions can hold for vortices located initially at  $y = 0$ ,  $z = n\lambda$ . By the first two assumptions, an average over an ensemble  $\{k_i, y_i, z_i\}$  gives

$$\overline{v^2} = \left(\frac{k}{2\pi}\right)^2 \sum_i \frac{1}{r_i^2}, \quad (69)$$

where  $\overline{k_i k_j} = k^2 \delta_{ij}$ . The error velocity  $v_e$  equals  $-\tau \underline{a}/2$ , and

$$\underline{a} = \frac{\partial \underline{v}}{\partial t} + \underline{v} \cdot \nabla \underline{v} = \frac{\partial \underline{v}}{\partial t} + \nabla \left( \frac{v^2 + w^2}{2} \right) + \xi \underline{j} \times \underline{v}.$$

The last term on the right is zero, since  $\xi$ , the component of vorticity in the  $x$  direction, is zero outside of the vortex singularities. The variance of  $\partial \underline{v}/\partial t$  would be hard to find, but the acceleration  $\underline{a}$  should be the same order as its convective part  $\nabla(v^2/2)$ . The variance of the error velocity

$$v_{e c}^2 = -\frac{\tau}{2} \nabla \left( \frac{v^2}{2} \right)$$

can be found about the same way equation 69 was found, but the algebra is complicated, and the derivation is deferred to Appendix F.

Under the three assumptions stated above equation 68, the result is

$$\overline{v_{e c}^2} = \frac{\tau^2}{4} \left(\frac{k}{2\pi}\right)^4 \left[ \sum_i \sum_j \frac{1}{r_i^2 r_j^4} + 2 \sum_i \frac{1}{r_i^6} \right]. \quad (70)$$

The averages in equations 69 and 70 are to be taken over an ensemble of vortex locations  $\{y_i, z_i\}$  with the particle position fixed.

Equations 69 and 70 both give infinity if the vortices are distributed with uniform density over the  $y, z$  plane. But suppose  $N$  vortices are distributed uniformly over an annulus around  $y, z$  of inner radius  $s$  and outer radius  $S$ . The density of vortices per unit area is

$$\rho = \frac{N}{\pi(S^2 - s^2)},$$

and the probability distribution function for  $r_1, \dots, r_N$  is

$$p(r_1, \dots, r_N) = P(r_1) \dots P(r_N),$$

since the vortices are distributed uniformly, where

$$P(r) = \begin{cases} \frac{2r}{S^2 - s^2}, & s < r < S, \\ 0, & \text{otherwise.} \end{cases}$$

Thus

$$\overline{y^2} = \left(\frac{k}{2\pi}\right)^2 \sum_i \int_s^S \frac{1}{r_i^2} \frac{2r_i dr_i}{S^2 - s^2}$$

or

$$\overline{y^2} = 2\pi \left(\frac{k}{2\pi}\right)^2 \rho \log \frac{S}{s}. \quad (71)$$

Similarly,

$$\overline{v_{\epsilon c}^2} = \frac{\tau^2}{4} \left(\frac{k}{2\pi}\right)^4 \left[ 3 \sum_i \int_s^S \frac{1}{r_i} \frac{2r_i dr_i}{S^2 - s^2} + \sum_{\substack{i,j \\ i \neq j}} \int_s^S \int_s^S \frac{1}{r_i^2 r_j^2} \frac{4r_i r_j}{(S^2 - s^2)^2} dr_i dr_j \right] .$$

For fixed  $\rho$  and large  $S$  and  $N$ , the result of integrating and summing is

$$\overline{v_{\epsilon c}^2} = \frac{\tau^2}{4} \left(\frac{k}{2\pi}\right)^4 \left[ \frac{3\pi}{2} \frac{\rho}{s} + 2\pi^2 \frac{\rho^2}{s^2} \log \frac{S}{s} \right] . \quad (72)$$

Non-dimensionalize  $\rho$  with the area excluded around each vortex,

$$\rho = \frac{\rho^*}{\pi s} .$$

Then the ratio of equations 72 and 71 is

$$\delta_c^2 = \frac{\overline{v_{\epsilon c}^2}}{\overline{v^2}} = \frac{3}{16} \left(\frac{\tau k}{2\pi s}\right)^2 \left( \frac{1 + \frac{4}{3} \rho^* \log \frac{S}{s}}{\log \frac{S}{s}} \right) . \quad (73)$$

Since  $\delta_c \sim \delta$ , equation 67 implies that the condition  $\delta_c \ll 1$  must be met for a numerical turbulence experiment to be valid.

What counterparts do  $S$ ,  $s$ ,  $\rho^*$  have in a numerical experiment? The computer can handle only a finite number of vortices distributed over a finite area of the  $y, z$  plane, and  $S$  can be taken as a linear dimension of that area.  $s$  is a distance of closest approach to a vortex, but it is not obvious that such a distance has any physical meaning. One thing is certain: if  $s$  could not be established physically, it would have to be incorporated in the computer program anyway.  $\delta_c$  is proportional to  $\tau k / 2\pi s^2$ , and that combination

must be small in a valid numerical experiment.

It may be that a passively convected particle has a hard time getting close to a vortex if it is not close at the start. As a particle approaches a line vortex, its motion is dominated by that vortex, and it tends to orbit at a constant radius. In the case of two approaching vortices, the argument is more solid. Equations 54 can be written in Hamiltonian form (Lamb [10]),

$$\dot{y}_i = \frac{\partial W}{\partial z_i} , \quad \dot{z}_i = - \frac{\partial W}{\partial y_i} ,$$

where

$$W = \sum_{i < j} k_i k_j \log r_{ij} ,$$

and

$$r_{ij} = \sqrt{(y_i - y_j)^2 + (z_i - z_j)^2} .$$

Then

$$\frac{dW}{dt} = \sum_i \left( \frac{\partial W}{\partial y_i} \dot{y}_i + \frac{\partial W}{\partial z_i} \dot{z}_i \right) = 0 ,$$

and the Hamiltonian  $W$  is conserved. No single  $r_{ij}$  can become very small unless an unusually large part of the energy  $W$  is concentrated in the interaction between  $i$  and  $j$ . Since such a concentration is improbable in a turbulent flow, close approaches are rare.

However, Abernathy and Kronauer, in their numerical experiments on vortex-street formation [11], found that vortices of the same sign tended to cluster into loosely packed clouds. The

important aspect of the flow is the motion of the clouds in the general field they induce, rather than the detailed motion of the vortices inside. If the computations were done by hand, clouds could be treated as single vortices once they form, and the detailed motions of the constituent vortices could be dropped from the calculations. The influence of one cloud on a vortex inside another cloud is small compared with the influence of adjacent vortices. If the computer does not notice the formation of clouds and concentrate them during the calculations, each cloud will tend to diffuse and wander at random under the errors accumulated in computing the trajectories of its constituent vortices, rather than move as a unit in the field induced by the other clouds.

A systematic way to concentrate clouds is to unite vortices which come close to each other. The clouds are cleaned up as they form. Furthermore,  $s$  has a precise meaning in a computer program which permits one vortex to capture another.  $s$  is an average capture radius. Once vortices of strengths  $k_1$  and  $k_2$  approach closer than  $s(k_1, k_2)$ , the computer assumes that they will orbit each other from then on and unites them into one vortex of strength  $k_1 + k_2$ . This is not just a computational expedient. The physical basis of vortex capture is explained in subsection E.

#### E. Vortex Capture

Suppose vortices 1 and 2 approach each other and interact strongly. If  $k_1$  and  $k_2$  have the same sign, the two lock into a mutual orbit until the strain field of the other vortices shears them apart

(the flow outside vortex singularities is irrotational, so the deformation is pure strain). Idealize the field of the other vortices in the vicinity of the pair singled for special attention as a uniform steady translation ( $V, W$ ) and strain  $\alpha$ . If the  $y, z$  axes are oriented parallel to the principal axes of strain with the flow diverging along the  $y$  axis, then the equations of motion 54 for vortices 1 and 2 are

$$\left. \begin{aligned} \dot{y}_1 &= V + \alpha y_1 + \frac{k_2}{2\pi} \frac{\zeta}{\eta^2 + \zeta^2}, \\ \dot{y}_2 &= V + \alpha y_2 - \frac{k_1}{2\pi} \frac{\zeta}{\eta^2 + \zeta^2}, \\ \dot{z}_1 &= W - \alpha z_1 - \frac{k_2}{2\pi} \frac{\eta}{\eta^2 + \zeta^2}, \\ \dot{z}_2 &= W - \alpha z_2 + \frac{k_1}{2\pi} \frac{\eta}{\eta^2 + \zeta^2}, \end{aligned} \right\} \quad (74)$$

where  $\alpha$  is positive, and the relative coordinates  $\eta, \zeta$  are

$$\eta = y_1 - y_2,$$

$$\zeta = z_1 - z_2.$$

Define the center of vorticity coordinates

$$Y = \frac{k_1 y_1 + k_2 y_2}{k_1 + k_2},$$

$$Z = \frac{k_1 z_1 + k_2 z_2}{k_1 + k_2}.$$

Equations 74 can be combined in an obvious way to give separated center of vorticity and relative equations of motion:

$$\begin{aligned}
 \text{(i)} \quad & \begin{cases} \dot{Y} = V + \alpha Y \quad , \\ \dot{Z} = W - \alpha Z \quad ; \end{cases} \\
 \text{(ii)} \quad & \begin{cases} \dot{\eta} = \alpha \eta + \frac{k_1+k_2}{2\pi} \frac{\zeta}{\eta^2+\zeta^2} \quad , \\ \dot{\zeta} = -\alpha \zeta - \frac{k_1+k_2}{2\pi} \frac{\eta}{\eta^2+\zeta^2} \quad . \end{cases}
 \end{aligned} \tag{75}$$

Equations 75(i) show that the center of vorticity of the vortex pair is convected like a passive particle in the idealized flow of the other vortices. Equations 75(ii) describe the motion of a particle around a vortex of strength  $k_1+k_2$  in a strain field  $\alpha$ . The phase plane trajectories of equations 75(ii) are the same as the streamlines of the combined vortex and strain fields. If  $\eta$  and  $\zeta$  lie on a closed trajectory, then vortices 1 and 2 remain bound in spite of the strain tending to shear them apart.

Equations 75(ii) can be written

$$\dot{\eta} = \frac{\partial \psi}{\partial \zeta} \quad , \quad \dot{\zeta} = - \frac{\partial \psi}{\partial \eta} \quad ,$$

where

$$\psi = \alpha \eta \zeta + \frac{k_1+k_2}{2\pi} \log \frac{r}{r_0} + K \quad .$$

$K$  and  $r_0$  are constants, and  $r^2 = \eta^2 + \zeta^2$ .  $\psi$  is conserved along trajectories, since

$$\dot{\psi} = \frac{\partial \psi}{\partial \eta} \dot{\eta} + \frac{\partial \psi}{\partial \zeta} \dot{\zeta} = 0 \quad .$$

$\psi$  is the stream-function for the combined vortex and strain fields.

From equations 75(ii),  $\dot{\eta}$  and  $\dot{\zeta}$  are both zero at

$$r_o = \sqrt{\frac{|k_1+k_2|}{2\pi\alpha}} ,$$

$$\theta_o = \begin{cases} 135^\circ, 315^\circ, & k_1+k_2 > 0 , \\ 45^\circ, 225^\circ, & k_1+k_2 < 0 , \end{cases}$$

where polar coordinates defined by  $\eta = r \sin \theta$ ,  $\zeta = r \cos \theta$  are used.

Set  $\psi = 0$  at these singular points, so that

$$K = \frac{k_1+k_2}{4\pi} .$$

Since  $\psi$ ,  $\partial\psi/\partial\eta$  and  $\partial\psi/\partial\zeta$  are zero at a singular point  $\eta_o$ ,  $\zeta_o$ , the expansion of  $\psi$  around the point begins

$$\psi = \frac{\tilde{\eta}^2}{2} \left( \frac{\partial^2 \psi}{\partial \eta^2} \right)_o + \tilde{\eta} \tilde{\zeta} \left( \frac{\partial^2 \psi}{\partial \eta \partial \zeta} \right)_o + \frac{\tilde{\zeta}^2}{2} \left( \frac{\partial^2 \psi}{\partial \zeta^2} \right)_o + \dots ,$$

where  $\tilde{\eta} = \eta - \eta_o$  and  $\tilde{\zeta} = \zeta - \zeta_o$ . But

$$\left( \frac{\partial^2 \psi}{\partial \eta^2} \right)_o = \left( \frac{\partial^2 \psi}{\partial \zeta^2} \right)_o = 0 , \quad \left( \frac{\partial^2 \psi}{\partial \eta \partial \zeta} \right)_o = 2\alpha .$$

Thus

$$\psi = 2\alpha \tilde{\eta} \tilde{\zeta}$$

near  $\eta_o$ ,  $\zeta_o$ , and the singularity is a saddle point (stagnation point) with principal axes aligned with the principal axes of the original strain field. The rate of strain at the singular points is  $2\alpha$ . A phase plane (streamline) diagram of the trajectories given by equations 75(ii) is sketched in figure 15 for  $k_1+k_2$  negative. The trajectories are closed in an eye-shaped region around the origin bounded

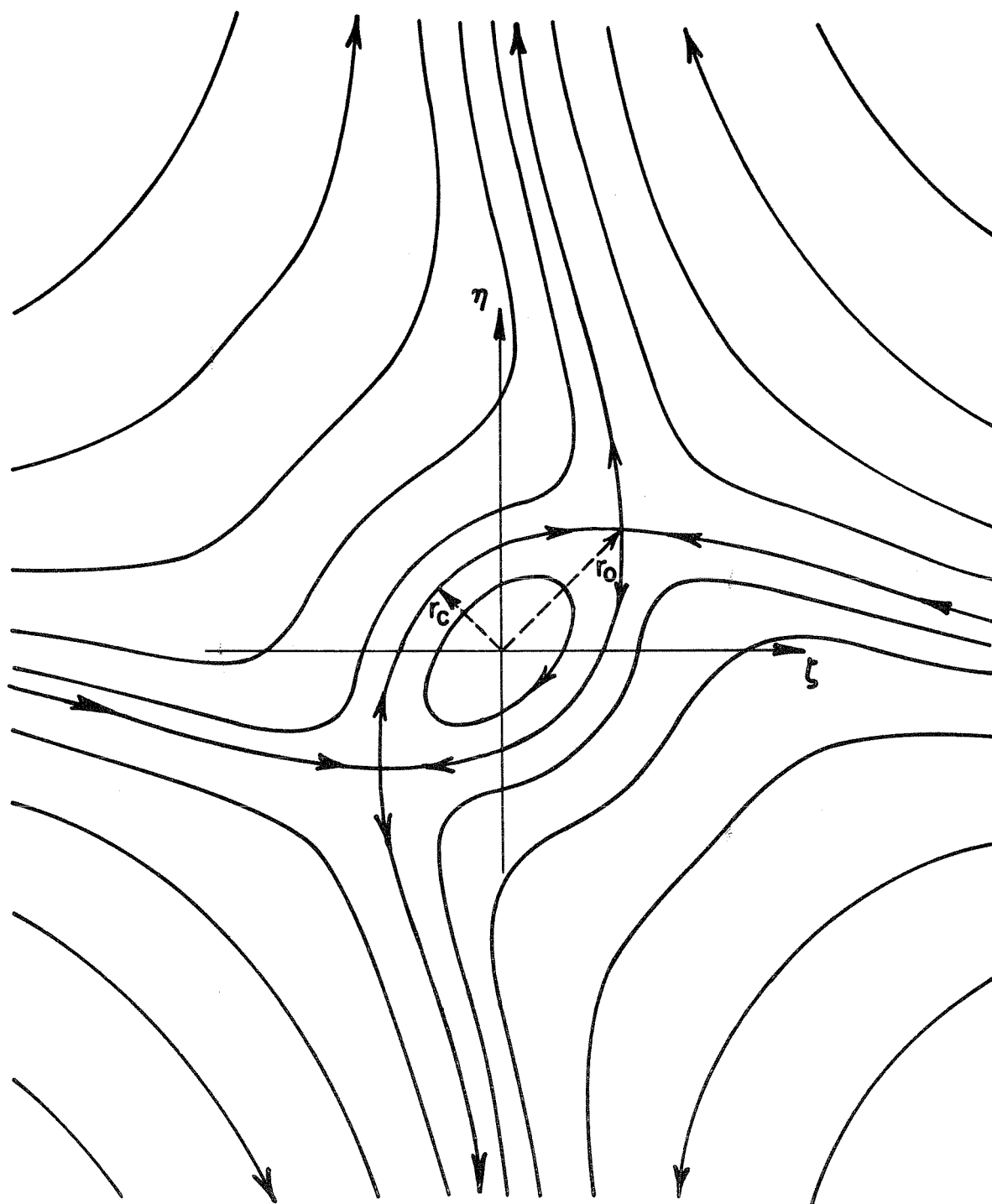


FIG. 15 RELATIVE TRAJECTORIES OF TWO VORTICES IN A STRAIN FIELD

by the stagnation trajectories  $\psi = 0$ . The closest approach to the origin of a  $\psi = 0$  trajectory occurs at  $\theta = 135^\circ$  in the figure, and the corresponding radius  $r_c$  is the solution of the equation

$$\frac{\alpha r_c^2}{2} + \frac{|k_1+k_2|}{2\pi} \log \frac{r_c}{r_o} + \frac{|k_1+k_2|}{4\pi} = 0 .$$

The solution  $r_c = .527 r_o$  can be found easily by iteration. Thus

$$r_c = .527 \sqrt{\frac{|k_1+k_2|}{2\pi\alpha}} . \tag{76}$$

If the distance between vortices of strengths  $k_1$  and  $k_2$  in a steady strain  $\alpha$  is ever smaller than  $r_c$ , the vortices are permanently bound and never shear apart. If the distance lies between  $r_c$  and  $r_o$ , the vortices may or may not be bound, and if the distance is greater than  $r_o$ , the vortex pair is not stable and will certainly shear apart. This is a simple mechanical explanation of the vortex clustering phenomenon discussed by Batchelor [13] and Onsager [14]. If  $k_1$  and  $k_2$  have the same sign, the capture cross section  $r_c^2$  (or more accurately, the area of the 'eye' in figure 15) tends to be large. If they have opposite signs, the cross section is small. Once two vortices of the same sign are bound tightly, the pair acts like a single strong vortex, and the capture cross section for interactions with third vortices is large.

Equation 76 provides a rational criterion, in a numerical experiment, for concentrating nearby vortices of strengths  $k_1$  and  $k_2$  into a single vortex of strength  $k_1 + k_2$ . But where should the new vortex be located? The answer depends on the physical process that 'capture' is supposed to represent. Equation 76 and the phase

plane eye were derived for a steady strain field. The actual strain encountered by a vortex pair varies in magnitude and orientation; the eye blinks. Line vortices are eventually knocked apart by strong interactions with other vortices no matter how strongly they are bound. If they are strongly bound, they stay bound for a long time. But real vortices have finite core diameters; if real vortices orbit together for several revolutions, they are smeared into concentric shells of vorticity by each other's strain field. Once that happens, they really are united and can never be knocked apart. Capture of line vortices should be a model of the physical smearing process. Suppose that at time  $t_0$ , before the smearing, a continuous vorticity distribution  $\xi$  is peaked near  $y_1, z_1$  and  $y_2, z_2$ , with total amounts  $2k_1$  around point 1 and  $2k_2$  around point 2. The y coordinate of the center of vorticity is

$$Y_0 = \frac{\int y \xi dA}{\int \xi dA} \approx \frac{k_1 y_1 + k_2 y_2}{k_1 + k_2}$$

at time  $t_0$ , with a similar equation for  $Z_0$ . As the vorticity is smeared under its own induction and convected by uniform translation  $(V, W)$  and strain  $\alpha$ , the center of vorticity moves according to the equation

$$\dot{Y} = V + \alpha Y$$

just as a single discrete vortex would move. That is shown in Appendix G. After the vorticity is smeared into shells, the shells are centered on the current center of vorticity. A single vortex

which started at  $(Y_0, Z_0)$  at time  $t_0$  would also be located there. Thus, if instantaneous concentration is supposed to simulate the eventual result of smearing, the new vortex must be located at the center of vorticity of the original pair. Two vortices of strengths and locations  $k_1, y_1, z_1$  and  $k_2, y_2, z_2$  must be united into a single vortex of strength

$$\left. \begin{aligned}
 k &= k_1 + k_2, \\
 \text{located at} \\
 y &= \frac{k_1 y_1 + k_2 y_2}{k}, \\
 z &= \frac{k_1 z_1 + k_2 z_2}{k}.
 \end{aligned} \right\} \quad (77)$$

Equation 76 cannot be used as a practical capture criterion for a non-steady and non-uniform flow until an effective  $\alpha$ , say  $\alpha_e$ , is estimated.  $\alpha_e$  is not the average strain (which is infinite for discrete vortices), but is an average intensity of that part of the strain field which is uniform over distances comparable to  $r_c$ .

Suppose the ensemble of initial conditions on the vortices is  $\{k_n, y_n(0) = 0, z_n(0) = n\lambda\}$ , with  $\overline{k_n^2} = k^2$  and nearest neighbor correlation only. Then  $\alpha_e$  is proportional to  $k/\lambda^2$  on dimensional grounds, but the constant of proportionality cannot be predicted exactly. In practice, the computer program unites vortices  $k_1, k_2$  if their separation  $r$  satisfies

$$r^2 < \sigma \lambda^2 \frac{|k_1 + k_2|}{k}, \quad (78)$$

where  $\sigma$  is an input parameter. Average results of the numerical experiments should not depend critically on  $\sigma$ .  $\sigma$  is selected to make the numerical error drift small rather than to satisfy a physical theory.

An estimate of  $\delta_c$  can be made from equation 73 based on effective values  $S_e$ ,  $s_e$ ,  $\rho_e^*$  and typical parameters used in the experiments. A very crude estimate of  $S_e$  is sufficient, since it enters equation 73 only as the argument of a log. About 50 vortices were usually run, and they dispersed over an area about  $50\lambda \times 4\lambda = 200\lambda^2$ . Thus  $S_e \sim 10 - 20\lambda$ . The effective distance of closest approach  $s_e$  can be taken as the average of the square root of the right hand side of inequality 78,  $s_e = \kappa\sqrt{\sigma} \lambda$ , with  $\kappa \sim 1$ .  $\sigma$  was usually .25, so  $s_e \sim .5\lambda$ . Thus  $\log S_e/s_e \sim \log 30 \sim 3$ . The vortex density  $\rho_e$  was about  $50/200\lambda^2$ , so  $\rho_e^* = \pi s_e^2 \rho_e \sim .2$ . By equation 73,

$$\delta_c \approx \frac{.25}{\kappa\sigma} \left( \frac{\tau\kappa}{2\pi\lambda^2} \right) .$$

Most experiments were run with  $\sigma = .25$  and  $\tau\kappa/2\pi\lambda^2 = .1$ . Thus the error velocity  $v_\epsilon$  was typically one-tenth the physical flow velocity  $u$ .

#### F. Flow Visualization Experiments

Equations 60, 54, 78 and 77 are the basis of numerical flow visualization experiments on the motion of line vortices. Random, correlated vortex strengths are generated by equations 60, the vortex paths are described by equations 54, vortices are united according to criterion 78, and the strength and location of the new vortex are given by equations 77. Variables in the computer program are

non-dimensionalized on the variance of the vortex strength,  $k^2$ , and the original vortex spacing,  $\lambda$ :

$$\begin{aligned} (y_i^*, z_i^*) &= \left( \frac{y_i}{\lambda}, \frac{z_i}{\lambda} \right), \\ k_i^* &= \frac{k_i}{k}, \\ \tau^* &= \frac{\tau k}{2\pi\lambda^2}, \\ t^* &= \frac{tk}{2\pi\lambda^2}. \end{aligned}$$

The input data are  $\tau^*$ , the non-dimensional time increment,  
 $\sigma$ , the constant in the capture criterion 78,  
 $N$ , the number of vortices,  
 $(N-1)/2$  correlations  $R$ ,  
 $(N-1)/2$  random phases  $\theta$ , and data for the output including  
 $T^*$ , the time between frames, and  
 $F$ , the number of frames desired.

Each frame shows the locations of the vortices at the time the frame is printed. The vortex strengths are symbolized by the letters used to show the locations according to the following table:

VORTEX STRENGTH	SYMBOL
$k^* < -2.0$	K
$-2.0 \leq k^* < -1.0$	L
$-1.0 \leq k^* < -0.5$	M
$-0.5 \leq k^* < 0$	N
$0 \leq k^* < 0.5$	P
$0.5 \leq k^* < 1.0$	Q
$1.0 \leq k^* < 2.0$	R
$2.0 \leq k^*$	S .

The graphing is done on-line, that is, the appropriate symbol for a vortex is typed in the line and column corresponding to its current location by the same machine that types ordinary arithmetical results. Figures 16 (i)-(vi) are six frames photographed directly from the computer output for a numerical experiment with the following input data:

$$\tau^* = .1$$

$$\sigma = .25$$

$$N = 45$$

$$R(1) = -0.5, R(2) = \dots = R(22) = 0$$

$$T^* = 1.0$$

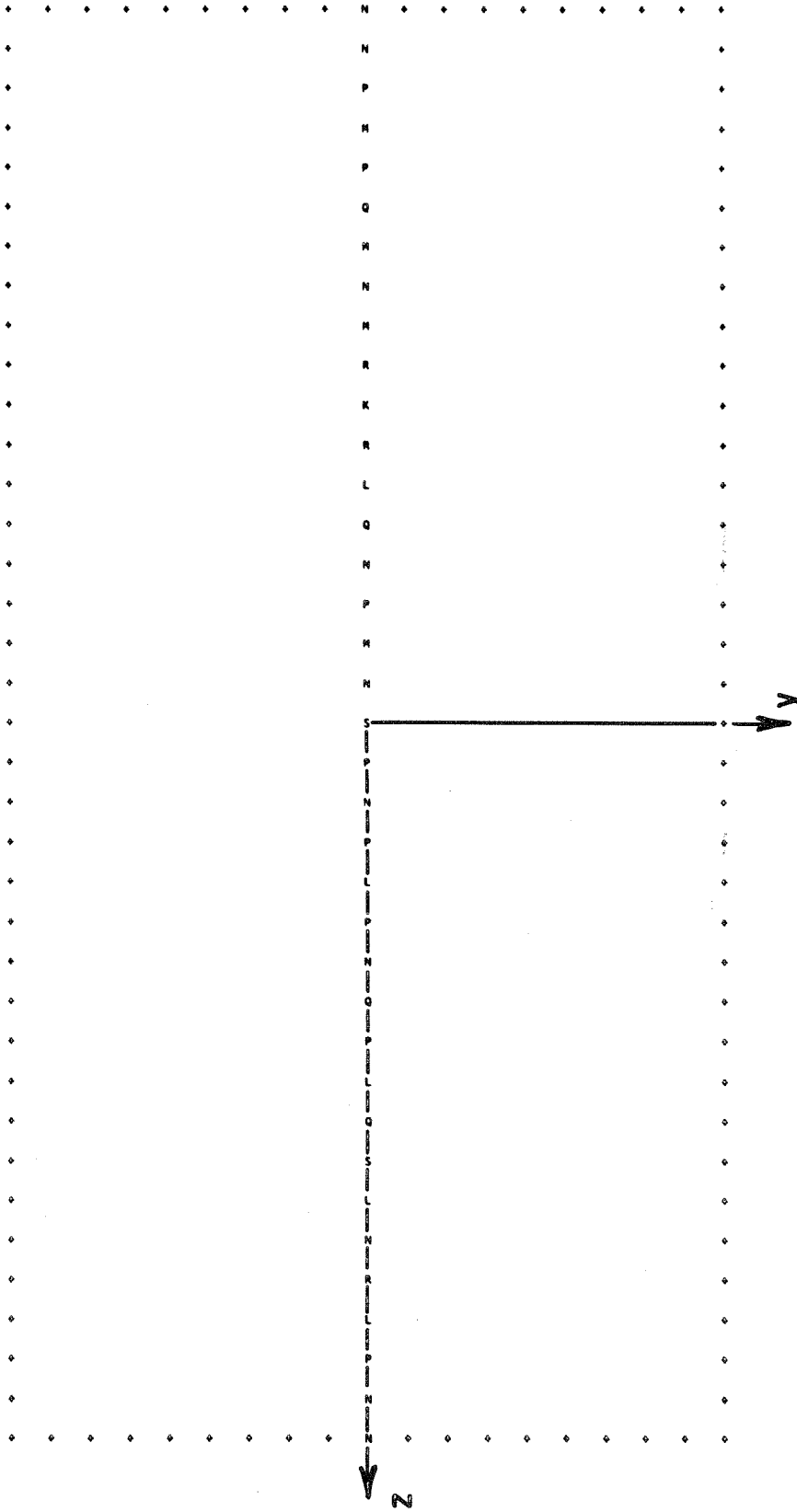
$$F = 6$$

The 22 random phases (each one having one of the values 0, 0.25, 0.5, 0.75) were chosen by rolling dice. The pluses around the border of each frame are spaced a unit distance apart. The first frame shows the conditions at  $t^* = 0$ , the second shows the vortex locations at  $t^* = 1$ , and so on up to  $t^* = 5$ . Each frame is centered on the original row of vortices and is 36 units long. Since the vortex row is 44 units long at the beginning, three or four vortices at either end fall outside of the picture. The particular results shown are typical for nearest neighbor correlation in every respect.

Two things are striking about figures 16: by  $t^* = 5$ , no clouds of vortices of the same sign have formed; instead, vortex dipoles consisting of vortices of opposite sign boil away from the original line. Up to  $t^* = 16$  at least, the clouds obtained by Abernathy and Kronauer never form. The vortices disperse too fast by

vigorous boiling of vortex dipoles. Equation 76 shows that a vortex dipole is not a very stable structure. If two vortices have strengths of equal magnitude but opposite sign, the vortices are sheared apart by any strain. But the strong dipoles escape the region of maximum turbulent agitation so fast that they are not split. They move in large orbits about their distant centers of vorticity almost unaffected by the other vortices. The vortex dipoles have been circumscribed by ellipses in figures 16(iv) and (vi). The size of an ellipse indicates how much fluid the dipole carries with it (cf. Lamb [10], p. 221). The dipoles can be visualized as columns of fluid which preserve their momentum and leave the region of agitation too fast to be stretched apart by non-linear convection. They correspond to the surges of turbulence found above wakes and boundary layers.

The dipoles arise because of the negative nearest neighbor correlation along the original line of vortices. Clouds would form if there were long sequences of positively correlated vortices as there were in Abernathy and Kronauer's experiments. Because clouds do not form, the analysis of error drift has little bearing on the numerical experiments of this chapter. Vortex captures rarely occur. On the average, about three vortices out of fifty are captured in a run up to  $t^* = 16$ . The analysis of error drift was carried out in great detail because of the intrinsic interest of the generalized random walk of subsection C, and because the mechanism of vortex capture would be essential in numerical experiments on more homogeneous initial distributions of line vortices.



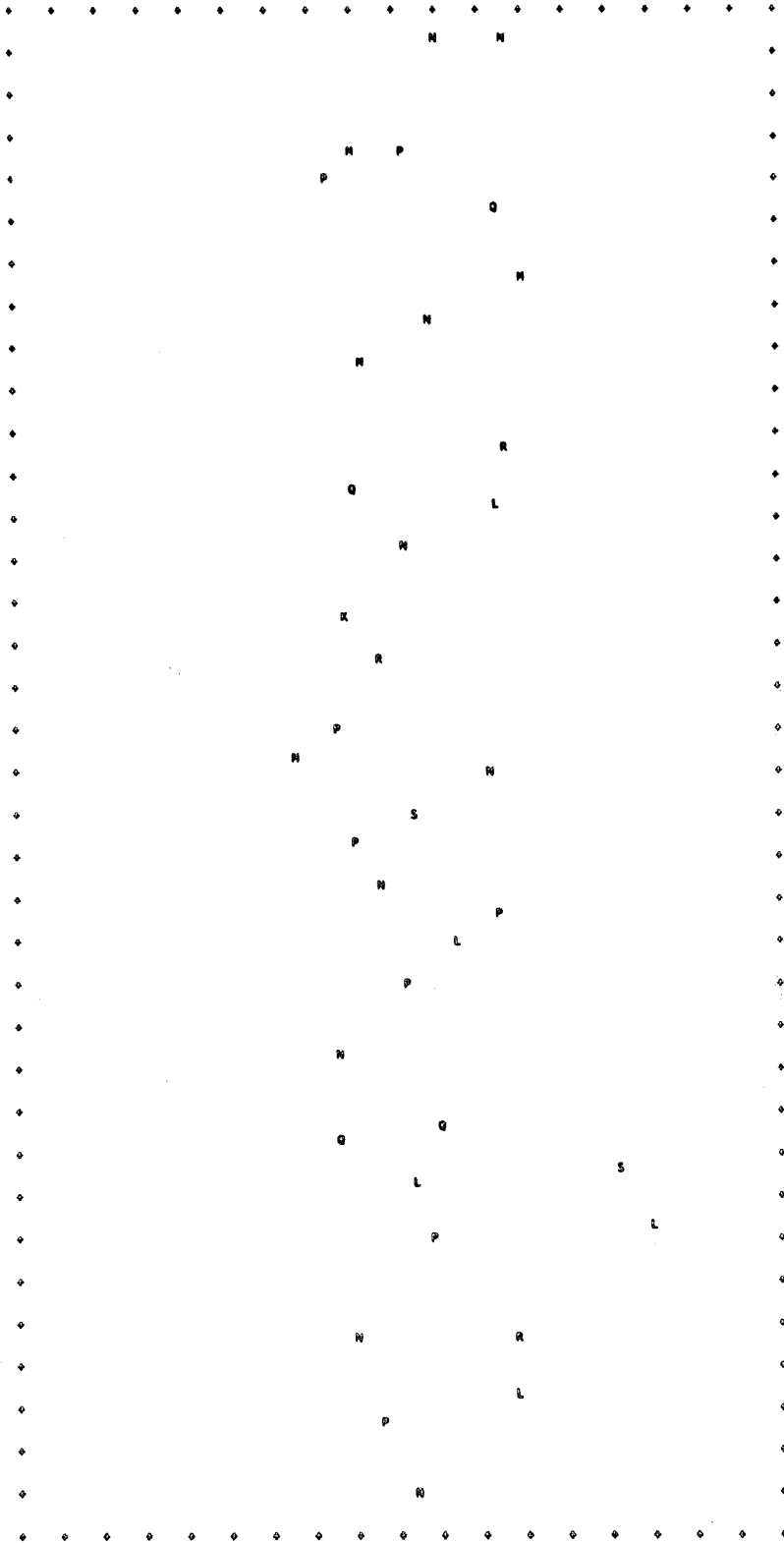
$t^* = 0$

FIG. 16(i) FLOW VISUALIZATION EXPERIMENT



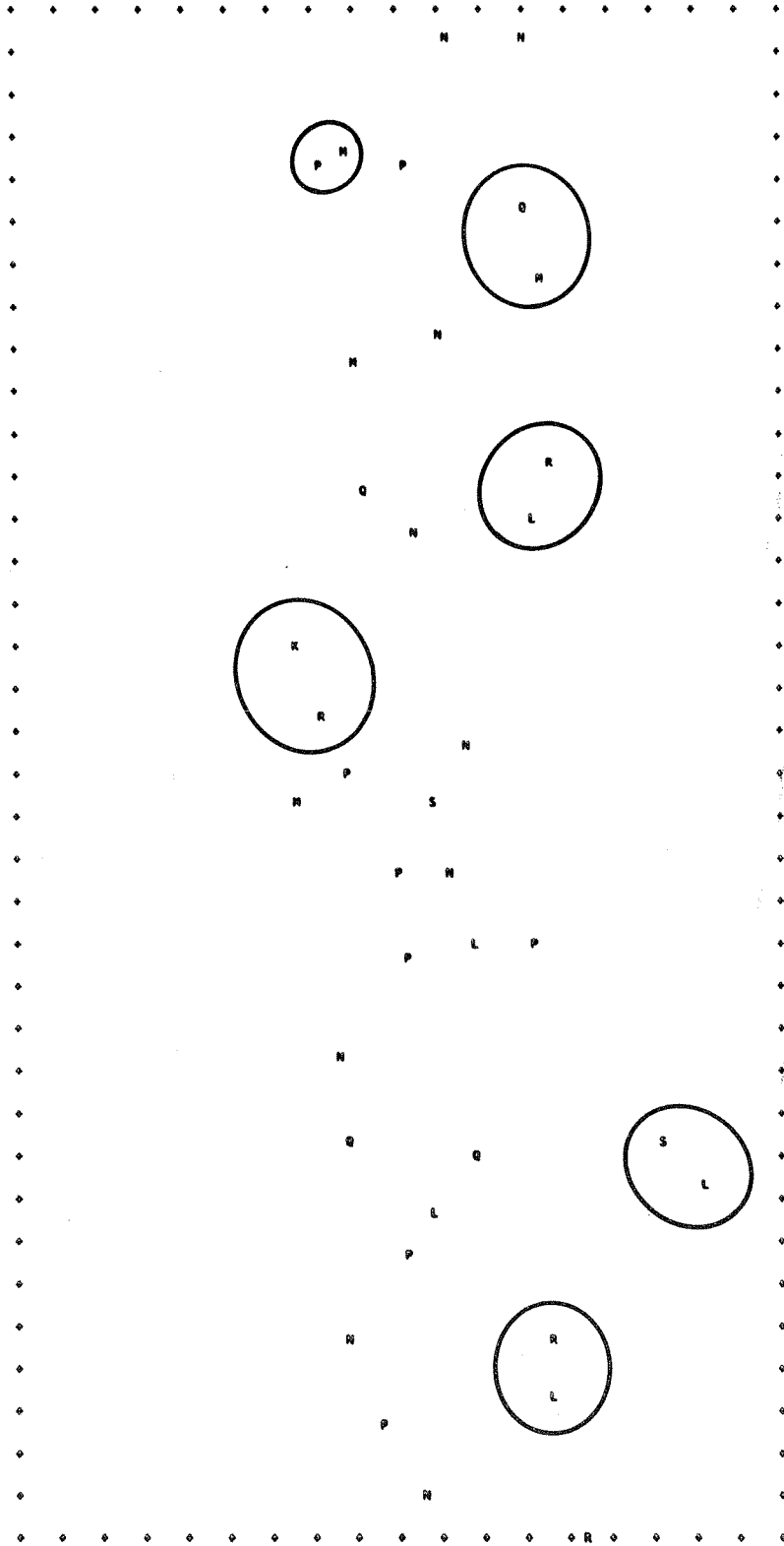






$t^* = 4$

FIG. 16(v) FLOW VISUALIZATION EXPERIMENT



\*  
t = 5

FIG. 16 (vi) FLOW VISUALIZATION EXPERIMENT

G. Background for the Momentum Transfer Experiments

Prior to time zero, fluid flows in the  $x$  direction at a speed  $U_0(y)$ . At time zero a random area-impulse independent of  $x$  is applied in the  $x, z$  plane to generate a row of line vortices. The initial random velocity component in the  $x$  direction is zero. The motion of the line vortices in the  $y, z$  plane is independent of the  $x$  momentum they transport. The flow visualization experiments of subsection F show how the vortices disperse, but give no indication of how rapidly the flow they induce distorts the mean speed profile  $U(y, t)$ . If the flow were studied in a physical experiment,  $U(y, t)$  would be found by taking a hot-wire traverse along  $z$  at height  $y$  and time  $t$ .  $U(y, t)$  would be the average  $x$  speed measured. A traverse over many eddy correlation lengths can be regarded as a sequence of measurements over an ensemble of independent experiments. This suggests the model experiment used here to define  $U(y, t)$  formally. Call it

Experiment 1.

The experiment is performed at time  $t$ . Let  $\tilde{p}(u|y)du$  be the probability that the speed at height  $y$  and random  $z$  lies between  $u$  and  $u + du$  ( $u$  is taken to be total velocity in the  $x$  direction here). Then the mean speed profile  $U(y)$  is defined by

$$U(y) = \int_{-\infty}^{\infty} u \tilde{p}(u|y) du .$$

Since  $x$  speed is conserved (equation 35) and the velocity fluctuations in the  $x$  direction are initially zero, the measured speed  $u$  is uniquely related to the original height  $y_0$  of the fluid column the measuring

instrument intercepts:

$$u = U_o(y_o) \ .$$

If  $U_o(y_o)$  is monotonic (like  $U_o = \Omega y_o$ ), then the inverse relation

$$y_o = Y_o(u)$$

is unique. Let  $p(y_o | y) dy_o$  be the probability that the fluid column intercepted at  $y$  originated between  $y_o$  and  $y_o + dy_o$ . Then

$$\int_{-\infty}^u \tilde{p}(u' | y) du' = \int_{-\infty}^{Y_o(u)} p(y_o' | y) dy_o' \ .$$

Differentiate with respect to  $u$ :

$$\tilde{p}(u | y) = p(Y_o(u) | y) \frac{dY_o}{du} \ .$$

Then

$$U(y) = \int_{-\infty}^{\infty} u p(Y_o(u) | y) \frac{dY_o}{du} du \ .$$

Substitute  $u = U_o(y_o)$  :

$$U(y) = \int_{-\infty}^{\infty} U_o(y_o) p(y_o | y) dy_o \ . \tag{79}$$

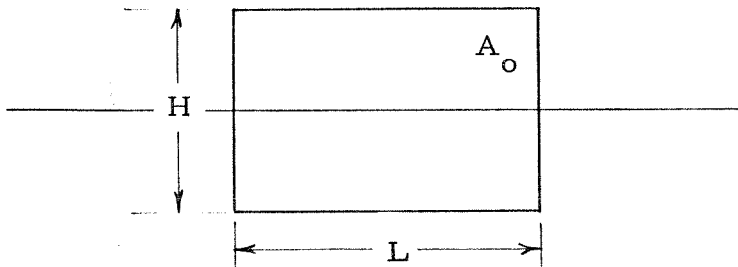
Equation 79 is the definition of  $U(y)$  in terms of the transition probability  $p(y_o | y)$ .

The trouble with Experiment 1 is that it cannot be performed on a computer. The only way to find  $y_o$  for a fluid column selected at specified  $y, t$  and random  $z$  is to reverse the calculation and carry the designated column back to its original location. That is

impossible in practice, because the computer solution is inherently unstable. Error drift (not to mention vortex capture) makes the flow irreversible and sustained, detailed backtracking impossible. An experiment that can be performed is

Experiment 2.

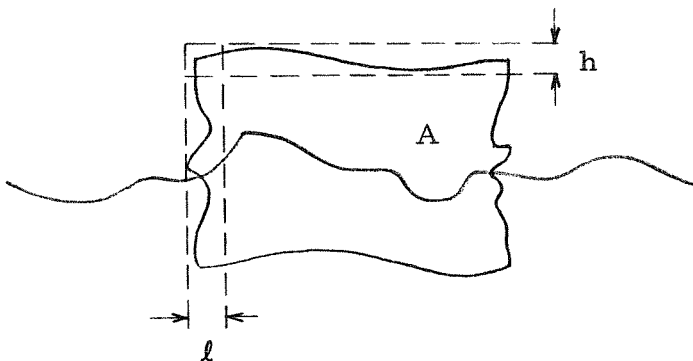
At time zero place a test particle at random inside a large area  $A_0$  straddling the vortex row:



If  $P(y_0, z_0)dy_0 dz_0$  is the probability that the particle originates between  $y_0$  and  $y_0 + dy_0$ ,  $z_0$  and  $z_0 + dz_0$ , then

$$P(y_0, z_0) = \begin{cases} (HL)^{-1}, & (y_0, z_0) \in A_0, \\ 0 & , \text{ otherwise.} \end{cases}$$

By time  $t$ , the converted boundary of the area is distorted:



The probability density for the current particle location is

$$P(y, z) = P(y, z | (y, z) \in A) P((y, z) \in A),$$

where

$P(y, z | (y, z) \in A)$  = the probability density at  $(y, z)$  given that  $(y, z)$  lies inside the convected boundary of  $A$ ,

$P((y, z) \in A)$  = the probability that  $(y, z)$  lies inside  $A$ .

By incompressibility,

$$P(y, z | (y, z) \in A) = (HL)^{-1} \neq \text{fn}(y, z, t).$$

If the horizontal boundaries distort a distance less than  $h$  and the vertical boundaries distort a distance less than  $\ell$ ,

$$P((y, z) \in A) = 1 \text{ for } \begin{aligned} -\frac{L}{2} + \ell < z < \frac{L}{2} - \ell, \\ -\frac{H}{2} + h < y < \frac{H}{2} - h, \end{aligned}$$

and  $P((y, z) \in A)$  drops rapidly to zero outside that area. If  $h \ll H$  and  $\ell \ll L$ ,

$$\begin{aligned} P(y, z) &= H^{-1} L^{-1} = P(y)P(z), \\ P(y) &= H^{-1} \neq \text{fn}(z, t), \\ P(z) &= L^{-1} \neq \text{fn}(y, t) \end{aligned} \tag{80}$$

almost everywhere inside the original area spanned by  $A_0$ . Thus  $y$  and  $z$  are independent, and sampling only those particles which happen to arrive at  $y$  at time  $t$  does not bias the distribution over  $z$ .

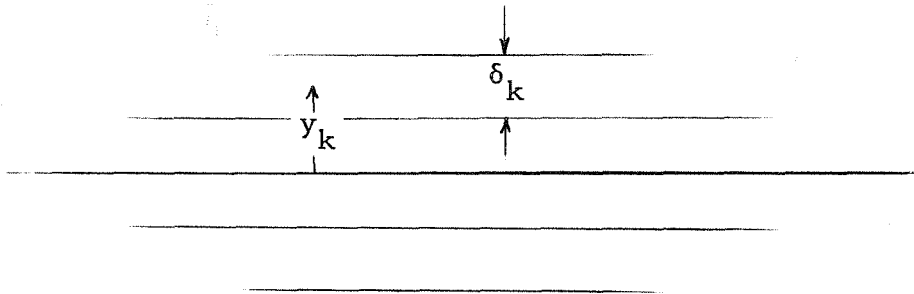
Let  $P(y_0 | y) dy_0$  be the conditional probability that the test particle was originally located between  $y_0$  and  $y_0 + dy_0$  given that it has arrived at  $y$ . Then

$$P(y_0 | y) = p(y_0 | y) ,$$

and sampling only those particles which arrive at  $y$  in Experiment 2 is equivalent to sampling at height  $y$  and random  $z$  in Experiment 1. From the definition of  $U(y)$ ,

$$U(y) = \int_{-\infty}^{\infty} U_0(y_0) P(y_0 | y) dy_0 . \quad (81)$$

Equation 81 is not usable as it stands, because a digital computer cannot handle continuous functions. Suppose the region  $-H/2 \leq y \leq H/2$  is broken into horizontal bands  $k$  with center height  $y_k$  and band height  $\delta_k$ :



Define the average speed in band  $k$ ,

$$U(k) = \frac{1}{\delta_k} \int_k U(y) dy ,$$

where the integration is carried from  $y_k - \delta_k/2$  to  $y_k + \delta_k/2$ . From equation 81,

$$U(k) = \int_{-\infty}^{\infty} dy_0 U_0(y_0) \frac{1}{\delta_k} \int_k dy P(y_0|y) .$$

This equation could be written

$$U(k) = \sum_{k_0} \int_{k_0} dy_0 U_0(y_0) \frac{1}{\delta_k} \int_k dy P(y_0|y)$$

exactly for any  $k$  if the stack of bands extended to  $y \rightarrow \pm \infty$ . But the computer can deal with a finite stack only. When  $k_0$  is summed over a finite sequence of bands, the equation still holds if band  $k$  is not too close to the top or bottom of the stack. For  $y_0 \in k_0$  and  $y \in k$ ,  $P(y_0|y)$  is then zero for the bands that fall outside the sum. If  $U_0(y_0)$  does not change too rapidly in band  $k_0$ ,

$$U(k) = \sum_{k_0} U_0(k_0) \left[ \frac{1}{\delta_k} \int_{k_0} dy_0 \int_k dy P(y_0|y) \right] , \quad (82)$$

where

$$U_0(k_0) = \frac{1}{\delta_{k_0}} \int_{k_0} U_0(y_0) dy_0 .$$

The double integral in brackets can be identified as follows.

The probability that the particle occupies band  $k$  at time  $t$  is

$$P(k) = \int_k P(y) dy = \delta_k H^{-1} ,$$

from equation 80. Let  $P(k_0, k)$  be the probability that the test particle originated in band  $k_0$  and occupies band  $k$  at time  $t$ , that is,

$$P(k_0, k) = \int_{k_0} dy_0 \int_k dy P(y_0, y) , \quad (83)$$

where  $P(y_o, y)dy_o dy$  is the probability that the particle started between  $y_o$  and  $y_o + dy_o$  and currently lies between  $y$  and  $y + dy$ . But

$$P(k_o, k) = P(k_o | k)P(k) = P(k_o | k) \delta_k H^{-1} ,$$

$$P(y_o, y) = P(y_o | y)P(y) = P(y_o | y) H^{-1} .$$

From equation 83,

$$P(k_o | k) = \frac{1}{\delta_k} \int_{k_o} dy_o \int_k dy P(y_o | y) . \quad (84)$$

Thus the bracketed factor in equation 82 is the band-transition probability  $P(k_o | k)$ , the probability that the particle originated in band  $k_o$  given that it occupies band  $k$  at time  $t$ . Equation 82 becomes

$$U(k) = \sum_{k_o} U_o(k_o)P(k_o | k) \quad (85)$$

when band  $k$  is deep enough in the stack of bands that fluid originating outside of the bands summed in equation 85 rarely enters  $k$ . Equation 85 is the discrete analog of equation 81.

The transition probabilities  $P(k_o | k)$  could be found by carrying one test particle per run (Experiment 2), but that would be absurdly wasteful. The numerical Monte Carlo experiments were run according to

### Experiment 3.

Each horizontal band is separated into cells as shown in figure 17. At time zero a test particle is placed at random in each cell (a conventional random number subroutine is used). If the cell area in band  $k_o$  is  $a(k_o)$ , then the number density of test particles convected

from band  $k_o$  is  $\rho(k_o) = a^{-1}(k_o)$ . At time  $t$  a survey is made of the test particles currently in each band  $k$ . If  $n(k_o, k)$  of them originated in  $k_o$  (transitions like  $c \rightarrow d$  in figure 17 are summed with transitions like  $a \rightarrow b$ ), then an unbiased estimator of  $P(k_o | k)$  is

$$P^e(k_o | k) = \frac{n(k_o, k)/\rho(k_o)}{\sum_{j_o} n(j_o, k)/\rho(j_o)} \quad (86)$$

Notice  $\sum_{k_o} P^e(k_o | k) = 1$  regardless of how untypical the particular experimental results happen to be. The Monte Carlo estimate for the mean speed  $U(y_k)$  at  $y_k, t$  is

$$U^e(y_k) = U^e(k) = \sum_{k_o} U_o(k_o) P^e(k_o | k) \quad (87)$$

for  $k$  not too close to the top or bottom bands. In practice that restriction meant that  $U(k)$  could not be estimated in the top or bottom bands of figure 17, but could be estimated in the second to the top or bottom bands. Since transitions  $c \rightarrow d$  are summed with transitions  $a \rightarrow b$ ,  $U^e(y_k) = \pm U^e(-y_k)$  if  $U_o(y_{k_o}) = \pm U_o(-y_{k_o})$ . Thus five independent speeds are obtained from the twelve band setup of figure 17.

The estimate  $U^e(k)$  is refined by running the experiment many times and averaging the results. Placing test particles in cells, grading  $\rho$  for maximum particle density near the vortices, and summing  $a \rightarrow b$  and  $c \rightarrow d$  transitions help to minimize the variance of the estimate for small times. If the particles were scattered at random in each band, the clustering characteristic of random distributions would occur. When the particles are placed at random in band cells

instead, the density over a band is still uniform and the clustering is eliminated. The particles remain spaced apart until the turbulent motion itself scrambles them into a random distribution. Grading  $\rho$  puts the most particles where the most action is — near the vortices. Summing transitions like  $a \rightarrow b$  and  $c \rightarrow d$  exploits continuity to cancel untypical results. If a particular set of vortices causes unusually many  $a \rightarrow b$  transitions, then  $c \rightarrow d$  transitions are unusually inhibited. Later, when the array of figure 17 is thoroughly mixed, none of these devices works.

Suppose the initial speed difference between bands  $k$  and  $k_0$  is

$$\Delta(k_0, k) = U(k_0) - U(k) .$$

From equation 85,

$$U(k) = \sum_{k_0} [U_0(k) + \Delta(k_0, k)] P(k_0 | k) = U_0(k) + \delta U(k) ,$$

where the speed change between times 0 and  $t$  is

$$\delta U(k) = \sum_{k_0} \Delta(k_0, k) P(k_0 | k) ,$$

and the fact that  $\sum_{k_0} P(k_0 | k) = 1$  has been used. The estimated speed change is

$$\delta U^e(k) = \sum_{k_0} \Delta(k_0, k) P^e(k_0 | k) .$$

A good estimate of the speed change is required. The square error of the estimate is

$$[\delta U^e(k) - \delta U(k)]^2 = \sum_{k_0} \sum_{k'_0} \Delta(k'_0, k) \Delta(k_0, k) [P^e(k'_0 | k) - P(k'_0 | k)] [P^e(k_0 | k) - P(k_0 | k)] .$$

Once the mixing is thorough, the estimates  $P^e(k'_0 | k)$  and  $P(k_0 | k)$  should be nearly independent for  $k'_0 \neq k_0$  (they cannot be strictly independent, since  $\sum_{k_0} P^e(k_0 | k) = 1$ ; however  $\Delta(k_0, k_0) = 0$ , so some of the slack is taken up by the terms with  $k'_0$  or  $k_0 = k$  which have zero coefficients anyway). Then the mean square error for one experiment is

$$\epsilon_1^e(k)^2 = \sum_{k_0} \Delta^2(k_0, k) \overline{[P^e(k_0 | k) - P(k_0 | k)]^2} .$$

Suppose  $\rho(k_0) = \text{constant}$  (the analysis for non-constant  $\rho$  is very complicated). Then

$$P^e(k_0 | k) = \frac{n(k_0, k)}{T(k)} ,$$

where  $T(k)$  is the total number of test particles in band  $k$  at time  $t$ ,

$$T(k) = \sum_{k_0} n(k_0, k) .$$

For the time being, the arguments  $(k_0, k)$ ,  $(k_0 | k)$ ,  $(k)$  are dropped.

Define a random variable  $a_a$  such that for every point  $a$  in band  $k$ ,

$$a_a = \begin{cases} 1-P, & \text{if } a \text{ came from } k_0; \\ -P, & \text{if not.} \end{cases}$$

Then

$$\sum_{\alpha} a_{\alpha} = (1-P)n - P(T-n) = n - TP .$$

Since  $P^e = n/T$ ,

$$P^e - P = \frac{\sum_{\alpha} a_{\alpha}}{T} .$$

$a_{\alpha}$  is independent of  $T$ , since the origin of a particular particle cannot be biased by the total number of particles in the band if  $\rho(k_0) =$  constant. Thus

$$\overline{(P^e - P)^2} = \left\langle \frac{\sum_{\alpha} \sum_{\beta} \overline{a_{\alpha} a_{\beta}}}{T^2} \right\rangle ,$$

where  $\langle \rangle$  is an average over  $T$ . But

$$\overline{a_{\alpha}} = (1-P)P - P(1-P) = 0 ,$$

$$\overline{a_{\alpha} a_{\alpha}} = (1-P)^2 P + P^2 (1-P) = P - P^2 ,$$

and if the mixing has been sufficiently thorough that the particle histories are almost independent.

$$\overline{a_{\alpha} a_{\beta}} = \overline{a_{\alpha}} \overline{a_{\beta}} = 0 .$$

Thus

$$\overline{(P^e - P)^2} = \left\langle \frac{\sum_{\alpha} (P - P^2)}{T^2} \right\rangle = (P - P^2) \left\langle \frac{1}{T} \right\rangle \approx \frac{(P - P^2)}{\langle T \rangle}$$

for large  $T$ . The mean square error in  $\delta U^e(k)$  is

$$\begin{aligned} \epsilon_1^2(k) &= \frac{1}{\langle T(k) \rangle} \sum_{k_0} \Delta^2(k_0, k) [P(k_0 | k) - P(k_0 | k)^2] \\ &\approx \frac{1}{\langle T(k) \rangle} \sum_{k_0} \Delta^2(k_0, k) P(k_0 | k) = \frac{\Delta^2(k)}{\langle T(k) \rangle} \end{aligned}$$

for thorough mixing.  $\Delta^2(k)$  is the mean square deviation of the speed in band  $k$  from the original speed  $U_0(k)$ . If  $Q$  experiments are run, the root mean square error divided by the speed change to be measured is

$$\frac{\epsilon_Q(k)}{\delta U(k)} \approx \frac{\Delta(k)}{\delta U(k)} \frac{1}{\sqrt{Q \langle T(k) \rangle}} \quad (87)$$

That ratio must be small for the results to be meaningful. The experiments of subsection H show that  $\Delta$  is much larger than  $\delta U$ , that is, the vortices transport  $x$  momentum rapidly, but the net transport is rather small. The number of experiments  $Q$  and the number of points per band  $T$  in each experiment must be large, and the Monte Carlo technique is barely feasible after the test particles are thoroughly mixed.

#### H. Momentum Transfer Experiments

The momentum transfer program begins an experiment by computing vortex strengths from random phase input data, and by locating test particles in cells of a specified matrix using pseudo-random numbers generated internally. Once the initial conditions are set, the momentum transfer program solves about the same

mechanical problem as the flow visualization program. Lengths, times and vortex strengths are non-dimensionalized the same way. A vortex is convected in the field induced by the other vortices; a test particle is convected in the field of all the vortices. The capture criterion treats test particles like vortices of zero strength. A test particle is not annihilated when it is captured – it rides its captor vortex. If that vortex is captured in turn, the test particle passes to the new captor. The number of vortices drops every time a vortex is captured, but test particles are conserved. The test particles are surveyed periodically to find the current band-transfer data  $n(k_o, k)$ . After the experiment has been run with fresh random phases and pseudo-random numbers as many times as desired, the accumulated data are passed through two data reduction programs.

The first program sums the  $n(k_o, k)$  for each survey over all the experiments and computes estimates of the band-transition probabilities  $P(k_o | k)$  by equation 86. The  $P(k_o | k)$  are related to a step-function approximation of the continuous transition probability  $P(y_o | y)$ . Define

$$g(y_o, y) = \frac{P(k_o | k)}{\delta k_o} \quad \text{for } y_o \in k_o, y \in k .$$

The expression ' $y \in k$ ' means  $y$  lies in band  $k$ , i. e.,  $(y_k - \delta_k/2) \leq y < (y_k + \delta_k/2)$ . From equation 84,

$$g(y_o, y) = \frac{1}{\delta_{k_o} \delta_k} \int_{k_o} dy_o \int_k dy P(y_o | y), \quad y_o \in k_o, y \in k ,$$

so  $g(y_0, y)$  is constant over the rectangle  $y_0 \leq k_0$ ,  $y \leq k$  and equals the average value of  $P(y_0 | y)$  there. Plots of  $g(y_0, y)$  show the probability distribution for original heights  $y_0$  spreading away from the current height  $y \leq k$ . Using data from all the experiments, the first data reduction program gives estimates  $P^e(k_0 | k)$  from which plots of  $g^e(y_0^*, y^*)$  can be made.

The second data reduction program computes transition probabilities, speeds and speed changes for each experiment using equations 86 and 87. If the initial speed profile is linear,  $U_0 = \Omega y$ , then the original vortex spacing  $\lambda$  is still the only length in the problem, and  $U$  is non-dimensionalized on  $\Omega \lambda$ :

$$U^* = \frac{U}{\Omega \lambda} .$$

The program averages the speed change estimates  $\delta U^{*e}(k)$  over all the experiments and computes empirical standard errors

$$\epsilon_Q^{*e}(k) = \sqrt{\frac{\sum [\delta U^{*e}(k) - \overline{\delta U^{*e}(k)}]^2}{Q(Q-1)}} , \quad (88)$$

where  $Q$  is the number of experiments.

Figures 18 and 19 show the results of the first and second data reduction programs for nine experiments run with the same values of  $\tau^*$ ,  $\sigma$ ,  $N$ ,  $R(l)$ ,  $T^*$  and  $F$  used to produce figures 16.  $T^*$  is the time between test particle surveys, and  $F$  is the number of surveys. The cell matrix, with 12 bands and 180 cells, is shown in figure 17. The band center locations  $y_k^*$ , band heights  $\delta_k^*$  and test particle densities  $\rho^*(k)$  for the upper half of the matrix are as follows:

BAND	$y^*$	$\delta^*$	$\rho^*$
1	7.1	1.8	.2778
2	5.4	1.6	.3750
3	3.9	1.4	.5000
4	2.6	1.2	.6667
5	1.5	1.0	.9000
6	.5	1.0	1.0000

The upper and lower halves of the matrix are symmetrical as shown.

The non-dimensional length and height of the matrix are

$$L^* = 20, \quad H^* = 16.$$

Both are large compared with the distance the boundary is distorted up to  $t^* = 5$ . The original row of 45 vortices extends 12 units beyond the vertical boundaries of the matrix. The transition probability estimates should be nearly the same as they would be if the test particles moved in a field truly homogeneous in  $z$ .

Figure 18 (i) shows  $g^e(y_0^*, y^*)$  for  $y^* \in 2$  plotted against  $y_0^*$  at times  $t^* = 0, 1, \dots, 5$ . Figures 18 (ii) and 18 (iii) show the same sequence for  $y^* \in 4$  and  $y^* \in 6$ . At  $t^* = 5$ , the probability distribution over  $y_0^*$  given  $y^* \in 2$  is still sharply peaked in band 2. The distribution is much more diffuse for  $y^* \in 4$ , and for  $y^* \in 6$ , the probability has spread almost uniformly over the band occupied by the vortices (cf. figures 16). Figures 19 show the speed change estimates  $\delta U^{*e}(y_k^*)$  for an initially linear shear profile at times  $t^* = 0, \dots, 5$ . Estimates in the top band are impossible, because fluid without test particles

intrudes there; no points at  $y^* = 7.1$  are shown. The heavy dots represent estimates averaged over the nine experiments, the vertical lines represent standard errors of the mean computed from equation 88, and the shaded bands represent speed change profiles as nearly as they can be specified. The oblique line  $\delta U^* = -y^*$  corresponds to fully stopped flow. The nine experiments took 20 minutes on an IBM 7094 computer.

No analytical theory can predict the curves of figures 19. A comparison of figures 16 and 19 shows that the speed change maximum and strong vortex dipoles propagate into the shear flow together. The time scales for Reynolds stress generation and mean flow change and for convection of turbulence in its own random field are the same. The maximum speed change at  $t^* = 5$  is  $-\delta U^* \sim .4 \rightarrow .5$  in band 4. The original speed there is  $U_o^* = 2 \rightarrow 3.2$ , so the mean speed changes about 20%. The last graph of figure 18 (ii) shows that the dispersion of the speed about its original value in band 4 is  $\Delta^*(4) \sim 2$  at  $t^* = 5$ . By  $t^* = 5$ , the speed range in band 4 is as large as the mean speed there, yet the mean speed change is small. It is surprising that flows as inhomogeneous on  $y$  as the flow in figure 16 could mix fluid columns as well as figures 18 show with such a small net transport of momentum.

Before the vortices have mixed the test particles thoroughly, the use of cells, grading of  $\rho$ , and summing of transitions like  $a \rightarrow b$  and  $c \rightarrow d$  in figure 17 keep down the standard errors in speed estimates. After thorough random mixing of the test particles, the errors cannot be reduced below the prediction of equation 87. About

20 test particles occupied band 4, and 20 more occupied its complement, band 9. Since transitions  $a \rightarrow b$  and  $c \rightarrow d$  are summed, the speed estimates in band 4 are based on  $\langle T(4) \rangle \sim 40$  particles per experiment and  $Q = 9$  experiments. The theoretical prediction of the standard error after thorough mixing is

$$\epsilon^* = \frac{\Delta^*}{\sqrt{Q\langle T \rangle}} \sim \frac{2}{\sqrt{9 \cdot 40}} \sim .1$$

from equation 87 (equation 87 was derived for  $\rho(k) = \text{constant}$ , but it is accurate enough for a crude estimate like this). The second data reduction program computed the following empirical standard errors:

$t^*$	$\epsilon^*$
0	0
1	.022
2	.060
3	.037
4	.103
5	.127

By  $t^* = 4$ , the fluid in band 4 is mixed well enough for equation 87 to be valid. As  $\Delta^*$  grows with time, the accuracy of a mean speed estimate drops. Since the vortices mix fluid columns thoroughly without having much effect on the mean flow, the expected error of a speed change estimate grows more rapidly than the speed change itself. The Monte Carlo method is time limited for practical purposes. There is no point in carrying the experiments much beyond  $t^* = 5$ .

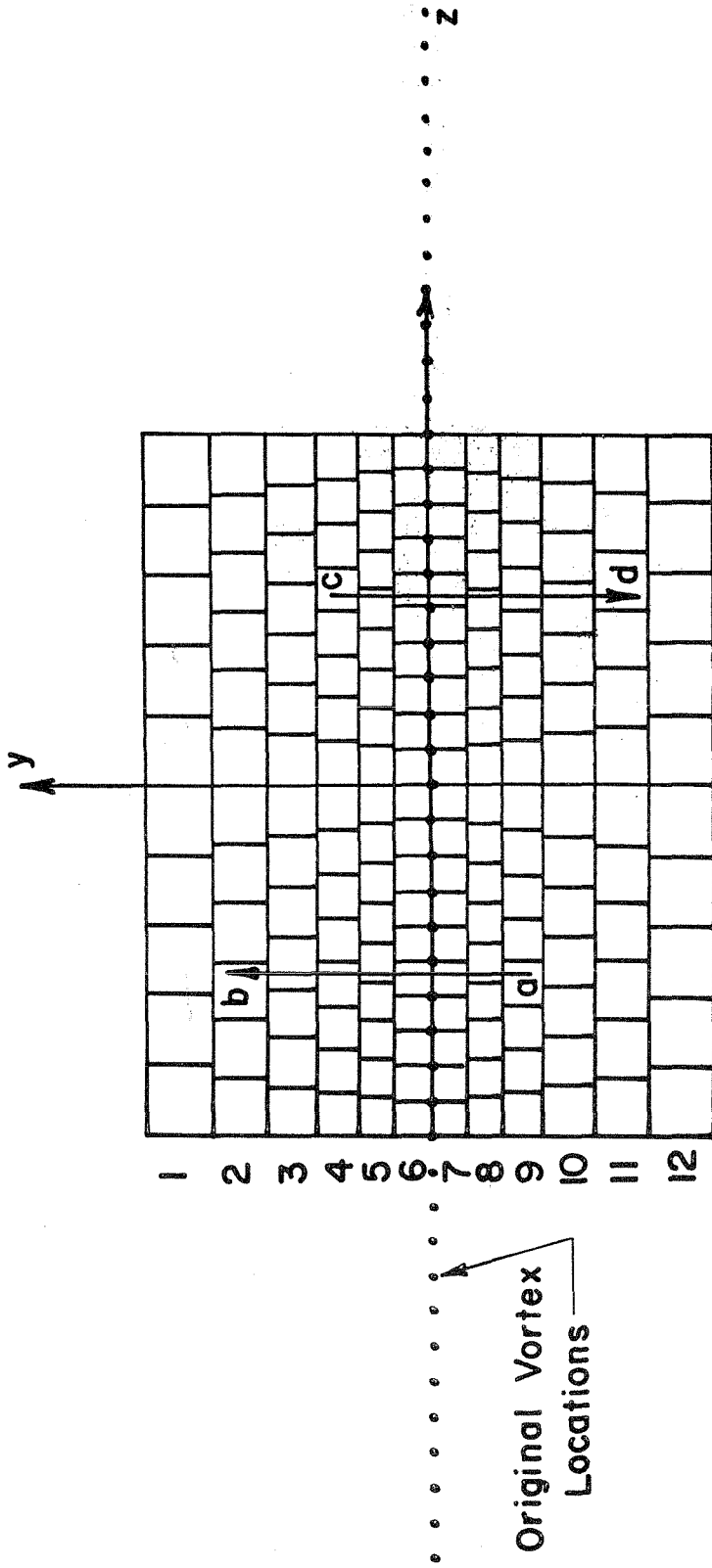


FIG. 17 CELL MATRIX FOR MOMENTUM TRANSFER EXPERIMENTS

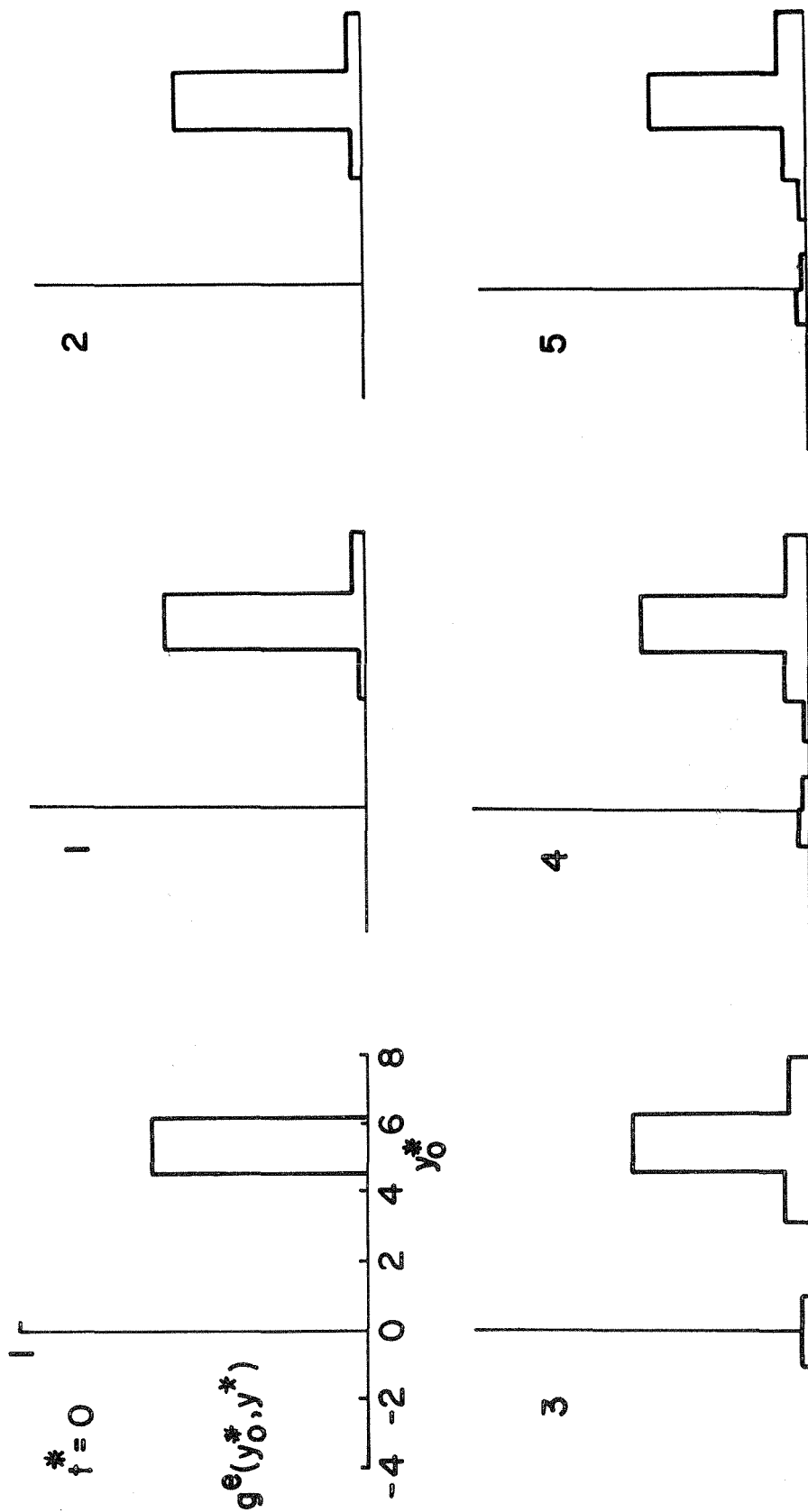


FIG. 18 (i) DISTRIBUTION OF ORIGINAL HEIGHTS  $y_0^*$  BAND 2

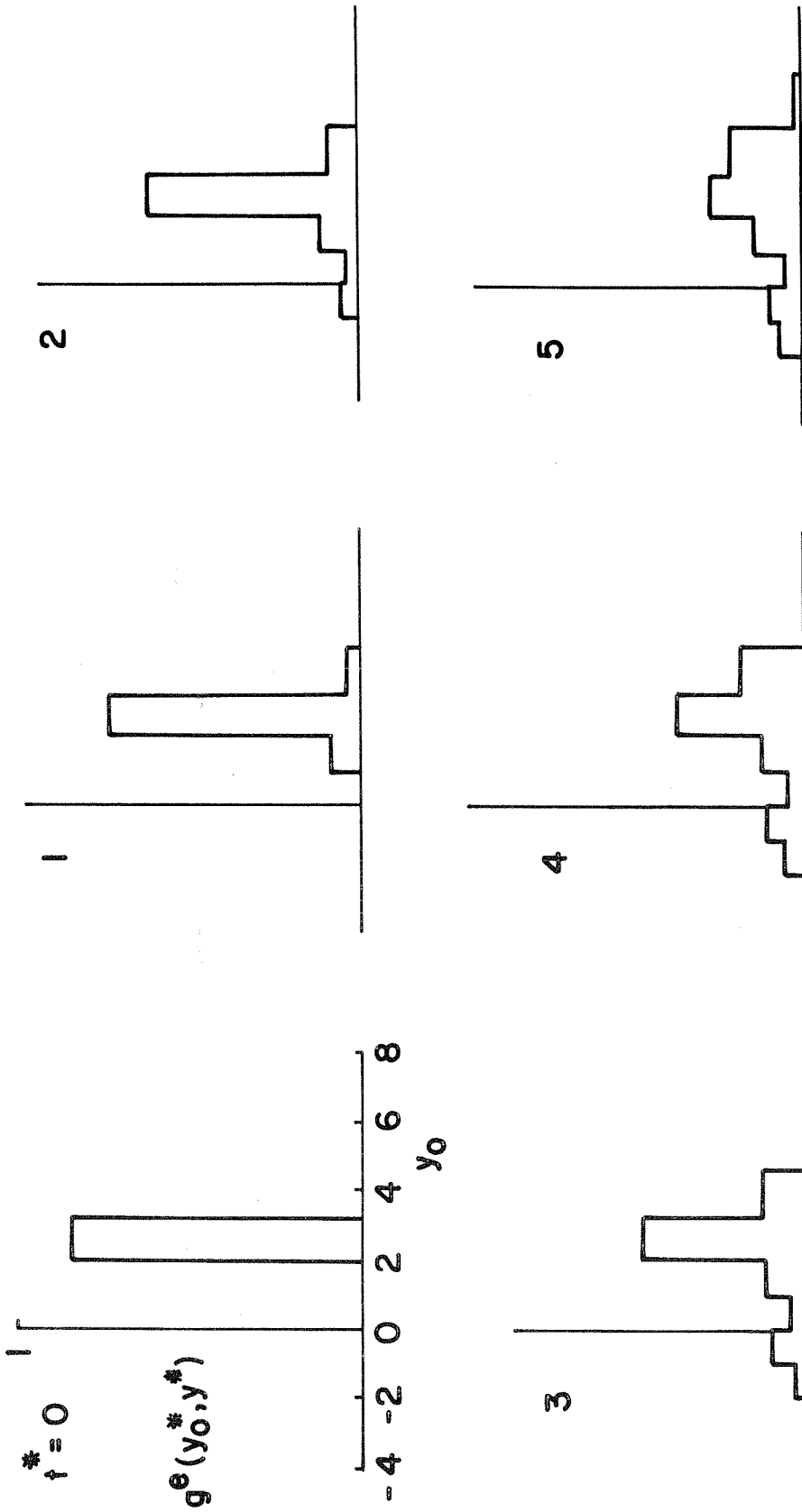


FIG. 18 (ii) DISTRIBUTION OF ORIGINAL HEIGHTS  $y_0^*$  BAND 4

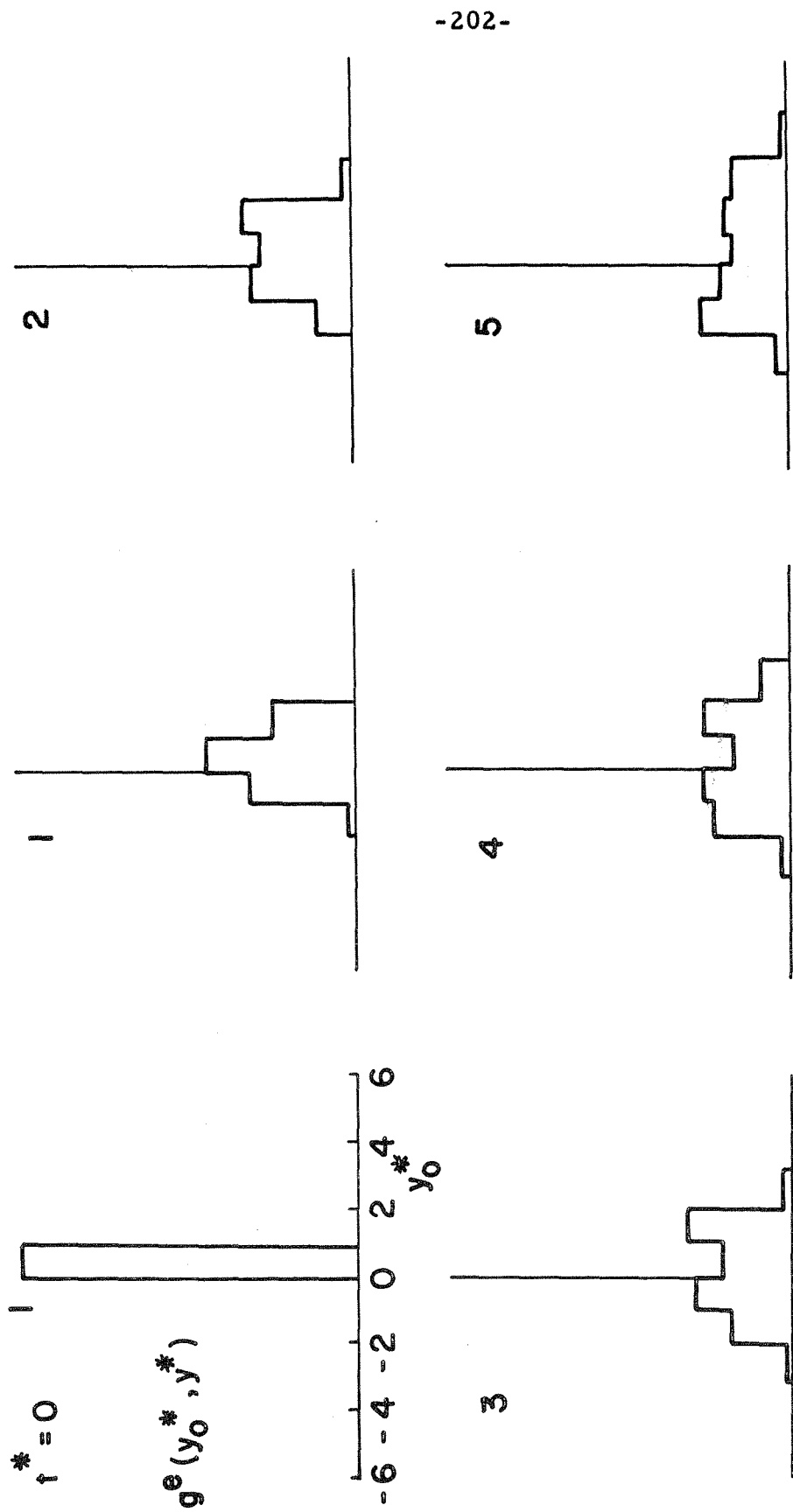


FIG. 18 (iii) DISTRIBUTION OF ORIGINAL HEIGHTS  $y_0^*$  BAND 6

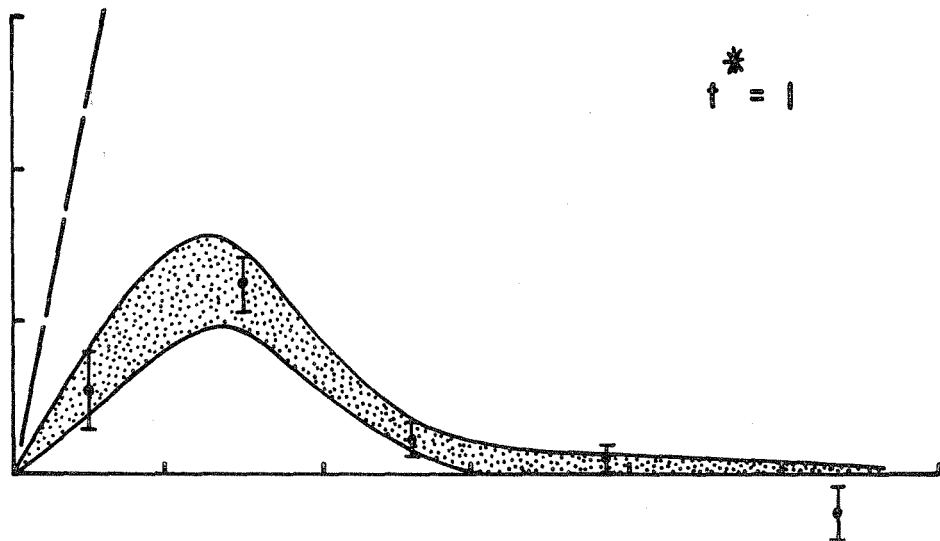
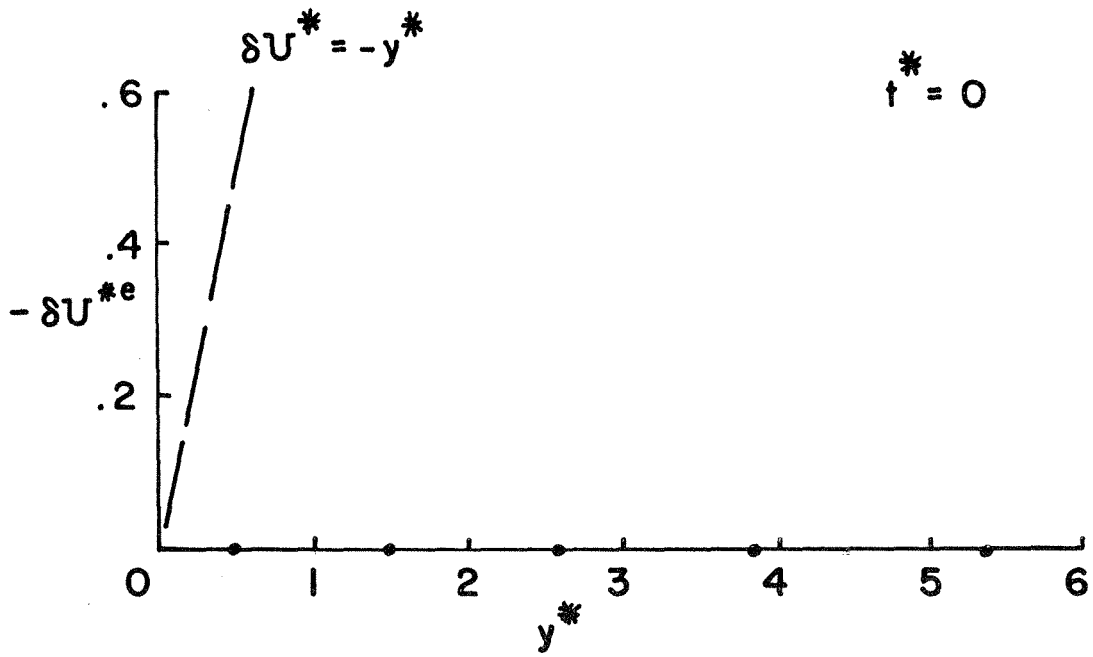


FIG. 19 (i) SPEED CHANGE PROFILE

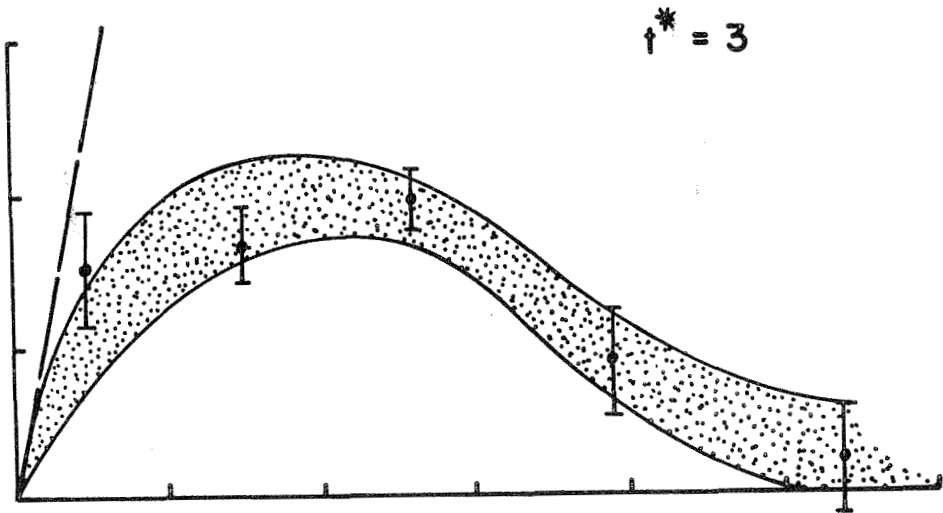
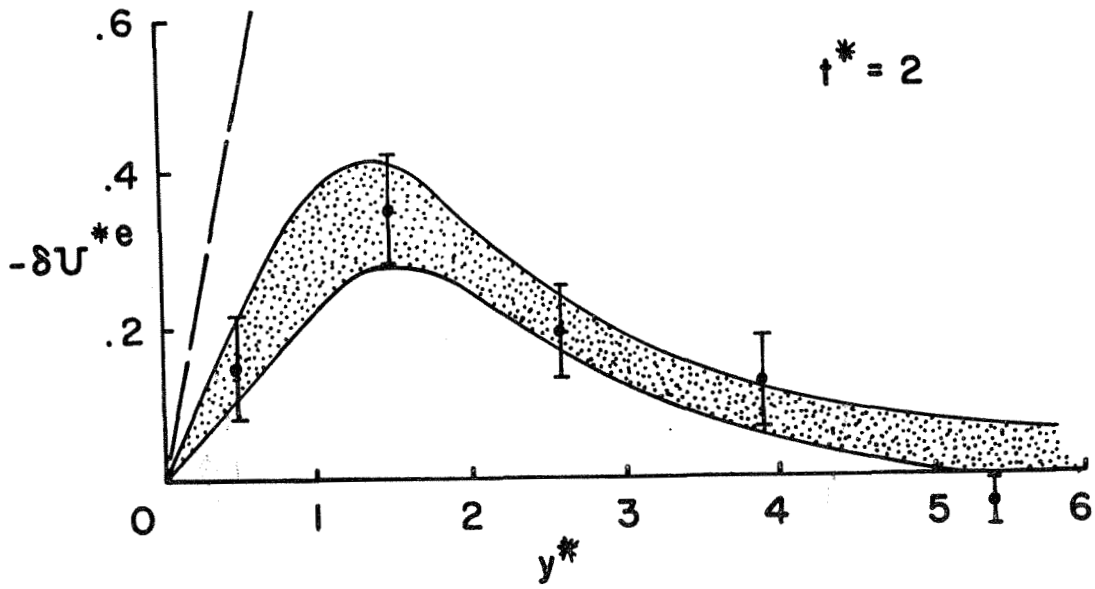


FIG. 19 (ii) SPEED CHANGE PROFILE

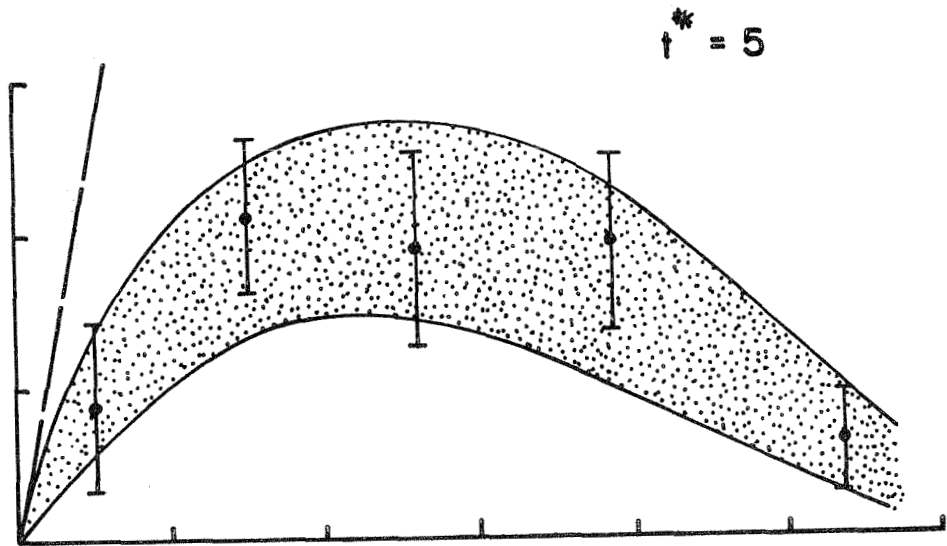
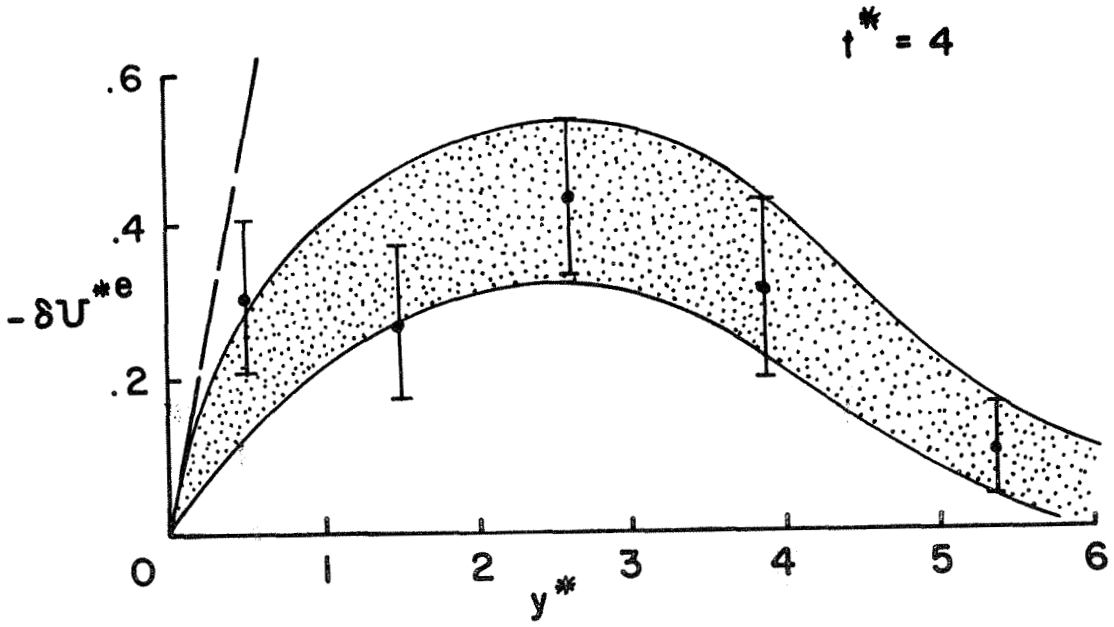


FIG. 19 (iii) SPEED CHANGE PROFILE

## 6. Summary

This chapter began with the assumption that the propagation of turbulence through a rapidly shearing flow depends primarily on random stretching of mean field vorticity. Reynolds stress was taken as the mechanical signature of random vorticity in a shear flow. Rapid shearing means  $U \ll \Omega L$ , where  $U$  is a fluctuation speed,  $L$  is an eddy size, and  $\Omega$  is a typical mean vorticity. The equations of turbulent motion were linearized under the assumption  $U \ll \Omega L$ , and the history of the Reynolds stress  $\sigma(y, t)$  acting on a mean flow  $U(y) = \Omega y$  in the  $x$  direction was studied. The original random vorticity was assumed to be generated at time zero by impulses homogeneous in  $x, z$  and concentrated near  $y = 0$ . Turbulence near  $y = 0$  was expected to catalyze the growth of random vorticity further out by stretching mean vorticity so that the turbulence would grow steadily more intense and propagate further and further through the mean flow. But the Reynolds stress was found to relax into a steady distribution as  $\Omega t \rightarrow \infty$ . As far as the Reynolds stress is a measure of turbulent intensity, random stretching of mean vorticity alone cannot yield steadily propagating turbulence.

The problem was simplified next by assuming that all flow properties are independent of  $x$ . In that case, the eddy motion in the  $y, z$  plane is independent of the  $x$  momentum it transports, and the mean speed  $U(y, t)$  is diffused like a passive scalar. The equations of motion were partially linearized by neglecting convection of eddies in the  $y, z$  plane, and wave equations for  $\sigma(y, t)$  and  $U(y, t)$  were derived. The solutions are worthless, however, for times  $t \gtrsim L/U$ .

Turbulence artificially steady in the  $y, z$  plane exerts a steady grip on the mean flow and forces  $U$  to become independent of  $y$  over a larger and larger interval  $-Y(t) < y < Y(t)$ . In a real flow the eddies disperse as fast as  $U$  diffuses. The core of the problem was found to be convection of eddies in their own random field.

The chapter ended with numerical turbulence experiments designed to find how quickly concentrated vortex columns parallel to  $x$  disperse over the  $y, z$  plane under their own induction, and how effectively they diffuse  $U(y, t)$ . The rate of error accumulation was analyzed carefully. The mean square error of the computed location of a vortex was found to diverge exponentially with time according to a generalized random walk equation. Detailed vortex locations are unimportant in a turbulence experiment; computed trajectories must not diverge too rapidly from current physical trajectories, but the accumulated displacements of computed locations from actual locations can be large. It was shown, however, that unless a lower limit on the distance between any two vortices is imposed, the velocity of error drift can dominate the flow velocity no matter how small a time increment is used in the computations. Vortices which approach each other closely must be united. Uniting vortices during the computations was justified by finding a capture cross section for the interaction of two vortices in a strain field. Numerical flow visualization and momentum transfer experiments confirmed the result that columnar eddies disperse as fast as they transport momentum. In case the flow properties are independent of  $x$ , the time scales for non-linear convection and turbulence propagation

are the same, and no analytical solution for the propagation is possible. That does not mean that the time scales for propagation and non-linear convection are the same in more realistic situations where turbulent quantities depend on  $x$ . The time scale for the propagation of random vorticity of strength  $U/L$  through a field of mean vorticity  $\Omega$  is not as short as  $\Omega^{-1}$ , as originally expected, but it may not be as long as  $L/U$ . Weak interaction among turbulent eddies may free the Reynolds stress, steady for  $t \gg \Omega^{-1}$  under the linear approximation, and allow its gradual diffusion.

REFERENCES

1. Corrsin, S., and Kistler, A. L., "The Free-Stream Boundaries of Turbulent Flows," NACA Tech. Note No. 3133 (1954).
2. Saffman, P. G., "The Motion of Turbulent Slugs along Pipes," JPL Space Programs Summary 37-22, Vol. 4 (1965).
3. Coles, D., "Interfaces and Intermittency in Turbulent Shear Flow," Mechanique de la Turbulence, Editions du Centre Nationale de la Recherche Scientifique, Paris (1962), pp. 224-250.
4. Phillips, O. M., "The Irrotational Motion outside a Free Turbulent Boundary," Proc. Cam. Phil. Soc., Vol. 51 (1955), pp. 220-229.
5. Moffatt, H. K., "The Interaction of Turbulence with Rapid Uniform Shear," SUDAER No. 242, Stanford University (1965).
6. Lighthill, M. J., Fourier Analysis and Generalized Functions, Cambridge (Eng.) University Press (1962).
7. Dwight, H. B., Tables of Integrals and Other Mathematical Data, 4th Ed., The Macmillan Company, New York (1961).
8. Townsend, A. A., The Structure of Turbulent Shear Flows, Cambridge (Eng.) University Press (1956), pp. 206-210.
9. Favre, A., Gaviglio, J., and Dumas, R., "Correlations Spatio-Temporelles en Ecoulements Turbulents," Mechanique de la Turbulence, Editions du Centre Nationale de la Recherche Scientic, Paris (1962), pp. 419-445.
10. Lamb, H., Hydrodynamics, 6th Ed., Dover Publications, New York (1932).

11. Abernathy, F. H., and Kronauer, R. E., "The Formation of Vortex Streets," Journal of Fluid Mechanics; Vol. 13 (1962), pp. 1-20.
12. Brillouin, L., Science and Information Theory, 2nd Ed., Academic Press Inc., New York (1962), pp. 78-79.
13. Batchelor, G. K., The Theory of Homogeneous Turbulence, Cambridge (Eng.) University Press (1960), pp. 186-187.
14. Onsager, L., "Statistical Hydrodynamics," Nuovo Cimento, Supplement, Vol. 6 (1949), pp. 279-282.

APPENDIX A

Evaluation of  $L_{ij}(k, k_{o2})$

The equation to be integrated is

$$\frac{\partial L_{ij}}{\partial k_2} = T_i(k_2)L_{2j} \quad , \quad L_{ij}(k_{o2}, k_{o2}) = \delta_{ij} \quad ,$$

where

$$T_i = \frac{1}{k_1} \left( \delta_{i1} - \frac{2k_1 k_1}{k^2} \right) \quad ,$$

and  $k_1, k_3$  are fixed.  $k^2$  is  $k_1^2 + k_2^2 + k_3^2$ , and  $k_1, k_3$  will often appear in the combination  $k_1^2 + k_3^2 = \ell^2$ . Thus

$$\frac{\partial L_{21}}{\partial k_2} = T_{22} L_{21} \quad ,$$

and by the initial condition,  $L_{21} = 0$ . Then

$$\frac{\partial L_{11}}{\partial k_2} = T_1 L_{21} = 0 \quad ,$$

so  $L_{11} = 1$ . It can likewise be shown that  $L_{31}, L_{13}, L_{23} = 0$  and  $L_{33} =$

1.  $L_{22}$  satisfies

$$\frac{\partial L_{22}}{\partial k_2} = \frac{-2k_2}{\ell^2 + k_2^2} L_{22} \quad .$$

Integration and use of the initial condition  $L_{22}(k_{o2}, k_{o2}) = 1$  gives

$L_{22} = k_o^2/k^2$ , where  $k_o^2 = \ell^2 + k_{o2}^2$ . Then  $L_{12}$  satisfies

$$\frac{\partial L_{12}}{\partial k_2} = T_1 L_{22} = \frac{1}{k_1} \left( 1 - 2 \frac{k_1^2}{k^2} \right) \frac{k_o^2}{k^2} \quad ,$$

and since  $L_{12}(k_{o2}, k_{o2}) = 0$ ,

$$\begin{aligned}
 L_{12} &= \frac{k_o^2}{k_1} \int_{k_{o2}}^{k_2} \left[ \frac{1}{l^2+x^2} - \frac{2k_1^2}{(l^2+x^2)^2} \right] dx \\
 &= \frac{k_o^2}{k_1} \left( \frac{k_3^2}{l^3} \tan^{-1} \left( \frac{x}{l} \right) - \frac{k_1^2}{l^2} \frac{x}{(l^2+x^2)} \right) \Bigg|_{k_{o2}}^{k_2} \\
 &= - \frac{k_3^2 k_o^2}{k_1 l^3} [\theta] - \frac{k_1 k_o^2}{l^2} \left[ \frac{k_2}{k} \right],
 \end{aligned}$$

where

$$[\theta] = \tan^{-1} \left( \frac{l}{k_2} \right) - \tan^{-1} \left( \frac{l}{k_{o2}} \right), \quad 0 \leq \theta \leq \pi,$$

and

$$\left[ \frac{k_2}{k} \right] = \frac{k_2}{k} - \frac{k_{o2}}{k_o} .$$

In the same way it can be shown that

$$L_{32} = \frac{k_o^2 k_3}{l^3} \left( [\theta] - l \left[ \frac{k_2}{k} \right] \right) .$$

APPENDIX B

Evaluation of the Stress Integrals in the Vortex Sheet Problem

From equations 27,

$$\sigma(y, t) = I_1 + I_2 + I_3 ,$$

where

$$I_1 = \int \frac{k_1 k_{o2}}{k'^2 k_o^2} \frac{\Theta}{\pi^2} e^{i(k_{o2} + k'_{o2})y} dk'_{o2} dk_{o2} d\ell ,$$

$$I_2 = \int \frac{k_3^2}{\ell k_1 k'^2} [\theta] \frac{\Theta}{\pi^2} e^{i(k_{o2} + k'_{o2})y} dk'_{o2} dk_{o2} d\ell ,$$

$$I_3 = \int \frac{k_1}{k'^2} \left[ \frac{k_2}{k^2} \right] \frac{\Theta}{\pi^2} e^{i(k_{o2} + k'_{o2})y} dk'_{o2} dk_{o2} d\ell .$$

But

$$\left[ \frac{k_2}{k^2} \right] = \frac{k_2}{k^2} - \frac{k_{o2}}{k_o^2} ,$$

so

$$I_1 + I_3 = \int \frac{k_1 k_2}{k^2 k'^2} \frac{\Theta(k_1, k_3)}{\pi^2} e^{i(k_{o2} + k'_{o2})y} dk'_{o2} dk_{o2} dk_1 dk_3 . \quad (B1)$$

From equations 21,

$$k_2 = k_{o2} - \Omega t k_1 ,$$

$$k'_2 = k'_{o2} + \Omega t k_1 ,$$

and since  $\Theta$  is the Fourier transform of a real function symmetric with respect to changes in sign of its arguments,

$$\Theta(-k_1, -k_3) = \Theta(k_1, k_3) .$$

Reversing the signs of  $k_1$  and  $k_3$  and switching the roles of  $k_{o2}$  and  $k'_{o2}$  alters the right hand side of B1 by a change of sign only, so

$$I_1 + I_3 = 0 .$$

The integral over  $k'_{o2}$  in  $I_2$  may be carried out as follows:

$$\begin{aligned} \int_{-\infty}^{\infty} \frac{e^{ik'_{o2}y}}{k'^2} dk'_{o2} &= \int_{-\infty}^{\infty} \frac{e^{ik'_{o2}y}}{\ell^2 + (k'_{o2} + \Omega tk_1)^2} dk'_{o2} \\ &= e^{-i\Omega tk_1 y} \int_{-\infty}^{\infty} \frac{e^{iky}}{\ell^2 + k^2} dk = \frac{2}{\ell} e^{-i\Omega tk_1 y} \int_0^{\infty} \frac{\cos(\ell y)x}{1+x^2} dx \\ &= \frac{\pi}{\ell} e^{-i\Omega tk_1 y} e^{-\ell |y|} , \end{aligned} \tag{B2}$$

from Dwight [7], p. 224. The integral over  $k_{o2}$  is

$$K = \int_{-\infty}^{\infty} [\theta] e^{ik_{o2}y} dk_{o2} ,$$

where

$$[\theta] = \cot^{-1} \left( \frac{k_{o2}}{\ell} - \frac{\Omega tk_1}{\ell} \right) - \cot^{-1} \left( \frac{k_{o2}}{\ell} \right) ,$$

from the definitions below equation 15. Substitute

$$\lambda = \frac{k_{o2}}{\ell} , \quad \xi = \frac{\Omega tk_1}{\ell} ,$$

so

$$K = \ell \int_{-\infty}^{\infty} [\cot^{-1}(\lambda - \xi) - \cot^{-1}(\lambda)] e^{i\ell y \lambda} d\lambda .$$

K can be regarded as a function of  $\xi$  satisfying

$$K(0) = 0 ,$$

$$\begin{aligned} \frac{dK}{d\xi} &= \ell \int_{-\infty}^{\infty} \frac{e^{i\ell y \lambda}}{1 + (\lambda - \xi)^2} d\lambda = 2\ell e^{i\xi \ell y} \int_0^{\infty} \frac{\cos(\ell y)x}{1+x^2} dx \\ &= \pi \ell e^{i\xi \ell y} e^{-\ell |y|} , \end{aligned}$$

since the integration is the same as that which led to B2. Thus

$$K = \frac{\pi}{iy} \left( e^{i\Omega t k_1 y} - 1 \right) e^{-\ell |y|} \quad (B3)$$

From equations B2 and B3,

$$\begin{aligned} I_2 &= \iint_{-\infty}^{\infty} \Theta(k_1, k_3) \frac{k_3^2}{\ell^2} \frac{(1 - e^{-i\Omega t k_1 y})}{ik_1 y} e^{-2\ell |y|} dk_1 dk_3 , \\ &= 2 \int_{-\infty}^{\infty} \int_0^{\infty} \Theta(k_1, k_3) \frac{k_3^2}{\ell^2} \frac{\sin(\Omega t k_1 y)}{k_1 y} e^{-2\ell |y|} dk_1 dk_3 , \\ &= \int_{-\infty}^{\infty} \int_{-\infty}^{\infty} \Theta(k_1, k_3) \frac{k_3^2}{\ell^2} \frac{\sin(\Omega t k_1 y)}{k_1 y} e^{-2\ell |y|} dk_1 dk_3 . \end{aligned}$$

The symmetry property of  $\Theta$  was used twice. Since  $\sigma = I_2 + (I_1 + I_3) = I_2$ , equation 28 in the text has been verified.

APPENDIX C

Proof that Equation 31 is Valid in the Limit  $\Omega t \rightarrow \infty$

The terms dropped from equation 31, analogous to  $I_1$  and  $I_3$  in the vortex sheet problem, are

$$J_1 = \int \frac{(\ell^2 + k'_{o2})}{[\ell^2 + (k'_{o2} + \Omega t k_1)^2]} A_{21}^o(k'_{o2}, k_1, k_{o2}, k_3) e^{i(k_{o2} + k'_{o2})y} dk'_{o2} dk_{o2} dk_1 dk_3,$$

$$J_3 = \int \frac{(\ell^2 + k_{o2}^2)(\ell^2 + k'_{o2})k_1}{\ell^2[\ell^2 + (k'_{o2} + \Omega t k_1)^2]} \left[ \frac{k_{o2} - \Omega t k_1}{\ell^2 + (k_{o2} - \Omega t k_1)^2} - \frac{k_{o2}}{\ell^2 + k_{o2}^2} \right] A_{22}^o(k'_{o2}, k_1, k_{o2}, k_3) e^{i(k_{o2} + k'_{o2})y} dk'_{o2} dk_{o2} dk_1 dk_3.$$

Under transformations 32 and 33, these become

$$J_1 = \frac{2}{\Omega t} \int_{-\infty}^{\infty} \int_{-\infty}^{\infty} \int_0^{\Omega t} \int_{-\Omega t}^{\Omega t} \frac{(1 + \beta'^2) \ell^3}{[1 + (\beta' - \xi)^2]} \frac{1}{\sqrt{1 - (\frac{\xi}{\Omega t})^2}} A_{21}^o(\beta' \ell, -\frac{\ell \xi}{\Omega t}, \beta \ell, \ell \sqrt{1 - (\frac{\xi}{\Omega t})^2}) e^{i(\beta + \beta') \ell y} d\xi d\ell d\beta d\beta',$$

$$J_3 = -\frac{2}{(\Omega t)^2} \int_{-\infty}^{\infty} \int_{-\infty}^{\infty} \int_0^{\Omega t} \int_{-\Omega t}^{\Omega t} \frac{(1 + \beta^2)(1 + \beta'^2) \ell^3}{[1 + (\beta' - \xi)^2]} \left[ \frac{\beta + \xi}{1 + (\beta + \xi)^2} - \frac{\beta}{1 + \beta^2} \right] \frac{\xi}{\sqrt{1 - (\frac{\xi}{\Omega t})^2}} A_{22}^o(\beta' \ell, -\frac{\ell \xi}{\Omega t}, \beta \ell, \ell \sqrt{1 - (\frac{\xi}{\Omega t})^2}) e^{i(\beta + \beta') \ell y} d\xi d\ell d\beta d\beta'.$$

Both integrals converge for large  $\xi$  even when the limit  $\Omega t \rightarrow \infty$  is

taken before the integrations are performed explicitly. Thus as  $\Omega t \rightarrow \infty$ ,

$$J_1 \Rightarrow \frac{2}{\Omega t} \int_{-\infty}^{\infty} \int_{-\infty}^{\infty} \int_0^{\infty} \int_{-\infty}^{\infty} \frac{(1+\beta'^2) l^3}{[1+(\beta'-\xi)^2]} A_{21}^0(\beta' l, 0, \beta l, l) e^{i(\beta+\beta')ly} d\xi dl d\beta d\beta' ,$$

$$J_3 \Rightarrow -\frac{2}{(\Omega t)^2} \int_{-\infty}^{\infty} \int_{-\infty}^{\infty} \int_0^{\infty} \int_{-\infty}^{\infty} \frac{(1+\beta^2)(1+\beta'^2) l^3 \xi}{[1+(\beta'-\xi)^2]} \left[ \frac{\beta+\xi}{1+(\beta+\xi)^2} - \frac{\beta}{1+\beta^2} \right] A_{22}^0(\beta' l, 0, \beta l, l) e^{i(\beta+\beta')ly} d\xi dl d\beta d\beta' .$$

Thus  $J_1$  is  $O(\Omega t)^{-1}$  and  $J_3$  is  $O(\Omega t)^{-2}$  as  $\Omega t \rightarrow \infty$ . It may seem inconsistent that these integrals cancel in the vortex sheet problem when they appear to be of different orders of magnitude in the limit  $\Omega t \rightarrow \infty$ . The answer is that in that special case  $A_{21}^0(\beta' l, 0, \beta l, l)$  is zero, and  $A_{21}^0$  is itself  $O(\Omega t)^{-1}$  under transformations 32 and 33.

APPENDIX D

Singular Perturbation Solution for  $s(\eta, \tau)$ ,  $r(\eta, \tau)$

The object is to solve equations 45, 46, 47 for all  $\eta$  and  $\tau \rightarrow 0$ . It is reasonable to use an expanded time coordinate  $\tilde{\tau} = \tau/\epsilon$  and to try to find asymptotic series expansions of  $s(\eta, \tilde{\tau}; \epsilon)$  and  $r(\eta, \tilde{\tau}; \epsilon)$ . The wave equations 45 are

$$\begin{aligned} \frac{\partial r}{\partial \tilde{\tau}} - \epsilon \frac{\partial s}{\partial \eta} &= 0, \\ \frac{\partial s}{\partial \tilde{\tau}} - \epsilon g \frac{\partial r}{\partial \eta} &= 0 \end{aligned} \tag{D1}$$

in terms of the expanded coordinate, and equations 46 and 47 are unchanged. Expand  $s$  and  $r$  as follows:

$$\begin{aligned} s &= s_0(\eta, \tilde{\tau}) + \epsilon s_1(\eta, \tilde{\tau}) + \epsilon^2 s_2(\eta, \tilde{\tau}) + \dots, \\ r &= r_0(\eta, \tilde{\tau}) + \epsilon r_1(\eta, \tilde{\tau}) + \epsilon^2 r_2(\eta, \tilde{\tau}) + \dots. \end{aligned}$$

The initial conditions of equations 47 are

$$\begin{aligned} r_0(\eta, 0) &= \eta, \quad r_1(\eta, 0) = r_2(\eta, 0) = \dots = 0, \\ s_0(\eta, 0) &= s_1(\eta, 0) = \dots = 0. \end{aligned}$$

When coefficients of separate powers of  $\epsilon$  are set equal to zero in the expansions of equations D1, the following system results:

$$\begin{aligned} O(\epsilon^0) \quad \frac{\partial r_0}{\partial \tilde{\tau}} &= 0, \quad \frac{\partial s_0}{\partial \tilde{\tau}} = 0, \quad \therefore r_0 = \eta, s_0 = 0; \\ O(\epsilon^1) \quad \frac{\partial r_1}{\partial \tilde{\tau}} &= \frac{\partial s_0}{\partial \eta}, \quad \frac{\partial s_1}{\partial \tilde{\tau}} = g \frac{\partial r_0}{\partial \eta}, \quad \therefore r_1 = 0, s_1 = \tau g; \\ O(\epsilon^2) \quad \frac{\partial r_2}{\partial \tilde{\tau}} &= \frac{\partial s_1}{\partial \eta}, \quad \frac{\partial s_2}{\partial \tilde{\tau}} = g \frac{\partial r_1}{\partial \eta}, \quad \therefore r_2 = \frac{\tau^2}{2} g', s_2 = 0. \\ \dots & \quad \dots \quad \dots \end{aligned}$$

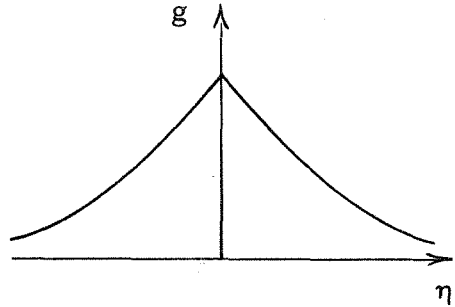
The equations have been solved step-by-step using the expanded initial conditions. Thus the power series for  $s$  and  $r$  begin

$$\begin{aligned} s &= \epsilon \tilde{\tau} g + O(\epsilon^3) , \\ r &= \eta + \epsilon^2 \frac{\tilde{\tau}^2}{2} g' + O(\epsilon^4) , \end{aligned} \tag{48}$$

equations 48 in the text. The ordering breaks down near  $n \sim \epsilon$ , and it is necessary to use an expanded space coordinate  $\tilde{\eta} = \eta/\epsilon$ . The wave equations become

$$\begin{aligned} \frac{\partial r}{\partial \tilde{\tau}} - \frac{\partial s}{\partial \tilde{\eta}} &= 0 , \\ \frac{\partial s}{\partial \tilde{\tau}} - g(\epsilon \tilde{\eta}) \frac{\partial r}{\partial \tilde{\eta}} &= 0 . \end{aligned}$$

$g(\eta)$  has the form shown in the sketch, and its expansion around  $\eta = 0$  begins



$$g = 1 - \alpha |\eta| + \dots = 1 - \epsilon \alpha |\tilde{\eta}| + \dots .$$

The 'inner' expansions of  $s(\tilde{\eta}, \tilde{\tau}; \epsilon)$  and  $r(\tilde{\eta}, \tilde{\tau}; \epsilon)$  begin

$$\begin{aligned} s &= S_0(\tilde{\eta}, \tilde{\tau}) + \epsilon S_1(\tilde{\eta}, \tilde{\tau}) + \epsilon^2 S_2(\tilde{\eta}, \tilde{\tau}) + \dots , \\ r &= R_0(\tilde{\eta}, \tilde{\tau}) + \epsilon R_1(\tilde{\eta}, \tilde{\tau}) + \epsilon^2 R_2(\tilde{\eta}, \tilde{\tau}) + \dots . \end{aligned}$$

The expanded initial conditions are

$$\begin{aligned} R_0(\tilde{\eta}, 0) &= 0, \quad R_1(\tilde{\eta}, 0) = \tilde{\eta}, \quad R_2(\tilde{\eta}, 0) = R_3(\tilde{\eta}, 0) = \dots = 0 , \\ S_0(\tilde{\eta}, 0) &= S_1(\tilde{\eta}, 0) = \dots = 0. \end{aligned}$$

The dependent variables r and s have been expanded in two forms suitable for 'inner' and 'outer' intervals of  $\eta$ ,

$$\text{(inner) } a = A_0(\tilde{\eta}, \tilde{\tau}) + \epsilon A_1(\tilde{\eta}, \tilde{\tau}) + \dots ,$$

$$\text{(outer) } a = a_0(\eta, \tilde{\tau}) + \epsilon a_1(\eta, \tilde{\tau}) + \dots ,$$

where a represents either r or s. The matching conditions between such expansions are

$$\lim_{|\tilde{\eta}| \rightarrow \infty} A_0(\tilde{\eta}, \tilde{\tau}) = a_0(0, \tilde{\tau}) ,$$

$$\lim_{|\tilde{\eta}| \rightarrow \infty} A_1(\tilde{\eta}, \tilde{\tau}) = a_1(0, \tilde{\tau}) + \tilde{\eta} \frac{\partial a_0}{\partial \eta}(0, \tilde{\tau}) ,$$

$$\lim_{|\tilde{\eta}| \rightarrow \infty} A_2(\tilde{\eta}, \tilde{\tau}) = a_2(0, \tilde{\tau}) + \tilde{\eta} \frac{\partial a_1}{\partial \eta}(0, \tilde{\tau}) + \frac{\tilde{\eta}^2}{2} \frac{\partial^2 a_0}{\partial \eta^2}(0, \tilde{\tau}) ,$$

...

Thus, from the outer solutions 48 and the expansion for g,

$$\lim_{|\tilde{\eta}| \rightarrow \infty} R_0 = 0 ,$$

$$\lim_{|\tilde{\eta}| \rightarrow \infty} S_0 = 0 ,$$

$$\text{" } R_1 = \tilde{\eta} ,$$

$$\text{" } S_1 = \tilde{\tau} ,$$

$$\text{" } R_2 = -\frac{\tilde{\tau}^2}{2} \alpha \text{sgn}(\tilde{\eta}) ,$$

$$\text{" } S_2 = -|\tilde{\eta}| \tilde{\tau} \alpha .$$

The coefficients of  $\epsilon^0$  and  $\epsilon^1$  in the expansions of D2 are

$$O(\epsilon^0) \quad \frac{\partial R_0}{\partial \tilde{\tau}} - \frac{\partial S_0}{\partial \tilde{\eta}} = 0 , \quad \frac{\partial S_0}{\partial \tilde{\tau}} - \frac{\partial R_0}{\partial \tilde{\eta}} = 0 ,$$

$$O(\epsilon^1) \quad \frac{\partial R_1}{\partial \tilde{\tau}} - \frac{\partial S_1}{\partial \tilde{\eta}} = 0 , \quad \frac{\partial S_1}{\partial \tilde{\tau}} + \alpha |\tilde{\eta}| \frac{\partial R_0}{\partial \tilde{\eta}} - \frac{\partial R_1}{\partial \tilde{\eta}} = 0 .$$

The solutions are

$$R_0 = 0, \quad S_0 = 0,$$

$$R_1 = \tilde{\eta}, \quad S_1 = \tilde{\tau},$$

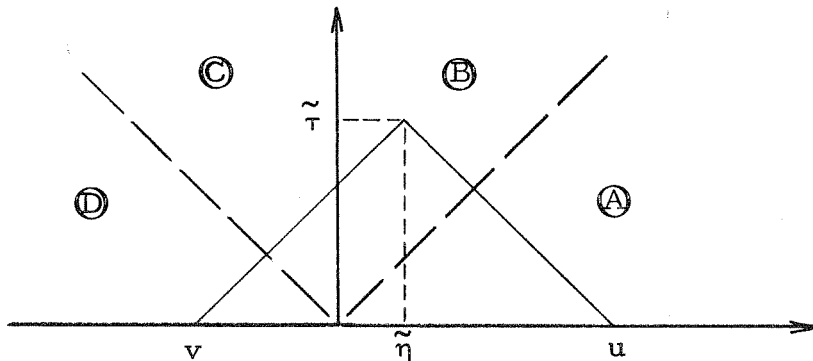
from the expanded initial and matching conditions. The  $O(\epsilon^2)$  set of equations is finally

$$\frac{\partial R_2}{\partial \tilde{\tau}} - \frac{\partial S_2}{\partial \tilde{\eta}} = 0, \quad \frac{\partial S_2}{\partial \tilde{\tau}} - \frac{\partial R_2}{\partial \tilde{\eta}} = -\alpha |\tilde{\eta}|,$$

$$R_2(\tilde{\eta}, 0) = S_2(\tilde{\eta}, 0) = 0,$$

$$\lim_{|\tilde{\eta}| \rightarrow \infty} R_2 = -\frac{\tilde{\tau}^2}{2} \alpha \operatorname{sgn}(\tilde{\eta}), \quad \lim_{|\tilde{\eta}| \rightarrow \infty} S_2 = -|\tilde{\eta}| \tilde{\tau} \alpha.$$

These equations contain the mean field approximation correction to the linear results. The equations can be solved by the method of characteristics. Some geometrical quantities are shown in the sketch:



Substitute

$$u = \tilde{\eta} + \tilde{\tau}, \quad v = \tilde{\eta} - \tilde{\tau}.$$

By adding and subtracting the transformed wave equations, the equations for the evolution of  $R_2 + S_2$  and  $R_2 - S_2$  along the characteristics specified by  $u$  and  $v$  are obtained:

$$\frac{\partial}{\partial v} (R_2 + S_2) = \frac{\alpha}{4} |u+v| ,$$

$$\frac{\partial}{\partial u} (R_2 - S_2) = \frac{\alpha}{4} |u+v| .$$

Thus

$$R_2 + S_2 = \frac{\alpha}{4} \int_u^v |u+x| dx ,$$

$$R_2 - S_2 = \frac{\alpha}{4} \int_v^u |v+x| dx .$$

$u$  and  $v$  switch signs in the four regions A, B, C, D of the  $\tilde{\eta}$ - $\tilde{\tau}$  diagram, so the integrations must be carried out separately in each region.

In region A, for example,  $u > 0$ ,  $v > 0$ , and the absolute value signs in the integrals can be ignored. The result is

$$\textcircled{A} \quad R_2 = -\frac{\tilde{\tau}^2}{2} \alpha , \quad S_2 = -\tilde{\eta}\tilde{\tau}\alpha .$$

In region C,  $u > 0$ ,  $v < 0$ , but  $u+v > 0$ . Thus the quantity  $v+x$  switches sign as  $x$  is integrated from  $v$  to  $u$ . The result is

$$\textcircled{B} \quad R_2 = -\frac{\alpha}{2} (\tilde{\eta}\tilde{\tau} - \frac{\tilde{\eta}^2}{2}), \quad S_2 = -\frac{\alpha}{2} (\tilde{\eta}^2 + \tilde{\tau}^2) .$$

The results in regions C and D can be found immediately from the symmetry of  $s$  and antisymmetry of  $r$  on  $\eta$ . Thus the inner expansions begin

$$\begin{aligned}
 s &= \epsilon \tilde{\tau} - \epsilon^2 |\tilde{\eta}| \tilde{\tau} \alpha + O(\epsilon^3) \\
 r &= \epsilon \tilde{\eta} - \epsilon^2 \frac{\tilde{\tau}^2}{2} \alpha \operatorname{sgn}(\tilde{\eta}) + O(\epsilon^3)
 \end{aligned}
 \tag{D3}$$

in regions A and D outside of the characteristics leaving  $(\tilde{\eta}, \tilde{\tau}) = (0, 0)$ , and

$$\begin{aligned}
 s &= \epsilon \tilde{\tau} - \epsilon^2 \frac{\alpha}{2} (\tilde{\eta}^2 + \tilde{\tau}^2) + O(\epsilon^3) \\
 r &= \epsilon \tilde{\eta} - \epsilon^2 \alpha \left( |\tilde{\eta}| \tilde{\tau} - \frac{\tilde{\eta}^2}{2} \right) \operatorname{sgn}(\tilde{\eta}) + O(\epsilon^3)
 \end{aligned}
 \tag{49}$$

in regions B and C between those characteristics. Equations D3 are the limit of equations 48 for  $\eta = \epsilon \tilde{\eta} \sim \epsilon$ . Thus equations 48 are the correct expansions wherever  $\eta > \tau$ . For  $\eta < \tau$ , or  $\tilde{\eta} < \tilde{\tau}$ , equations 49 are valid and represent the effect of mean flow distortion lost in the linear approximation.

APPENDIX E

Derivation of  $T(\psi)$  and  $\psi(y, 0)$  for the Steady Vortex Street

Complex variables with the sign conventions of Lamb [10] are used. Thus the location  $y, z$  is assigned a complex number  $Z = z+iy$ , and  $\phi$  and  $\psi$  are written as a complex potential  $W = \phi + i\psi$ . The complex potential for an infinite row of vortices of strength  $k$  located at  $z = 0, \pm\ell, \pm 2\ell, \dots$  is

$$\tilde{W} = \frac{ik}{2\pi} \log \sin \frac{\pi Z}{\ell} ,$$

from Lamb. The potential for the vortices of alternating sign spaced  $\lambda$  apart is then

$$W = \frac{ik}{2\pi} \log \sin \frac{\pi Z}{2\lambda} - \frac{ik}{2\pi} \log \sin \frac{\pi(Z-\lambda)}{2\lambda} = \frac{ik}{2\pi} \log \left(-\tan \frac{\pi Z}{2\lambda}\right) .$$

Thus

$$\psi = \text{Im}(W) = \frac{k}{2\pi} \log \left[ \frac{\sqrt{\sin^2 \frac{\pi x}{\lambda} + \sinh^2 \frac{\pi y}{\lambda}}}{\cos \frac{\pi x}{\lambda} + \cosh \frac{\pi y}{\lambda}} \right] .$$

In particular

$$\psi(y, 0) = \frac{k}{2\pi} \log \left( \frac{\sinh \frac{\pi y}{\lambda}}{1 + \cosh \frac{\pi y}{\lambda}} \right) ,$$

which is the second of equations 51 in the text. The complex velocity is

$$w-iv = - \frac{dW}{dZ} = \frac{ik/4\lambda}{\sin \frac{\pi Z}{2\lambda} \cos \frac{\pi Z}{2\lambda}} .$$

The expression for  $W(Z)$  can be inverted to give

$$Z(W) = -\frac{2\lambda}{\pi} \tan^{-1} e^{2\pi W/ik},$$

and the complex velocity can be written as a function of  $W$ :

$$w-iv = \frac{-ik}{2\lambda} \cos \frac{2\pi W}{k}.$$

The square of the speed is

$$V^2 = v^2 + w^2 = (w-iv)(w-iv)^*$$

Thus

$$\begin{aligned} V^2 &= \frac{k^2}{4\lambda^2} \cos \frac{2\pi W}{k} \cos \frac{2\pi W^*}{k} \\ &= \frac{k^2}{8\lambda^2} \left[ \cos \frac{2\pi}{k} (W+W^*) + \cos \frac{2\pi}{k} (W-W^*) \right], \end{aligned}$$

from Dwight [7], p. 79. In terms of  $\phi$  and  $\psi$ ,

$$V^2(\phi, \psi) = \frac{k^2}{8\lambda^2} \left( \cos \frac{4\pi\phi}{k} + \cosh \frac{4\pi\psi}{k} \right).$$

The orbit time  $T(\psi)$  is then

$$T(\psi) = \int_0^k \frac{d\phi}{V^2(\phi, \psi)} = \frac{8\lambda^2}{\pi k} \int_0^\pi \frac{d\theta}{a + \cos\theta},$$

from equation 50 of the text, where

$$a = \cosh \frac{4\pi\psi}{k} > 1.$$

From Dwight, p. 105,

$$T(\psi) = \frac{8\lambda^2}{k\sqrt{a^2-1}}.$$

Again from Dwight, p. 152,  $2|\sinh x \cosh x| = \sqrt{\cosh^2 2x - 1}$ , and

$$T(\psi) = \frac{4\lambda^2}{k \left| \sinh \frac{2\pi\psi}{k} \right| \left| \cosh \frac{2\pi\psi}{k} \right|},$$

which is the first of equations 51 in the text.

APPENDIX F

Derivation of the Mean Square Error Velocity  $\overline{v_{\epsilon c}^2}$

Write the convective part of the acceleration

$$\underline{a}_c = \nabla \left( \frac{v^2 + w^2}{2} \right) .$$

Then  $\overline{v_{\epsilon c}^2} = -\tau \overline{a}_c / 2$ . Equation 68 is

$$v^2 + w^2 = \frac{1}{4\pi^2} \sum_i \sum_j k_i k_j \frac{\zeta_i \zeta_j + \eta_i \eta_j}{r_i^2 r_j^2} \quad (68)$$

From the definitions of  $\eta_i, \zeta_i, r_i,$

$$\frac{\partial}{\partial x} \left[ \frac{\zeta_i \zeta_j + \eta_i \eta_j}{r_i^2 r_j^2} \right] = \frac{\{i, j; \zeta\}}{r_i^2 r_j^2} ,$$

where

$$\{i, j; \zeta\} = \left\{ \zeta_i + \zeta_j - 2 \left( \frac{\zeta_i}{r_i^2} + \frac{\zeta_j}{r_j^2} \right) (\zeta_i \zeta_j + \eta_i \eta_j) \right\} .$$

Similarly

$$\frac{\partial}{\partial y} \left[ \frac{\zeta_i \zeta_j + \eta_i \eta_j}{r_i^2 r_j^2} \right] = \frac{\{i, j; \eta\}}{r_i^2 r_j^2} ,$$

where  $\{i, j; \eta\}$  is the same as  $\{i, j; \zeta\}$  except that the roles of  $\eta$  and  $\zeta$  are reversed. Thus

$$\underline{a}_c = \frac{1}{8\pi^2} \sum_i \sum_j \frac{k_i k_j}{r_i^2 r_j^2} \left( \underline{j} \{i, j; \eta\} + \underline{k} \{i, j; \zeta\} \right) .$$

If the vortices are distributed symmetrically around  $y, z$ , then  $\overline{\underline{a}_c} = 0$ .

If the location of each vortex is independent of its strength,

$$\overline{a_c^2} = \frac{1}{64\pi^2} \sum_i \sum_j \sum_m \sum_n \overline{k_i k_j k_m k_n} \left[ \frac{\{i,j;\zeta\}\{m,n;\zeta\} + \{i,j;\eta\}\{m,n;\eta\}}{r_i^2 r_j^2 r_m^2 r_n^2} \right]$$

If  $k_i$  and  $k_j$  are independent for  $i \neq j$ ,

$$\overline{k_i k_j k_m k_n} = k^4 (\delta_{ij} \delta_{mn} + \delta_{im} \delta_{jn} + \delta_{in} \delta_{jm}) .$$

Thus

$$\begin{aligned} \overline{a_c^2} = \frac{k^4}{64\pi^4} & \left\{ \sum_i \sum_j \left[ \frac{\{i,i;\zeta\}\{j,j;\zeta\} + \{i,i;\eta\}\{j,j;\eta\}}{r_i^4 r_j^4} \right] \right. \\ & \left. + 2 \sum_i \sum_j \left[ \frac{\{i,j;\zeta\}^2 + \{i,j;\eta\}^2}{r_i^4 r_j^4} \right] \right\} . \end{aligned}$$

From the definition of the brackets,

$$\{i,i;\zeta\} = -2\zeta_i ,$$

$$\{i,i;\eta\} = -2\eta_i ,$$

$$\{i,j;\zeta\}^2 + \{i,j;\eta\}^2 = r_i^2 + r_j^2 + 6(\zeta_i \zeta_j + \eta_i \eta_j) + 8 \frac{(\zeta_i \zeta_j + \eta_i \eta_j)^3}{r_i^6 r_j^6} .$$

Thus

$$\overline{a_c^2} = \frac{k^4}{32\pi^4} \sum_i \sum_j \left\{ \frac{r_i^2 + r_j^2}{r_i^4 r_j^4} - 8 \frac{(\zeta_i \zeta_j + \eta_i \eta_j)}{r_i^4 r_j^4} + 16 \frac{(\zeta_i \zeta_j + \eta_i \eta_j)^3}{r_i^6 r_j^6} \right\} .$$

If the vortices are distributed isotropically around  $y, z$ , then quantities like  $\zeta_i \zeta_j / r_i^4 r_j^4$  are zero unless  $i = j$ , and

$$\overline{a}_c^2 = \left(\frac{k}{2\pi}\right)^4 \left[ \sum_i \sum_j \frac{1}{r_i r_j^4} + 2 \sum_i \frac{1}{r_i^6} \right] .$$

Since  $\overline{y}_{\epsilon_c}^2 = \tau^2 \overline{a}_c^2 / 4$ , equation 70 in the text follows immediately.

APPENDIX G

Motion of the Center of a Continuous Vorticity

Distribution in a Uniform Translation and Strain Field

The speed of the center of vorticity in the y direction is

$$\dot{Y} = \frac{d}{dt} \left[ \frac{\int y \xi dA}{\int \xi dA} \right] = \frac{1}{\int \xi dA} \frac{d}{dt} \int y \xi dA$$

since vorticity is conserved. But

$$\begin{aligned} \frac{d}{dt} \int y \xi dA &= \int y \frac{\partial \xi}{\partial t} dA = - \int y \left( v \frac{\partial \xi}{\partial y} + w \frac{\partial \xi}{\partial z} \right) dydz \\ &= - \int y \left[ \frac{\partial}{\partial y} (v \xi) + \frac{\partial}{\partial z} (w \xi) \right] dydz, \end{aligned}$$

where the vorticity convection equation and continuity equation were used. If the vorticity  $\xi$  goes to zero sufficiently fast toward infinity,

$$\begin{aligned} \int_{-\infty}^{\infty} \int_{-\infty}^{\infty} y \frac{\partial}{\partial z} (w \xi) dydz &= \int_{-\infty}^{\infty} y \left( w \xi \Big|_{-\infty}^{\infty} \right) dy = 0, \\ \int_{-\infty}^{\infty} \int_{-\infty}^{\infty} y \frac{\partial}{\partial y} (v \xi) dydz &= - \int_{-\infty}^{\infty} \int_{-\infty}^{\infty} v \xi dydz. \end{aligned}$$

Thus

$$\frac{d}{dt} \int y \xi dA = \int v \xi dA.$$

Since the velocity field consists of a uniform translation plus a strain plus the velocity induced by the vorticity distribution  $\xi$ ,

$$v(y, z) = V + \alpha y + \frac{1}{4\pi} \int \xi(y', z') \frac{(z-z')}{r^2} dA',$$

where  $r^2 = (y-y')^2 + (z-z')^2$ . Then

$$\frac{d}{dt} \int y \xi dA = V \int \xi dA + \alpha \int y \xi dA + \frac{1}{4\pi} \iint \xi(y, z) \xi(y', z') \frac{(y-y')}{r^2} dA dA' .$$

The last integral is zero since it switches sign when the dummy variables  $y$  and  $y'$  are exchanged. Division by  $\int \xi dA$  gives

$$\dot{Y} = V + \alpha Y .$$

The equation  $\dot{Z} = W - \alpha Z$  follows from a similar argument.